SPECIAL COMBINED ISSUE ON

# FULLERENES

Indian J Chem
May 1992
CODEN : IJOCAP 31 A&B (5) F1-F112 (1992)
ISSN : 0376-4710
0376-4699

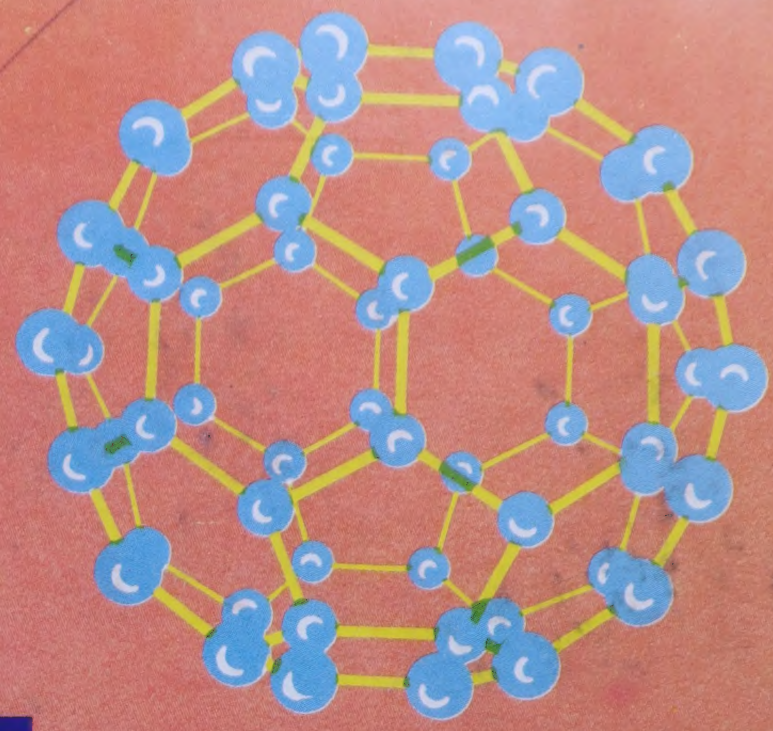

27/4/92

# INDIAN JOURNAL OF CHEMISTRY

SECTION A & SECTION B

LIBRARY
REGIONAL CENTRE
LUDHIANA-141 008

Published by
PUBLICATIONS & INFORMATION DIRECTORATE, CSIR, NEW DELHI
In association with
THE INDIAN NATIONAL SCIENCE ACADEMY, NEW DELHI

# GOLDEN OFFER

You can now book your copies of the popular science titles under

# CSIR GOLDEN JUBILEE SERIES

in advance

**Titles now available**

## BODY'S BATTLES

**BY BAL PHONDKE**

This attractive and lavishly illustrated book unfolds the dramatic story of our inner defence organisation, the diversity and specificity of its armament, and the methodical way in which it maintains round the clock vigil to meet squarely every imaginable threat to the human body and also how it wins the Body's Battles most of the time.

*ISBN-81-85038-99-6*
*(Paperback)*
*84 pages, price Rs. 9.00*

*ISBN-81-7236-003-7*
*(Hardcover)*
*84 pages, price Rs. 18.00*

## HIS MASTER'S SLAVE

**BY TAPAN BHATTACHARYA**

This book, full of illustrations, explains even to the non-specialist the core concepts of computers. Against the backdrop of a canvas rich in detail is revealed the riveting story of modern day genie of the bottle, the PC.

*ISBN 81-7236-018-5*
*(Paperback)*
*88 pages, price Rs. 10.00*

*ISBN 81-7236-019-3*
*(Hardcover)*
*88 pages, price Rs. 18.00*

## MINING THE OCEAN

**BY T.K.S. MURTHY**

*ISBN 81-7236-014-2*
*(Paperback)*
*106 pages,*
*price Rs. 12.00*

*ISBN 81-7236-015-0*
*(Hardcover)*
*106 pages,*
*price Rs. 20.00*

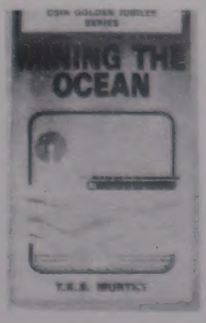


This well illustrated book written especially for the non-specialist, reveals the timeless secrets of the seas. It unfolds in exquisite detail the bounty that seas hold in reserve and highlights man's attempts at mining the oceans.

## INSIDE STARS

**BY BIMAN BASU**

This attractive and lavishly illustrated book written especially for the non-specialist provides a privileged glimpse into star nurseries, tracking their luminescent trail to an ultimate fiery senescence and death. It reveals the mysteries and marvels that reign inside stars.

*ISBN 81-7236-022-3*
*(Paperback)*
*90 pages,*
*price Rs. 10.00*

*ISBN 81-7236-023-1*
*(Hardcover)*
*90 pages,*
*price Rs. 18.00*

## FORTHCOMING TITLES

- PLASTIC FEAST
- ARTIFICIAL INTELLIGENCE
- VERSATILE CERAMICS
- HARDY COMPOSITES
- ALTERNATIVE ENERGY
- DESIGNER MOLECULES

You may place order for all the 10 titles by sending Rs.120.00 (for paperback) or Rs.200 (for hardcover) including postage, by Demand Draft/M.O. payable to "Publications and Information Directorate". Each title will be sent to you by post as soon as it is published, one every month. The titles already published will be sent to you as soon as the payment is received by us.

**For further information write to:**

**Senior Sales and Distribution Officer**
Publications & Information Directorate (CSIR)
Dr K.S. Krishnan Marg
New Delhi - 110 012.

# Indian Journal of Chemistry

## Sections A&B

Special issue on

## FULLERENES

Guest Editor

C.N.R. Rao

CSIR Centre of Excellence in Chemistry,
Solid State & Structural Chemistry Unit

and

Jawaharlal Nehru Centre of Advanced Scientific Research
Indian Institute of Science
Bangalore 560 012, India

# INDIAN JOURNAL OF CHEMISTRY

## Section A: Inorganic, Bio-inorganic, Physical, Theoretical & Analytical Chemistry



**Editorial Board**

Prof. R C Mehrotra
Vice-Chancellor
Allahabad University
Allahabad 211 002

Prof. D V S Jain
Chemistry Department
Panjab University
Chandigarh 160 014

Prof. A Chakravorty
Department of Inorganic Chemistry
Indian Association for the
Cultivation of Science
Calcutta 700 032

Prof. V Krishnan
Department of Inorganic
& Physical Chemistry
Indian Institute of Science
Bangalore 560 012

Prof. K K Rohatgi Mukherjee
Department of Chemistry
Jadavpur University
Calcutta 700 032

Dr J P Mittal
Chemistry Division
Bhabha Atomic Research Centre
Bombay 400 085

Prof. S K Rangarajan
Director
Central Electrochemical Research Institute
Karaikudi 623 006

Prof. R C Srivastava
Department of Chemistry
Banaras Hindu University
Varanasi 221 005

Prof. E D Jemmis
Department of Chemistry
University of Hyderabad
Hyderabad 500 134

Dr S K Date
Physical Chemistry Division
National Chemical Laboratory
Pune 410 008

Prof. I Gutman
Faculty of Science
Yu. 34000, Kragnjevan
Radoja Domanovica
Yugoslavia

Prof. A B Sannigrahi
Department of Chemistry
IIT, Kharagpur 721 302

Dr D Papousek
J. Heyrovsky Institute
of Physical Chemistry
Prague
Czechoslovakia

Prof. P P Singh
Department of Chemistry
M.D. University
Rohtak 124 001

Dr Pradip K Mascharak
Department of Chemistry
University of California
Santa Cruz
California 65064
USA

Dr G P Phondke Director, PID

**Editors** : Dr B.C. Sharma, Dr S. Sivakamasundari and Dr S.K. Bhasin
**Sr. Scientific Assistant** : Geeta Mahadevan



**Published by the Publications & Information Directorate (CSIR), Hillside Road, New Delhi 110 012**
**Director:** Dr G P Phondke



Copyright, 1992, by the Council of Scientific & Industrial Research, New Delhi 110 012



The Indian Journal of Chemistry is issued monthly in two sections: A and B. Communications regarding contributions for publication in the journal should be addressed to the Editor, Indian Journal of Chemistry, Publications & Information Directorate, Hillside Road, New Delhi 110 012.

Correspondence regarding subscriptions and advertisements should be addressed to the Sales & Distribution Officer, Publications & Information Directorate, Hillside Road, New Delhi 110 012.

The Publications & Information Directorate (CSIR) assumes no responsibility for the statements and opinions advanced by contributors. The Editorial Board in its work of examining papers received for publication is assisted, in an honorary capacity by a large number of distinguished scientists, working in various parts of India.

Annual Subscription: Rs. 400.00 £ 100.00 $ 150.00; 50% discount admissible to research workers and students and 25% discount to non-research individuals on annual subscription.

Single Copy: Rs. 40.00 £ 10.00 $ 15.00

Payments in respect of subscriptions and advertisements may be sent by cheque, bank draft, money order or postal order marked payable to Publications & Information Directorate, Hillside Road, New Delhi 110 012.

**Claims for missing numbers of the journal will be allowed only if received within 3 months of the date of issue of the journal plus the time normally required for postal delivery of the journals and the claim.**

# INDIAN JOURNAL OF CHEMISTRY

## Section B: Organic Chemistry including Medicinal Chemistry



**Editorial Board**

Dr A V Rama Rao
Indian Institute of Chemical Technology
Hyderabad 500 007

Dr S Rajappa
National Chemical Laboratory
Pune 411 008

Prof. S V Kessar
Department of Chemistry
Panjab University
Chandigarh 160014

Prof. R P Gandhi
Department of Chemistry
Indian Institute of Technology
New Delhi 110 016

Prof. Goverdhan Mehta
School of Chemistry
University of Hyderabad
Hyderabad 500 134

Prof. H Junjappa
Chemistry Department
North-Eastern Hill University
Shillong 793 003

Prof. U R Ghatak
Indian Association for the Cultivation of Science
Calcutta 700 032

Dr Anil Saran
Chemical Physics Group
Tata Institute of Fundamental Research
Bombay 400 005

Dr Bansi Lal
Chemistry Department
Hoechst India Ltd
Bombay 400 080

Dr R S Kapil
Regional Research Laboratory
Jammu 180 001

Prof. S Chandrasekaran
Department of Organic Chemistry
Indian Institute of Science
Bangalore 560 012

Dr G P Phondke, Editor-in-Chief, *Ex-officio*

**Editors:** Dr S A I Rizvi, Dr L M Mathur and S Hotchandani
**Asstt Editor**: N B Bhoi



**Published by the Publications & Information Directorate (CSIR), Hillside Road, New Delhi 110 012**
**Director:** Dr G P Phondke



Copyright, 1992, by the Council of Scientific & Industrial Research, New Delhi 110 012



The Indian Journal of Chemistry is issued monthly in two sections: A and B. Communications regarding contributions for publication in the journal should be addressed to the Editor, Indian Journal of Chemistry, Publications & Information Directorate, Hillside Road, New Delhi 110 012.

Correspondence regarding subscriptions and advertisements should be addressed to the Sales & Distribution Officer, Publications & Information Directorate, Hillside Road, New Delhi 110 012.

The Publications & Information Directorate (CSIR) assumes no responsibility for the statements and opinions advanced by contributors. The Editorial Board in its work of examining papers received for publication is assisted, in an honorary capacity by a large number of distinguished scientists, working in various parts of India.

Annual Subscription: Rs. 400.00 £ 100.00 $ 150.00; 50% discount admissible to research workers and students and 25% discount to non-research individuals on annual subscription.

Single Copy: Rs. 40.00 £ 10.00 $ 15.00

Payments in respect of subscriptions and advertisements may be sent by cheque, bank draft, money order or postal order marked payable to Publications & Information Directorate, Hillside Road, New Delhi 110 012.

**Claims for missing numbers of the journal will be allowed only if received within 3 months of the date of issue of the journal plus the time normally required for postal delivery of the journals and the claim.**

# Indian Journal of Chemistry (A&B)

## Special Issue on Fullerenes†

VOLUME 31 A&B NUMBER 5 MAY 1992

CONTENTS

Preface . . . . . F1
C N R Rao

Preparation, characterization and properties of $C_{60}$ and $C_{70}$: Spectroscopy, structure, anion interaction with electron donors and superconductivity . . . . . F5
C N R Rao*, T Pradeep, Ram Seshadri, R Nagarajan, V Narasimha Murthy, G N Subbanna, F D'Souza, V Krishnan, G A Nagannagowda, N R Suryaprakash, C L Khetrapal & S V Bhat

Investigations of iron adducts of $C_{60}$: A novel $FeC_{60}$ in the solid state with Fe inside the $C_{60}$ cage. . . . . F17
T Pradeep, G U Kulkarni, K R Kannan, N Y Vasanthacharya, T N Guru Row & C N R Rao*

A photoelectron spectroscopic study of the interaction of oxygen, nitrogen and transition metals with $C_{60}$ films . . . . . F22
V Vijayakrishnan, A K Santra, Ram Seshadri, R Nagarajan, T Pradeep & C N R Rao*

Nitrogen derivatives of $C_{60}$ and $C_{70}$: Interaction of fullerenes with nitrogen in gas phase and with amines in solution phase . . . . . F27
C N R Rao*, T Pradeep, Ram Seshadri & A Govindaraj

Extraction of fullerenes in organic solvents and the development of superior isolation procedures . . . . . F32
R Dhamodaran, I Kaliappam, N Sivaraman, T G Srinivasan, P R Vasudeva Rao & C K Mathews*

Organic chemistry with buckminsterfullerene ($C_{60}$) . . . . . F36
S Chandrasekaran

Spreading of $C_{60}$ on air-water interface . . . . . F42
P Ganguly*, D V Paranjape, K R Patil, S K Chaudhari & S T Kshirsagar

Photophysical studies on buckminsterfullerene: $C_{60}$ . . . . . F46
D K Palit, A V Sapre & J P Mittal*

Simple structural and bonding representations of fullerenes . . . . . F51
A Rathna & J Chandrasekhar*

Towards a correlated electronic structure of fullerenes. . . . . F56
S Ramasesha* & Bhargavi Srinivasan

Physics of undoped and doped $C_{60}$ fullerene . . . . . F64
H R Krishnamurthy & A K Sood*

Structural and microstructural characteristics of solid $C_{60}$ . . . . . F79
N P Lalla & O N Srivastava*

27 APR
REGIONAL CENTRE LUDHIA

CONTENTS

Studies on structural and electronic properties of undoped and doped fullerenes $C_{60}$ and $C_{70}$ . . . . . F92
C S Sundar*, Y Hariharan, A Bharathi, V S Sastry, G V N Rao, J Janaki, T Geethakumari, T S Radhakrishnan, A K Arora, T Shakuntala, M Yousuf, P Ch Sahu, N Subramanian, V S Raghunathan & M C Valsakumar

The problem of conducting and superconducting fullerides. . . . . F100
Ratan Lal & S K Joshi*

On the origin of superconductivity and anomalous normal state properties of doped solid $C_{60}$ . . . . . F104
G Baskaran

Announcement . . . . . F112

Authors for correspondence are indicated by (*)

†This special combined issue of Indian J. Chem., Sections A and B has been paginated independently of the regular issues of the two sections. Pagination of the June 1992 issues will be in continuation of the April 1992 issues of the respective sections.

# AUTHOR INDEX

## (Special Issue on Fullerenes)


| | |
|---|---|
| Arora A K | F92 |
| Baskaran G | F104 |
| Bharathi A | F92 |
| Bhat S V | F5 |
| Chandrasekaran S | F36 |
| Chandrasekhar J | F51 |
| Chaudhari S K | F42 |
| Dhamodaran R | F32 |
| D'Souza F | F5 |
| Ganguly P | F42 |
| Geethakumari T | F92 |
| Govindaraj A | F27 |
| Guru Row T N | F17 |
| Hariharan Y | F92 |
| Janaki J | F92 |
| Joshi S K | F100 |
| Kaliappam I | F32 |
| Kannan K R | F17 |
| Khetrapal C L | F5 |
| Krishnamurthy H R | F64 |
| Krishnan V | F5 |
| Kshirsagar S T | F42 |
| Kulkarni G U | F17 |
| Lalla N P | F79 |
| Mathews C K | F32 |
| Mittal J P | F46 |
| Nagannagowda G A | F5 |
| Nagarajan R | F5,F22 |
| Narasimha Murthy V | F5 |
| Palit D K | F46 |
| Paranjape D V | F42 |
| Patil K R | F42 |
| Pradeep T | F5,F17,F22,F27 |
| Radhakrishnan T S | F92 |
| Raghunathan V S | F92 |
| Ramasesha S | F56 |
| Rao C N R | F1,F5,F17,F22,F27 |
| Rao G V N | F92 |
| Ratan Lal | F100 |
| Rathna A | F51 |
| Sahu P Ch | F92 |
| Santra A K | F22 |
| Sapre A V | F46 |
| Sastry V S | F92 |
| Seshadri Ram | F5,F22,F27 |
| Shakuntala T | F92 |
| Sivaraman N | F32 |
| Sood A K | F64 |
| Srinivasan Bhargavi | F56 |
| Srinivasan T G | F32 |
| Srivastava O N | F79 |
| Subbanna G N | F5 |
| Subramanian N | F92 |
| Sundar C S | F92 |
| Suryaprakash N R | F5 |
| Valsakumar M C | F92 |
| Vasanthacharya N Y | F17 |
| Vasudeva Rao P R | F32 |
| Vijayakrishnan V | F22 |
| Yousuf M | F92 |

Indian Journal of Chemistry
Vol. 31 A& B, May 1992, pp. F1-F4

# PREFACE

There has been considerable interest in understanding the nature of carbon in the universe for some time. It was found a few years ago that some of the features in the absorption spectra of the interstellar region arise from large molecules of carbon. In an attempt to generate these molecules in the laboratory, Harold Kroto, Richard Smalley and coworkers[1] studied the mass spectra of carbon vapours resulting from the ablation of graphite crystals with high energy lasers. To their surprise, they found mass peaks due to various carbon species in the vapour, the most abundant amongst them being a cluster containing 60 carbon atoms. The cluster of 60 carbon atoms has remarkable stability and has a shape similar to a soccer ball involving a framework with an icosahedral hollow cage (Fig. 1). Since geodesic domes of a similar shape had earlier been designed by the famous American architect Buckminster Fuller, the $C_{60}$ molecule was named *buckminsterfullerene.* Popularly, this molecule has been called *buckyball.*

Along with buckminsterfullerene, $C_{60}$, the other prominent carbon cluster molecule found in graphite vapours is $C_{70}$, containing 70 atoms of carbon. The $C_{70}$ molecule has the shape of a rugby ball (Fig. 1). This entire family of carbon molecules is referred to as *fullerenes.* Other interesting species (e.g. $C_{76}$) have also been identified. One of the large fullerenes one can visualise is $C_{540}$ made up of 540 carbon atoms. The fullerenes clearly constitute a new allotrope of carbon, different from graphite and diamond.

In spite of its stability, it was not possible to study $C_{60}$ in the laboratory until recently, since it was not possible to obtain sufficient quantities of the material. Theoreticians predicted some properties based on various types of calculations, but they could not be verified. The situation however changed towards the end of 1990, when Krätschmer and coworkers[2] found a simple laboratory method to prepare macroscopic quantities of $C_{60}$ and $C_{70}$. The method involves vapourizing graphite in a conventional bell-jar by passing high current through two

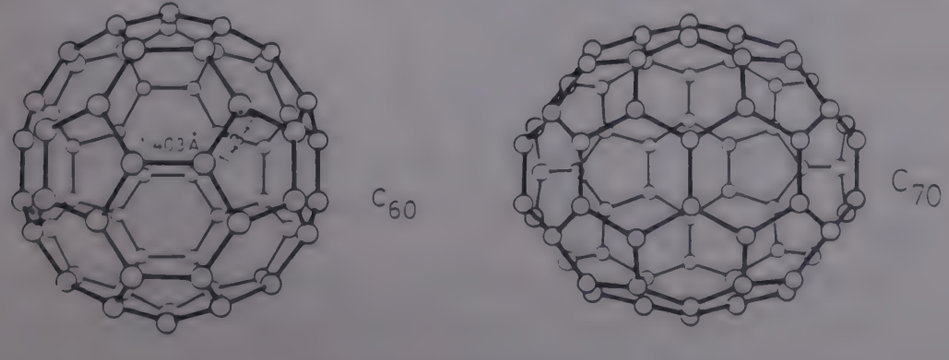


Fig. 1—Structures of fullerenes $C_{60}$ and $C_{70}$

graphite electrodes in an atmosphere of helium. The soot collected from the arc is digested with an organic solvent such as toluene. The solid obtained after removing the solvent from the toluene solution contains $C_{60}$ mixed with a smaller proportion of $C_{70}$. $C_{60}$ and $C_{70}$ can be separated by column chromatography[3]. $C_{60}$ when dissolved in organic liquids gives a magenta coloured solution while the solution of $C_{70}$ is wine red.

$C_{60}$ and $C_{70}$ have been found to be present in the soot produced from benzene flames[4,5]. These molecules have also been found in the soot obtained by vapourizing coal[6]. They are not present in soots from flames of kerosene or aliphatic hydrocarbons. Presence of $C_{60}$ and $C_{70}$ in certain soots is of relevance in understanding the origin of these carbon molecules and also the mechanism of formation of soot itself.

With the availability of a method to produce fullerenes in the laboratory, the topic has become the rage of the day. It has created great excitement in the scientific world comparable only to that of high-temperature superconductors in early 1987. $C_{60}$ and $C_{70}$ (partly) have been characterized[8] in terms of the crystal structure[7], UV-visible[9], NMR[10], infrared[11] and Raman[12] spectra as well as high-resolution electron microscopy[13]. At room temperature, $C_{60}$ has a face-centered cubic structure. The X-ray study confirms the high symmetry of $C_{60}$ and shows an intercluster separation of 10 Å in the crystal. The icosahedral hollow cage has a diameter of 7 Å (Fig. 1). It is to be noted that the icosahedral symmetry, $I_h$, of $C_{60}$ is the highest possible point group symmetry. Since the crystals at room temperature contain spherical molecules which can randomly orient themselves, there is considerable orientational disorder (plastic state). On cooling to 250K, the molecules order themselves, giving rise to a more crystalline phase.

In diamond, the distance between two carbon atoms is that of a C-C single bond (1.54 Å) while in graphite, it is smaller (1.39 Å). In buckminsterfullerene, $C_{60}$, there are two distinct C-C bond lengths of around 1.40 Å and 1.43 Å (Fig. 1). These distances are in between those in diamond and graphite. Diamond is a perfect insulator while graphite is a conductor; $C_{60}$ is an insulator with a band gap of 2.2 eV. The compressibility of $C_{60}$ is comparable to that of diamond. The chemical behaviour of fullerenes would also be expected to be in between that of diamond an graphite. Actually $C_{60}$ is a reactive molecule and can undergo several types of reactions. It has been reduced to give $C_{60}H_{18}$ and $C_{60}H_{36}$ and methylated to get $C_{60}(CH_3)_6$. It is of considerable interest to functionalise $C_{60}$, and use the derivatives for other reactions. A problem that one faces while functionalising $C_{60}$ is the large number of isomers that are possible in these derivatives. For example, $C_{60}H_2$ can have 59 isomers. Separation and characterization of the isomers would be a formidable task.

One of the interesting aspects of intense interest today is the incorporation of an external atom in the spheroidal cavity. A variety of metal atoms can, in principle, be trapped in this cavity. Some of the stud-

ies have claimed that it is posible to push atoms such as lanthanum, iron and helium inside the spheroidal cavity[14,15]. Substitution of the carbon in $C_{60}$ by boron and nitrogen have been attempted. Interestingly nitrogen not only substitutes for carbon in the cage but also adds on to $C_{60}$ and $C_{70}$[16].

Excitement in fullerene research has been enhanced by the discovery of superconducting fullerene compounds. Hebard *et al.*[17] discovered that the potassium derivative of $C_{60}$ is superconducting at 18K. The rubidium-cesium analogues are also superconducting with higher transition temperatures (up to 35K)[18]. One of the important differences between these carbon superconductors and high-temperature cuprate superconductors is that the latter are two-dimensional oxides while the $C_{60}$ derivatives are three-dimensional molecular solids. It is noteworthy that the other organic molecular superconductors show superconductivity at temperatures of 10K or less.

A variety of problems related to $C_{60}$ and other fullerenes will undoubtedly occupy the interest of chemists, physicists and materials scientists in the next few years. In addition to high-temperature superconductivity, the possibility of making molecular ferromagnets, molecular traps and molecular bearings would be of interest. $C_{60}$ offers immense possibilities in synthetic organic chemistry. Use of $C_{60}$ in catalysis and organometallic chemistry and also as part of polymeric structures deserves to be explored. Properties of fullerenes other than $C_{60}$ and $C_{70}$ are equally fasciriating; thus, $C_{76}$ has a chiral $D_2$ symmetry[19]. Many new fullerenes are yet to be prepared and characterized. It has already been shown that extraction of the soot from graphite with quinoline gives higher fullerenes[20] (e.g. $C_{120}$, $C_{180}$, $C_{300}$). The possibility of obtaining carbon cluster molecules such as $C_{240}$ and $C_{540}$ (Fig. 2) in macroscopic quantities is real. Inside the cavity of $C_{240}$, it would be possible to locate a $C_{60}$ molecule. Clearly, fullerenes promise exciting times ahead[21].

In this special issue of the Indian Journal of Chemistry (sections A and B), we have got together articles by Indian scientists engaged in fullerene research to highlight the activities in the country. The arti-

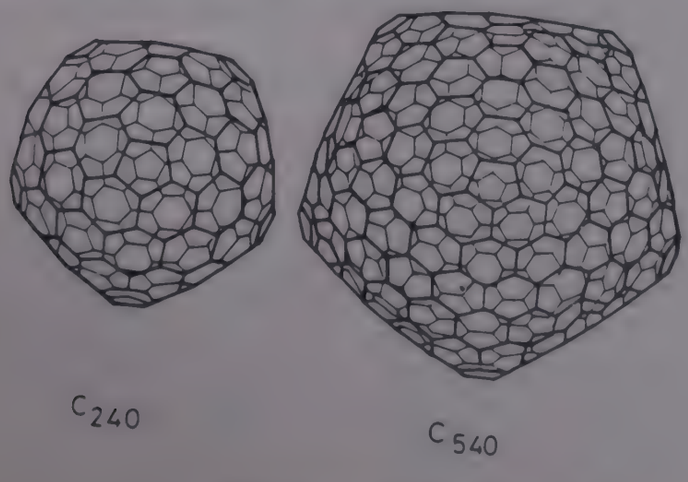


Fig. 2—Structures of fullerenes $C_{240}$ and $C_{540}$

cles are, by and large, based on research carried out in India, but also include reviews of the pertinent literature. It is hoped that practitioners in the field as well as teachers and students will find the special issue to be useful and instructive.

C N R Rao
Guest Editor

**References**


1 Kroto H W, Heath J R, O'Brien S C, Curl R F & Smalley R E, *Nature*, 318 (1985) 162.
2 Krätschmer W, Lamb L D, Fostiropoulous K & Huffman D R, *Nature*, 347 (1990) 354.
3 Taylor R, Hare J P, Abdul-Sada A K & Kroto H W, *J chem Soc Chem Commun*, (1990) 1423.
4 Howard J B, McKinnon J T, Makarovsky Y, Lafleur L & Johnson M E, *Nature*, 352 (1991) 139.
5 Pradeep T & Rao C N R, *Current Science (India)*, 61 (1991) 432.
6 Pang L S K,Vassallo A M & Wilson M A, *Nature*, 352 (1991) 480.
7 David W I F, Ibberson R M, Matthewman J C, Prassides K, Dennis T J S, Hare J P, Kroto H W, Taylor R & Walton D R M, *Nature*, 353 (1991) 147.
8 Cox D M, Behal S, Disko M, Gorun S N, Greaney M, Hsu C S, Kollin E B, Millar J, Robbins J, Robbins W, Sherwood R D & Tindall P, *J Am chem Soc*, 113 (1991) 2940.
9 Hare J P, Kroto H W & Taylor R, *Chem Phys Lett*, 177 (1991) 394.
10 Johnson R D, Meijer G & Betune D S, *J Am chem Soc*, 112 (1990) 8983.
11 Hare J P, Dennis T J, Kroto H W, Taylor R, Allaf A W, Balu S & Walton D R M, *J chem Soc Chem Commun*, (1991) 412.
12 Bethune D S, Meijer G, Tang W C & Rosen H J, *Chem Phys Lett*, 174 (1990) 219.
13 Wang S & Buseck P R, *Chem Phys Lett*, 182 (1991) 1.
14 Chai Y, Guo T, Jin C, Haufler R E, Chibante L P F, Fure J, Wang L, Alford J M & Smalley R E, *J phys Chem*, 95 (1991) 7564.
15 Pradeep T, Kulkarni G U, Kannan K R, Guru Row T N & Rao C N R, *J Am chem Soc*, 114 (1992) 2272.
16 Pradeep T, Vijayakrishnan V, Santra A K & Rao C N R, *J phys Chem*, 95 (1991) 10564.
17 Hebard A F, Rosseinsky M J, Haddon R C, Murphy D W, Glarum S, Glarum S H, Palstra T T M, Ramirez A P & Kortan A R, *Nature*, 350 (1991) 600.
18 Tanikagi K, Ebbesen T W, Saito S, Mizuki J, Tsai J S, Kubo Y & Kurushima S, *Nature*, 352 (1991) 222.
19 Ettl R, Chao I, Diederich F & Whetten R L, *Nature*, 353 (1991) 149.
20 Shinohara H, Sato H, Saito Y, Takayama H, Izouka A & Sugawara T, *J phys Chem*, 95 (1991) 8449.
21 Kroto H W, Allaf A W & Balm S P, *Chem Rev*, 91 (1991) 1213.

Indian Journal of Chemistry
Vol. 31 A& B, May 1992, pp. F5-F16

# Preparation, characterization and properties of $C_{60}$ and $C_{70}$: Spectroscopy, structure, anions, interaction with electron donors and superconductivity

C N R Rao*[1,2], T Pradeep[1], Ram Seshadri[2], R Nagarajan[2], V Narasimha Murthy[2], G N Subbanna[3], F D'Souza[4], V Krishnan[4], G A Nagannagowda[5], N R Suryaprakash[5], C L Khetrapal[5] & S V Bhat[6]

[1]CSIR Centre of Excellence in Chemistry,
[2]Solid State & Structural Chemistry Unit,
[3]Materials Research Centre,
[4]Department of Inorganic & Physical Chemistry,
[5]Sophisticated Instruments Facility, and
[6]Department of Physics,
Indian Institute of Science, Bangalore 560 012, India

Received 20 February 1992

Preparation and characterization of the fullerenes, $C_{60}$ and $C_{70}$, are described in detail, including the design of the generators fabricated locally. The characterization techniques employed are UV-visible, IR, Raman and $^{13}C$ NMR spectroscopies, scanning as well as transmission electron microscopy and mass spectrometry. The electron energy level diagram of $C_{60}$ as well as the one-electron reductions of $C_{60}$ and $C_{70}$ leading to various anions are discussed. Electronic absorption spectra of $C_{60}^-$ and $C_{60}^{2-}$ are reported. Phase transitions from the plastic to the crystalline states of $C_{60}$ and $C_{70}$ are examined. Based on a $^{13}C$ NMR study in a mixture of nematic liquid crystals, it has been demonstrated that $C_{60}$ retains its extraordinary symmetry in solution phase as well. Interaction of $C_{60}$ and $C_{70}$ with strong electron-donor molecules has been investigated employing cyclic voltammetry. Superconductivity of $K_xC_{60}$ has been studied by non-resonant microwave absorption; $Na_xC_{60}$ as well as $K_xC_{70}$ are shown to be non-superconducting. Doping $C_{60}$ with iodine does not make it superconducting. Interaction of $C_{60}$ with $SbCl_5$ and liquid $Br_2$ gives rise to halogenated products.

The closed-cage molecules of carbon, the fullerenes, and in particular buckminsterfullerene, $C_{60}$, first discovered by Kroto *et al.*[1] have become a topic of intense research after the preparative procedure involving vapourization of graphite in an arc, to prepare macroscopic quantities, became available[2]. In our efforts[3] to investigate the structure, properties and reactivity of $C_{60}$ and $C_{70}$, we have designed generators which produce $C_{60}$ and $C_{70}$ in high yields at a fast rate. Besides producing $C_{60}$ and $C_{70}$ by contact-arc vapourization of graphite employing locally designed generators, we show that these fullerenes are formed in simple benzene-air flames in minute quantities. We describe here characterization of $C_{60}$ and $C_{70}$ by a variety of techniques including optical and NMR spectroscopy, mass spectrometry and electron microscopy. An electron energy level scheme of $C_{60}$ consistent with the electronic absorption spectrum and the UV photoelectron spectrum is given. Also reported are four one-electron reversible reduction potentials of $C_{60}$ giving rise to different anions, besides reliable electronic absorption spectra of the mono- and di-anions. The interaction of $C_{60}$ and $C_{70}$ with a few electron donor molecules has also been investigated employing cyclic voltammetry.

Since $C_{60}$ is a highly symmetrical molecule with $I_h$ symmetry, we have investigated its $^{13}C$ NMR spectrum in a mixture of nematic crystals of opposite diamagnetic anisotropies to find out if any distortions are induced in the molecule in such an environment just as those found in the case of spherical molecules such as methane. Also examined are the phase transitions of $C_{60}$ and $C_{70}$ involving orientational disorder by means of differential scanning calorimetry. We have also studied the superconducting properties of doped fullerenes by employing non-resonant microwave absorption.

## Materials and Methods

In order to prepare $C_{60}$ and $C_{70}$, we have built two generators wherein contact-arc vapourization of graphite is carried out in a helium atmosphere. A schematic diagram of one of the generators fabricated by us[3] is shown in Fig.1. Two water-cooled copper electrodes and a water-cooled double-walled copper vessel form the essential parts of the generator. The graphite electrodes and the copper vessel are housed in a 30" long stainless steel vacuum vessel of 8" diameter mounted on a 4" diffusion pump through a liquid nitrogen trap. Graphite rods of 5 mm diameter (Johnson Matthey Chemicals Ltd., England) were used in the evaporation.

In order to facilitate the evaporation process,

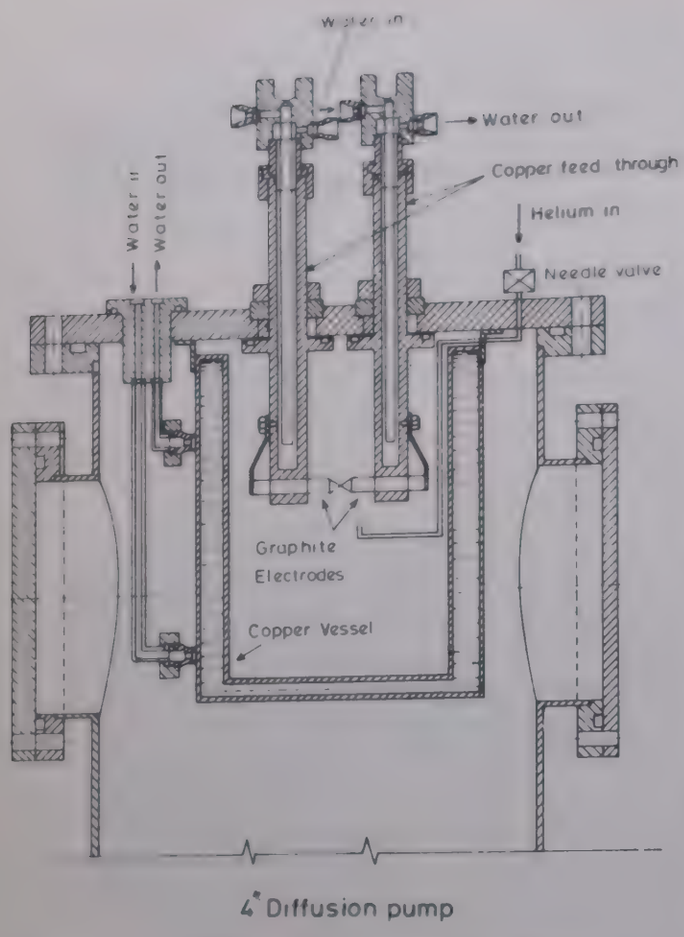


Fig. 1—Schematic diagram of a fullerene generator

both the graphite electrodes were sharpened to a conical shape and held in loose contact with each other with the help of two tungsten springs. The system was pumped to ~$10^{-6}$ torr and helium let into the copper vessel through a liquid nitrogen trap. The pressure of helium was maintained around 180 torr with slow pumping and by controlling the leak rate with the help of a variable leak valve. A current in the 100-180 amp range (5-8 volts AC, 60 Hz) was passed through the electrodes to initiate the arc. A gray plume was observed under these conditions. After three hours of evaporation, about 500 mg of soot could be collected from the copper vessel and the electrode surfaces. Still larger quantities of soot could be obtained after prolonged evaporation. The soot was extracted with toluene and filtered. The resulting red solution was evaporated to yield a solid which was characterised by mass spectrometry, $^{13}C$ NMR spectroscopy, etc. We have recently incorporated another set of electrodes in the system shown in Fig.1 in a manner that enables us to move them from outside. This helps to sustain the arc for longer periods. With this design, larger quantities of $C_{60}$ could be produced in a shorter period (50 mg in less than an hour). The yield of $C_{60}$ + $C_{70}$ mixtures obtained by us were 10-30% of the soot and $C_{70}$ content in the mixture was ~ 10% or less.

In Fig.2 is shown the diagram of another generator fabricated by us. This consists of a water cooled stainless steel vessel of 8" dia. pumped to ~ $10^{-6}$ torr by a 4" oil diffusion pump through a liquid $N_2$ trap. The graphite rods were connected to 1" copper feed-throughs and a current of 100-300 Å (10V AC) was passed through the rods to obtain the arc. One of the electrodes is movable from outside so that a graphite rod of 4 cm could be evaporated completely in 10 min. Once the system is pumped to ~ $10^{-6}$, the vacuum valve is closed and helium admitted to ~ 100 torr through a needle valve. The arc could be maintained continuously by keeping the distance between the electrodes constant. The design of this generator makes it possible to change the graphite rods and to remove the soot by opening just one flange. It is also possible to drive the copper feedthrough by means of an electrical motor and automate soot generation.

In order to obtain pure $C_{60}$ and $C_{70}$, the toluene extract was passed through alumina columns. After chromatographic separation, we could get pure $C_{60}$ and $C_{70}$. The purity was ascertained by TLC, mass spectrometry, Raman spectroscopy and others techniques. One should note that $C_{60}$ samples are often contaminated by $C_{70}$ and vice-versa.

Mass spectrometry was carried out with a JEOL (direct inlet 70 eV EI source) instrument. UV-visible spectra were recorded with a Pye-Unicam instrument. Infrared spectra were recorded with a Brüker FT spectrometer and Raman spectra with a Spex Ramalog unit. $^{13}C$ NMR spectra were recorded with a 400 MHz Brüker spectrometer. High resolution electron micrographs were recorded with a JEOL 200CX instrument while scanning electron micrographs were obtained with a Cambridge microscope. Cyclic voltammograms were recorded with a PAR instrument. Differential scanning calorimetry was carried out with a Perkin-Elmer instrument at a cooling rate of 20°/min under nitrogen flow.

We have prepared $K_xC_{60}$ and $K_xC_{70}$ by the solution route wherein ~ 75 mg of potassium metal was refluxed with ~ 15 mg of pure $C_{60}$ or $C_{70}$ in toluene for ~ 2 h under Ar flow. The black solid thus obtained was filtered under Ar flow and the powder was packed in a capillary tube of 0.1 mm diameter. $Na_xC_{60}$ was prepared by reaction of Na with $C_{60}$ in refluxing toluene. The samples were studied by non-resonant microwave absorption and ESR spectroscopy, using a Brüker ER-200D X-band spectrometer working at a nominal frequency of 9.4 GHz. Magnetic field modulation of 100 kHz with phase sensitive detection was employed to record the re-

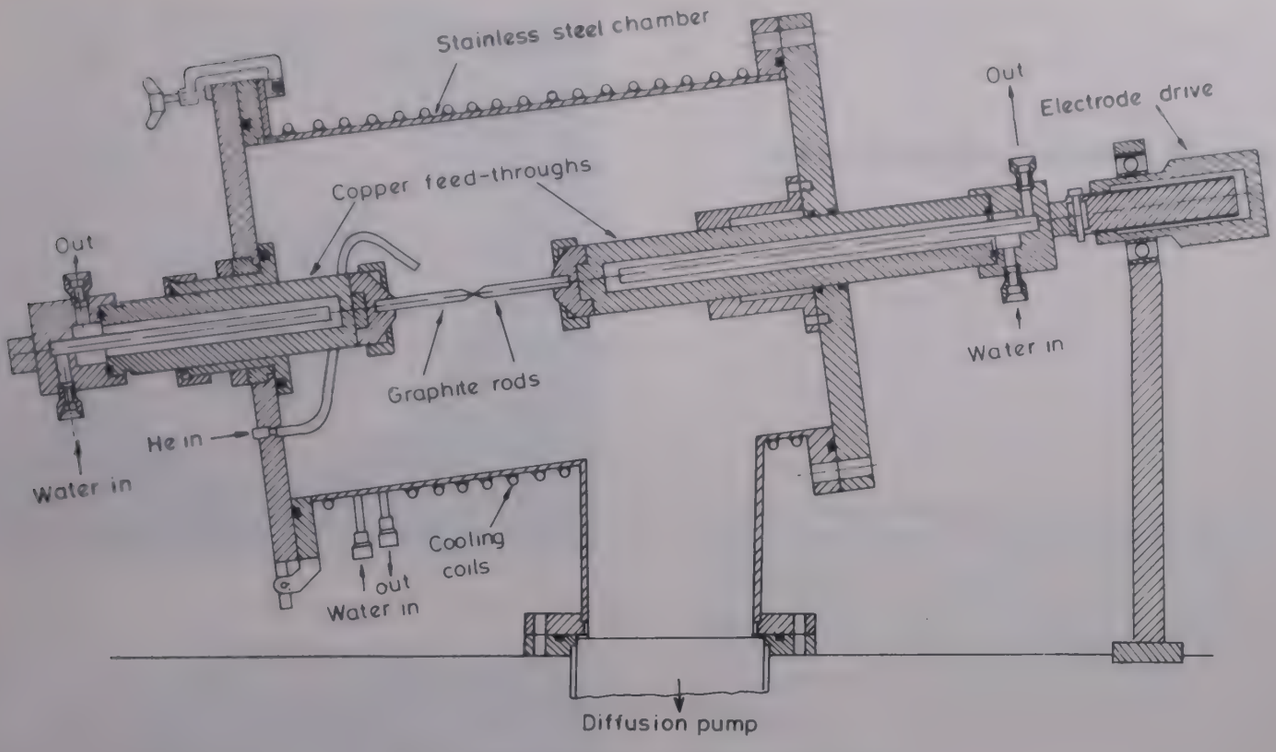


Fig. 2—Second design of a fullerene generator

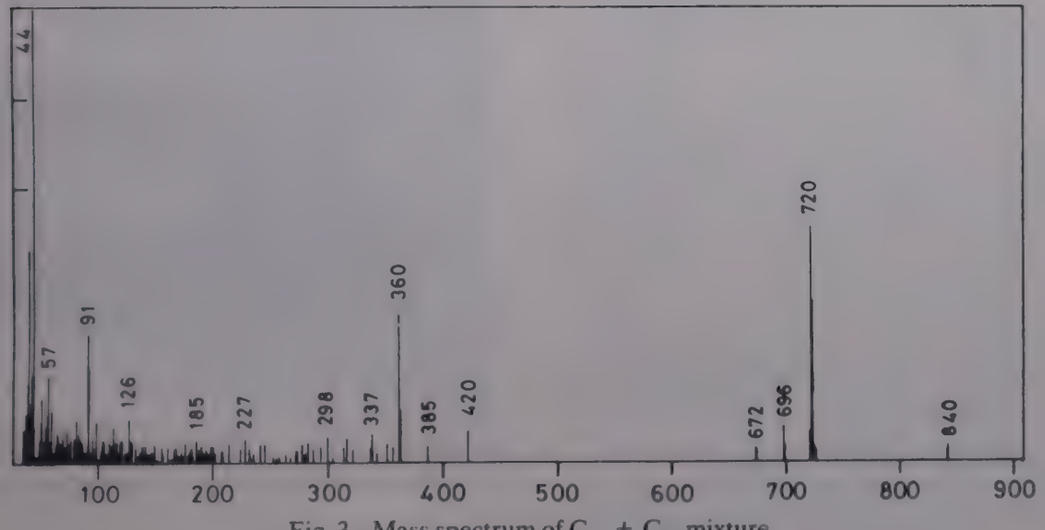


Fig. 3—Mass spectrum of $C_{60}$ + $C_{70}$ mixture

sponse in the derivative form. A continuous flow He cryostat (Oxford Instruments) was used to vary the temperature down to 4.2 K with ± 0.1 K accuracy. The Na salt of $C_{60}$ was prepared in a manner analogous to $K_xC_{60}$ and it was also examined by non-resonant microwave absorption. $C_{60}$ samples, subjected to interaction with iodine, were also similarly examined. Efforts to examine adducts of $C_{60}$ with liquid $Br_2$ and $SbCl_5$ (in an organic solvent) failed since halogenated products were obtained. Rb and Rb-Cs derivatives of $C_{60}$ were prepared by reaction in sealed tubes.

## Results and Discussion

### *Characterization*

Over the last few months we have been able to generate $C_{60}$ and $C_{70}$ at fairly rapid rates. We have used mass spectrometry routinely to characterize $C_{60}$ and $C_{70}$ (Fig.3). $^{13}C$ NMR spectroscopy is also a good tool to distinguish $C_{60}$ and $C_{70}$. While $C_{60}$ shows a single line around 143 ppm, $C_{70}$ shows five lines at 130.9, 145.2, 147.3, 148.6 and 150.5 ppm with intensity ratios of 10/20/10/20/10 as can be seen from Fig.4. $C_{60}$ and $C_{70}$ show characteristic infrared spectra (Fig.5), the remarkable simplicity of the spectrum of $C_{60}$ due to its high symmetry being noteworthy. The Raman spectrum of $C_{60}$ is shown in Fig.6.

Scanning electron micrographs of the $C_{60}$ particles obtained after removal of the solvent show spherical aggregates of 1-5 microns (Fig.7a). High-resolution electron micrographs not only show lat-

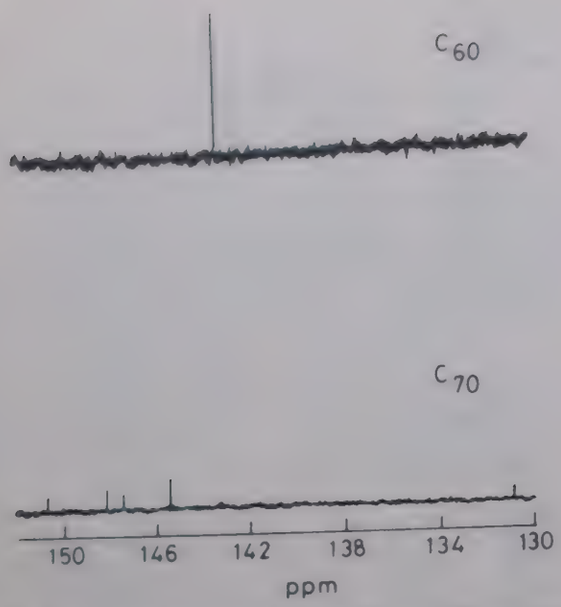


Fig. 4—$^{13}C$ NMR spectra of $C_{60}$ and $C_{70}$ in $CCl_4$ solution

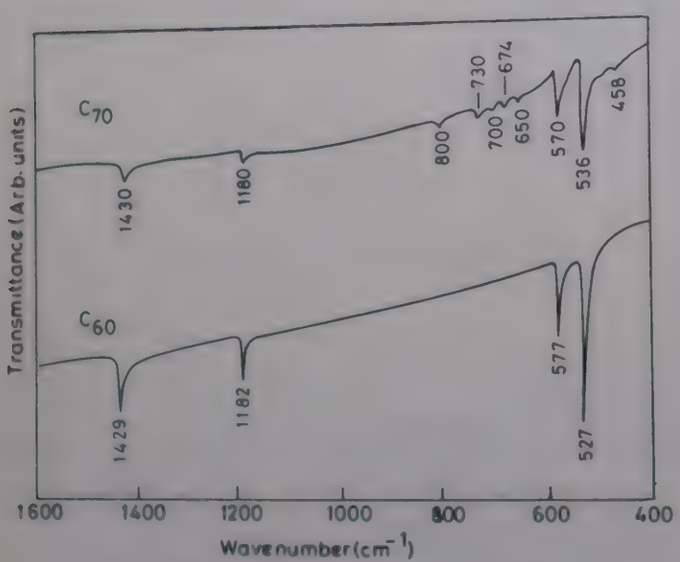


Fig. 5—Infrared spectra of $C_{60}$ and $C_{70}$

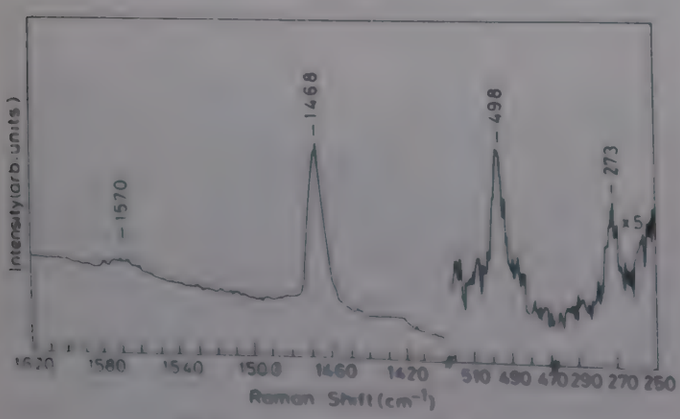


Fig. 6—Raman spectrum of $C_{60}$

tice fringes corresponding to $a/2$ (~8Å) as in Fig. 7b, but also the closed packed arrangement of $C_{60}$ molecules with a diameter of ~7Å. In the inset of Fig. 7b, we show an image in which the nearly cir-

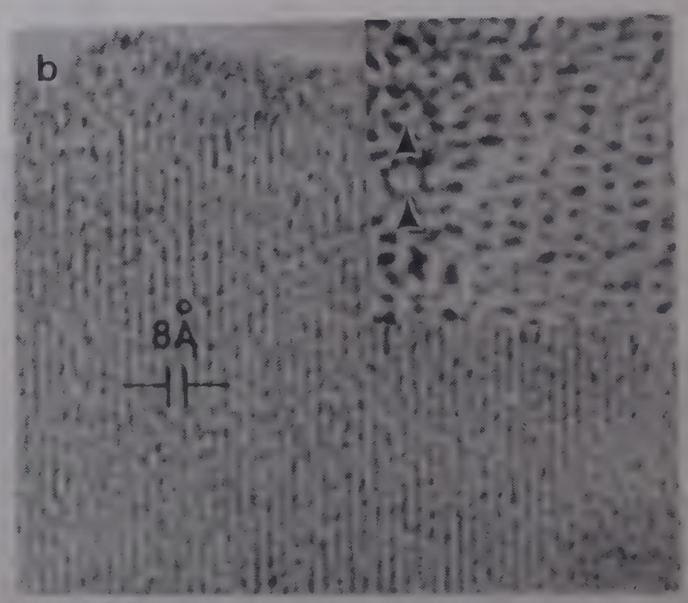


Fig. 7—(a) Scanning electron micrograph showing a spherical aggregate of $C_{60}$; (b) Lattice fringes in the transmission electron micrograph; inset shows close-packed $C_{60}$ molecules

cular white features with central black spots represent the projection of the hollow cage.

The electronic absorption spectrum of $C_{60}$ in *n*-hexane solution (Fig.8) recorded by us shows distinct maxima at 213, 257 and 328 nm (log ε, 5.1, 5.2 and 4.7 respectively) and a broad band centred around 555 nm; there is also a sharp feature at 404 nm in agreement with Hare *et al.*[4]. This spectrum can be understood by taking the first three π orbital energies to be approximately equal to the ionization energies from the UV photoelectron spectrum[5]. The ionization energies are at 7.6 ($h_u$), 8.9 ($g_g$ + $h_g$) and 10.8 eV ($g_u$ + $t_{2u}$). In Fig.9 we show the energy level diagram[3] of $C_{60}$ which also indicates the various $\pi$-$\pi^*$ transitions; in this diagram we have made use of the fact that the differences in some of the transition energies are close to the differences in the

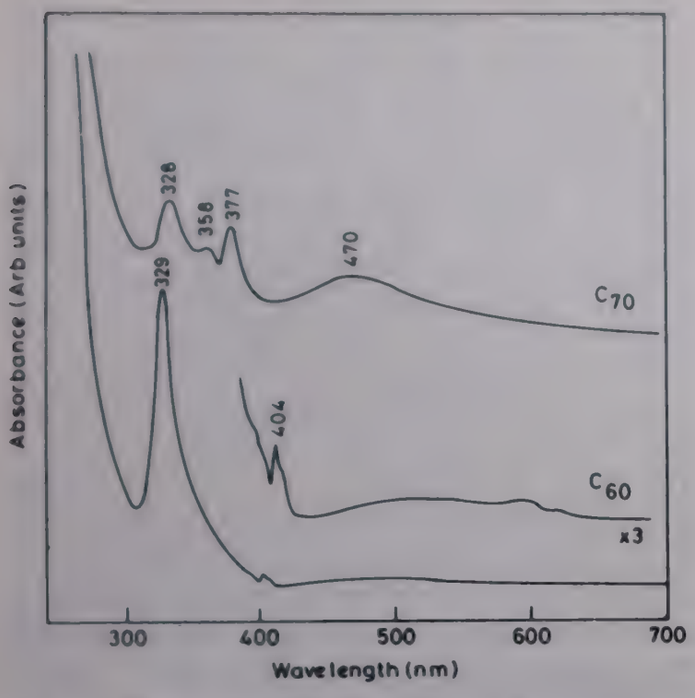


Fig. 8—Electronic absorption spectra of $C_{60}$ and $C_{70}$ in hexane solution

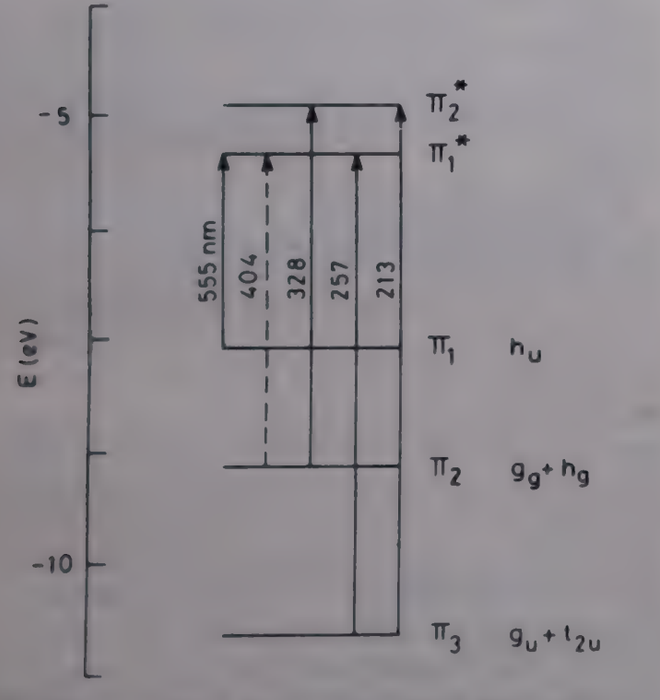


Fig. 9—Approximate electron energy level scheme of $C_{60}$

$\pi$ orbital energies. The longest wavelength $\pi$-$\pi^*$ transition around 550 nm corresponds to HOMO-LUMO separation of 2.2 eV, in agreement with theoretical expectations and the electron energy loss spectrum. The sharp 404 nm feature is likely to be due to the $\pi_2$-$\pi_1^*$ (rather than $\pi_1$-$\pi_2^*$) transition as shown in Fig.9. Some of the structures in the 550 nm band seems to correspond to the known vibrational frequencies of the molecule. The UV absorption bands of $C_{60}$ show solvent red-shifts in polar solvents indicating an increase in the dipole moment

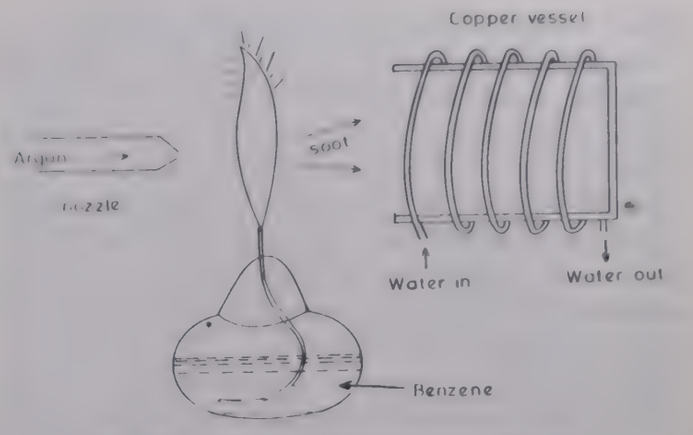


Fig. 10—Fullerenes from benzene-air flame

on excitation. The red-shifts of the 328 nm band in $CH_3CN$ and DMSO solvents are 92 and 278 $cm^{-1}$ respectively with respect to *n*-hexane. In Fig.8 we have also shown the electronic absorption spectrum of $C_{70}$, but are unable to provide the energy level diagram due to the absence of information on orbital ordering.

*Fullerenes from benzene flames*

Recently, Howard *et al.*[6] have found $C_{60}$ and $C_{70}$ in varying proportions in laminar flames of benzene and oxygen. These authors stabilized the flame in a partial helium atmosphere employing a specially designed low-pressure chamber and found the fullerenes to occur preferentially in non-sooty flames. We have been examining the nature of condensible compounds and soot in benzene-air flames for some time and have found fullerenes, $C_{60}$ and $C_{70}$, in sooty flames obtained from a simple laboratory spirit lamp using benzene as the fuel (Fig.10). We consider this to be of some general interest.

The technique employed by us involved quenching of a part of the sooting end of the flame by argon coming through a glass nozzle (1 mm dia) at a stagnation pressure of 1.5 atm and collecting the soot on a cooled copper surface positioned opoosite to the nozzle (Fig.10). We could collect ~5 g of the soot after 3 hr of operation, expending 250 ml of benzene. The soot was washed with ether and the toluene extract of the residue dried and analysed by mass spectrometry. The mass spectrum showed the 720 and the 840 mass peaks (as well as the m/2 peaks). The proportion of $C_{60}$ was higher and the total yield of fullerenes was ~0.1% with respect to the soot. The yield can be improved by quenching a larger area of the flame. The observation of fullerenes in such simple benzene flames is not only of significance in understanding the origin of fullerenes as well as the formation of soot, but also suggests the possible occurrence of these species in the environment.

*Phase transitions due to orientational disorder*

Buckminsterfullerene, $C_{60}$, being a spherical molecule, would be expected to show a high degree of orientational disorder in the solid state. We were interested in examining whether $C_{60}$ showed evidence for a transition from an orientationally disordered (plastic) state to an ordered state. We indeed found such a phase transition around 250 K. In the meantime, however, we noticed the paper of Heiney *et al.*[7] who found the transition at 250 K to be accompanied by a change in crystal symmetry. We were equally interested to examine whether a plastic to crystalline phase transition is exhibited by $C_{70}$ which has a near-spherical symmetry. For this purpose, we have carried out a study on $C_{70}$ by differential scanning calorimetry. The sample of $C_{70}$ was pure, although presence of minute quantities of $C_{60}$ cannot entirely be ruled out.

In Fig.11, we show the differential scanning calorimetric trace of $C_{70}$ after subtracting the baseline. For purpose of comparison, we also show the DSC trace for $C_{60}$ in this figure. The transition in $C_{70}$ (218K) occurs at a lower temperature than that in $C_{60}$. The transition takes place over a slightly wider temperature range than in the case of $C_{60}$. The enthalpy change of the transition in $C_{70}$ from the area under the curves is around 5.4 kJ/mol, which is large showing that the transition is thermodynamically first-order. This can be compared with the enthalpy change of 4.8 kJ/mol of the corresponding transition in $C_{60}$. The presence of a single phase transition in $C_{70}$ and $C_{60}$ at 218 K and 250 K respectively leads us to believe that the two transitions found at 221 and 252 K in $C_{60}$ by Tse *et al.*[8] arise because of the presence of $C_{70}$ impurity in $C_{60}$. We find no noticeable changes in the IR and Raman spectra of $C_{70}$ across the phase transition.

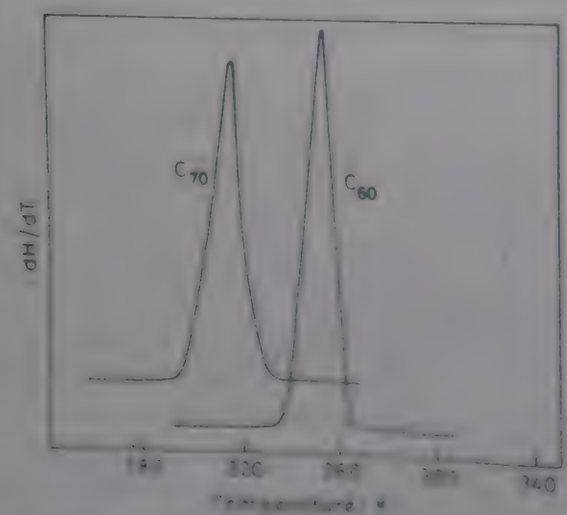


Fig. 11 - [illegible] scanning calorimetric traces of powdered samples of $C_{70}$ and $C_{60}$

*$^{13}C$ NMR spectrum of $C_{60}$ in nematic liquid crystal mixtures and the extraordinary symmetry of $C_{60}$ in solution phase*: Buckminsterfullerene, $C_{60}$, is a molecule with the highest finite point group symmetry, $I_h$, and the room-temperature crystalline phase is orientationally disordered ($Fm\bar{3}$ space group). In the low-temperature ordered phase ($Pa3$ space group), weak bonding between $C_{60}$ units appears to produce appreciable geometrical deviations from the $m\bar{5}m$ to the $\bar{3}$ point group[9]. Theoretical calculations show that in the free state, the $C_{60}$ molecule prefers the $I_h$ symmetry and does not have a more stable lower symmetry structure[10]. The $^{13}C$ NMR spectrum of $C_{60}$ in $CCl_4$ solution shows a single line with an isotropic chemical shift of 142.5 ppm establishing the exact equivalence of all the 60 atoms, consistent with the $I_h$ symmetry. In order to determine whether slight distortions from the $I_h$ symmetry occur in the solution phase, we have employed a novel method wherein the $^{13}C$ NMR spectrum of $C_{60}$ was recorded in a mixture of nematic liquid crystals of opposite diamagnetic anisotropies[11,12]. This method is distinct from the well-known NMR technique[13] wherein precise molecular geometries are obtained from the anisotropic NMR parameters of molecules dissolved in nematic liquid crystals.

In the method employed by us, we make use of the change in the anisotropic parameters resulting from the switching of the order parameters at the critical point of a nematic liquid crystal mixture; the change can be by a factor of $-2$ or $-1/2$ depending on the direction of approach of the critical point. By an adjustment of the concentration and temperature, it is possible to render both types of orientations to coexist, the shift between the two spectra providing the chemical-shift anisotropy. In tetrahedral molecules such as methane such a coexistence of spectra with shifts of $\sim 0.5$ ppm has indeed been observed. Observation of a single line spectrum near the critical point would, therefore, indicate the absence of any detectable distortions. In the present study, we have examined the $^{13}C$ NMR spectra of $C_{60}$ and tetramethylsilane in liquid-crystal mixtures in order to compare the behaviour of $C_{60}$ with that of another nearly spherical molecule.

$^{13}C$ spectra were recorded with a temperature stability of better than $\pm$ 0.1 K. The proton decoupled $^{13}C$ spectra were accumulated with the decoupler being "on" only during acquisition period. This prevents heating of the samples and eliminates the temperature inhomogeneities arising from the decoupling powers used while accumulating the spectra. A delay of 10s was introduced between the successive scans. Nearly 25,000 scans were accumulated and

Fourier transformed in each case. Spectra of the following systems were recorded: (i) pure S-1114 (*trans*-4-pentyl-4,4'-cyanophenylcyclohexane) with a positive diamagnetic anisotropy at 323.0 K in the nematic phase and 358.0 K in the isotropic phase; (ii) pure ZLI-1167 (a ternary eutectic mixture of propyl-, pentyl- and heptyl-bicyclohexyl carbonitriles) with a negative anisotropy at 323.0 K in the nematic phase and at 358.0 K in the isotropic phase; (iii) solution containing 0.2 wt% of $C_{60}$in S-1114 at 323.0 K in the nematic and at 358.0 K in the isotropic phases; and (iv) 0.2 wt% solution of $C_{60}$ in ZLI-1167 at 323.0 and 358.0 K in the nematic and isotropic phases respectively. We then studied the spectra of a 1:1 mixture of (iii) and (iv) containing 4.2 wt% of tetramethylsilane (hereafter referred to as solution (v) in both the nematic and the isotropic phases. The mixture showed spectra due to the coexistence of the two phases at 333.4 K.

Figure 12 shows intense, well-separated lines due to the $^{13}C$ resonances from the liquid crystal solvent carbons. The vertically expanded versions show the lines due to tetramethylsilane and fullerene $C_{60}$ around 0.00 and 140.37 ppm respectively. Since the $^{13}C$ NMR signal of $C_{60}$ was weak, in order to ensure that the assignment of the line at 140.37 ppm to $C_{60}$ in the nematic phase was correct, experiments were performed with (i), (ii), (iii) and (iv) under identical conditions. Comparison of the various spectra with and without $C_{60}$ unambiguously established that the line at 140.37 ppm was due to $C_{60}$. Figure 13 shows the spectra due to the coexistence of the two types of orientations. Coexistence of the two $^{13}C$ lines separated by 0.54 ppm is clearly observed for tetramethylsilane. This was stable for over a week while the sample was in the magnet, indicating the stability of the temperature as well as the concentration homogeneity of the solution. The tetramethylsilane line in the isotropic phase is 0.18 ppm upfield with respect to the lower field tetramethylsilane line in Figure 13. The corresponding separation from the higher field line is 0.36 ppm downfield which is twice that for the lower field line. $C_{60}$ gives only a single sharp line at $-140.37$ ppm with respect to tetramethylsilane. This is exactly at the same position as in the isotropic phase. This observation shows that the order parameter, S, rather than the chemical shift anisotropy, $\Delta\sigma$, is zero and conclusively establishes that there are no detectable distortions from the $I_h$ symmetry in $C_{60}$ in solution. $C_{60}$ is the first molecule found to be undistorted in a nematic liquid-crystalline media. It should serve as a reference in the study of chemical shift anisotropies in nematic phases.

*Anions of $C_{60}$.*

$C_{60}$ is clearly very electrophilic as evidenced by cyclic voltammetry. Cyclic voltammetry carried out by Haufler *et al.*[14] in $CH_2Cl_2$ solution with a glassy carbon electrode showed two reversible anionic

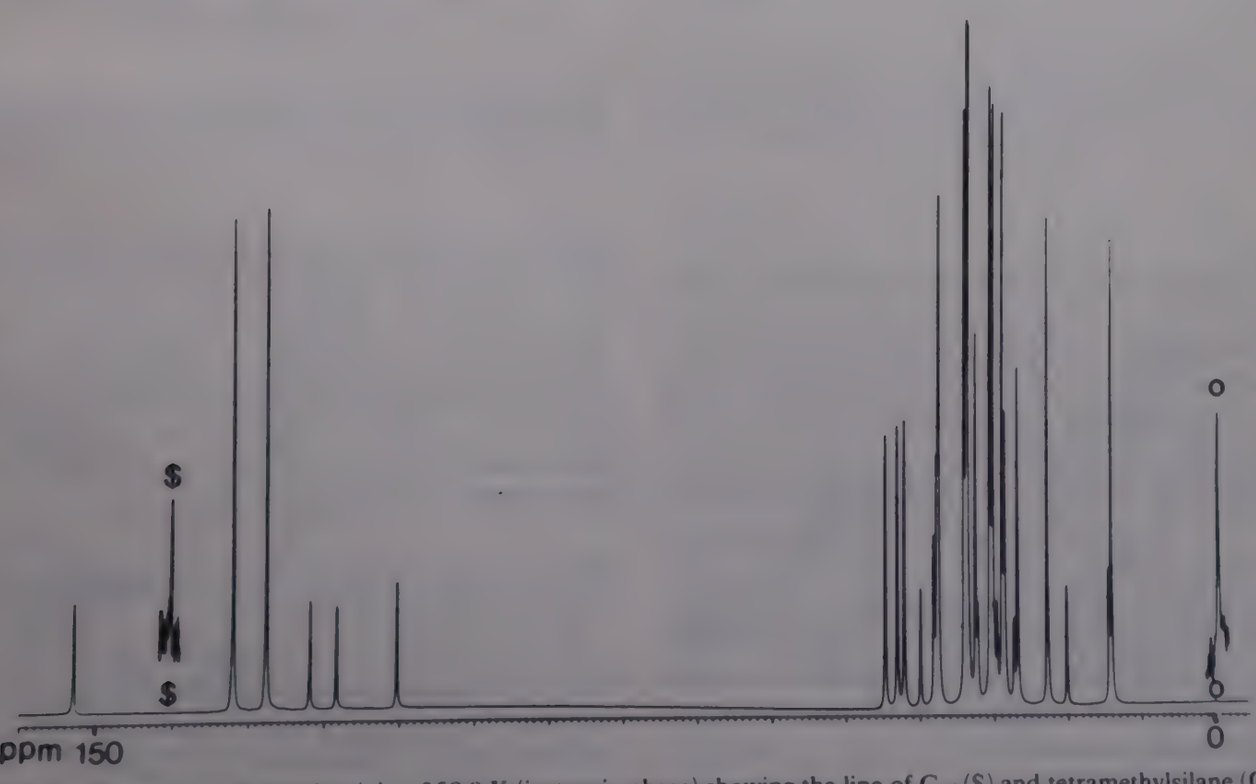


Fig. 12—$^{13}C$ NMR spectrum of solution (v) at 358.0 K (isotropic phase) showing the line of $C_{60}$ (S) and tetramethylsilane (O). The lines due to $C_{60}$ and tetramethylsilane are also shown with a magnified vertical scale

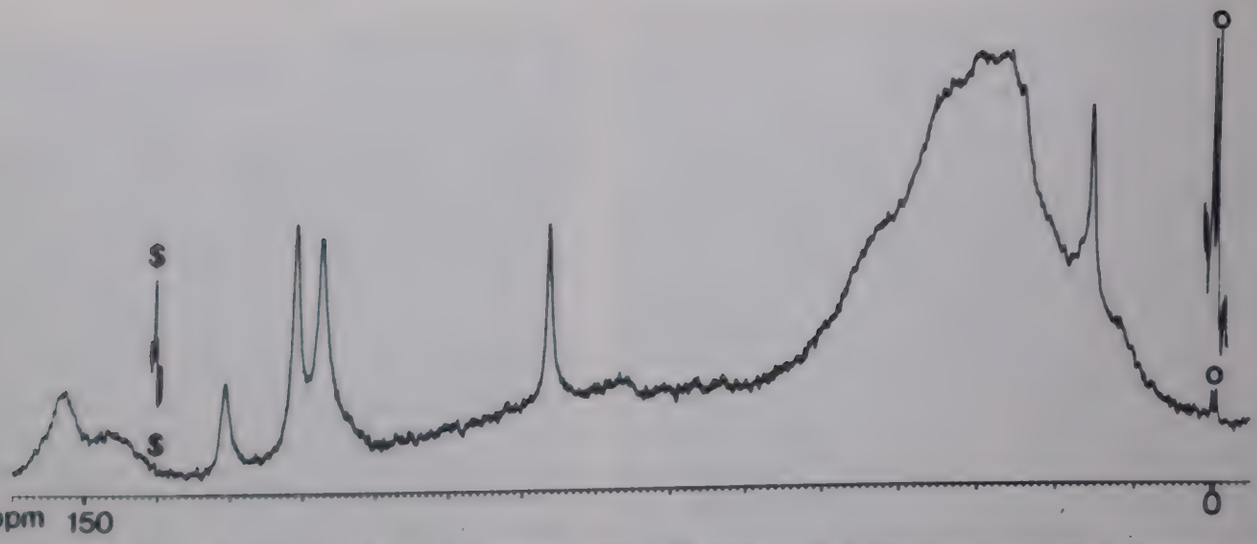


Fig. 13—$^{13}C$ NMR spectrum of solution (v) at 332.4 K (nematic phase). The coexistence of two types of spectra is evident in the case of tetramethylsilane

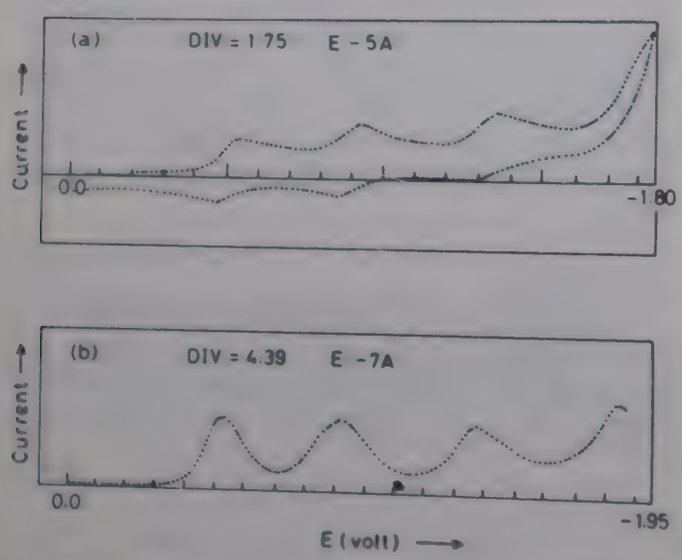


Fig. 14—(a) Cyclic voltammogram of $C_{60}$ in $CH_2Cl_2$ solution (~ 1 mM). Au electrode with 0.05 $M$ $(Bu)_4NPF_6$ as supporting electrolyte was used (scan rate 300 mV/s). b. Differential pulse voltammogram of $C_{60}$

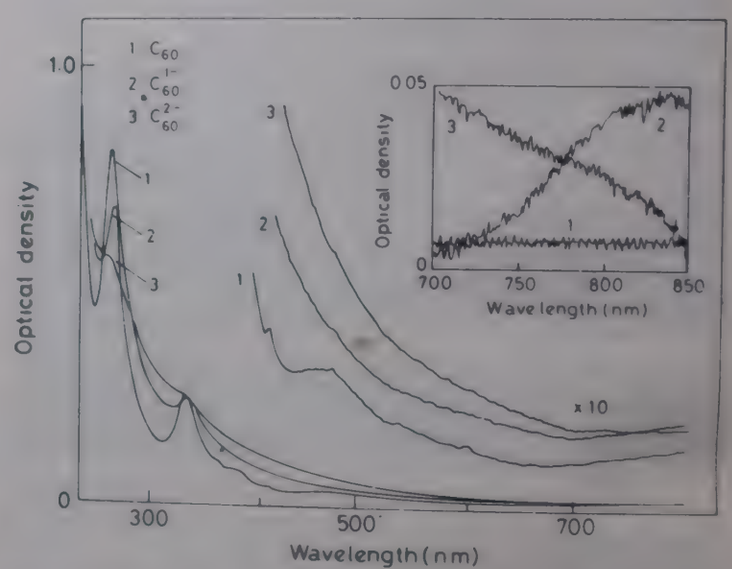


Fig. 15—Electronic absorption spectra of $C_{60}$, $C_{60}^{-}$ and $C_{60}^{2-}$ obtained using a thin-layer spectroelectrochemical cell (electrolysis time 300 s). Inset shows the spectrum in the 700-850 nm region

forms. Dubois *et al*[15] found four reductions in the −0.4 to −1.7 eV range at a high scan rate of 20V/s of which only the first two at 0.44 and 0.82 V were reversible. We have carried out cyclic voltammetry as well as differential pulse voltammetry in $CH_2Cl_2$ solution with Pt, glassy carbon and Au electrodes and found four one-electron reduction peaks in the range −0.4 to −1.9 V (Fig.14). The reduction potentials are −0.464, −0.856, −1.292 and −1.661 V vs Ag/AgCl, of which the first three are fully reversible while the fourth is quasi-reversible at a slow scan of 100-500 mV/s. The four successive reduction potentials are independent of the electrodes and indicate the formation of $C_{60}^{-}$, $C_{60}^{2-}$, $C_{60}^{3-}$ and $C_{60}^{4-}$.

The thin-layer spectroelectrochemical measurements carried out with an optically transparent grid mini-grid electrode have enabled us to obtain good electronic absorption spectra of $C_{60}^{-}$ and $C_{60}^{2-}$ (Fig.15). The UV absorption bands of $C_{60}^{-}$, besides showing red-shifts with respect to $C_{60}$, are less intense as expected. Also seen is a characteristic band at 830 nm due to $C_{60}$ which disappears in the dianion. Our measurements also show that the two anions could be reversibly oxidized back to $C_{60}$.

*Electron donor-acceptor interaction of fullerenes : a cyclic voltammetric study*:

Recent studies have shown that $C_{60}$ and $C_{70}$ exhibit five one-electron reductions leading to the formation of mono, di, tri, tetra and penta anions and an irreversible oxidation at 1.76V vs SCE. The last involves a four-electron oxidation process[16]. In our cyclic voltammetric (CV) studies, we observed the

formation of fulleronium ion at 1.71V (vs Ag/AgCl). The first reversible one-electron reduction of $C_{60}$ and $C_{70}$ occurs around −0.40V (vs Ag/AgCl) in $CH_2Cl_2$ resulting in the formation of a mono-fulleride anion radical with a characteristic visible absorption band around 8.30 nm[3]. Pericaud *et al.*[17] and Krusic *et al.*[18] have shown that fulleride ion ($C_{60}^-$) can function as a coordinating anion resulting in the formation of tetraphenylporphinatochromium (III) fulleride, [(CrTTP)$^+$ $C_{60}^-$]. Photolysis experiments involving $C_{60}$ with diverse donors result in formation of stable fulleride mono anion adducts. We have investigated the ground state electron donor-acceptor properties of fullerenes by cyclic voltammetry.

The donors chosen for the study are tetramethyl-para-phenylenediamine (TMPD), tetrakis-2,3,5,6-(N,N-dimethylamino)benzene (TDAB) and N,N,N′,N′-tetramethylbenzidine (TMB) (Fig.16). Clearly, TDAB is a very powerful electron donor. It is recognized that CV studies of a mixture of an electron donor and an electron acceptor should reveal the existence and the strength of interaction in solution. In view of the fact that $C_{60}$ and $C_{70}$ are good electron acceptors, it is possible to observe the changes in their reduction potentials on interaction with the donors. Figure 17 displays the one-electron oxidation of the free donor TMPD in $CH_2Cl_2$. The voltammograms of solutions containing TMPD and the fullerenes reveal a marginal anodic shift of all the three reversible one-electron reduction peaks of $C_{60}$ and $C_{70}$. The fourth one-electron reduction of the fullerenes is irreversible and hence not reported. Interestingly, the oxidation peak of TMPD in the presence of the fullerenes is found to be split, suggesting interaction of TMPD with the fullerenes in the ground state. Tetramethylbenzidine in $CH_2Cl_2$ solution exhibits two reversible one-electron oxidations at +0.52 and +0.76V (vs Ag/AgCl). These peak potentials remain unchanged on the addition of fullerenes; the one-electron reduction peaks of the fullerenes show no significant changes. These observations indicate that charge-transfer interaction of the fullerenes is minimal in these two donors.

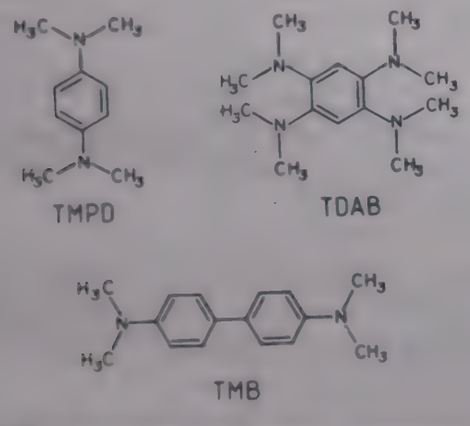


Fig. 16—Structures of the electron donors employed

We have obtained interesting results from our study of the interaction of $C_{60}$ with the powerful donor TDAB. TDAB in $CH_2Cl_2$ displays two oxidations at +0.22 and +0.30 V each corresponding to a two-electron process (Fig.18). On addition of $C_{60}$, each of the peaks is split into two peaks (with anodic and cathodic shift) exhibiting a four-step oxidation process. On the other hand, the first three reduction potentials of $C_{60}$ in the presence of TDAB are found to be shifted to the anodic side. The second reduction at −0.84V becomes irreversible and possibly involves a two-electron process. These observations suggest that TDAB interacts fairly

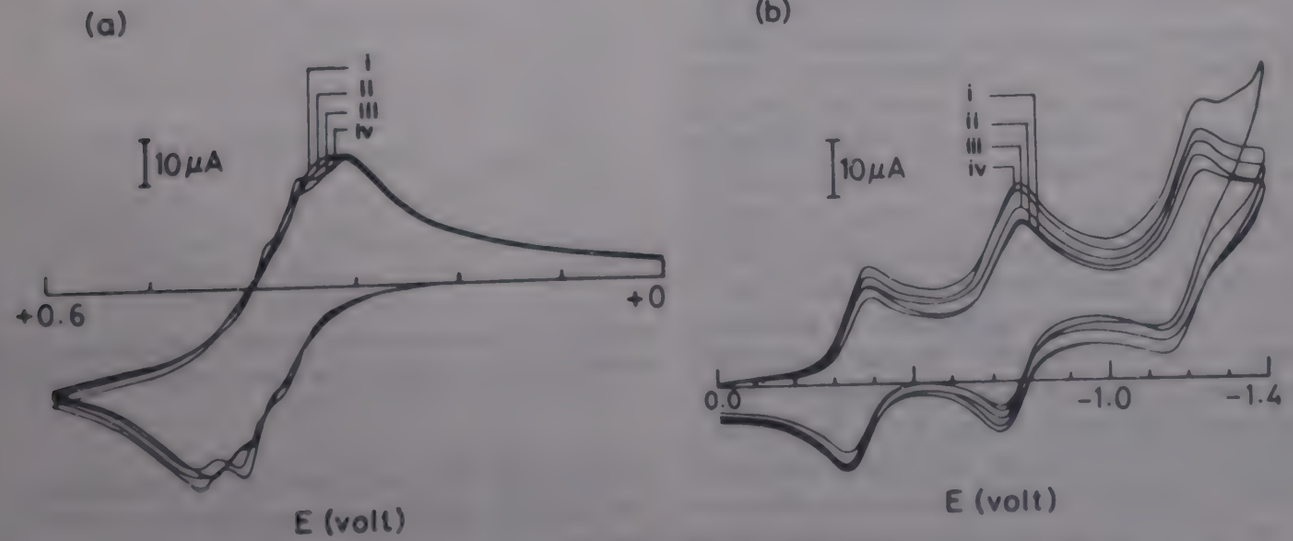


Fig. 17—(a) CV of (i) TMPD (0.5 mM) and (ii-iv) in the presence of different amounts of $C_{70}$ (1 m*M* - 5 m*M*) in $CH_2Cl_2$. (b) CV of (i) $C_{60}$ (0.5 m*M* and (ii-iv) on successive addition of TMPD

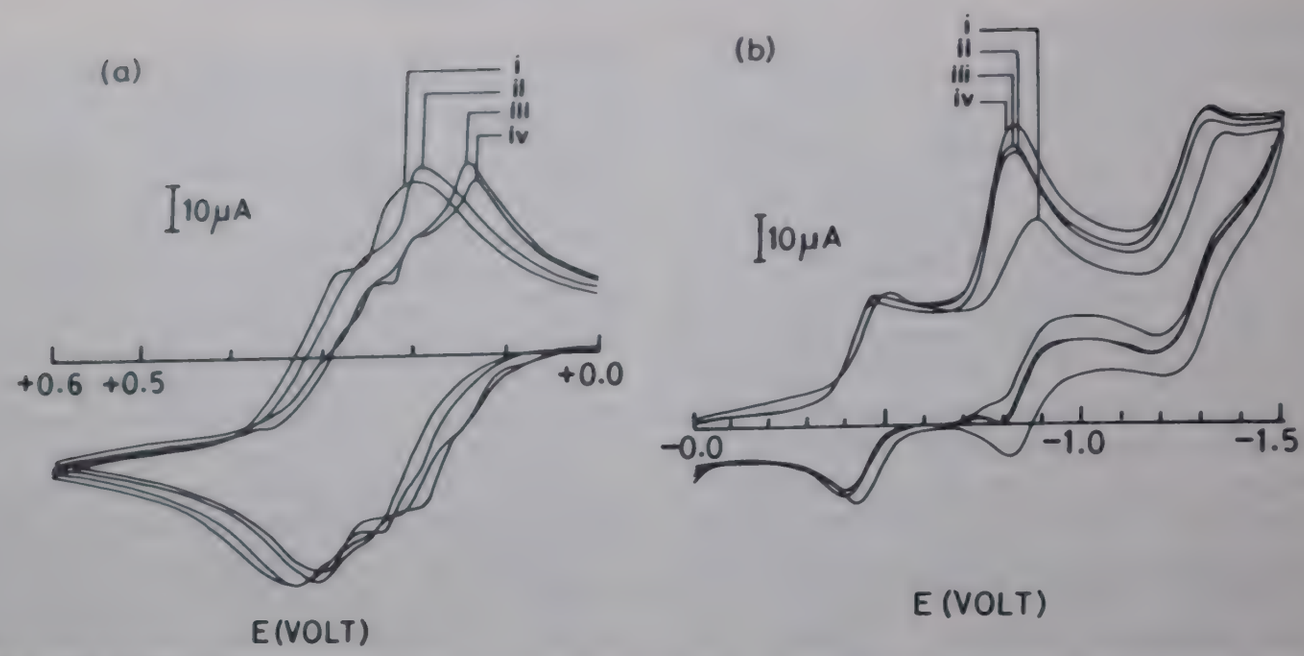


Fig. 18—(a) CV of (i) TDAB (0.5 m*M*) and (ii-iv) on successive addition of $C_{60}$ (1 m*M* – 10 m*M*) in $CH_2Cl_2$. (b) CV of (i) $C_{60}$ (0.5 m*M*) and (ii-iv) in presence of different amounts of TDAB (1 m*M* – 10 m*M*) in $CH_2Cl_2$

strongly with $C_{60}$. The magnitudes of the shift is larger in case of the TDAB interaction relative to that obtained with the other two donors. These results agree with the recent finding[19] that N,N-dimethylaniline forms a weak complex with $C_{60}$ ($K_{ass}$ = 0.0047 $dm^3\ mol^{-1}$).

Preliminary CV studies on the interaction of fullerenes with tetraphenylporphinato cobalt(II) in $CH_2Cl_2$ indicate that the oxidation of Co(II) (0.93V vs Ag/AgCl) in the porphyrin is shifted to lower potentials by about 80 mV. This indicates possible formation of fulleride anion coordinated Co(III) TPP species. However, use of ferrocene and ferricinium hexaflurophosphate does not seem to reveal any significant changes in their respective oxidation and reduction potentials on addition of $C_{60}$.

*Superconducting properties of fullerene derivatives*

Superconductivity around 20 K was first reported in potassium doped $C_{60}$ by Hebard *et al.*[20]. Since then, higher $T_c$'s upto 35 K have been achieved in Rb-Cs doped $C_{60}$[21]. While $C_{60}$ doped with rubidium alone shows a $T_c$ of 28 K[22], $C_{60}$ doped with cesium is not superconducting. We have carried out several experiments on the superconducting properties of doped fullerenes and we present our results here.

In Fig.19 we show the appearance of non-resonant microwave absorption[23] by the controlled cooling of $K_xC_{60}$ in zero-field signifying the presence of superconductivity below 21 K. We observe hysterisis on the forward and backward sweeps of the H-field confirming the granular nature of this superconductor. In Fig.20, we have plotted the intensity of the microwave signal against temperature to

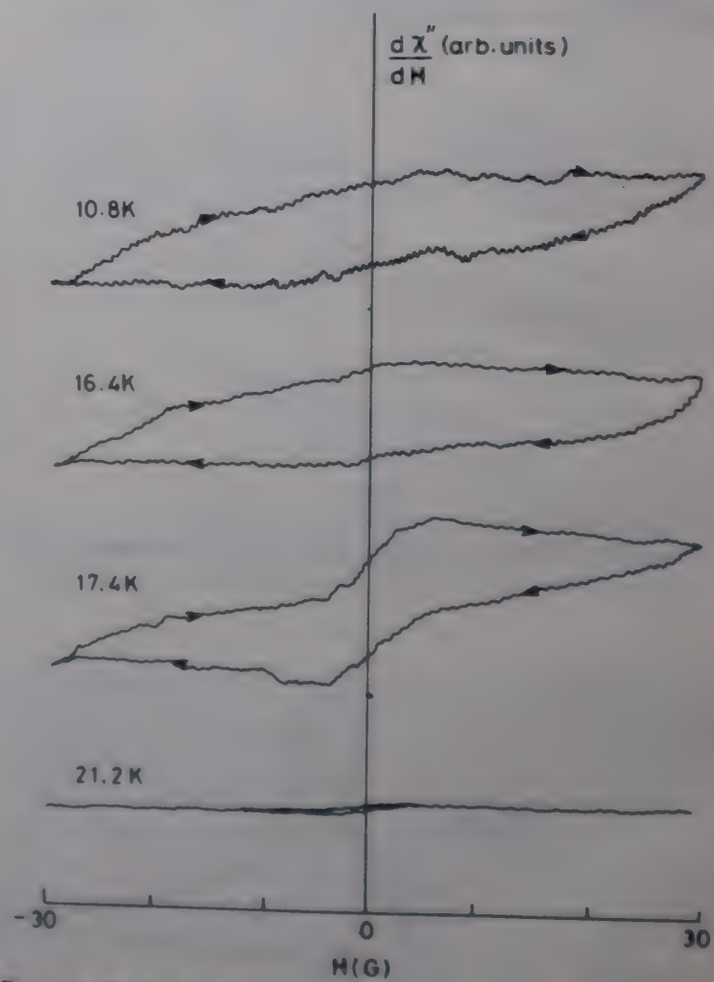


Fig. 19—Derivative microwave absorption by $K_xC_{60}$ at various temperatures. Temperature dependence of the hysteresis is to be noted

demonstrate the sharp onset of superconductivity at 20 K. ESR studies of these samples showed the presence of a signal at room temperature as well as in the superconducting state which indicates the

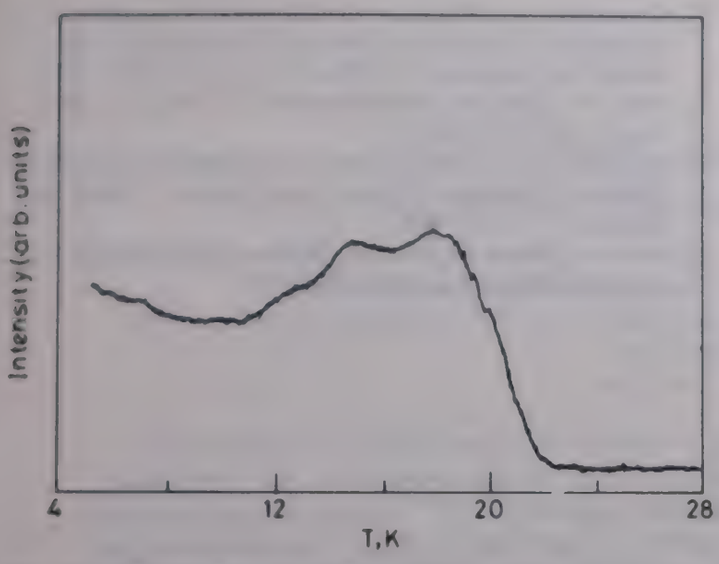


Fig. 20—Temperature dependence of the microwave absorption of $K_xC_{60}$

presence of a non-superconducting impurity phase as reported previously[24]. However, the nature of the ESR signal found by us is different in that at room temperature there is some structure in the signal whereas in the superconducting state there is only a single signal without structure. Although we do not have any control over the stoichiometry of the $K_xC_{60}$ prepared by the solution route employed by us, the onset is sharp unlike in the case of the product obtained from solid state reaction.

We have carried out tests for superconductivity for the sodium salt of $C_{60}$ which was synthesized by the reaction of a known excess of sodium metal with ~ 15 mg of $C_{60}$ in toluene solution under conditions similar to those used for the preparation of $K_xC_{60}$ sample. The black product of the reaction did not show any non-resonant microwave absorption above 4.5 K confirming the absence of superconductivity. We have also prepared potassium salt of $C_{70}$ by the solution route. Although we got a black solid as the reaction product, there was no indication of superconductivity above 4.5 K.

Following a Japanese report[25] that $C_{60}$ doped with iodine showed a superconducting transition around 60 K, we prepared several samples of $C_{60}$ heated with iodine. Samples of nominal compositions $I_2C_{60}$ and $I_3C_{60}$ were prepared by the solid state reaction of pure $C_{60}$ with iodine in a quartz tube of 5 mm diameter. The evacuated tubes were sealed under $10^{-2}$ torr of helium and heated first at 480 K for 50 h and later at 530 K for 25 h. Some of the samples of nominal composition $I_2C_{60}$ were heated at 570 K for 50 h and for extended periods of time. The samples so obtained were examined by non-resonant microwave absorption. We found no evidence for superconductivity in any of the samples above 4.5 K. It appears that the superconductivity in iodine-doped $C_{60}$ reported in the literature is an artefact.

We tried to interact $C_{60}$ with $SbCl_5$ to explore the possibility of superconductivity since $SbCl_5$ is a well-known electron acceptor. By refluxing a 1:1 mixture of $SbCl_5$ and $C_{60}$ in $CCl_4$ solution, we got a brown product, due to the chlorination of $C_{60}$. Reacting $C_{60}$ with liquid $Br_2$ gave a brominated product.

We have obtained results with Rb and Rb-Cs derivatives of $C_{60}$ similar to those in the literature. We are now examining superconductivity in $Pb_xC_{60}$ and other compounds.

## Acknowledgement

The authors thank Professor H A Staab, Heidelberg, for a gift of the sample of the donor TDAB. Their thanks are due to Dr C K Mathews, IGCAR, Kalpakkam, for help in handling Rb and Cs.

## References

1 Kroto H W, Heath J R, O'Brien S C, Curl R F & Smalley R E, *Nature*, 318 (1985) 162.
2 Kratschmer W, Lamb L D, Fostiropoulous K & Huffman D R, *Nature*, 347 (1990) 354.
3 (a) Pradeep T & Rao C N R, *Mat Res Bull*, 26 (1991) 1101. (b) Pradeep T, D'Souza F, Subbanna G N, Krishnan V & Rao C N R, *Proc Ind Acad Sci (Chem Sci)*, 103 (1991) 685.
4 Hare J P, Kroto H W & Taylor R, *Chem Phys Lett*, 1991 (177) 394.
5 Lichtenberger D L, Nebesny K W, Ray C D, Huffman D R & Lamb L D, *Chem Phys Lett*, 176 (1991) 203.
6 Howard J B, McKinnon J, Makarovsky Y, Lafleur A L, Johnson M E, *Nature*, 352 (1991) 139.
7 Heiney P A, Fischer J E, McGhite A R, Romanow W J, Denenstein A M, McCauley (Jr) J P, Smith (III) A B & Cox D E, *Phys Rev Lett*, 66 (1991) 2911.
8 Tse J S, Lug D D, Wilkinson D A & Handa Y P, *Chem Phys Lett*, 183 (1991) 387.
9 David W I F, Ibberson R M, Matthewman J C, Prassides K, Dennis T J S, Hare J P, Kroto H W, Taylor R & Walton D R M, *Nature*, 353 (1991) 147.
10 Bakowies D & Thiel W, *J Am chem Soc*, 113 (1991) 3704.
11 Burnell E E & DeLange C A, *Chem Phys Lett*, 136 (1987) 87.
12 Khetrapal C L, Kunwar A C & Lakshminarayana M R, *Molec Cryst Liq Cryst*, 111 (1984) 189.
13 Emsley J W & Lindon J C, *NMR Spectroscopy using liquid crystal solvents* (Pergamon Press, Oxford), 1975.
14 Haufler R E, Conciecao J, Chibante L P F, Chai Y, Byrne N E, Flanagan S, Haley M M, O'Brien S C, Pan C, Xiao Z, Billups W E, Cinfolini M A, Hauge R H, Margrave J L, Wilson L J, Curl R F & Smalley R E, *J phys Chem*, 94 (1990) 8634.
15 Dubois D, Kadish K M, Flanagan S, Haufler R E, Chibante L P F & Wilson L J, *J Am chem Soc*, 113 (1991) 4364.
16 Dubois D, Kadish K M, Flanagan S & Wilson L J, *J Am chem Soc*, 113 (1991) 7773.
17 Pericaud A, Hsu J, Reed C A, Koch A, Khemani K C, Allemand P M & Wudl F, *J Am chem Soc*, 113 (1991) 6698.

18 Krusic P J, Wasserman P, Parkinson B A, Malone B, Holler (Jr) E R, Keizer P N, Morton J R & Preston K F, *J Am chem Soc*, 113 (1991) 6274.
19 Sension R J, Szarka A Z, Smith G R & Hochstrasser R M, *Chem Phys Lett*, 185 (1991) 179.
20 Hebard A F, Rosseinsky M J, Haddon R C, Murphy D W, Glarum S, Glarum S H, Palstra T T M, Ramirez A P & Kortan A R, *Nature*, 350 (1991) 600.
21 Tanigaki K, Effesen T W, Saito S, Mizuki J, Tsai J S, Kubo Y & Kuroshima S, *Nature*, 352 (1991) 222.
22 Rosseinsky M J, Ramirez A P, Glarum S H, Murphy D W, Haddon R C, Hebard A F, Palstra T T M, Kartan A R, Zahurak S M & Makhija A V, *Phys Rev Lett*, 66 (1991) 2830.
23 Bhat S V, Ganguly P, Ramakrishnan T V & Rao C N R, *J Phys C*, 20 (1987) L559.
24 Zakhidov A A, Ugawa A, Imaeda K, Yakushi K, Inokuchi H, Kikuchi K, Ikemoto I, Suzuki S & Achiba Y, *Solid State Commun*, 79 (1991) 939.
25 Sekine H, Maeda H, Suzuki T, Kadowaki K & Tanaka Y, as reported in *High $T_c$ update*, 5 (1991) 1.

Indian Journal of Chemistry
Vol. 31 A&B, May 1992, pp. F17-F21

# Investigations of iron adducts of $C_{60}$: Novel $FeC_{60}$ in the solid state with Fe inside the $C_{60}$ cage

T Pradeep, G U Kulkarni, K R Kannan, N Y Vasanthacharya, T N Guru Row & C N R Rao*
CSIR Centre of Excellence in Chemistry & Solid State and Structural Chemistry Unit, Indian Institute of Science, Bangalore 560 012, India

Received 20 February 1992

By carrying out contact-arc vaporization of graphite in a partial atmosphere of $Fe(CO)_5$, an iron-adduct with $C_{60}$ has been obtained. The adduct has been characterized by various techniques including mass spectrometry, $^{57}Fe$ Mössbauer spectroscopy and Fe K-EXAFS. Properties of this adduct are compared with those of an adduct prepared by solution method where Fe is clearly outside the cage. Results suggest that $FeC_{60}$ obtained from the gas phase reaction has the Fe atom in the cage.

The 7 Å diameter cavity in buckminsterfullerene has long been considered as a possible host for various atoms and molecules[1]. There have been several attempts to incorporate metal atoms such as La in this cavity. In all these studies[2-6] the species identified were generally in the gas phase and were characterized by mass spectrometry. The question whether the metal atom is inside or outside the spheroidal hollow cage in these species has not been resolved fully. Freiser and coworkers[4] have generated a $FeC_{60}$ complex in the gas phase by means of a ligand-exchange reaction and have also characterized $NiC_{60}$ and $Ni(C_{60})_2$ in the gas phase.

One example where an atom has been entrapped in $C_{60}$ is that where a high-energy beam of $C_{60}$ was made to interact with helium to give $HeC_{60}$ in the gas phase[5]. Chai *et al.*[6] have more recently prepared fullerenes with La trapped in the cages by laser vaporization. Metal complexes of $C_{60}$ where the metal is present outside the cavity have been prepared by solution methods and characterized[7,8]. We have investigated an iron adduct of $C_{60}$, $FeC_{60}$(I), where iron atoms were introduced during the contact-arc vaporization of graphite, expecting that this would result in the entrapment of Fe in the cavity. In order to understand some of the unique features of this adduct prepared by the gas phase reaction, we have compared its properties with those of a solid $FeC_{60}$(II) adduct prepared by solution method, wherein Fe was clearly bound externally to the fullerene. We have primarily employed mass spectrometry, $^{57}Fe$ Mössbauer spectroscopy and extended X-ray absorption fine structure (Fe K-EXAFS) in these investigations.

## Materials and Methods

In our effort to obtain the Fe adduct of $C_{60}$ with the metal inside the cage, we carried out the contact-arc vaporization of graphite in an atmosphere of $Fe(CO)_5$. The arc chamber was pumped to a base vacuum of $\sim 10^{-6}$ torr and He gas admitted to about 50 torr through a needle valve. $Fe(CO)_5$ was admitted to the system from a reservoir at the same rate as He. $^{57}Fe$ Mössbauer spectrum of the soot so obtained was recorded with a constant acceleration spectrometer with a $^{57}Fe$ source. The spectrum showed a 6-finger pattern due to $Fe_3C$ and $\alpha$-Fe along with a singlet due to a new species. The soot was soxhlet-extracted with toluene for about 3 hours and the extract vacuum-dried at 380 K to remove any volatile iron compounds. The mass spectrum of the product of solvent extraction was then recorded. It showed the presence of mass peaks other than those due to $C_{60}$ and $C_{70}$ which could be ascribed to $FeC_{60}$. The mass spectrum of the residue left over after solvent extraction did not show any volatile species upto 400°C. The product of solvent extraction showed an additional spot in the TLC other than those due to $C_{60}$ and $C_{70}$ with an $R_f$ value close to that of $C_{70}$. After separating out $C_{60}$ by column chromatography, the new product was eluted out along with a small proportion of $C_{70}$. The product was then examined by mass spectrometry and $^{57}Fe$ Mössbauer spectroscopy. Magnetic susceptibility (with a Lewis Coil magnetometer) and X-ray diffraction (STOE diffractometer) measurements as well as UV-visible and infrared spectroscopic measurements were also carried out.

In order to compare $FeC_{60}$(I) obtained from the

gas-phase reaction with that of an adduct where Fe is definitely outside the cage we prepared $FeC_{60}$(II) by the reaction of the solid Na compound with $C_{60}$ (prepared by the reaction of Na with $C_{60}$ in toluene solution) with $FeCl_2$ in THF solution. $FeC_{60}$(II) was also investigated by the various techniques mentioned earlier.

EXAFS measurements were carried out at room temperature, using a Rigaku spectrometer attached to a rotating anode X-ray generator (Ru-200B, Rigaku, Japan). A Ge(220) monochromator was used with a 0.1 mm slit for X-rays from a Mo-target. The spectral resolution was about 5 eV at 9 keV incident energy. The samples were pressed into self-supporting wafers after mixing with polyethylene powder (Merck). The thickness of the wafer was adjusted so that the edge jump ($\mu$.d) was $\approx 1.5$. The pre-edge data were collected in steps of 5 eV for 100 eV and data upto 700 eV after the edge were collected in steps of 1 eV. EXAFS of the reference compound, ferrocene (Fe-C: N = 10, R = 2.05 Å), was also recorded under similar conditions. The EXAFS data were treated using the multishell model involving the additive relationship of EXAFS function. Fourier transforms (FT) were obtained with $k_{min} \approx 3.5$ and $k_{max} \approx 12.0$ Å$^{-1}$ after weighing the data by $k^3$.

## Results and Discussion

The mass spectrum of $FeC_{60}$(I), in mixture with $C_{70}$, obtained after column chromatography (Fig. 1) showed peaks at 776, 752 and 728 ascribable to $FeC_{60}$, $FeC_{58}$ and $FeC_{56}$, besides peaks at 720 and 840; we must note the *m/z* 720 is also found in the mass spectrum of $C_{70}$. A mass peak at 388 is seen due to the half-mass of $FeC_{60}$. The presence of $C_2$-loss peaks in the decreasing order of intensity suggests that Fe may be internally bound to the $C_{60}$ frame. Similar $C_2$ losses found in He-$C_{60}$ and La-$C_{60}$ have been attributed to the entrapment of He and La in the hollow cage[5,6]. The $^{57}$Fe Mössbauer spectrum of the adduct (anal. Fe 7.2%) shows a singlet with an isomer shift of −0.083 mm/sec with respect to $\alpha$-Fe, (Fig. 2), characteristic of iron in a near-zero oxidation state. The sharpness of the spectrum suggests a strongly bound Fe species. The compound was weakly paramagnetic over the 10-300 K range. Its electronic absorption spectrum (Fig. 3) showed a slight red shift relative to that of $C_{60}$. The infrared spectrum was not very different from that of $C_{60}$. The powder X-ray diffraction pattern of $FeC_{60}$(I) could best be fitted into a primitive tetragonal structure ($a$ = 15.43 Å, $c$ = 9.08 Å) rather than an FCC structure. The most intense line due to the (221) reflection was not consistent with the FCC structure. The tetragonal structure can be understood as resulting from a cell determined primarily from the Fe atoms and the intense line in the diffraction pattern could be simulated with Fe cage atoms 8 Å apart.

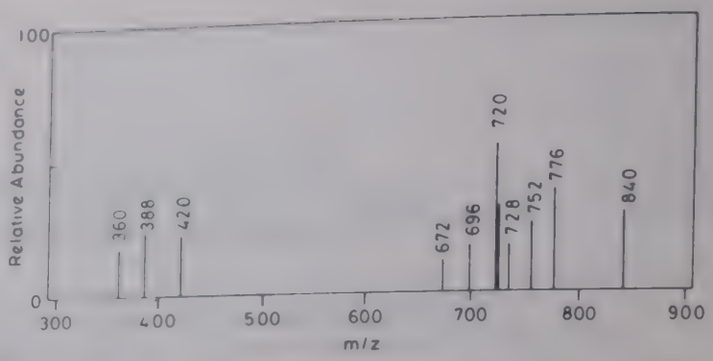


Fig. 1—Mass spectrum of $FeC_{60}$(I) (in mixture with $C_{70}$) from the gas-phase reaction. Peaks at 840, 720, 696 and 672 arise from the parent fullerenes.

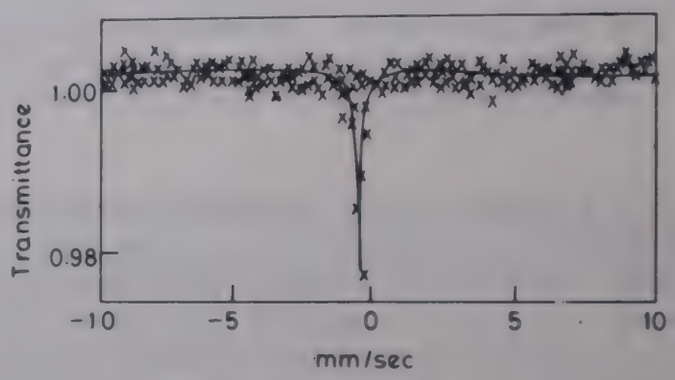


Fig. 2—$^{57}$Fe Mössbauer spectrum of $FeC_{60}$(I).

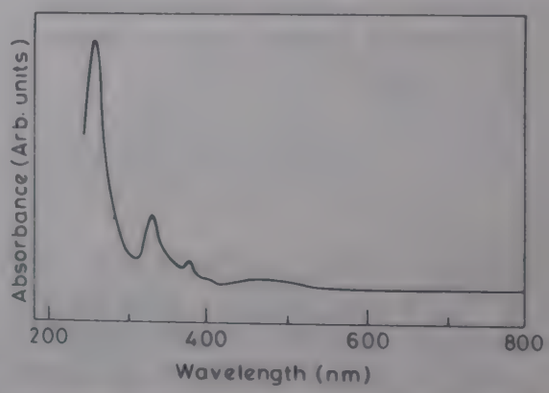


Fig. 3—Electronic absorption spectrum of $FeC_{60}$(I) in hexane solution.

Unlike the $FeC_{60}$(I) prepared by the gas-phase reaction, solid $FeC_{60}$(II) where Fe was bound externally to the fullerene showed a doublet in the Mossbauer spectrum (Fig. 4) with an isomer shift of 0.45 mm/sec due to Fe(III). Magnetic susceptibility measurements showed evidence for antiferromagnetic interaction (Fig. 5). Both the electronic and infrared spectra were different from those

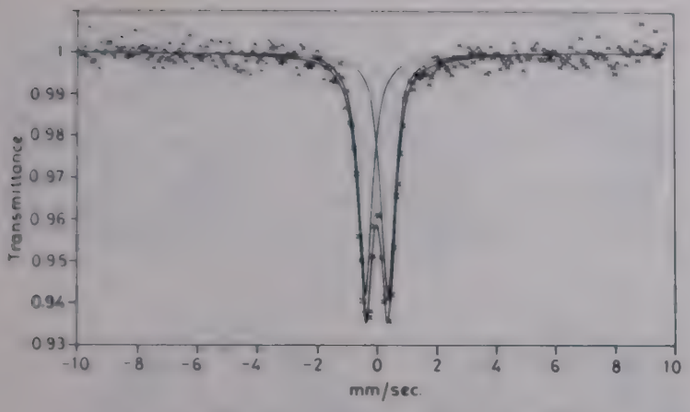


Fig. 4—$^{57}$Fe Mössbauer spectrum of $FeC_{60}$(II)

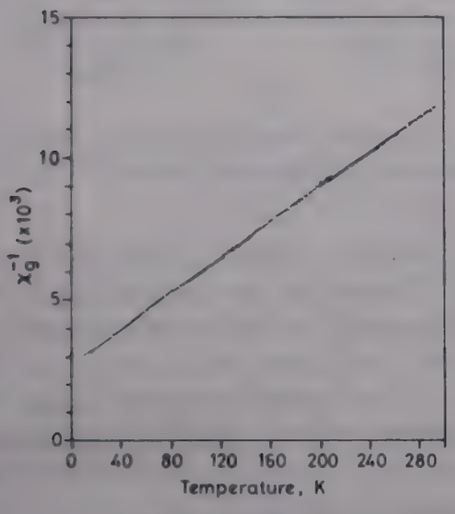


Fig. 5—Magnetic susceptibility of $FeC_{60}$(II)

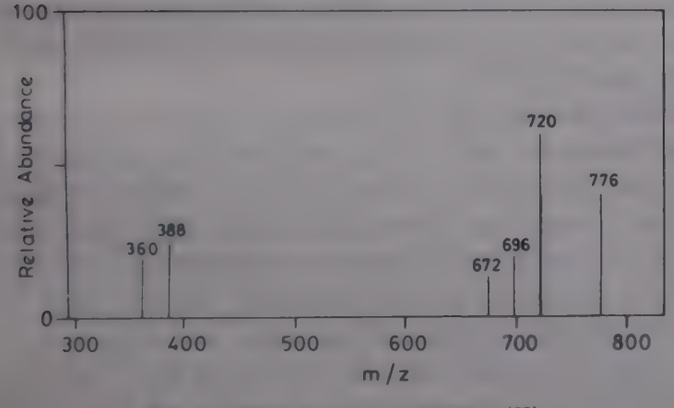


Fig. 6—Mass spectrum of $FeC_{60}$(II)

of $C_{60}$. Furthermore, the mass spectrum did not show $C_2$ losses (Fig. 6).

We have examined the structures of the two $FeC_{60}$ adducts (I) and (II) by means of Fe K-EXAFS measurements. In Fig. 7 we show the Fourier transforms of the EXAFS data of the $FeC_{60}$ adducts along with the FT of the reference compound, ferrocene. We see significant differences in the FTs though the main peak occurs around the same position (1.62 Å) in all the cases. The FT of

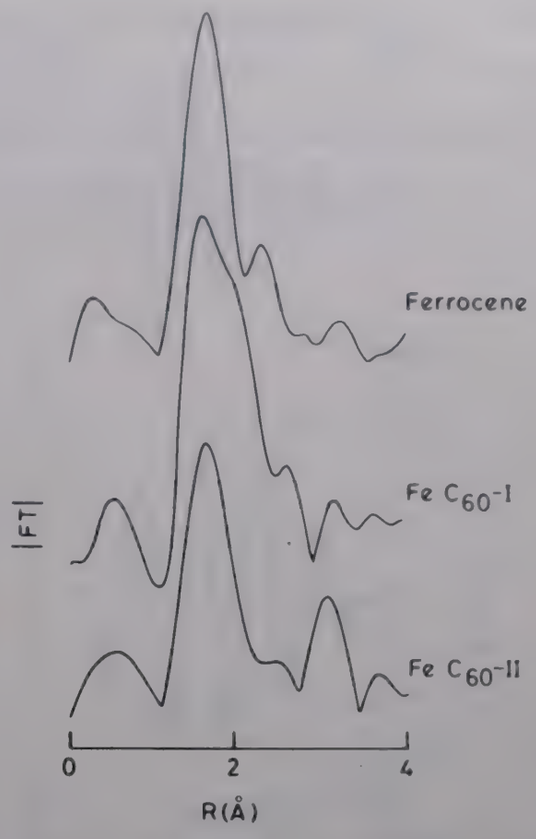


Fig. 7—Fourier transforms of the Fe K-EXAFS of $FeC_{60}$(I), $FeC_{60}$(II) and of ferrocene

the adduct-I has a shoulder on the main peak around 2.0 Å whereas that of the adduct-II shows a distinct peak at 3.0 Å. We have carried out the curve-fitting analysis on the inverse transformed data using phase and amplitude parameters of Fe-C from ferrocene. The best fits obtained are depicted in Fig. 8 and the r-windows employed are also given. The inverse transformed data of the main peak of $FeC_{60}$(I) required two Fe-C distances, 2.06 and 2.34 Å, unlike the case of $FeC_{60}$(II) which gave a good fit just with one short Fe-C distance. The data of $FeC_{60}$(II) comprising the second peak were fitted with a Fe-C distance of 3.46 Å. Interestingly, the $FeC_{60}$(I) adduct showed slightly negative $\Delta\sigma^2$ while $FeC_{60}$(II) adduct gave a high positive value of $\Delta\sigma^2$. The results of the curve-fitting analysis are listed in Table 1. The negative $\Delta\sigma^2$ indicates strong Fe-C bonding.

In order to interpret the EXAFS results we have simulated the local coordinations of the Fe atom by placing it inside and outside the $C_{60}$ unit and imposing a constraint that the first Fe-C distance should be 2.05 Å. This was done by generating the (x,y,z) coordinates of the 60 carbon atoms and calculating the Fe-C distances for different positions of the Fe atom. A high coordination number was ensured by placing the Fe atom in

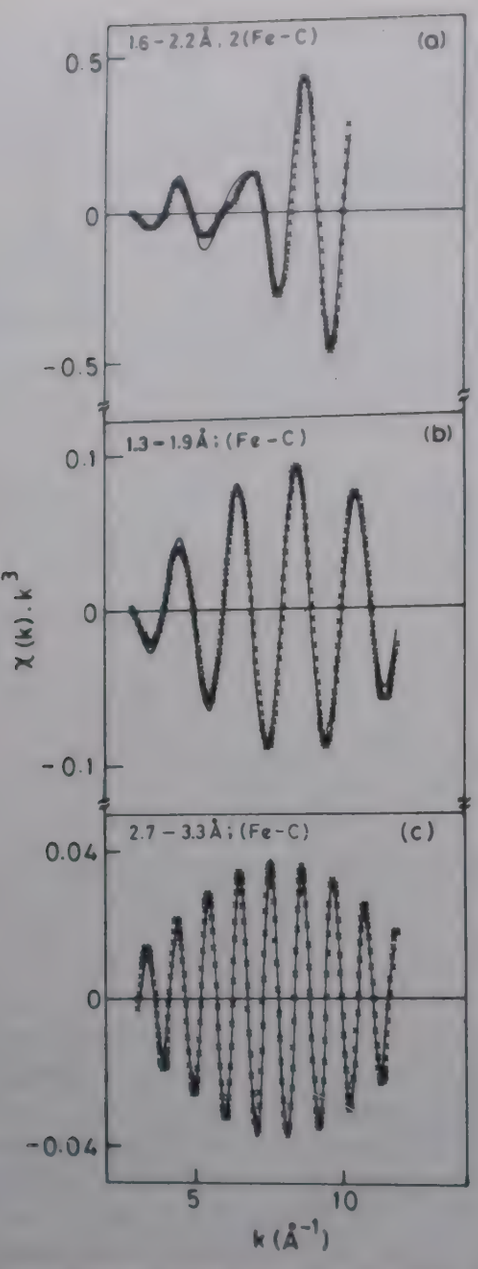


Fig. 8—Curve fitting of the inverse transformed data. The phase and amplitude parameters as well as the r-windows are indicated: (a), $FeC_{60}$(I); (b) & (c) $FeC_{60}$(II)

Table 1—EXAFS results on $FeC_{60}$ adducts

| System | N | R (Å) | $\Delta\sigma^2$ (Å²) |
|---|---|---|---|
| Ferrocene (reference) | 10 | 2.05 | — |
| $FeC_{60}$(I) | 11 | 2.06 | −0.0002 |
| | 8 | 2.34 | −0.0003 |
| $FeC_{60}$(II) | 8 | 2.03 | 0.0003 |
| | 10 | 3.46 | 0.001 |

front of a pentagon or a hexagon of carbon atoms. We find marked differences in the local coordination of the Fe atom when it is placed inside and outside. In the situation wherein Fe atom is

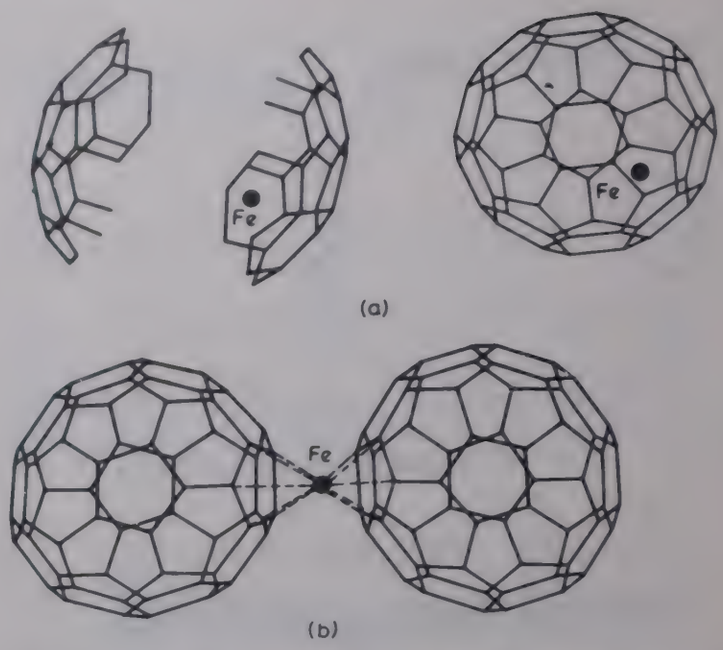


Fig. 9—(a) Formation of endohedral $FeC_{60}$ with Fe in the $C_{60}$ cage (schematic); (b) Ferrocene analogue of $C_{60}$ ($C_{60}$ $FeC_{60}$)

bonded externally to the $C_{60}$ unit, we find the second Fe-C distance to be around 3.4 Å which exactly corresponds to the results obtained with adduct-II. We could not obtain two short Fe-C distances (< 3.0 A) with Fe being outside the cage. The possibility wherein the Fe atom is coordinated to three or more $C_{60}$ units involving short Fe-C distances is negligible because it would bring the $C_{60}$ units at a distance shorter than the vander Waals' sphere. The presence of short Fe-C distances (< 3.0Å) as found in the case of adduct-I can only be reconciled if the Fe atom is inside the cage (Fig. 9).

We have sought to prepare $(C_{60})_2Fe$ by reacting the mono-Na salt of $C_{60}$ with $FeCl_2$ in solution. A brown solid thus obtained has a different electronic spectrum. Electron-impact mass spectroscopy unfortunately seems to fragment the species. Fe-C distances in this ferrocene analog (Fig. 9) cannot be distinguished from those in $FeC_{60}$(II).

The near-zero oxidation state of Fe, $C_2$ losses in the mass spectrum, occurrence of two short Fe-C distances as well as some of the other features indicate that $FeC_{60}$(I) obtained by the gas phase reaction during arc-vaporization of graphite is likely[9] to be an endohedral species with the Fe atom inside the cage of $C_{60}$. A possible mode of formation is indicated in Fig. 9.

## References

1 Kroto H W, Heath J R, O'Brien S C, Curl R F & Smalley R E, *Nature*, 318 (1985) 162.

2 Heath J R, O'Brien S C, Zhang Q, Liu Y, Curl R F, Kroto H W, Tittel F K & Smalley R E, *J Am chem Soc*, 107 (1985) 7779.

3 Cox D M, Trevor D J, Reichmann K C & Kaldor A J, *J Am chem Soc*, 108 (1986) 2457.
4 Roth L M, Huang Y, Schwedler J T, Cassady C J, Ben-Amotz D, Kahr D & Freiser B S, *J Am chem Soc*, 113 (1991) 6298; Huang Y & Freiser B S, *J Am chem Soc*, 113 (1991) 8186.
5 Ross M M & Callahan J H, *J phys Chem*, 95 (1991) 5720.
6 Chai Y, Guo T, Jin C, Haufler R E, Chibante L P F, Fure J, Wang L, Alford J M & Smalley R E, *J phys Chem*, 95 (1991) 7568.
7 Hawkins J M, Meyer A, Lewis T A, Loren S & Hollander F J, *Science*, 252 (1991) 312.
8 Fagan P J, Calabrese J C & Malone B, *Science*, 252 (1991) 1160.
9 Pradeep T, Kulkarni G U, Kannan K R, Guru Row T N & Rao C N R, *J Am chem Soc*, 114 (1992) 2272.

Indian Journal of Chemistry
Vol. 31 A&B, May 1992, pp. F22-F26

# A photoelectron spectroscopic study of the interaction of oxygen, nitrogen and transition metals with $C_{60}$ films

V Vijayakrishnan, A K Santra, Ram Seshadri, R Nagarajan, T Pradeep & C N R Rao*
Solid State and Structural Chemistry Unit and CSIR Centre of Excellence in Chemistry
Indian Institute of Science, Bangalore 560 012, India

Received 20 February 1992

Evidence is presented for the strong interaction of oxygen and nitrogen with solid films of buckminsterfullerence based on core-level spectroscopic studies. Cr, Ni and Cu deposited on $C_{60}$ films interact strongly giving rise to large changes in the C(1*s*) and C(2*p*) binding energies as well as the (2*p*) binding energies of the transition metals.

The chemistry of buckminsterfullerene, $C_{60}$, has attracted world-wide attention in the last few months. $C_{60}$ exhibits many novel properties. It undergoes facile one-electron reduction to give various anionic species[1,2] and produce singlet oxygen with high quantum yields[3]. It is reported that $C_{60}$ gets oxidised by solid $O_2$ on exposure to low or high energy photons[4]. Interaction of $C_{60}$ with $N_2$ has not been studied hitherto although one would expect interesting adsorbed species to be formed on the surface, considering that strongly bound molecular species with a bond order between 1 and 2 have been found on a carbided Ni surface[5,6]. We have studied the interaction of $N_2$ with multilayer $C_{60}$ films by employing X-ray photoelectron spectroscopy. For the purpose of comparison, we have examined the interaction of $O_2$ with $C_{60}$ films. We have also investigated the interaction of chromium, nickel and copper clusters deposited on $C_{60}$ films, since we felt that transition metal atoms may bind strongly by the $\pi$ system of $C_{60}$. We have employed core-level spectra of the transition metal and $C_{60}$ as well as the valence bands to examine the $C_{60}$-transition metal interaction.

## Materials and Methods

$C_{60}$, prepared by the contact-arc vapourization of graphite in a He atmosphere by employing a locally fabricated generator[7], was purified by chromatography[8] and the identity ascertained by mass spectrometry, UV-visible spectroscopy and $^{13}C$ NMR spectroscopy. Layers of $C_{60}$ were deposited on a polycrystalline Au foil. Photoelectron spectra were recorded with a VG ESCA 3 MkII spectrometer fitted with a sample preparation chamber, by employing Al $K_\alpha$ (1486.6 eV) or HeII (40.8 eV) radiation under an operating vacuum of $\sim 4 \times 10^{-10}$torr. The C(1*s*), O(1*s*) and N(1*s*) binding energies were referenced with respect to the Au(4*f*) binding energy (84.0 eV). The $C_{60}$ films were exposed to $N_2$ and $O_2$ under different conditions in the sample preparation chamber. Different coverages of Ni, Cr or Cu were deposited on the $C_{60}$ film by resistive evaporation of the metal, the quantity deposited being determined by the $I_M/I_C$ intensity ratio (of the transition metal $2p_{3/2}$ and C 1*s* levels). For the purpose of comparison we have examined all these systems by employing amorphized graphite substrate.

## Results and Discussion

*Nitrogen*

In Fig. 1 we show the N(1*s*) spectrum of $N_2$ adsorbed on a multilayer film of $C_{60}$ at 80K. We observe a single sharp feature around 400.6 eV, unlike $N_2$ adsorbed on most transition metal surfaces (in the $\gamma$-state[6]) wherein two relatively broad features around 401 eV and 405 eV are generally found due to the screened and the unscreened final states respectively[6]. A single N(1*s*) feature in the 399-400 eV range is found on transition metal surfaces when $N_2$ is strongly chemisorbed in the $\alpha$-state[6] with a N-N bond order between 1 and 2. We believe that the N(1*s*) peak around 400.6 eV found at 80K on the $C_{60}$ films is due to a strongly chemisorbed molecular species, I, the sharpness of the feature being suggestive of the presence of a well-defined single species (Note that graphite does not interact with $N_2$ at 80K or 300K). The absence of a feature due to the unscreened state also suggests that the $N_2$ species

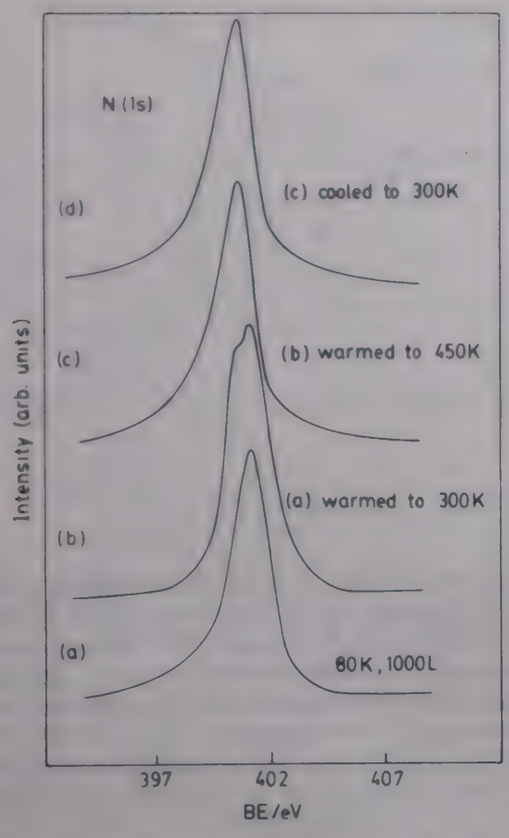


Fig. 1—N(1*s*) spectra of $N_2$ adsorbed on $C_{60}$.

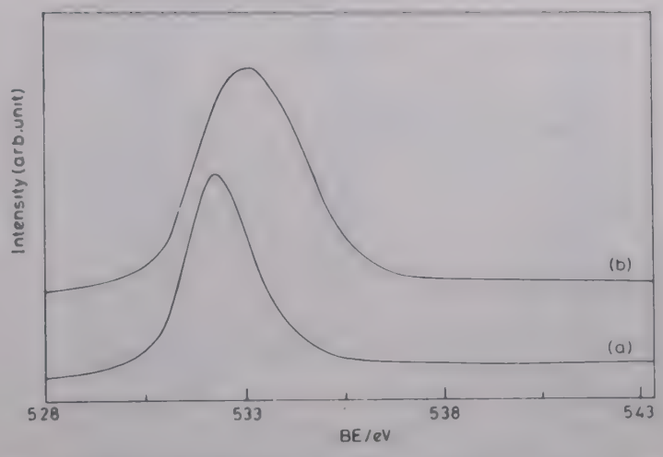


Fig. 2—O(1*s*) spectrum of $O_2$ adsorbed on $C_{60}$: (a) $C_{60}$ film exposed to oxygen at 300K; (b) $O_2$ adsorbed at 80K in (a) showing physisorbed species; on warming to 300K spectrum (a) is found again.

does not desorb even at 300K, unlike the weakly chemisorbed γ-species on transition metal surfaces which desorbs well below 300K. The N(1*s*) spectrum at 300K (Fig. 1) also shows the emergence of a new sharp feature at a lower binding energy (400.2 eV). This would represent another chemisorbed state, II, of $N_2$ on $C_{60}$. On warming at 450K, we only see the 400.2 eV feature indicating that species I completely transforms to II. We consider the occurrence of such chemisorbed states of $N_2$ on $C_{60}$ to be most interesting. It is possible that the structure of this species is one where a weakened N-N bond (1.3-1.4 Å long) is lying side-on on a C-C bond of $C_{60}$. We have not found any evidence for the formation of dissociated nitrogen species on $C_{60}$ up to 450K.

*Oxygen*

Unlike in the case of $N_2$, $C_{60}$ films exposed to oxygen or air (without any special irradiation) show evidence for reactive interaction with a O(1*s*) feature around 532.5 eV at 300K (Fig. 2) due to oxygenated $C_{60}$, probably involving an epoxide-like linkage as in graphitic oxide, rather than a carbonyl function. Accordingly, the 532.5 feature remains on the surface even at 450K. Graphite itself does not interact with oxygen at 300K; oxidation of graphite occurs only on interaction with atomic oxygen or oxygen plasma[9]. It is likely that the oxidation of $C_{60}$ probably occurs through the $O_2^-$ species[10] (O 1*s*, 534.2 eV) initially formed on the surface on adsorption of $O_2^-$ at low temperatures; the $O_2$ species disappears below 200K from the surfaces of clean as well as oxygenated $C_{60}$.

*Nickel*

As mentioned earlier, the coverages of the Ni were quantitified by means of the intensity of the Ni($2p_{3/2}$) feature, $I_{Ni}$, relative to that of the C(1*s*) signal of the support, $I_C$. The $I_{Ni}/I_C$ ratios so obtained provide a measure of the amount of Ni deposited or the Ni cluster size[11]. The surface coverage at the lowest $I_{Ni}/I_C$ ( ~ 0.1) employed by us was $5 \times 10^{13}$ atoms $cm^{-2}$ as estimated by the method of Carley and Roberts[12]; this corresponds roughly to 80 Ni atoms per cluster.

We first examined the variation in the Ni ($2p_{3/2}$) binding energy relative to bulk Ni (852.9 eV) with the Ni coverage in order to characterize the nature of the metal clusters deposited on the substrates. In Fig. 3 we show plots of $\Delta E$ Ni ($2p_{3/2}$) against $I_{Ni/IC}$ on both $C_{60}$ and amorphized graphite substrates. The $\Delta E$ ($2p_{3/2}$) increases with the decrease in $I_{Ni}/I_C$ on the graphite surface; at the smallest coverage studied by us, the shift is around ~ 0.7 eV. The increase in the 2*p* binding energy relative to the bulk accompanying the decrease in the coverage or the cluster size, signifies the occurrence of a metal to non-metal transition. That is, at small Ni coverages, the deposited clusters are on average, non-metallic. The increase in the Ni(2*p*) binding energy with decrease in Ni coverage arises because the core-hole created in the photoemission process is more poorly screened in the small clusters compared to the bulk metal causing a reduction in the relaxation energy. What is noteworthy is that the increase in

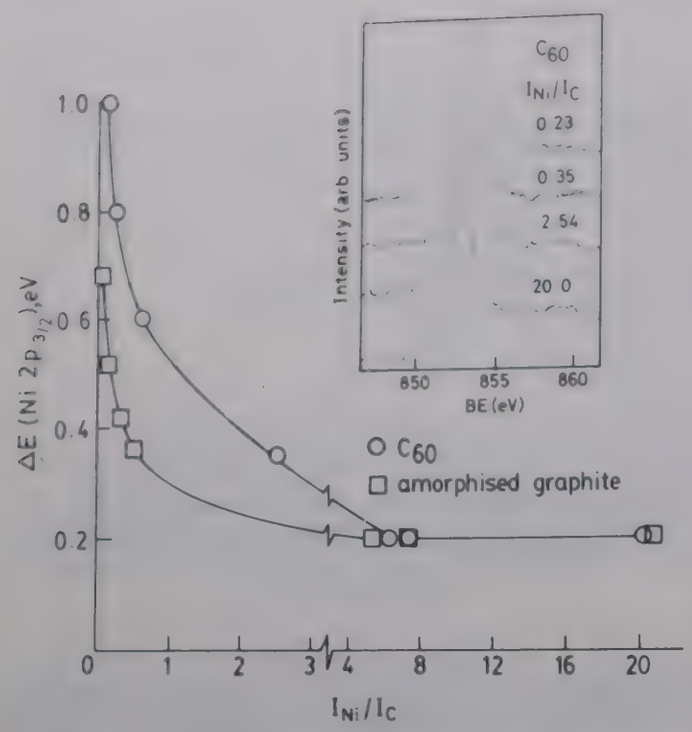


Fig. 3—Variation of the Ni($2p_{3/2}$) binding energy (relative to the bulk Ni value) with the Ni coverage ($I_{Ni}/I_C$) on $C_{60}$ and amorphized graphite substrates. Each experimental point represents an independent measurement on a freshly deposited cluster. Inset shows Ni($2p_{3/2}$) spectra on $C_{60}$.

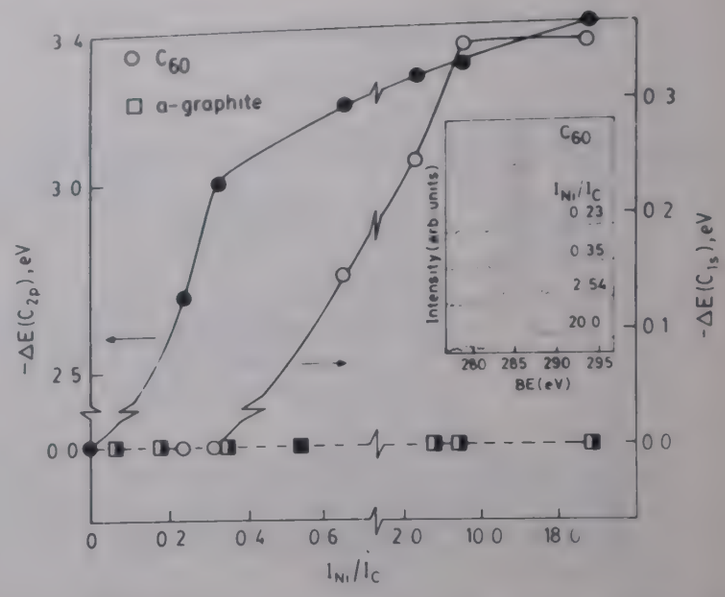


Fig. 4—Variation of the C($1s$) and C($2p$) binding energies of $C_{60}$ with Ni coverage ($I_{Ni}/I_C$) relative to those of the clean substrate. Note that the C($1s$) and C($2p$) binding energies do not change with Ni coverage in the case of the graphite substrate. Inset shows C($1s$) spectra of $C_{60}$ at different Ni coverages.

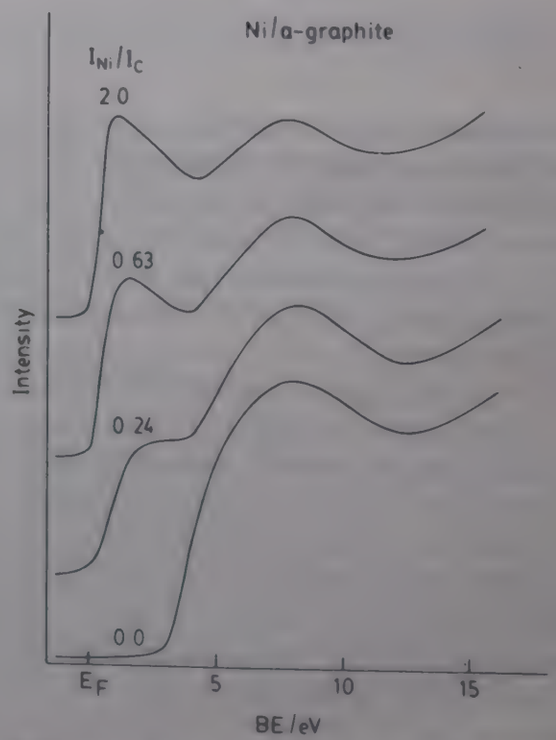


Fig. 5—HeII valence band spectra of Ni clusters deposited on amorphized graphite at different coverages. All spectra are normalized to equal height at the top of C($2p$) band of the blank graphite substrate.

the Ni($2p$) binding energy is significantly larger on the $C_{60}$ support than on graphite for an equivalent Ni coverage[13]. Thus, at the smallest coverage, $\Delta E$ Ni ($2p_{3/2}$) is ~ 1.0 eV on $C_{60}$. This implies that the core-hole is more weakly screened on the $C_{60}$ substrate and is consistent with the fact that $C_{60}$ is less conducting than graphite.

When Ni is deposited on the amorphized graphite substrate no change occurs in the C($1s$) binding energy of graphite at all coverages. However, when Ni is deposited on the $C_{60}$ support, we observe a progressive decrease in the C($1s$) binding energy (relative to the value of 284.9 eV of $C_{60}$) with increasing Ni coverage, showing a maximum shift of ~ 0.4 eV at large Ni coverages (Fig. 4). This observation suggests that as Ni is deposited on the $C_{60}$ film, the carbon atoms acquire a slight negative charge[13]. The C($1s$) binding energy at large Ni coverages (284.5 eV) is slightly higher than that of carbidic carbon (284.2 eV).

In Fig. 5, we show the evolution of the Ni ($3d$) band in the valence region with the increase in the coverage of Ni on an amorphized graphite substrate. The broad feature due to C($2p$) is centered around 9.5 eV relative to $E_F$. The Ni $3d$ band shifts to lower energies with increase in Ni coverage. This new C($2p$) feature is considered the C($2p$) region due to interaction of the graphite surface with Ni. However, when Ni is deposited on the $C_{60}$ film, we observe a feature derived from C($2p$) at a lower binding energy (Fig. 6). The position of this feature progressively shifts to lower binding energy with the increase in Ni coverage. This new C($2p$) feature is consdedred to result from the interaction of Ni atoms with

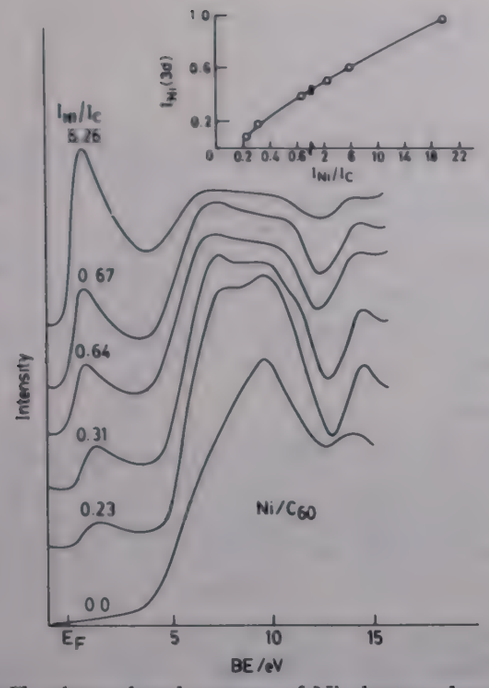


Fig. 6—HeII valence band spectra of Ni clusters deposited on a multilayer $C_{60}$ film. Note the new C($2p$) feature moving towards lower binding energy with increase in Ni coverage. Inset shows the variation of the intensity of the Ni($3d$) band with $I_{Ni}/I_C$.

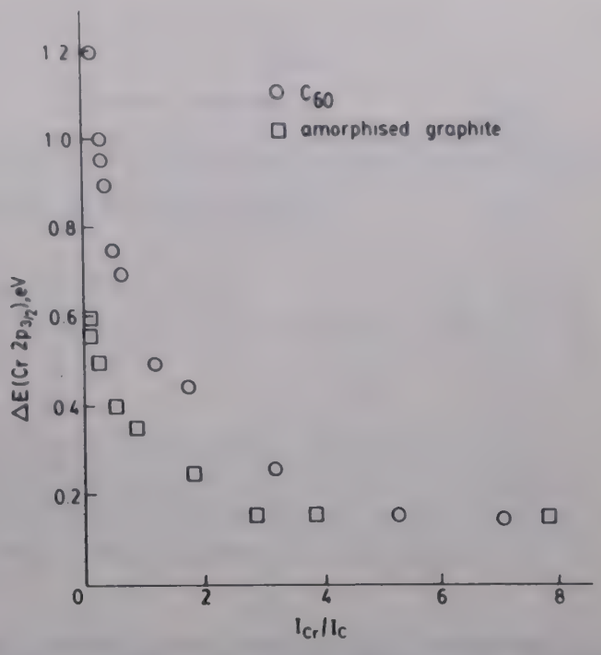


Fig. 7—Variation of the Cr($2p_{3/2}$) binding energy (relative to bulk Cr) with Cr coverage )$I_{cr}/I_c$) on $C_{60}$ and amorphized graphite substrates.

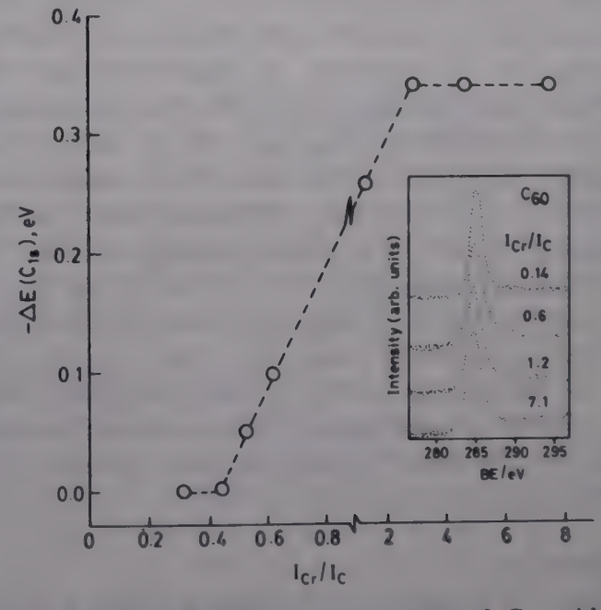


Fig. 8—Variation of C($1s$) binding energy of $C_{60}$ with Cr coverage ($I_{cr}/I_C$) relative to the clean substrate. In the inset we show C($1s$) spectra.

$C_{60}$[13]. In the case of the $C_{60}$ substrate also, the Ni($3d$) band shifts to higher binding energies with decrese in Ni coverage. In the inset of Fig. 6 we show the variation of the Ni($3d$) band intensity with Ni coverage; we see that the intensity approaches zero at the smallest coverage showing the cluster size to be very small.

In Fig. 4 we have plotted the shift in the binding energy of the new C($2p$) feature (relative to the binding energy of 9.5 eV of pure $C_{60}$) against the Ni coverage. We notice that it shifts by ~ 3.4 eV at large coverages. The progressive decrease in the binding energies of the C($1s$) and the C($2p$) levels in the $C_{60}$ surface with the increase in $I_{Ni}/I_C$ as well as the higher Ni ($2p_{3/2}$) binding energies on $C_{60}$ imply that at low coverages, the Ni atom forms a "complex" with $\pi$-system of $C_{60}$. With increase in Ni coverage, more $\pi$-bonds of $C_{60}$ interact with the metal atoms giving rise to the observed shifts in binding energies.

*Chromium and copper*

In Fig. 7 we show the variation of the shift in the Cr($2p_{3/2}$) binding energy, $\Delta E$, relative to the bulk metal (574.3 eV) with Cr coverage on both $C_{60}$ an amorphized graphite substrates. The shift increases with decrease in coverage or cluster size. Furthermore, the shift is much larger on $C_{60}$ than on amorphized graphite for any given coverage. The maximum $\Delta E$ found for the smallest coverage studied by us is around 1.2 eV. This shift is larger than that found with Ni (Fig. 3). The C($1s$) binding energy of $C_{60}$ also shifts progressively to lower binding energies with increasing Cr coverage showing a maximum shift of ~ 0.35 eV for large Cr coverage (Fig. 8). In the inset of the Fig. 8, we have shown the C($1s$) spectra of $C_{60}$ for different coverages of Cr. It appears that the interaction of Cr with $C_{60}$ is similar to that of Ni, involving strong metal-carbon bonding.

We have also studied the interaction of $C_{60}$ films with Cu at different coverages. Here again

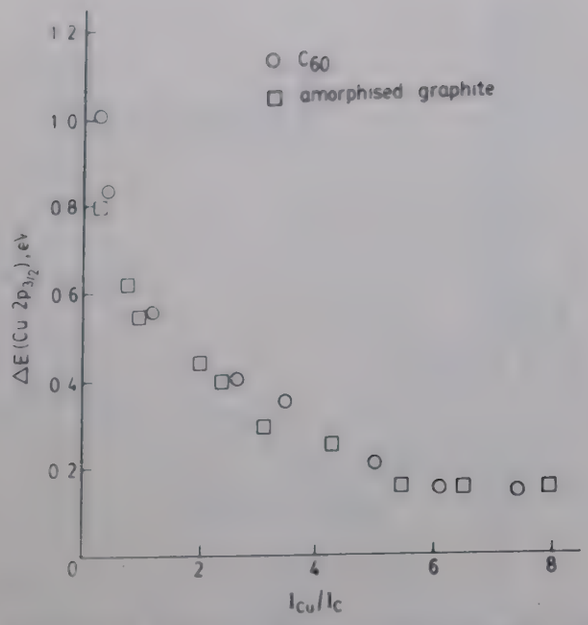


Fig. 9—Variation of Cu($2p_{3/2}$) binding energy (relative to bulk Cu) with Cu coverage ($I_{Cu}/I_C$) on $C_{60}$ and amorphized graphite substrates.

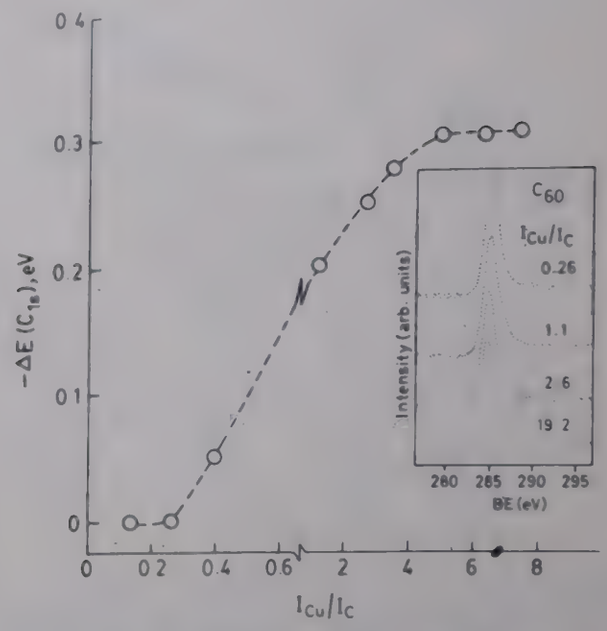


Fig. 10-Variation of C($1s$) binding energy of $C_{60}$ with Cu coverage ($I_{Cu}/I_c$). In the inset we show C($1s$) spectra.

we find large shifts in the Cu($2p_{3/2}$) binding energies relative to the bulk metal (933.1 eV) with the decrease in Cu coverage. In Fig. 9, we show the shifts of $2p_{3/2}$ binding energy for various coverage of Cu deposited on $C_{60}$ as well as amorphized graphite supports. In the case of Cu, unlike with Ni and Cr, we see little difference with the two supports. The C($1s$) binding energy of the $C_{60}$ however decreases by ~0.3 eV for the highest Cu deposition (Fig. 10) suggesting strong interaction between Cu clusters and $C_{60}$. The present study on the interaction of Ni, Cr and Cu clusters with $C_{60}$ shows the interaction to be uniformly strong and suggests that $C_{60}$ may have a role in heterogeneous catalysis[13].

## References


1 Dubois D, Kadish K M, Flanangan S, Haufler R E, Chibante L P F & Wilson L J, *J Am chem Soc*, 113 (1991) 4364.

2 Pradeep T, D'Souza F, Subbanna G N, Krishnan V & Rao C N R, *Proc Indian Acad Sci (Chem Sci)*, 103 (1991) 685.

3 Arbogast J W, Darmanyan A P, Foots C S, Rubin Y, Diederich F N, Alvarez M M, Anz S J & Whetten R L, *J phys Chem*, 95 (1991) 11.

4 Kroll G H, Benning P J, Chen Y, Ohno T R, Weaver J H, Chibante L P H & Smalley R E, *Chem Phys Lett*, 181 (1991) 112.

5 Ranga Rao G & Rao C N R, *Appl Surf Sci*, 45 (1990) 65.

6 Rao C N R & Ranga Rao G, *Surf Sci Repts*, 13 (1991) 221.

7 Pradeep T & Rao C N R, *Mat Res Bull*, 26 (1991) 1101.

8 Taylor R, Hare J P, Abdul-Sada A K & Kroto H W, *J chem Soc Chem Commun*, (1990) 1423.

9 Evans S & Thomas J M, *Proc R Soc (London)*, A 353 (1977) 103.

10 Rao C N R, Prabhakaran K & Rajumon M K, *Rev Solid State Sci*, 4 (1990) 843.

11 Vijayakrishnan V & Rao C N R, *Surf Sci Lett*, 255 (1991) L 561.

12 Carley A F & Roberts M W, *Proc R Soc London*, A 363 (1978) 403.

13 Vijayakrishnan V, Santra A K, Pradeep T, Seshadri R, Nagarajan R & Rao C N R, *Surf Sci Lett*, 262 (1992) L87.

Indian Journal of Chemistry
Vol. 31 A& B, May 1992, pp. F27-F31

# Nitrogen derivatives of $C_{60}$ and $C_{70}$: Interaction of fullerenes with nitrogen in gas phase and with amines in solution phase

C N R Rao*, T Pradeep, Ram Seshadri & A Govindaraj

CSIR Centre of Excellence in Chemistry and Solid State and Structural Chemistry Unit, Indian Institute of Science, Bangalore 560 012, India

Received 20 February 1992

Mass spectrometric studies show that contact-arc vaporization of graphite in a partial atmosphere of $N_2$ or $NH_3$ yields nitrogenous products tentatively assigned to species such as $C_{70}N_2$, $C_{59}N_6$, $C_{59}N_4$ and $C_{59}N_2$ involving addition of or substitution by nitrogen along with the species due to $C_2$ and $C_4$ losses. Mass spectrometry and other techniques have been employed to identify products of the nucleophilic addition of aliphatic amines to $C_{60}$ and $C_{70}$ in solution phase.

Research on $C_{60}$ has progressed at an enormous pace in the last few months. One of the important aspects of research in this area relates to the reactivity of $C_{60}$. It is known that $C_{60}$ readily produces singlet oxygen in high quantum yields[1] and reacts with oxygen[2]. $C_{60}$ interacts strongly with nickel deposited on it as discussed in an earlier paper in this issue of the Journal. Our studies on the interaction of $C_{60}$ films with gaseous nitrogen[3] by X-ray photoelectron spectroscopy showed evidence of strong binding with a sharp feature around 400 eV in the N(1*s*) spectrum[4]. (Note that graphite does not interact with $N_2$). Prompted by this observation and encouraged by the finding of Guo *et al.*[5] that carbon can be replaced by boron in $C_{60}$, we sought to explore whether we can produce nitrogenous derivatives of $C_{60}$ and $C_{70}$ by carrying out the contact-arc vaporization of graphite in a partial atmosphere of gaseous $N_2$ or $NH_3$. We have indeed found that nitrogen containing derivatives of $C_{60}$ and $C_{70}$ involving the addition of nitrogen as well as substitution of carbon by nitrogen are formed in such a process. We report the results of our study in this article. In addition, we report results of our studies of the addition of aliphatic amines to $C_{60}$ and $C_{70}$. These fullerenes are shown to readily undergo nucleophilic additions of amines giving products involving the addition of 1,2,6,12 and even a larger number of amine molecules.

## Materials and Methods

We carried out contact-arc vaporization of graphite in the presence of $N_2$ or $NH_3$ by leaking the gas at a rate of 1cc $sec^{-1}$. Helium was simultaneously leaked at the same rate. The soot obtained was soxhlet-extracted with toluene. After the solvent was evaporated from the toluene solution, the resulting product was light brown (in the case of $N_2$ reaction) or pale yellow (in the case of $NH_3$ reaction) in colour. Elemental analysis established the presence of nitrogen in the products. These products were subjected to mass spectrometric analysis and also other spectroscopic characterization. A JEOL direct inlet mass spectrometer (70 eV EI source) was used for the study.

$C_{60}$ (and $C_{70}$) were reacted with aliphatic amines such as $CH_3NH_2$ and $(CH_3)_2NH$ in toluene solution at room temperature. Reaction took place instantaneously and the yellow products of the reactions were subjected to spectroscopic and mass spectrometric examination. Long chain amines were also reacted with $C_{60}$ in toluene solution under reflux.

## Results and Discussion

### *Gas phase reactions with $N_2$ and $NH_3$*

The product of the reaction between $N_2$ and the graphite vapour obtained after toluene extraction gave peaks in the mass spectrum at *m/z* 792, 764 and 736 along with the corresponding dication peaks (Fig. 1). Since the 792 peak is unlikely to arise from the substitution of 36 carbons of $C_{60}$ by nitrogen, we suggest that this is due to the addition of 5 nitrogen ($N_a$) and substitution of one carbon atom by nitrogen ($N_s$) giving a composition $C_{59}N_6$. Other possible alternatives are compounds with $(5\text{-}n)N_a + (1+7n)N_s$ with n = 1, 2 or 3; even with n = 1, the formula works out to be $C_{52}N_{12}$ with more nitrogen than the structure can probably tolerate. We, therefore, feel that the assignment of the 792 peak to $C_{59}N_6$ may be reasonable; this is also justified by the internally consistent set of assignments of the other observed features that become possible on this basis. The 764 peak can be considered to be due to $C_{59}N_4$ (with $3N_a + 1N_s$) arising from a loss of $N_2$ from $C_{59}N_6$ while the 736 feature is due to $C_{59}N_2$

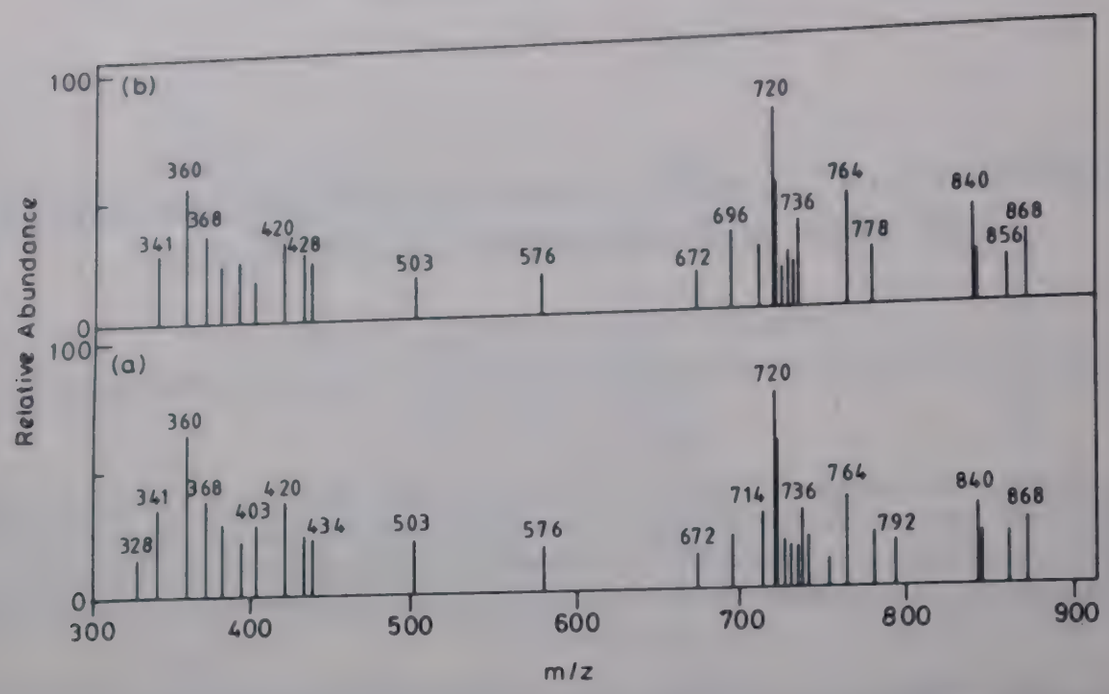


Fig. 1—Typical mass spectra of the toluene extract of the soot obtained from the contact-arc vaporization of graphite in a partial nitrogen atmosphere; (a) and (b) are spectra from different runs

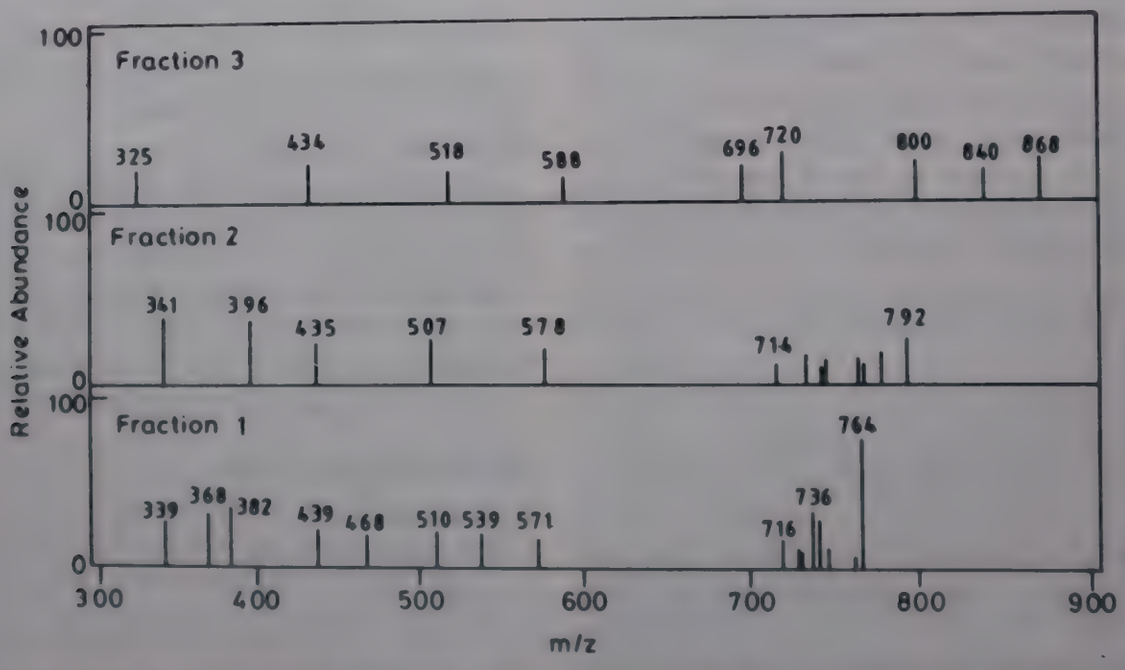


Fig. 2—Mass spectra of the chromatographic fractions of the toluene extract of the soot obtained from the contact-arc vaporization of graphite in a partial atmosphere of ammonia

(with 1 $N_3 + N_2$) arising from a further $N_2$ loss. The other peaks in the mass spectra (Fig. 2) at $m/z$ 778, 768 and 744 can be explained as due to loss of N, $C_2$ and $C_4$ respectively from $C_{58}N_6$. We also see peaks at $m/z$ 722-728 which can be due to nitrogen substitution in $C_{60}$ giving molecules in the range $C_{60}N$-$C_{56}N_4$. The $m/z$ 868 peak (dication peak at 434) in the mass spectrum is clearly due to $C_{58}N_2$ with two $N_2$; the feature around 856 can also be due to $C_{56}N_2$ with 1 $N_3$ and 1 $N_2$.

The yellow product of the $NH_3$ reaction with graphite vaporization gave three fractions in column chromatography (with neutral alumina) which could be eluted out with $CH_2Cl_2$, leaving one band at the top of the column. Mass spectra of the three fractions showed the total absence of the $m/z$ 720 peak due to $C_{60}$ (Fig. 2), but instead showed peaks which can be assigned to nitrogenous products similar to those obtained in the vaporization of graphite in the presence of $N_2$. Accordingly, the mass spectrum of fraction 1 showed peaks at $m/z$ 764 and 736 (along with the corresponding dication peaks at $m/z$ 382 and 368) due to $C_{58}N_2$ and $C_{56}N_2$. The peaks at $m/z$ 740 and 716 are considered to be due to $C_2$ and $C_4$ loss respectively from $C_{56}N_2$; the other peaks in the mass spectra can also be interpreted in terms of si-

milar combinations of $N_a$ and $N_s$. Fraction 2 showed peaks at *m/z* 792 and 764 due to $C_{59}N_6$ and $C_{59}N_4$ (Fig. 2); peaks at *m/z* 778, 768 and 744 are likely to be due to loss of N, $C_2$ and $C_4$ respectively from $C_{59}N_6$ while the other peaks in the *m/z* 714-742 range can be interpreted as due to combinations of $N_a$ and $N_s$. Fraction 2 also showed peaks at *m/z* 868 and 434 due to $C_{70}N_2$; the peak at *m/z* 842 could be due to $C_{69}N$ with one carbon substituted by nitrogen. Fraction 3 showed a peak at *m/z* 868 due to $C_{70}N_2$.

The compounds present in these fractions only show absorption in the ultraviolet region (Fig. 3). The infrared spectra are completely different from those of $C_{60}$ and $C_{70}$. While there could be some hydrogenation, we have not found evidence for C−H or N−H bonds. Contact-arc vaporization of graphite in a partial atmosphere of $CH_3NH_2$ also gives similar nitrogenous products, completely transforming $C_{60}$; $C_{59}N_4$, $C_{59}N_2$ and the associated peaks have been found by us in the mass spectrum.

In summary, the present study demonstrates that $C_{60}$ interacts strongly with nitrogen[6]. The reaction products of the contact-arc vaporization of graphite in a partial atmosphere of $N_2$ or $NH_3$ can be identified by mass spectrometry. In Table 1, we list the approximate description of the nitrogenous products; the exact characterization of these products, however, has to await more detailed mass spectrometric and chemical studies. It is possible that $C_{70}N_2$, $C_{59}N_6$ and $C_{59}N_4$ and possibly some of the species with mass numbers in the range 722-728 ($C_{56}N_4 - C_{56}N$ with only $N_s$) are bonafide compounds formed in the vaporization of graphite while the others are fragmentation features[6]. We are not able to comment on the nature of the nitrogen added to $C_{60}$ or $C_{70}$ at this stage, although one possibility is the formation of 3- or 4-membered rings. A noteworthy feature is that they seem to eliminate $N_2$ (e.g. $C_{59}N_6 \rightarrow C_{59}N_4 \rightarrow C_{59}N_2$). The likely reason that we have found formation of nitrogeneous derivatives in the present study is because we did not backfill the reactor completely with $N_2$, but only leaked $N_2$ gas at a slow rate. On backfilling, we found a polymeric product.

Table 1—Nitrogen derivatives of $C_{60}$ and $C_{70}$ identified by mass spectrometry

| Mass No. | Molecular formula | Approximate description[a] |
|---|---|---|
| 868 | $C_{70}N_2$ | $2\,N_a$ |
| 856 | $C_{69}N_2$ | $1\,N_a + 1\,N_s$ |
| 842 | $C_{69}N$ | $1\,N_s$ |
| 792 | $C_{59}N_6$ | $5\,N_a + 1\,N_s$ ($4\,N_a + 8\,N_s$)[b] |
| 764 | $C_{59}N_4$ | $3\,N_a + 1\,N_s$ ($2\,N_a + 8\,N_s$)[b] |
| 736 | $C_{59}N_2$ | $1\,N_a + 1\,N_s$ ($8\,N_s$)[b] |
| 728 to 722 | $C_{56}N_4$ to $C_{59}N$ | $4\,N_s$ to $1\,N_s$ |

(a) $N_a$ and $N_s$ stand for addition of nitrogen and substitution of a carbon by nitrogen respectively. Alternative combinations of $N_a$ and $N_s$ are possible.

(b) Alternative descriptions of *m/z* 792, 764 and 736 features shown in parentheses would be $C_{52}N_{12}$, $C_{52}N_{10}$ and $C_{52}N_8$, but these seem unlikely.

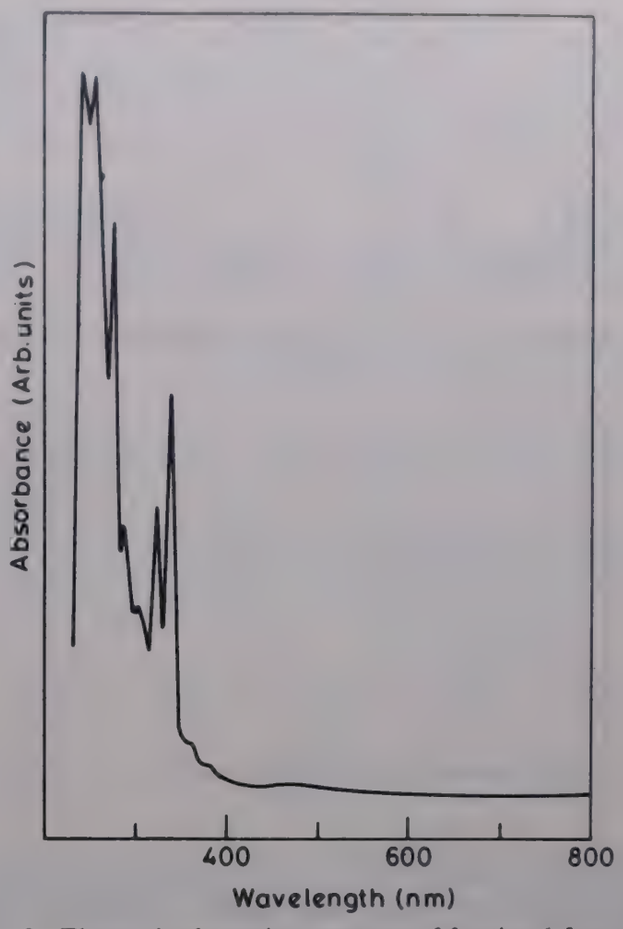


Fig. 3—Electronic absorption spectrum of fraction 1 from the $NH_3$ reaction

*Reactions with amines in solution phase*

Addition of methylamine to $C_{60}$ was carried out by passing dry methylamine gas into a solution of $C_{60}$ in toluene at 298K. Such an addition gave rise to a yellow product almost instantaneously. This product was studied by mass spectrometry. A typical mass spectrum is shown in Fig. 4. The mass spectra showed a large number of addition products involving multiple addition of the amine to $C_{60}$. The intense peak with *m/z* around 751 corresponds to the addition of one $CH_3NH_2$ to $C_{60}$. Peaks with *m/z* of 727 and 703 could arise from $C_2$ and $C_4$ losses. The weaker peak at *m/z* of 782 could be assigned to the product with two $MeNH_2$ units. More interestingly, we see features which correspond to the addition of six $CH_3NH_2$ at *m/z* of 906 with associated fragmentation loss peaks at *m/z* of 882 and 858. Features

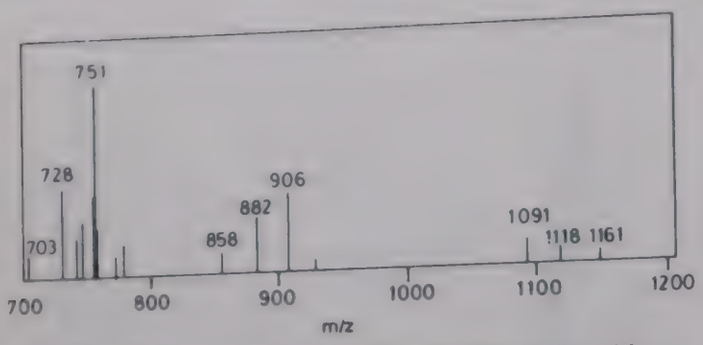


Fig. 4—Mass spectrum of the addition product of $C_{60}$ with methylamine

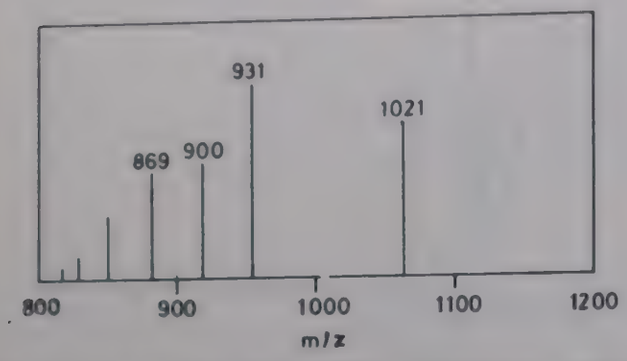


Fig. 5—Mass spectrum of the addition product of $C_{70}$ with methylamine

which can be attributed to seven and eight $CH_3NH_2$ units were also seen in some scans. The highest *m/z* seen by us could be assigned to 12, 13 and 14 $CH_3NH_2$ units at *m/z* of around 1091, 1118 and 1148 respectively.

We carried out a similar reaction with $C_{70}$. A typical mass spectrum is shown in Fig. 5. Here we see peaks at *m/z* of 869, 900, 931 and 1021 which could be assigned to products with one, two, three or five $CH_3NH_2$ additions. We did not see evidence for the addition of a large number of amine molecules.

We carried out a reaction of $C_{60}$ with dimethylamine in the same fashion. The mass spectra do not show strong molecular ion peaks (Fig. 6). However, based on fragmentation loss peaks at *m/z* 717 and 762, we assign the peaks at *m/z* of 765 and 808 to mono- and di-adducts. Peaks at *m/z* of 922 and 967 are considered to arise from the penta- and hexa-adducts respectively. In Fig. 7, we show the UV spectrum of the mixture of adducts with $CH_3NH_2$ along with the fluorescence spectrum. In Fig. 8, we show the infrared spectra of the amine adducts. The $CH_3NH_2$ adduct shows the N–H stretching band (3400 $cm^{-1}$) absent in the $(CH_3)_2NH$ adduct.

Mass spectrometry of the product of reaction of $C_{60}$ with methylamine shows that we get a mixture of addition products, the predominant ones being the mono- and hexa-adducts. We attempted a separation of the components by thin-layer chromatography on silica using ethyl acetate-petroleum ether (40:60, v/v). We obtained separation into three

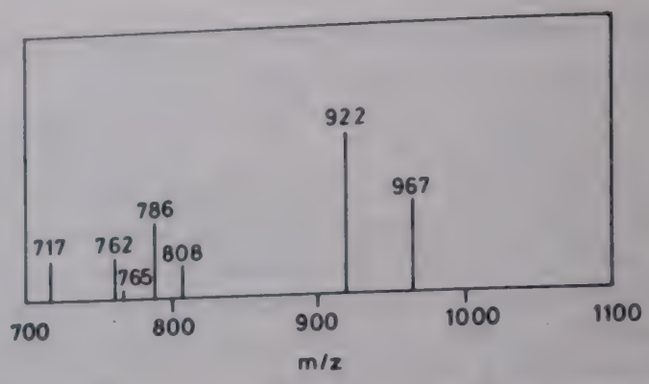


Fig. 6—Mass spectrum of the addition product of $C_{60}$ with dimethylamine

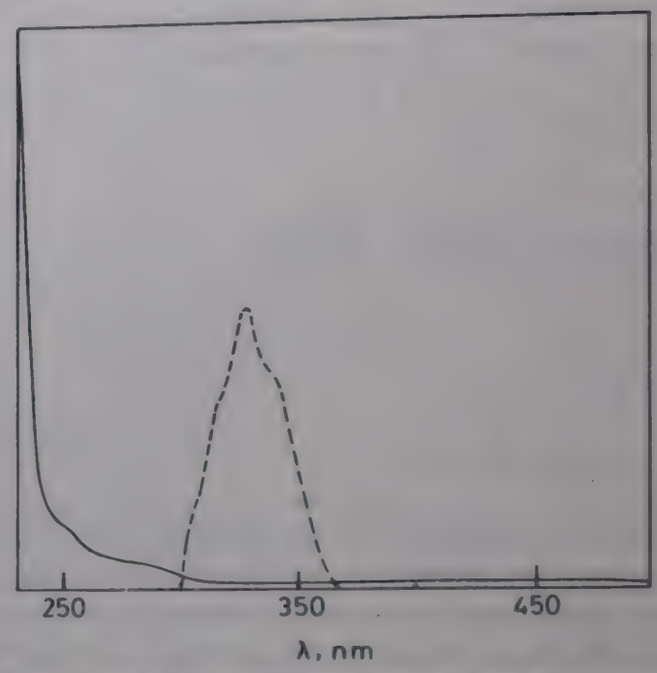


Fig. 7—UV-visible absorption (solid curve) and fluorescence (broken curve) spectra of the addition product of $C_{60}$ and methylamine in methanol solution

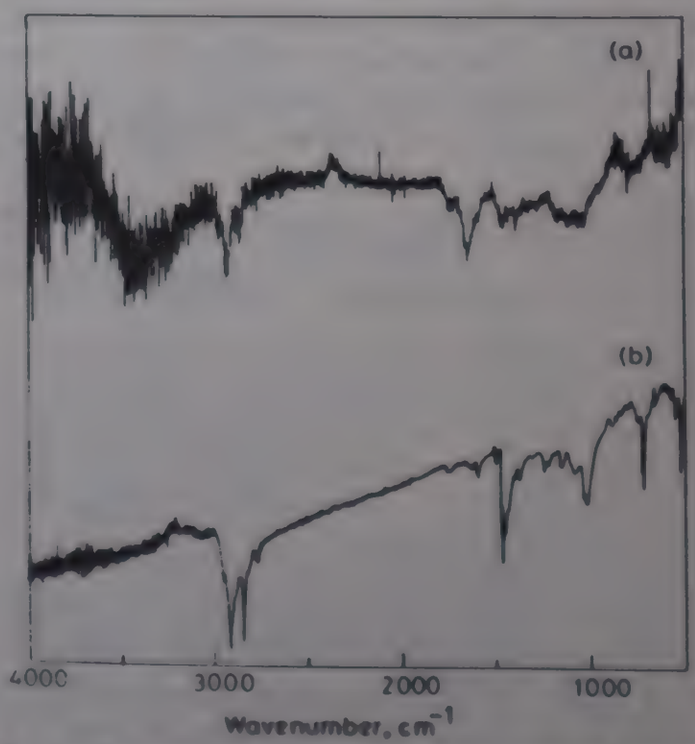


Fig. 8—IR spectra of the adducts of (a) $CH_3NH_2$ and (b) $(CH_3)_2NH$ with $C_{60}$. Notice the NH stretching band in (a)

bands 1, 2 and 3 with R.F. values of 0.61, 0.73 and 0.94. The highest mass peaks in the mass spectrum of 1 corresponds to the addition of 4 to 6 $CH_3NH_2$ units, although peaks corresponding to the addition of 8 to 11 amine units are occasionally seen. Fraction 2 seemed to give, predominantly, features corresponding to addition of 6 to 8 $CH_3NH_2$ units and some weak features due to the addition of up to 12 units. Fraction 3 was predominantly composed of products from the addition of 9 to 18 $CH_3NH_2$ units with a few of the lower adducts. We did not see these large adducts in the mass spectrum of the as-reacted product (Fig. 4) probably due to poor volatalization.

We have ben able to prepare an essentially pure mono adduct of $C_4H_9NH_2$ with $C_{60}$ by refluxing a 2:1 mixture in toluene solution. The UV spectrum of the product shows peaks at 328, 286, 271, 265 and 257 nm in the THF solution. The compound shows a fluorescence maximum at 394 nm (excitation maximum 330 nm). The mass spectrum showed the expected molecular ion peak at *m/z* 793.

## References

1 Arbogast J W, Darmanyan A P, Foote C S, Rubin Y, Diederich F N, Alvarez M M, Anz S J & Whetten R L, *J phys Chem*, 95 (1991) 11.

2 Kroll G H, Benning P J, Chen Y, Ohno T R, Weaver J H, Chibante L P F & Smalley R E, *Chem Phys Lett*, 181 (1991) 112.

3 Vijayakrishnan V, Santra A K, Pradeep T, Nagarajan R, Seshadri R & Rao C N R, *J chem Soc Chem Commun*, (1992) 198.

4 Rao C N R & Ranga Rao G, *Surface Sci, Repts*, 13 (1991) 221.

5 Guo T, Jin C & Smalley R E, *J phys Chem*, 95 (1991) 4948.

6 Pradeep T, Vijayakrishnan V, Santra A K & Rao C N R, *J phys Chem*, 95 (1991) 10564.

Indian Journal of Chemistry
Vol. 31 A&B, May 1992, pp. F32-F35

# Extraction of fullerenes in organic solvents and the development of superior isolation procedures

R Dhamodaran, I Kaliappam, N Sivaraman, T G Srinivasan, P R Vasudeva Rao & C K Mathews*
Indira Gandhi Centre for Atomic Research, Kalpakkam 603 102, Tamil Nadu, India

Received 20 February 1992

Development of methods for the isolation of fullerenes depends to a great extent on the identification of suitable solvents. In the present work, extraction of fullerenes from carbon soot by a number of aliphatic, alicyclic and aromatic solvents has been examined at a constant temperature of 60°C. The results indicate that the extraction power of aliphatic straight chain hydrocarbons increases with increase in carbon chain length. The aromatic solvents have superior extracting power as compared to the aliphatic solvents. The higher extraction power of the aromatic solvents is attributed to their better solubilising action. Based on the experimental data, it was possible to develop efficient procedures for the chromatographic separation of $C_{60}$ and $C_{70}$ employing cyclohexane and a normal paraffin hydrocarbon mixture with average carbon number of 12 as solvents. $C_{60}$ and $C_{70}$ could both be isolated completely in pure form in much smaller volumes of eluant than in the hexane system.

The recent isolation of macroquantities of $C_{60}$ and $C_{70}$ has led to a veritable explosion in scientific literature on the properties of these all-carbon clusters called fullerenes. Superconductivity has been observed in alkali metal-doped $C_{60}$, a number of chemical reactions involving $C_{60}$ have been reported, and "endohedral complexes" of the fullerness, where a metal atom is trapped inside the ball shaped cage of the fullerene molecule, have also been reported. These as well as many other aspects of fullerenes are covered in several reviews[1-3].

The major advancement that was responsible for the developments mentioned above was the discovery of a procedure for the preparation and isolation of the fullerenes in bulk quantities. Preparation of fullerenes is carried out by the "contact arc" method[4] or "resistance heating" method[5], the former being more popular. High yields (upto 40% of the soot as soluble material) have been obtained by suitable modifications in the design and operation of the arcing set up[6].

The procedure widely used for the isolation of fullerenes involves the soxhlet extraction of the soluble material in the soot (with toluene or benzene as solvent) followed by rotary evaporation to obtain a mixture of fullerenes. From this mixture, $C_{60}$ is separated by chromatographic separation on neutral alumina[5,7]. $C_{60}$ is eluted from the column by using hexane-5% toluene as eluant. $C_{70}$ is eluted by using hexane containing ~ 25% toluene.

The poor solubility of fullerenes in hexane makes this separation procedure tedious, and large volumes of solutions have to be handled. Further, the use of toluene means that for recycling of the solvents, fractional distillation has to be resorted to.

It has been observed that by using aromatic solvents with higher boiling points such as 1, 2, 3, 5-tetramethylbenzene, fullerenes with high carbon numbers (as high as 300) could be extracted from soot[6,8]. However, in the absence of any systematic data on the solubility of various fullerenes in different solvents as a function of temperature, it cannot be concluded whether the efficient extraction of higher fullerenes is due to the nature of the solvent used, or the higher boiling points of the solvents.

In the present work, the extraction of fullerenes from carbon soot by a number of organic solvents was studied at a constant temperature (60°C), with the following objectives: (a) to examine the relative solubilities of fullerenes in these solvents and (b) to arrive at procedures for chromatographic separations based on single solvent systems. The results of our studies indicate trends in the solubilities of fullerenes based on the nature of the solvent, and thus point to better chromatographic procedures. Two new solvents for fullerene separation are also suggested.

## Materials and Methods

Carbon soot obtained by the contact arc method was subjected to toluene soxhlet extraction to

recover the fullerenes. The details of the apparatus and the separation methods are reported in an earlier paper[9].

The paraffin solvent (Normal Paraffin Hydrocarbon-NPH) used in the present work was a mixture of *n*-decane, *n*-undecane, *n*-dodecane, *n*-tridecane and *n*-tetradecane, with an average carbon number of 12 supplied by M/s Tamilnadu Petroproducts Ltd., Madras. It contained less than 0.003% of aromatics, as confirmed by its absorption spectrum. The absorbance at 270 nm, usually considered as an indicator of the concentration of aromatics, was measured to be 0.150 absorbance units. All other solvents used were either of HPLC grade or AR grade. The NPH solvent, as well as *n*-hexane and *n*-octane were used without any further purification. *n*-Decane, *n*-dodecane and *n*-tetradecane, which were found to contain some aromatic impurities, were purified by passing through neutral alumina to remove aromatic impurities in the solvent. The absence of aromatic impurities was confirmed by measuring the UV-visible absorption spectrum.

In the experiments to study the extraction of fullerenes from soot, approximately 10 g of soot was homogenised and a 100 mg aliquot was suspended in 10 ml of the solvent taken in an equilibration tube. This tube was kept in a water bath maintained at a constant temperature of $60 \pm 0.1$°C by circulating water from a thermostat through a glass jacket surrounding the bath. The entire apparatus was kept on top of a magnetic stirrer, and the contents of the glass equilibration tube were mixed by using a teflon coated magnetic stirring bar. The equilibration was continued for 4 hr, after which the tube was centrifuged, and a sample of the solvent phase withdrawn for the measurement of the absorption spectrum.

UV-visible absorption spectra were measured using a Shimadzu model UV-2100 spectrophotometer.

## Results and Discussion

Figures 1 and 2 show the absorption spectra of the solutions obtained by equilibration of the soot with various solvents. The absorbance values at appropriate wavelengths were taken to indicate the extent of extraction. Fig. 1 shows the spectra of the extracts in aliphatic solvents and Fig. 2 shows the spectra of the extracts in some aromatic solvents as well as cyclohexane and carbon tetrachloride. The spectra in Figs 1 and 2 were recorded with extract solutions as such without dilution. Table 1 gives some data on absorbance values measured from these spectra, for a more quantitative comparison.

Since the studies have been made on raw soot, the absorption spectral information obtained indicates the combined solubility of $C_{60}$ and $C_{70}$ (ignoring the higher fullerenes which are formed in much lower amounts). Still, the data reported here bring out clearly the role of the chemical nature of the solvent in solubilising the fullerenes.

The spectra in Fig. 1 as well as the data in Table 1 clearly show that the solubility of the fullerenes in aliphatic straight chain hydrocarbons increases with chain length. It is seen that the extraction power of *n*-dodecane is approximately six times that of *n*-hexane. This trend is contrary to that normally observed in the solubilities of organic compounds. On the basis of the theory of regular solutions, the solubility is expected to dec-

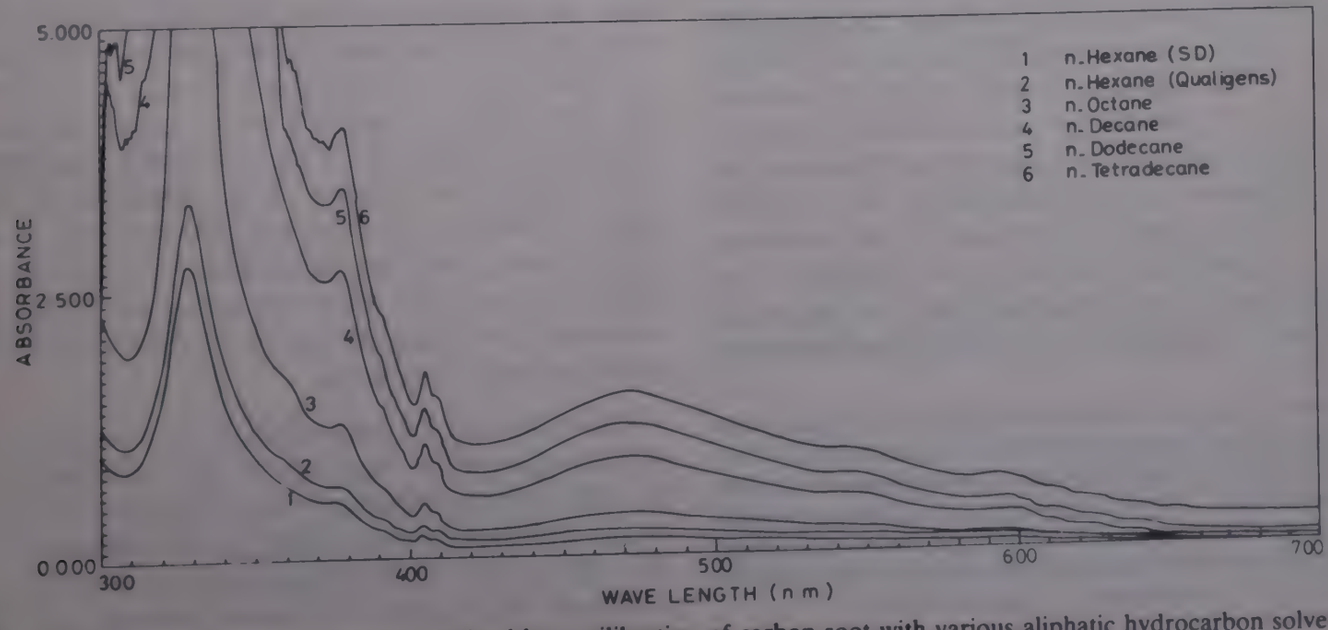


Fig. 1—Absorption spectra of extracts obtained by equilibration of carbon soot with various aliphatic hydrocarbon solvents.

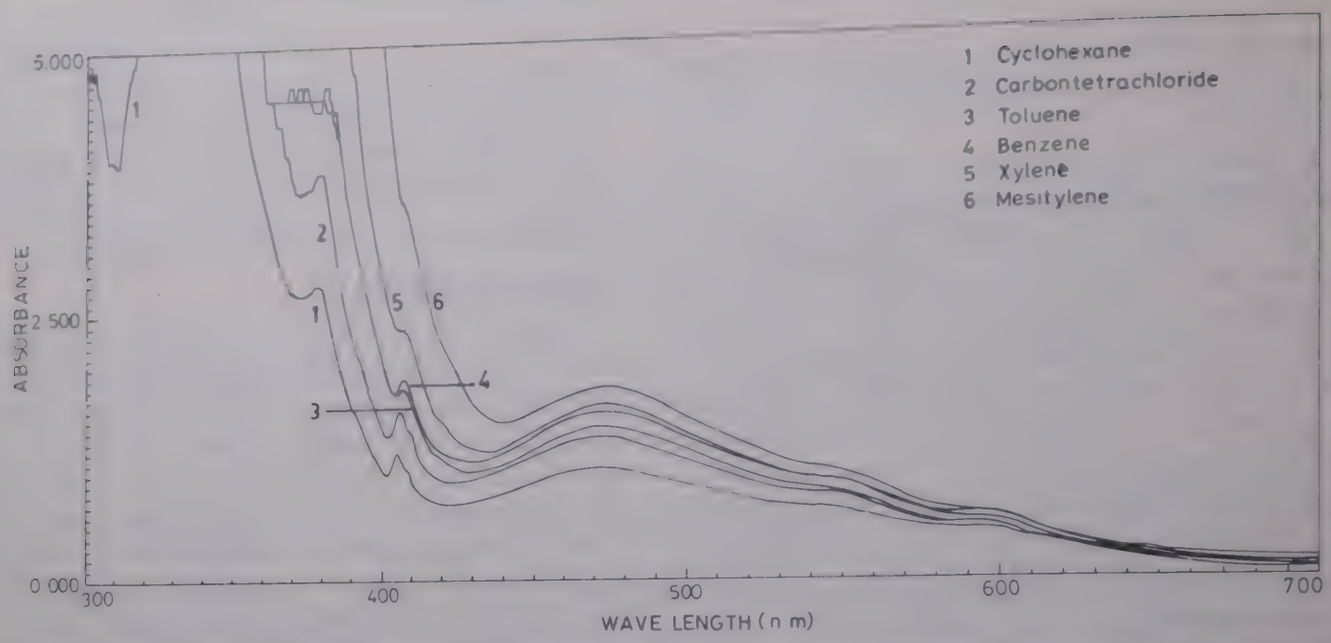


Fig. 2—Absorption spectra of extracts obtained by equilibration of carbon soot with benzene, toluene, xylene, mesitylene, $CCl_4$ and cyclohexane

Table 1—Absorbance values for fullerene extracts in various solvents at selected wavelengths

| Solvent | Wavelength (nm) | | | |
|---|---|---|---|---|
| | 468 | 403 | 378 | 330 |
| *n*-Hexane (SD) | 0.159 | 0.199 | 0.539 | 2.706 |
| *n*-Hexane (Qualigens) | 0.235 | 0.282 | 0.691 | 3.287 |
| *n*-Octane | 0.402 | 0.461 | 1.277 | >5 |
| *n*-Decane | 0.909 | 0.931 | 2.700 | >5 |
| *n*-Dodecane | 1.219 | 1.228 | 3.476 | >5 |
| *n*-Tetradecane | 1.507 | 1.529 | 4.038 | >5 |
| Cyclohexane | 1.042 | 1.058 | 2.775 | >5 |
| Carbontetrachloride | 1.333 | 1.362 | 3.817 | >5 |
| Toluene | 1.409 | 1.785 | 4.516 | >5 |
| Benzene | 1.554 | 1.776 | 4.396 | >5 |
| Xylene | 1.606 | 2.459 | >5 | >5 |
| Mesitylene | 1.761 | 4.245 | >5 | >5 |

rease with increase in carbon number, since the solubility parameter, which reflects the cohesion of the solvent molecules, increases with carbon number. The differing behaviour in the present case may be due to the near spherical shape of the fullerene molecules. Long chain hydrocarbons may accommodate the "buckyballs" more readily between them, with a minimum of net breakage of the intermolecular bonds in the solvent. More detailed studies are underway with the individual fullerenes to understand the solvation mechanism†.

† The solubility of pure $C_{60}$ in various solvents of differing solubility parameter has since been measured in our laboratory, and the results are being published separately. These results indicate that the solubility of $C_{60}$ first increases with the increase in solubility parameter, and then decreases. Such a behaviour may be explained on the basis of the regular solution theory and the solubility parameter of $C_{60}$ which has now been estimated

Fig. 2 and the absorbance data provided in Table 1 show that the extraction in the aromatic solvents as well as carbon tetrachloride and cyclohexane is higher than that in the aliphatic hydrocarbons. This higher solubility of the fullerenes obviously results from better interaction of the fullerenes with these solvents. It is seen that extraction by mesitylene is the highest amongst the aromatic hydrocarbons studied. Since these studies were carried out at the same temperature (60°C), the better extraction power of this solvent can be attributed to its better solvation properties and not to the higher extraction temperature.

Fig. 1 also indicates a difference in the extraction power of *n*-hexane obtained from two different sources (M/s SD Fine Chemicals and M/s Glaxo). Even after the hexane from both the sources was purified by passing through alumina, a clear difference was seen in their extraction behaviour. The reason for this is not clear. It is possible that the hexane contained some polar impurity that does not show up in the UV-visible spectrum. Due to the poor soluility of the fullerenes in aliphatic solvents of low carbon number, the presence of even small concentrations of polar impurities can drastically affect the measured solubility behaviour, and thus the purity of solvent used becomes an important factor.

The efficiency of separation of $C_{60}$ and $C_{70}$ by chromatography is decided by the difference in the affinity of alumina for these fullerenes, as well as the difference in solubility of the fullerenes in the solvent used for chromatography. The use of a solvent with higher solvation capacity has the

advantage of loading the mixture and eluting the individual fullerenes in smaller volumes.

The extraction data obtained by us indicated that cyclohexane can be a good solvent for extraction/isolation of fullerenes. We have carried out a few column runs using this solvent, and excellent separation of $C_{60}$ and $C_{70}$ was realised using this solvent. Further, all the $C_{70}$ could be eluted from the column by this solvent. The solvent coming out of the column in the loading step could be directly reused for preparing feed solutions or for elution; the $C_{60}$ and $C_{70}$ eluates were evaporated in a rotary evaporator, and the solvent recovered used in elution. The complete separation of approx. 200 mg of fullerene mixture could thus be accomplished using just 4 litres of the solvent, whereas in similar runs with hexane-toluene system we had to use more than 10 litres of the solvents, with the added problem of having to separate toluene and hexane by distillation for reuse.

The aliphatic hydrocarbon NPH was also used in some column runs; it also led to complete isolation and separation of $C_{60}$ and $C_{70}$. In fact, use of NPH resulted in lesser solvent volumes due to the higher solubility of the fullerenes in NPH. However, since the boiling range of this solvent is high, high vacuum must be used with the rotary evaporator to be able to evaporate away the solvent for recovery of the fullerenes. Cyclohexane possesses an advantage in this respect, as fullerenes can be conveniently recovered from it by simple evaporation or distillation.

In conclusion, it can be said that aliphatic hydrocarbons of higher chain length extract fullerenes from soot better than hexane does, and aromatic solvents in general extract better than the aliphatic solvents. The solvents studied in this work can be ranked in terms of their extraction power (based on the absorbance of the extract at 468 nm) as follows: *n*-hexane < *n*-octane < *n*-decane < cyclohexane < *n*-dodecane < carbon tetrachloride < toluene < *n*-tetradecane < benzene < xylene < mesitylene.

The extraction of higher percentages of soluble matter from soot by mesitylene is due to its better solvation properties. It is possible to arrive at more efficient and convenient methods for the extraction and purification of the fullerenes by a proper choice of the solvents. Two examples of such solvents are described above. More experiments are being conducted to understand the solubility behaviour of $C_{60}$ and $C_{70}$ in various solvents.

## References


1 Kroto H W, Allaf A W & Balm S P, *Chem Rev*, 91 (1991) 1213.

2 Huffman D R, *Physics Today*, 44(11) (1991) 22.

3 Curl R F & Smalley R E, *Scientific American*, 265(4) (1991) 32.

4 Haufler R E, Conceicao J, Chibante L P F, Chai Y, Byrne N E, Flanagan S, Haley M M, O'Brien S C, Pan C, Xiao Z, Billups W E, Ciufolini M A, Hauge R H, Margrave J L, Wilson L J, Curl R F & Smalley R E, *J phys Chem*, 94 (1990) 8634.

5 Ajie H, Alvarez M M, Anz S J, Beck R D, Diedrich F, Fostiropoulos K, Huffman D R, Kratschmer W, Rubin Y, Schriver K E, Sensharma D & Whetten R L, *J phys Chem*, 94 (1990) 8630.

6 Parker D H, Wurtz P, Chatterjee K, Lykke K R, Hunt J E, Pellin M J, Hemminger J C, Gruen D M & Stock L M, *J Am chem Soc*, 113 (1991) 7499.

7 Diederich F, Ettl R, Rubin Y, Whetten R L, Beck R & Alvarez M, Anz S, Sensharma D, Wudl F, Khemani K C & Koch A, *Science*, 252 (1991) 548.

8 Shinohara H, Sato H, Saito Y, Takayama M, Izuoka A & Sugawara T, *J phys Chem*, 95 (1991) 8449.

9 Mathews C K, Vasudeva Rao P R, Srinivasan T G, Ganesan V, Sivaraman N, Lakshmi Narasimhan T S, Kaliappan I, Chandran K & Dhamodaran R, *Curr Sci*, 61 (1991) 834.

Indian Journal of Chemistry
Vol. 31 A&B, May 1992, pp. F36-F41

# Organic chemistry with buckminsterfullerene ($C_{60}$)

S Chandrasekaran

Department of Organic Chemistry, Indian Institute of Science, Bangalore 560 012

Received 20 February 1992

A brief review of the organic chemical reactions with buckminsterfullerene ($C_{60}$) – Birch reduction, reductive alkylation, halogenation, Friedel-Crafts reaction, dipolar cycloaddition – that have been reported in the literature is presented. Some preliminary results on hydroboration-protonolysis, cycloaddition of diazomethane and chlorosulfonyl isocyanate with $C_{60}$ have been discussed.

Carbon is the all important element that anchors the molecules of everything from crude oil to DNA and is thus a kind of natural backbone. In recent years, a number of groups of scientists have been pursuing an exotic form of carbon believed to have a particularly elegant configuration: 60 atoms of carbons arranged like a miniature soccer ball[1]. In 1990, a team of astronomers led by Krätschmer and Huffmann[2] reported that this new allotrope of carbon, $C_{60}$, named buckminsterfullerene, can be produced in reasonable quantities through resistive heating of graphite under inert atmosphere.

They found that the sublimate from the arc-processed graphite was soluble in benzene and contained a range of fullerenes, $C_{60}$ and $C_{70}$ in particular. This material was chromatographed by using hexane/alumina and $C_{60}$ and $C_{70}$ were thereby separated into magenta and red coloured fractions respectively[3]. $^{13}C$ NMR measurements of $C_{60}$ showed a single line ($\delta$ 142.68) suggesting that all the 60 atoms are equivalent. The $^{13}C$ NMR spectrum of $C_{70}$ consisted[4] of a set of five lines indicating five different types of carbons in the ratio 10:10:20:20:10[4]. The structures in Fig. 1 and Fig. 2 for $C_{60}$ and $C_{70}$ are also supported by IR[1,5], Raman[6] and photoelectron spectroscopy[7]. The ultimate configuration and the detailed parameters of the soccer ball shaped framework had to wait for X-ray crystallographic analysis. But the crystals of $C_{60}$ were disorganised piles of buckyballs and there was no way of viewing the individual molecules, because $C_{60}$ is the most symmetric molecule possible in three-dimensional Euclidean space; it is the roundest of round molecules: edgeless, chargeless, and unbound. The major difficulty arises from the fact that when the buckyballs are on their own, they spin like tiny planets completing more than billion rotations in a second. They do not stay still long enough to have their picture taken. To break the symmetry of $C_{60}$ and prevent its rapid spinning in the crystal, Hawkins *et al.* prepared by osmylation a 1:1 $C_{60}$-osmium tetroxide adduct[8]. (Eq. 1).

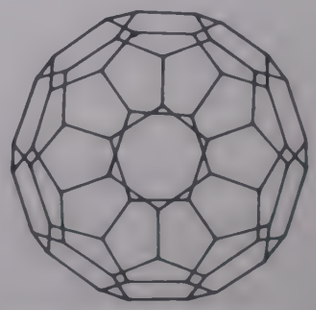

Fig. 1 – Structure of $C_{60}$

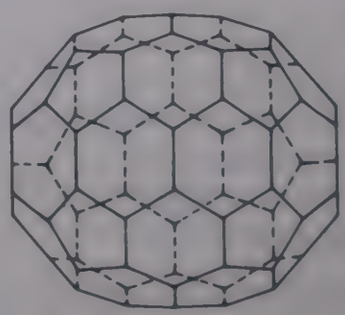

Fig. 2 – Structure of $C_{70}$

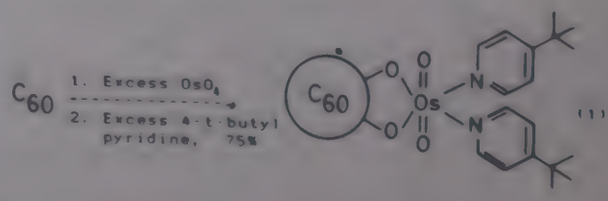


The crystal structure of this adduct was finally solved which clearly confirms the soccer ball structure of $C_{60}$ consisting of 20 six-membered rings fused to 12 five-membered rings[9]. All tricoordinate carbon atoms of $C_{60}$ are pyramidalized

and lie at an average distance of 3.5 Å from the center of the sphere. The bond length at the six-six ring fusion is 1.39 Å and the bond length at the five-six ring fusion is 1.43 Å The UV/vis spectrum showed absorption at 213, 257, 329 ($\varepsilon_{max}$ 135000, 175000, 51000), 404(w), 440-670 (br) ($\lambda_{max}$ 500, 540, 570, 600, 625) nm[10] and infrared spectrum had absorptions at 528, 579, 1183 and 1429 $cm^{-1}$ (refs 1,5).

The name chosen for the molecule buckminsterfullerene is long but definitely not as long as the IUPAC nomenclature (Fig. 3)[1a]. The the name 'fullerene' is conveniently used for the whole family of closed carbon cages with the 12 pentagons and N (other than one) hexagons in an $sp^2$ network[4a,11].

## Organic chemical reactivity of fullerene-60

Since improved and simple experimental set up and techniques for the production of fullerenes in significant quantities are available now[12-14], a new era of polycyclic aromatic chemistry has started. $C_{60}$, however, differs in many respects from the planar aromatic molecules and exhibits "ambiguous" aromatic character[15]. The structural framework in $C_{60}$ is generally very stable and it possesses a relatively small $\pi$-electron ring current magnetic susceptibility compared to graphite or benzene[16]. Based on electrochemical studies, $C_{60}$ has been found to be as strong an oxidizing agent as methyl viologen and flavin chromophores and its first reduction potential is more positive than that for most of the polycyclic aromatic hydrocarbons[5,17]. A few organic chemical reactions that have been successfully carried out with $C_{60}$ so far owe their origin to the inherent electron deficient nature of the molecule.

## Reduction and reductive alkylation on $C_{60}$

Smalley *et al.*[12] were the first to effect an organic chemical reaction on $C_{60}$. In a remarkably successful experiment underscoring the aromatic character of fullerene-60, Birch reduction was performed with lithium and liquid ammonia in the presence of *t*-butanol as proton source to obtain a light cream to off white solid. This material was homogeneous on thin layer chromatographic analysis ($R_f$ = 0.37, 30% $CH_2Cl_2$ in hexanes). However, mass spectral analysis showed this to be a mixture of two hydrocarbons. The major product with the molecular ion at *m/z* 756 corresponds to the hydrocarbon of formula $C_{60}H_{36}$. It was not clear whether the minor product with molecular ion at *m/z* 738 ($C_{60}H_{18}$) was a genuine coproduct in Birch reduction or the pyrolysis product of $C_{60}H_{36}$. Based on $^1H$ NMR spectrum of $C_{60}H_{36}$ (broad multiplet between $\delta$ 2.5 and 4.2) and its analogy with the spectrum of dodecahedrane, the structure of one possible isomer of $C_{60}H_{36}$ has been postulated as in Fig. 4. Smalley *et al.* have a convincing explanation for the observation that 36 hydrogens have been added to $C_{60}$ on Birch reduction. Since Birch reduction affects only conjugated double bonds, 36 is the number of hydrogens required to leave 12 double bonds which are isolated from each other, one on each pentagon (Fig. 4)[18].

The IR spectrum (KBr) of this material exhibited bands at 2925, 2855, 1620, 1450, 1400 and 675 $cm^{-1}$ strongly supporting the structure with C–H and C=C bonds. To substantiate the point that in the Birch reduction of $C_{60}$ the basic molecular skeleton of the fullerene has not been al-

IUPAC Nomenclature for $C_{60}$

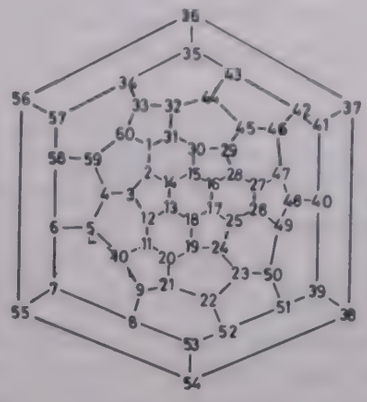

Hentriacontacyclo[29.29.0.$O^{2,14}$.$O^{3,12}$.$O^{4,59}$.$O^{5,10}$.$O^{6,58}$.$O^{7,55}$.$O^{8,53}$.$O^{9,21}$.$O^{11,20}$.$O^{13,18}$.$O^{15,30}$.$O^{16,28}$.$O^{17,25}$.$O^{19,24}$.$O^{22,52}$.$O^{23,50}$.$O^{26,49}$.$O^{27,47}$.$O^{29,45}$.$O^{32,44}$.$O^{33,60}$.$O^{34,57}$.$O^{35,43}$.$O^{36,56}$.$O^{37,41}$.$O^{38,54}$.$O^{39,51}$.$O^{40,48}$.$O^{42,46}$] hexaconta 1,3,5(10),6,8,11,13(18),14,16,19,21,23,25,27,29(45),30,32(44),33,35(43),36,38(54),39(51),40(48),41,46,49,52,55,57,59 -triacontaene.

Fig. 3 – IUPAC nomenclature for buckminsterfullerene

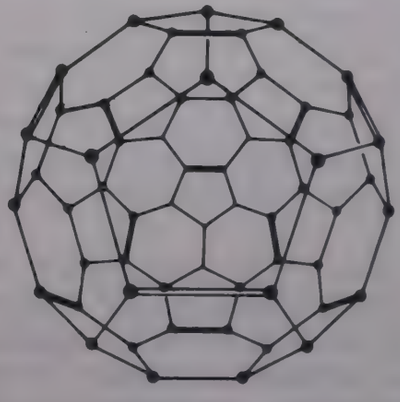

Fig. 4 – Structure of an isomer of $C_{60}H_{36}$

tered, Smalley *et al.* elegantly demonstrated that the reduction is fully reversible. Thus, dehydrogenation of the hydrocarbon $C_{60}H_{36}$ with DDQ in toluene under reflux resulted in the formation of $C_{60}$[12].

Olah *et al.* reduced a mixture of $C_{60}$ and $C_{70}$ (approximately 85:15 ratio) using lithium metal in deuterated THF with the aid of ultrasound[19]. Although the fullerenes are only slightly soluble in THF, the reduced fullerenes are highly soluble and generate a deep reddish brown solution of diamagnetic polyanions. The $^{13}C$ NMR spectrum at room temperature showed a single resonance at $\delta$ 156.7 for the reduced $C_{60}$. This deshielding of 14 ppm is a remarkable observation since carbanion carbons are generally shielded compared to their neutral precursors. The reduced $C_{70}$ also showed a similar deshielding effect in the $^{13}C$ NMR compared to $C_{70}$. Subsequent alkylations of these anions with excess methyl iodide yielded a light brown solid. Based on field ionisation mass spectral analysis Olah[19] concluded that it is a mixture of polymethylated fullerenes: all the way up to 24 methyl groups are covalently added to the sphere. This report is the first successful attempt at functionalization of $C_{60}$ and $C_{70}$ via alkylative carbon-carbon bond formation. Obviously this opens up the possibility of functionalization with other alkyl halides and other substituents like trialkylhalosilanes.

Olah *et al.* also carried out oxidation studies on $C_{60}$ and $C_{70}$ using $SbF_5$ in $SO_2ClF$ solution, a system which has been shown to be efficient for the oxidation of polycyclic aromatics to their dications. Green coloured solution thus obtained showed broad $^{13}C$ NMR spectra at all temperatures studied. It is very likely that radical cations are generated and no diamagnetic di or polycations are formed[19].

**Halogenation studies with fullerene-60**

There has been some speculation as to the possible lubricant properties of the fully fluorinated fullerene. Initially when fluorination was carried out with $XeF_2$, a mixture of partially fluorinated fullerenes was obtained[20] containing mostly of $C_{60}F_6$ and $C_{60}F_{42}$. Holloway *et al.*[20] carried out fluorinations on $C_{60}$ with fluorine gas (3-4 days) which reacts slowly in a stepwise manner to obtain finally an almost colourless crystalline product (m.p. 287°C). This compound showed sharp singlet at $\delta$ 153.9 in $^{19}F$ NMR spectrum suggesting the environment of fluorine is similar to that expected for $C_{60}F_{60}$. The IR spectrum had strong absorptions at 1060 and 1035 $cm^{-1}$ indicating the presence of C–F stretching band. The results have been interpreted suggesting fluorination is initially slow owing to the high stability of the fullerene cage. But once the first fluorine molecule has been added the other two bonds in a given benzenoid ring gets fluorinated more rapidly to give $C_{60}F_6$. It is then possible to get a second derivative of enhanced stability, possibly $C_{60}F_{42}$.

Recently Olah reported studies on chlorination and bromination of fullerenes[21]. Although chlorination was found to be sluggish at room temperature, in a hot glass tube under a slow stream of chlorine gas at 200°C for 5 h, chlorination took place readily to yield a dark brown product containing on an average 24 chlorine atoms (Eq. 2).

$$C_{60} \xrightarrow[\Delta]{Cl_2(g)} C_{60}Cl_n \qquad \ldots (2)$$

Efforts to obtain the mass spectrum of this compound were not successful. The polychlorofullerene mixture on treatment with excess methanol/KOH under reflux provided a polymethoxylated product (polymethoxylation upto 26 methoxy groups, $M^+$, 1256) (Eq. 3)

$$C_{60}Cl_n \xrightarrow[\text{reflux}]{MeOH,\ KOH} C_{60}(OMe)_n \qquad \ldots (3)$$

The replacement of methoxy groups has been rationalized by a unique front side substitution.

Interestingly Olah *et al.*[21] have also shown that the polychlorinated fullerenes undergo Friedel-Crafts reaction (Eq. 4).

$$C_{60}Cl_n \xrightarrow[AlCl_3]{C_6H_6} C_{60}(Ph)_n \qquad \ldots (4)$$

The brown solid obtained on Friedel-Crafts reaction with benzene showed a broad absorption at $\delta$ 7.2 in the $^1H$ NMR spectrum and a broad absorption at $\delta$ 128 was observed in the $^{13}C$ NMR spectrum. Analysis of the FAB mass spectrum revealed substitution of 22 phenyl groups in the molecule.

It was also demonstrated by these authors that bromination of fullerene-60 however takes place at lower temperature (20-50°C) to afford a product with an uptake of two to four bromine atoms (Eq. 5)

$$C_{60} \xrightarrow[20-50°C]{Br_2\ (neat)} C_{60}Br_n \qquad \ldots (5)$$
$$n = 2 \text{ or } 4$$

The halogenated fullerenes have been found to undergo thermal dehalogenation to give back fullerenes.

Independently Rao *et al.*[22] have carried out the

reaction of $C_{60}$ with excess $SbCl_5$ in $CCl_4$ solution to obtain the chlorine adduct as a brown solid which showed C–Cl stretching bands around 812 $cm^{-1}$ in the IR and UV absorption maxima at 250 nm. They have also shown that liquid bromine reacts with $C_{60}$ to give an orange colored product containing the dibromo adduct (C–Br stretching, 515-575 $cm^{-1}$; UV 282 and 330 nm). Attempted reaction of $C_{60}$ with $I_2$ vapor in a sealed tube around 250°C failed to yield any product[22].

**Acid catalysed fulleration of aromatics**

In a related development on the functionalization of fullerenes, Olah *et al.*[23] observed that $C_{60}$ as well as $C_{60}/C_{70}$ mixture undergo Friedel-Crafts reaction with aromatics such as benzene and toluene under catalysis with $AlCl_3$ or strong acids to form polyarenefullerenes (Eq-6).

$$C_{60} \xrightarrow[AlCl_3]{H-Ar\ (excess)} C_{60}(H-Ar)_n \qquad \ldots (6)$$

In the reaction with benzene at room temperature after 2 h fullerenes gave a major product identified as $C_{60}(Ph)_{12}$ ($M^+$, 1656). There were other products corresponding to various species containing various amount of benzene adducts. Similarly Friedel-Crafts reaction product with toluene has been identified as $C_{60}(PhCH_3)_{12}$. A mechanism that has been proposed to explain the formation of the polyarenefullerenes (Scheme-1)[23] is similar to the alkylation with alkenes under acid catalysis.

**Systematic inflation of fullerene $C_{60}$ with diphenyldiazomethane: Synthesis of fulleroids**

Recently Wudl *et al.*[24] have demonstrated the dipolarophilicity of $C_{60}$ by reacting it with diphenyldiazomethane at room temperature (1 h) to obtain a monoadduct diphenyl fulleroid $C_{61}$ (Fig. 5). Since the electronic spectrum of this compound was strikingly similar to the spectrum of $C_{60}$, the structure in Fig. 5 has been favoured over structure depicted in Fig. 6 for the product. The mechanism of formation of this product has been rationalized by these authors as depicted in Scheme-2 which involves a crucial norcaradiene-cycloheptatriene rearrangement. It has also been found that more extended reaction times with different stoichiometries afforded the diphenyl fulleroids $C_{62}$, $C_{63}$, $C_{64}$, $C_{65}$ and $C_{66}$. These results clearly indicate that one could prepare essentially any functionalized fulleroid.

**Nucleophilic addition to $C_{60}$**

The electron deficient character of $C_{60}$ has

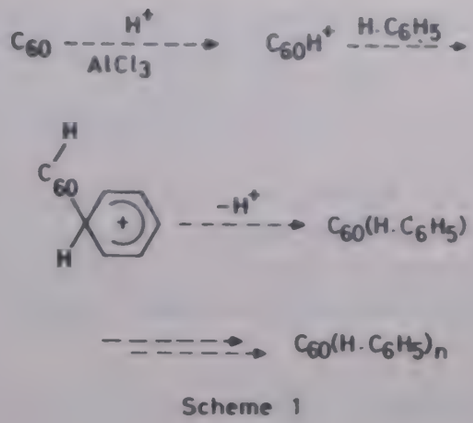


Scheme 1

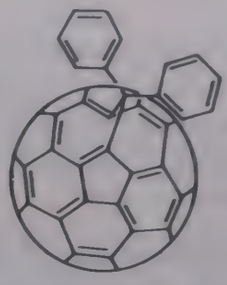

Fig. 5 – Structure of a monoadduct diphenylfulleroid, $C_{61}$

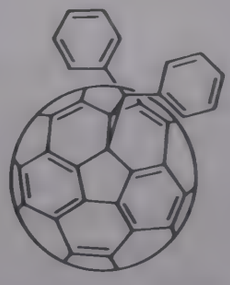

Fig. 6 – An alternative structure of monoadduct diphenyl fulleroid $C_{61}$

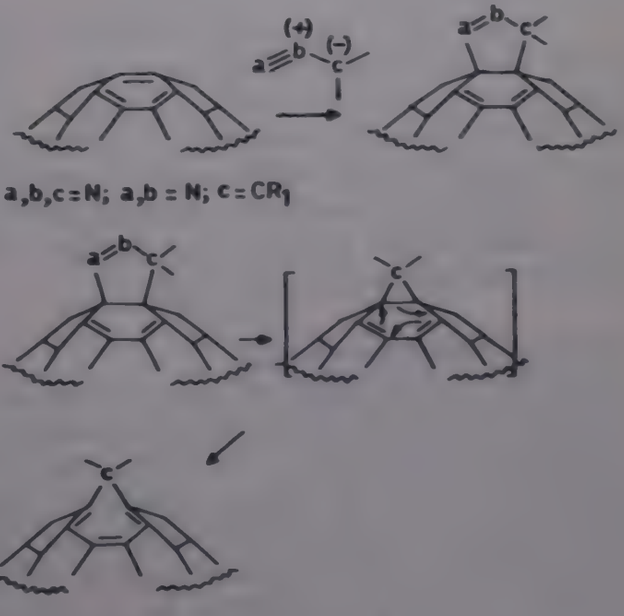


Scheme 2

been further confirmed by effecting nucleophilic additions to $C_{60}$. Wudl *et al.* observed multiple additions of amine nucleophiles to $C_{60}$ and were able to prepare polyaminated derivatives that are soluble in water[25].

Rao *et al.* have carried out detailed studies of addition of aliphatic amines to $C_{60}$ and $C_{70}$. They have obtained an essentially 1:1 amine adduct by refluxing $C_{60}$ with *n*-butylamine in toluene[22] (Eq. 7).

$$C_{60} + n\text{-}C_4H_9NH_2 \xrightarrow[\blacktriangle]{\text{Toluene}} n\text{-}C_4H_9NHC_{60}H \quad \ldots (7)$$

Reaction of $C_{60}$ with excess methylamine, however has been shown to give a mixture of adducts. Mass spectral analysis revealed this mixture to contain predominantly addition products arising out of 1, 2 and 6 amine units[22].

**Hydroboration and protonolysis of $C_{60}$[26]**

Since it has earlier been shown that $C_{60}$ is rather easily reduced and undergoes nucleophilic addition reactions, not many successful electrophilic addition reactions have been reported. Study of electrophilic addition of borane ($BH_3$) to $C_{60}$ appeared quite attractive. Accordingly when $C_{60}$ in toluene was treated with an excess of $BH_3.S(Me)_2$ at room temperature (12 h) it resulted in the complete disappearance of the magenta colour of $C_{60}$ and a pale brown solid was obtained as the product. The compound showed a broad singlet ($\delta$ 23.0) in the $^{11}B$ NMR and the IR spectrum revealed the presence of B−H and C−H stretching bands. Efforts to obtain mass spectrum (electron impact) were not successful. However, protonolysis of the organoborane with propionic acid (reflux, 12 h) afforded a hydrocarbon mixture. Mass spectral analysis revealed the presence of two major products $C_{60}H_{42}$ ($M^+$ 762) and $C_{60}H_{20}$ ($M^+$ 740). Efforts are being continued to optimise the reaction conditions and characterize the products fully. It appears as though this methodology can be extended further to obtain the elusive, fully saturated, buckminsterfullerane-$C_{60}H_{60}$[26].

**Dipolar cycloaddition with $C_{60}$**

In an independent study, we have carried out a 1,3-dipolar cycloaddition reaction of $C_{60}$ with diazomethane. Reaction of $C_{60}$ in toluene and diazomethane in ether takes place readily at room temperature to produce a light brown solid. The product shows C−H stretching bands in the IR spectrum and the UV spectrum has strong absorptions at 272, 312 and 334 nm (cyclohexane).

Although the compound needs to be fully characterized, from mass spectral analysis it appears as though 10 diazomethane units have been added and that the pyrazoline derivative readily eliminates 10 molecules of nitrogen to give a cyclopropyl derivative-$C_{60}(CH_2)_{10}$.

Since $C_{60}$ readily undergoes dipolarcycloaddition a study of the reaction of a number of dipolarphiles like phenylazide, nitrones and nitrile oxides would be of much interest. It would thus be possible to make a variety of heterocycles based on $C_{60}$[26].

**(2+2) Cycloaddition with chlorosulfonyl isocyanate**

Although it has been reported that $C_{60}$ does not undergo 4+2 cycloaddition in Diels-Alder fashion, it seems possible to effect 2+2 cycloaddition with $C_{60}$. In an exploratory reaction chlorosulfonyl isocyanate was allowed to react with $C_{60}$ in toluene at room temperature. No reaction occurred under these conditions. However when the reaction mixture was heated to 80-100°C, the colour of the solution of $C_{60}$ disappeared completely within two hours to produce a mixture of products. Work is under progress to purify and characterize the components[26]. We believe that this methodology would lead to a 1,2-functionalized $C_{60}$ – a $\beta$-amino acid with a $C_{60}$ skeleton.

Already fullerene chemistry is a vibrant field of study and the prospects for new materials with novel properties is most promising. There will be rich organic chemistry associated with the 'outside' of the molecule in the years to come.

**Acknowledgement**

The author is thankful to Mr Shridhar Bhat for help in the preparation of the manuscript and to Prof C N R Rao and Prof J Chandrasekhar for useful discussions.

**References**

1 a) Kroto H W, Allaf A W & Balm S P, *Chem Rev*, 91 (1991) 1213.
b) Stoddart J F, *Angew Chem Intern Edn Engl*, 30 (1991) 70.
c) Diederich F & Whetten R L, *Angew Chem Intern Edn Engl*, 30 (1991) 678.
2 Krätschmer W, Lamb L D, Fostiropoulos K & Huffmann D R, *Nature*, 347 (1990) 354.
3 Taylor R, Hare J P, Abdul Sada A K & Kroto H W, *Chem Commun*, (1990) 1423.
4 a) Kroto H W, *Nature*, 329 (1987) 529.
b) Schmalz T G, Seitz W A, Klein D J & Hite G E, *J Am chem Soc*, 110 (1988) 1113.
5 Cox D M, Behal S, Disko M, Gorun S M, Greaney M, Hsu C S, Kollin E B, Miller J, Robbins W, Sherwood R D & Tindall P, *J Am chem Soc*, 113 (1991) 2940.

6 Bethune D S, Meifer G, Tang W C, Rosen H J, Golden W G, Seki H, Brown C A & de Vries M S, *Chem Phys Lett*, 179 (1991) 181.
7 Lichtenberger D L, Nebesny K W, Ray C D, Huffmann D R & Lamb L D, *Chem Phys Lett*, 176 (1991) 203.
8 Hawkins J M, Lewis T A, Loren S D, Meyer A, Heath J R, Shibato Y & Saykally R J, *J org Chem*, 55 (1990) 6250.
9 Hawkins J M, Meyer A, Lewis T A, Loren S & Hollander F J, *Science*, 252 (1991) 312.
10 Hare J P, Kroto H W & Taylor R, *Chem Phys Lett*, 177 (1991) 394.
11 Nickon A & Silversmith E F, *Organic chemistry—The name game: Modern coined terms and their origins* (Pergamon, New York), 1987, p. 214.
12 Haufler R E, Conceicao J, Chibante L P F, Chai Y, Byrne N E, Flanagen S, Haley M M, Obrien S C, Pan C, Xiao Z, Billups W E, Chiufolini M A, Hange R H, Margrave J L, Wilson L J, Curle R & Smalley R E J, *J phys Chem*, 94 (1990) 8634.
13 Koch A S, Khemani K C & Wudl F, *J org Chem*, 56 (1991) 4543.
14 Pradeep T D, D'Souza F, Subbanna G N, Krishnan V & Rao C N R, *Proced Indian Acad Sci*, 103 (1991) 685.
15 Haddon R C, Schneemeyer L F, Waszczak J V, Glarum S H, Tycko R, Dabbagh G, Kortan A R, Muller A J, Mufsee A M, Rossemsky M J, Zahurak S M, Makhija A V, Thiel F A, Raghavachari K, Cockayne E & Elser V, *Nature*, 350 (1991) 46.
16 Ruoff R S, Beach D, Cuomo J, McGuire T, Whetten R L & Diederich F, *J phys Chem*, 95 (1991) 3457.
17 Allemand P M, Koch A, Wudl F, Rubin Y, Diederich F, Alvarez M M, Anz S J & Whetten R L, *J Am chem Soc*, 113 (1991) 1050.
18 Kaifer I M, *Synthesis*, (1972) 391.
19 Bausch J W, Surya Prakash G K, Olah G A, Tse D S, Lorents D C, Bae Y K & Malhotra R, *J Am chem Soc*, 113 (1991) 3205.
20 Holloway J H, Hope E G, Taylor R, Langley G J, Avent A G, John D T, Hare J P, Kroto H W & Walton D R M, *Chem Commun*, (1991) 966.
21 Olah G A, Bucsi I, Lambert C, Aniszfeld R, Trivedi N J, Sensharma D K & Surya Prakash G K, *J Am chem Soc*, 113 (1991) 9385.
22 Seshadri R, Govindaraj A, Nagarajan R, Pradeep T & Rao C N R, *Tetrahedron Lett*, (1992) to be published. [Recent studies indicate that $C_{60}$ can be reduced with 'diimide' to yield a mixture of hydrocarbons, Rao C N R, private communication].
23 Olah G A, Bucsi I, Lambert C, Aniszfeld R, Trivedi N J, Sensharma D K & Surya Prakash G K, *J Am chem Soc*, 113 (1991) 9387.
24 Suzuki T, Li Q, Khemani K C, Wudl F & Almarsson O, *Science*, 254 (1991) 1186.
25 Wudl F, in Amato I: Bucky balls, Hairy balls, Dopey balls, *Science*, 252 (1991) 646.
26 Baskaran S & Chandrasekaran S, (unpublished results).

Indian Journal of Chemistry
Vol. 31 A&B, May 1992, pp. F42-F45

# Spreading of $C_{60}$ at air-water interface†

P Ganguly*, D V Paranjape, K R Patil, S K Chaudhari & S T Kshirsagar
Materials Research Division, National Chemical Laboratory, Pune 411 008

Received 20 February 1992

The spreading of $C_{60}$ films at the air-water interface as Langmuir monolayers has been studied by examining the pressure-area ($\pi$-A) isotherms. The films spread on the air-water interface is found to be rather unstable collapsing above a surface pressue of ~ 15 dynes/cm. The area per mole in the compressed state as obtained from the extrapolation of the $\pi$-A isotherms is found to be sensitive to the source of the $C_{60}$ molecules. However, the nature of the $\pi$-A isotherms has been found to be the same once they are normalised to some reference point. This could be attributed to the sensitivity of the $\pi$-A isotherms to small amounts of impurities. The influence of the addition of various molecules both in the aqueous subphase as well as at the air-water interface has been examined. A globular amine such as *t*-butyl amine considerably stabilises the $C_{60}$ films at the interface. Long chain amines such as *n*-octadecylamine form a mixed monolayer at the air-water interface. Alcohols and acids do not show much influence. The characterisation of the films deposited on substrates by Raman spectroscopy is carried out for the first time.

The recent developments in the methods of synthesis of $C_{60}$ and $C_{70}$ have led to a number of studies of their physical and chemical properties as well as their possible aplications[1]. Obeng and Bard[2] have reported the pressure-area ($\pi$-A) isotherms of $C_{60}$ films at air-water interface. They have also commented on their deposition as Langmuir Blodgett (LB) films. The attractive aspect of the results of Obeng and Bard[2] is that the films at the air-water interface are highly incompressive and withstand high pressures (>65 dynes/cm) over a long time. However, the limiting area per molecule calculated from the $\pi$-A isotherms is about 100 Å$^2$ giving a radius of about 5.6 Å for the $C_{60}$ molecule. This is too high since the effective radius[3] of $C_{60}$ is only 3.54Å. It is also not clear how the $C_{60}$ molecules, which in the solid state form a plastic crystal with orientational disorder[4], at room temperature, could form such a stable solid-like film at the air-water interface. We have, therefore, reinvestigated the $\pi$-A isotherms for $C_{60}$ at the air-water interface with and without various dissolved molecules in the aqueous subphase such as the globular *t*-butyl amine or with molecules at the the air-water interface such as *n*-octadecyl amine. Such molecules could interact more strongly with $C_{60}$. The interest in adding *t*-butyl amine to the subphase is to study the effect of possible increase $C_{60}$-subphase interaction on the stability of the films at the air-water interface.

## Materials and Methods

The samples of $C_{60}$ were kindly supplied to us from the laboratory of Prof. C N R Rao. The $C_{60}$ compound was synthesised[5] by modifying the procedure of Kratschmer *et al.*[1d]. Monomolecular films of the material were obtained by dissolving the compound in benzene and spreading it on a Langmuir through containing doubly distilled water. MilliQ water was also used and this made no difference. The benzene in the solution was allowed to evaporate for 15-20 min. *p*H of the subphase was adjusted by adding HCl. $\pi$-A isotherms have been recorded in the manner reported earlier[6].

We had earlier used[7] oleic acid (30 dynes/cm) as a piston for depositing LB films of fatty acid salts. Because of the instability of $C_{60}$ films at this pressure an attempt was made to deposit LB films (35 layers) on silicon (111) substrate at a pressure of 16.5 dynes/cm using castor oil piston. The rate of deposition was controlled at 0.5 cm/min. The Raman spectra of the deposited film of $C_{60}$ were taken on spectrophotometer between 200-1600 $cm^{-1}$ range.

## Results and Discussion

The $\pi$-A plots for $C_{60}$ spread on water at *p*H 6.0 and 3.0 are shown in Fig. 1. The $\pi$-A iso-

†NCL Commun No 5389

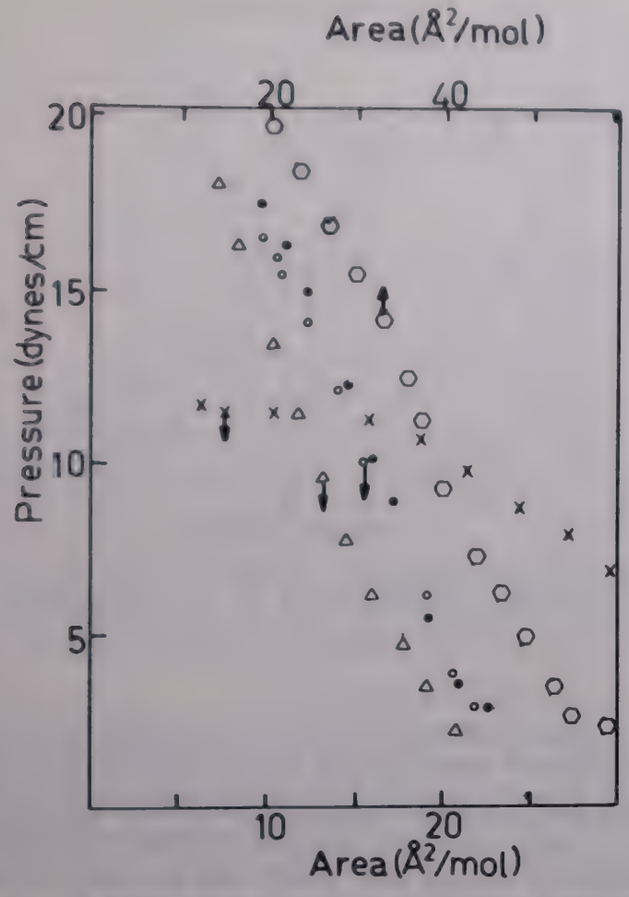


Fig. 1—π-A isotherms of $C_{60}$ (sample A) on water at *p*H ≈ 6.0 (open circles) and *p*H ≈ 3.0 (filled circles). The π-A siotherms obtained at *p*H ≈ 6.0 with sample B (triangles) and sample C (hexagons) of $C_{60}$ as well as with $C_{70}$ (crosses) are shown

therms for $C_{60}$ do not depend strongly on *p*H in the given range studied. The plot is very different from that reported by Obeng and bard[2]. Indeed the $C_{60}$ layer as spread by us is very unstable to pressure. This is what is actually expected for these molecules. Since $C_{60}$ molecules have only weak interactions between them the solid phase has orientational disorder[4] and behaves as a plastic crystal at room temperature. A truly solid phase at the air-water interfaced such as that obtained with fatty acids is not thus expected.

The limiting area as obtained from the extrapolation of the π-A isotherms at higher pressures to $\pi = 0$ was found to be sensitive to the preparation conditions of the $C_{60}$ molecule. We show in Fig. 1 the changes in the π-A isotherms as recorded for different samples of $C_{60}$ which did not show in the mass spectra evidence for contamination with other phases. It is apparent from the figure that the π-A isotherms would be superimposable on each other once they were normalised at some reference point. This could indicate either an error in the actual amount weighed in the sense that there could be considerable impurity in the $C_{60}$ sample. It could also be due to the presence of small amounts of impurities which are extremely surface specific. This has to be further investigated. The Raman spectra obtained by us are typical of $C_{60}$ and do not show the presence of other impurity phases (such as $C_{70}$) as we shall discuss later. The reflection electron energy loss as well as ESCA spectra of the several batches are identical in the *C*1s region[8].

The extrapolated π-A plots of samples A and B (circles and trinagles in Fig. 1) give limiting areas which are rather small being only about 20 Å²/mol. This is less than the area (~40 Å²) expected for the $C_{60}$ molecule which has a radius ~3.5 Å. The extrapolated area of ~20 Å² is thus suggestive of the formation of a $C_{60}$ bilayer. The rapid decrease in the area with increasing pressure would then be suggestive of multilayer formation. Sample C, on the other hand, gives a very large area (~60 Å² per mol) which is inconsistent with the area of $C_{60}$ molecule but is in the direction of the area obtained by Obeng and Bard[2].

Bard[2] has also given evidence to show that $C_{60}$ may be trapped in the hydrocarbon chains of arachidic acid ($C_{20}$) monolayer when $C_{60}$ and the acid is spread at the same time. Taking a cue from this observation we have studied the effect of the addition of quasi-globular hydrocarbon molecule such as *t*-butyl amine in the water subphase. This is expected to increase the interaction of $C_{60}$ with the subphase because of the possibility of the interaction with the hydrophobic alkyl groups of the molecule the concentration of which could increase at the air-water interface due to such an interaction[9]. Such an interaction could increase the surface pressure. The choice of the amine has been further dictated by the electronegative nature[10] of $C_{60}$ which accepts electrons in $K_3C_{60}$. Rao and cowerkers[11] have shown that $C_{60}$ forms stable complexes with amines.

There is a marked change in the π-A curves in the presence of *t*-butyl amine in water as shown in Fig. 2. The films are always unstable to pressures greater than 20 dynes/cm. The extrapolated area obtained from the π-A plot at *p*H 9.0 is now 40 Å² with sample-B, which is close to the area of $C_{60}$ molecule. Sample-C also shows a marked change in the π-A plot as can be seen in Fig. 2, so that the effect of *t*-butyl amine may be considered to be genuine.

The π-A plots in the presence of amine in the aqueous subphase are dependent on the *p*H as shown in Fig. 2 with sample A. The nature of the changes are consistent with the assumption that there is an interaction between $C_{60}$ and the free amine in the aqueous phase which stablises the

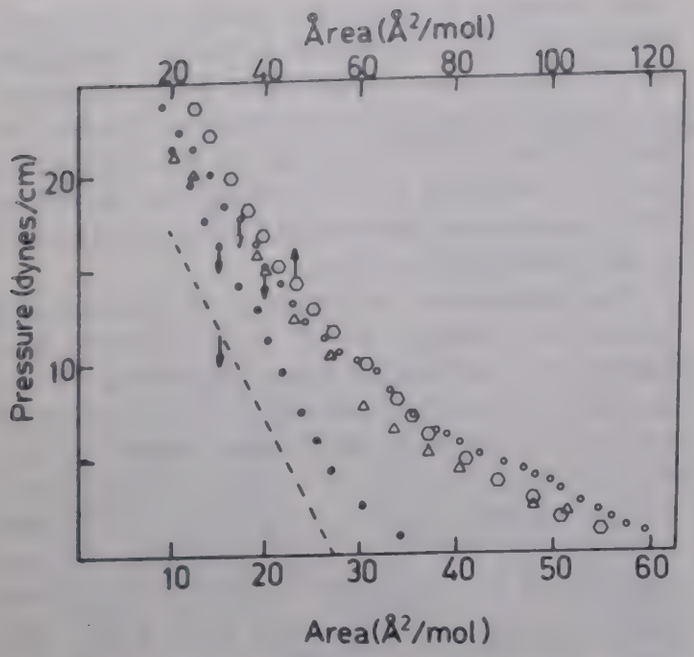


Fig. 2—π-A isotherms for $C_{60}$ (sample A, open circles) in the presence of *t*-butyl amine dissolved in water ($10^{-4}$ molar) at *p*H ≈ 9.0. Triangles represent the isotherm for $C_{60}$ obtained when both $C_{60}$ (sample A) and the amine were dissolved in benzene and then spread at *p*H ≈ 9.0. Filled circles is the isotherm obtained with sample A for a *p*H ≈ 3.0 with *t*-butyl amine being predissolved in water. The dashed line shows the isotherm obtained with pure water as shown in Fig. 1. Hexagons represent the isotherm obtained with sample C of $C_{60}$ in the precne of *t*-butyl amine dissolved in the subphase at *p*H ≈ 9.0

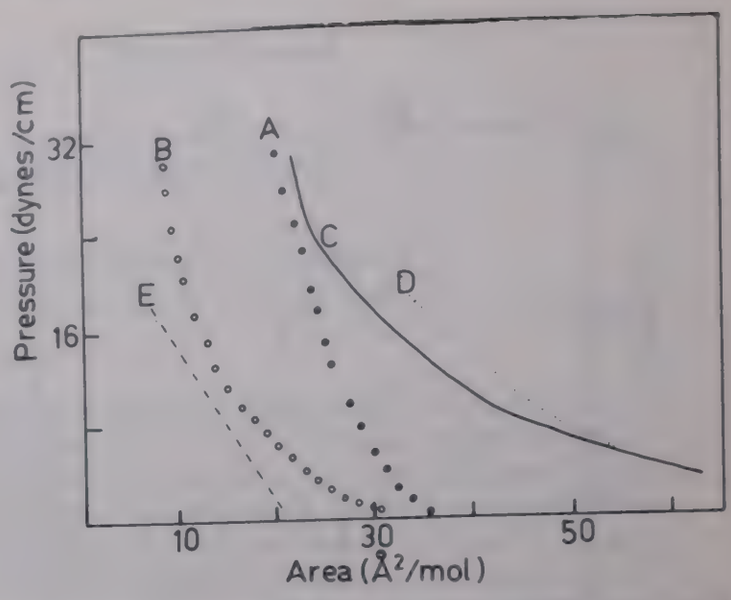


Fig. 3—π-A isotherms of $C_{60}$ spread along with *n*-octadecyl amine at the air-water interface as compared with that of pure $C_{60}$ (see text for details)

monolayer of $C_{60}$ at the interface. At lower *p*H the amine hydrochloride is formed which is more soluble in water thereby reducing the interaction with $C_{60}$ and thence the stability of the layer at the air-water interface. The pressure of the monolayer was not much changed when *t*-butanol was mixed in the subphase. The film was destabilised by *n*-butyl amine so that it seems that the globular nature as well as the presence of free amino group is necessary for the partial stabilisation of the $C_{60}$ layer.

In Fig. 3 we have shown the π-A isotherms of *n*-octadecyl amine spread on water at *p*H 6.0 (curve A) as well as that of *n*-octadecyl amine mixed with $C_{60}$ (sample a) in the ratio 60:40 with the area being calculated for the total number of molecules (curve B). Curve C is obtained when curve B is replotted in terms of the area per mole of $C_{60}$. Curve D is obtained when the π-A isotherm of pure $C_{60}$ (dashed line) is added to that of curve C to give a total ratio of 40:60 between $C_{60}$ and *n*-octadecyl amine. We see that curve C is a composite of $C_{60}$ and *n*-octadecyl amine at low pressures and that at high pressures the $C_{60}$ component is not seen and only the amine component is able to withstand the pressure. These results are again in conflict with that reported by Obeng and Bard[2] who studied the mixture of arachidic acid and $C_{60}$ and found that $C_{60}$ stabilised the layer of arachidic acid. We have repeated the experiments of Obeng and Bard[2] and do not obtain a considerable change in the π-A isotherm of arachidic acid in the presence of $C_{60}$. Our results are, however, more consistent with the reported properties of $C_{60}$. These results suggest that $C_{60}$ does not form a complex with the hydrocarbon end of octadecyl amine present at the air-water interface. The expanded film kind of structure shown by curve C relative to that of curve A is consistent with the presence of an interaction between $C_{60}$ and the $-NH_2$ group of *n*-octadecyl amine. Apparently the $C_{60}$ molecule does not interact with the $-COOH$ group of arachidic acid at the interface.

We have tried to pick up the $C_{60}$ layers at the air-water interface as LB films. We find that the films are patchy and have a yellowish colour as reported by Obeng and Bard[2]. The Raman spectra from the LB films obtained from sample A have been taken for the first time. The Raman band characteristic[12] of $C_{60}$ is seen for the films (Fig. 4a and 4b) albeit shifted slightly to lower frequencies by about 5 $cm^{-1}$ in the case of our films. This shift is not an artefact of the measurement. It has to be investigated whether the shift is due to the small thickness of the films (~200 Å) so that the orientational melting is dominant and reduces cohesive interactions between the $C_{60}$ molecules in the film.

The films picked up from the $C_{60}$ layers at the air-water (*t*-butyl amine) subphase show very

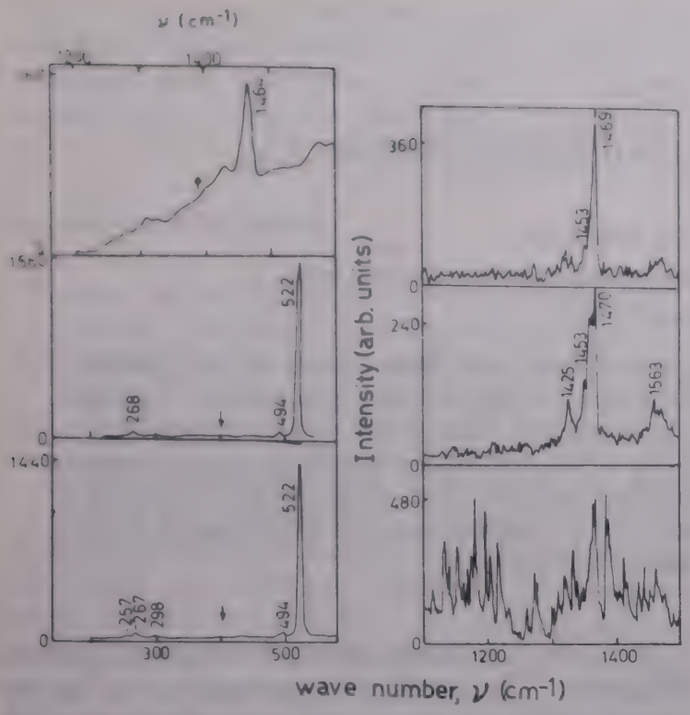


**Fig. 4—Raman spectra of$C_{60}$ films picked up (a) and (b) from the air-water interface. (c)-(f) from air-water (*n*-octadecyl amine) interface. (a)-(d) spectra were taken at 400 mW and slow scan rate of 10 sec per cycle; (e) 200 mW and 10 sec/scan; (f) 200 mW and 1 sec/scan, (see text for more details)**

complex Raman spectra (Fig. 4d) when high powers and long scan times are used. The complex spectra are probably due to transitions in new photoreaction species of $C_{60}$. When the spectraum is taken at 200 mW and at the same scan rate the features (Fig. 4e) being to resemble more the features of $C_{60}$ although the main line (at ~ 1470 $cm^{-1}$) is split. An important feature is the appearance of a band at 1570 $cm^{-1}$ which is usually associated with $C_{70}$. The spectra taken at 200 mW and at a faster scan rate (1 sec per cycle) show sharp features more typical of $C_{60}$ with a relative diminution of the intensity of the band at 1570 $cm^{-1}$. This would suggest that $C_{70}$, if present at all, is not an initial contaminant. This films picked up from the air-pure water interface also show the pure $C_{60}$ Raman lines (Fig. 4b) while those picked up from the air-water (*t*-butyl amine) interface show more lines (Fig. 4c). Preliminary XPS studies show no evidence for the presence of hydrogenated carbons or nitrogen in the films. The reasons for the peculiar Raman sensitivity requires further investigation.

**Acknowledgement**

The authors thanks Prof. C N R Rao for the sample of $C_{60}$.

**References**

1 (a) Kroto H W, Heath J R, O'Brien S C, Curl R F & Smalley R E, *Nature (London)*, 318 (1985) 162.
(b) Kroto H W, *Nature (London)*, 329 (1987) 529.
(c) Hare J P, Kroto H W & taylor R, *Chem Phys Lett*, 177(4,5) (1991) 394.
(d) Kratschmer W, Lamb L D, Fostiropolour K & Huffman D R, *Nature (London)*, 47 (1990) 354.
2 Obeng Y S & Bard A J, *J Am chem Soc*, 113 (1991) 6279.
3 Hawkins J M, Meyer A, Lewis T A, Loren S & Hollander F J, *Science*, 252 (1991) 312.
4 Heiney P A, Fischer J E, McGhie A R, Romanov W J, Demenstein A M, McCauley(Jr) J P, Smith III A M & Cox D E, *Phys Rev Lett*, 66 (1991) 2911.
5 Pradip T, D'Souza V, Krishnan V & Rao C N R, *Proc Indian Acad Sci (Chem Sci)*, 103 (1991) 68.
6 Katti S S, Kulkarni M G & Paranjape D V, *J Surface Sci Technol*, 6(6) (1990) 317.
7 Sastry M, Ganguly P, Badrinarayan S, Mandale A B, Sainkar S R, Paranjape D V, Patil K R & Chaudhari S K, *J chem Phys*, 95 (1991) 8631.
8 Sastry M (unpublished results).
9 Shin S & Stuart Rice A, *J chem Phys*, 93 (1990) 5247; Cai Z & Stuart Rice A, *J chem Phys*, 90 (1989) 6717.
10 Stephens P W, Mihaly L, Lee P L, Whetten R L, Huang S, Kaner R, Deidrich F & Holczer K, *Nature (London)*, 351 (1991) 632.
11 Rao C N R Pradeep T, Seshadri R & Govindaraj A, *Indian J Chem*, 31 (1992) F27.
12 Bethune D S, Meijer G, Tang W C & Rosen H J, *Chem Phys Lett*, 174 (1990) 219.

Indian Journal of Chemistry
Vol. 31 A&B, May 1992, pp. F46-F50

# Photophysical studies on buckminsterfullerene: $C_{60}$

D K Palit, A V Sapre & J P Mittal*
Chemistry Division, Bhabha Atomic Research Centre, Bombay 400 085, India

Received 20 February 1992

Picosecond and nanosecond laser flash photolysis experiments have been carried out on buckminsterfullerene $C_{60}$ in solution phase. $S_0 \rightarrow S_n^*$ and $T_1^* \rightarrow T_n^*$ absorption spectra have been studied. The singlet state lifetimes for $C_{60}$ are found to be 1.3, 1.5, 1.6 ns in benzene, toluene and *n*-hexane respectively. The $T_1^* \rightarrow T_n^*$ absorption spectrum of $C_{60}$ is blue shifted by 10 nm in the entire spectrum range in hexane as compared to benzene solutions. At the low laser intensities used the triplet decays by first order with a rate constant of $2.1 \times 10^4$ $s^{-1}$ in benzene. Contributions from T-T anihilations and triplet-singlet ground state reactions are discussed. The work done so far in this area is discussed.

## Introduction

The recently discovered all carbon hollow spheroidal shell-structured clusters, called fullerenes have captured the imagination of both experimental as well as theoretical scientists[1]. The cluster consisting of sixty carbon atoms $C_{60}$ also known as buckminsterfullerene, after the inventor of the geodesic dome, the structure which this molecule possesses, is regarded as the third allotrope of carbon. Although identified first by Smalley and coworkers[2] in the cluster beam produced by laser ablation of graphite, the research on this exotic molecule has been speeded up by discovery of an easy method to prepare and separate macroscopic quantities of $C_{60}$ as solid crystals and in solution form[3] from soot. Several studies have been carried out to characterise the basic properties of $C_{60}$ by techniques like NMR, photoelectron spectroscopy, mass spectroscopy, ground state absorption spectroscopy, magnetic circular dichroism etc. in condensed phase[4-8]. Buckminsterfullerene should possess interesting photophysical properties since it has a hollow truncated icosahedral cage type of structure in which all the carbon atoms are connected to each other by $sp^2$ and pi bonds which gives rise to the three dimensional aromaticity[1]. The X-ray and C-13 NMR spectra exhibiting a single resonance line confirmed this type of structure for $C_{60}$. The present work was undertaken to investigate some of the interesting properties of $C_{60}$ using nanosecond and picosecond laser flash photolysis techniques and in this communication we present some of our recent data and their comparison with those from other laboratories.

## Materials and Methods

Pure $C_{60}$ samples were kindly provided by Prof. C.N.R. Rao, Director, Indian Institute of Science, Bangalore. The details of preparation, etc. are reported[9]. All the solvents used were of spectroscopic grade. Nanosecond laser flash photolysis studies were carried out on a Laser Kinetic Spectrometer (Applied Photophysics, UK) using either KrF excimer laser (248 nm, 100 mJ, 10 ns) or nitrogen laser (337 nm, 1.5 mJ, 0.6 ns) as excitation source[10]. The transient optical absorptions were monitored using 300 W pulsed Xe lamp, f/3.4 monochromator, R-928 photomultiplier and Gould-Biomation 4500 digital oscilloscope. The signals were processed on PDP 11/23 computer and plotted on HP 7470 plotter.

Picosecond flash photolysis unit is similar to that of Ebbesen[11] and is described elsewhere in details[12]. Briefly, a pulse mode locked Nd-YAG laser (Continuum USA model 501-C-10) giving 35 ps pulses with Kodak dye 1 is used for excitation after frequency doubling (532 nm), tripling (355 nm) and quadrupling (266 nm). The transient species generated were probed by an analysing white light continuum (range 400-900 nm) produced by focussing the residual laser fundamental at 1064 nm on to a cell of $H_2O$:$D_2O$ (50-50%). The arrival of the probe pulses at the sample cell were delayed by using a combination of different lengths of optical fibers (core dia 200 μ) and home made delay rail, giving a continuous delay variation in the 0-4200 psec range. The probe light is bifurcated in two parts (50-50%) by a fibre optic beam splitter (canstar), one part of which passes through the laser irradiation zone and the other is used as reference. Both these beams are then dispersed through a spectrograph (Acton) and monitored by an Optical Spectroscopic Multichannel Analyser System (Spectroscopy Instruments, Ger-

many) consisting of a dual diode array, ST 180 controller and analysed by HP Vectra ES12 computer.

Ground state absorption spectra were recorded on Shimazdu model UV 160A double beam spectrophotometer.

## Results and Discussion

*Electronic absorption spectra in the ground state*

Hare and coworkers[13] first reported the UV-visible spectrum of chromatographically separated $C_{60}$ in *n*-hexane. The wavelength maxima for $C_{60}$ and their molar extinction coefficients are given in Table 1. The UV absorption bands show solvent red shifts in polar solvents indicating an increase in the dipole moment on excitation. Red shifts for 328 nm band in acetonitrile and dimethyl sulfoxide solvents are reported to be 92 and 278 $cm^{-1}$ respectively with respect to *n*-hexane[9]. The transitions are $\pi \rightarrow \pi^*$ type, typical of aromatic molecules. The low $\varepsilon$ value of $< 750$ $dm^3\ mol^{-1}\ cm^{-1}$ for the absorption band between 490-620 nm is probably due to $S_0 \rightarrow S_1^*$ transition of $C_{60}$ which is strongly forbidden[13].

Recently, Gasyna *et al.*[14] have studied the magnetic circular dichroism and the absorption spectra of $C_{60}$ isolated in Argon matrices and proposed detailed assignments for the observed well resolved spectral lines. The most intense UV bands at 208, 253 and 326 nm arise out of the dipole allowed transitions $^1A_g \rightarrow {}^1T_{1u}$ of $C_{60}$ which belong to the point group $I_h$. Shoulders observed at 225 and 295 nm in Argon matrices arise out of $^1A_g \rightarrow {}^3T_{1u}$ transition. Sharp but weak vibronic structure in the 400-600 nm region shows clear evidence for the Jahn-Teller activity. The sharp features near 404 nm, 420-580 nm, and near 600 nm result from dipole forbidden $^1A_g \rightarrow {}^1T_{2u}$ and $^1A_g \rightarrow {}^1T_{1g}$ transitions. Detailed Jahn-Teller assignments for the vibronic bands are given by the authors and are in reasonable agreement with the theoretical calculations of Negri *et al.*[15]. The frequencies in the argon matrices are blue shifted by $\sim 180$ $cm^{-1}$ as compared to those in hydrocarbon solvents in the region 580-650 nm. The spin orbit coupling is expected to be unusually large in $C_{60}$ and hence significant intensity to the $^3T_{1u}$ states is predicted. A weak triplet absorption in the region 630-680 nm is reported[16].

Table 1—Photophysical properties of buckminsterfullerene $C_{60}$

*Electronic absorption spectrum in the ground state* (*ref.* 13)

| $\lambda_{max}$ (nm) | 231 | 257 | 329 | 404 | 440-670 |
|---|---|---|---|---|---|
| $\varepsilon$ ($dm^3 mol^{-1} cm^{-1}$) | 135000 | 175000 | 51000 | | $< 750$ |

*Singlet singlet absorption spectrum* (*ref.* 22)

| $\lambda_{max}$ (nm) | 513 | 759 | 885 |
|---|---|---|---|
| $\varepsilon$ ($dm^3 mol^{-1} cm^{-1}$) | 5400 | 3700 | 6300 |

*Triplet triplet absorption spectrum* (*ref.* 22)

| $\lambda_{max}$ (nm) | 457 | 509 | 747 |
|---|---|---|---|
| $\varepsilon$ ($dm^3 mol^{-1} cm^{-1}$) | 3400 | 3000 | 15000 |

| | | |
|---|---|---|
| *Singlet energy* | 46.1 kcal $mol^{-1}$ | (ref. 18) |
| *Triplet energy* | 37.5 kcal $mol^{-1}$ | (ref. 18) |
| *Ionization energy* | $7.61 \pm 0.02$ eV | (ref. 5) |
| *Electron affinity* | 2.6-2.8 eV | (ref. 8) |
| *Reduction potential* | $-0.61$ V | (ref. 28) |

*Singlet decay rate constants* ($s^{-1}$): $3 \times 10^{10}$ (ref. 21)
$8.3 \times 10^8$ [22], $1.5 \times 10^9$ [23], $7.2 \times 10^8$ (this work)

*Triplet decay constants*: $2.1 \times 10^4$ $s^{-1}$

*T-T anihilation rate constants*: $2.3 \times 10^9$ $dm^3\ mol^{-1} cm^{-1}$

T-$S_0$ reaction rate constant $2 \times 10^8$ $dm^3\ mol^{-1} cm^{-1}$ (this work)

*Excited state dynamics*

Figure 1 gives the absorption spectrum for the singlet-singlet ($S_0 \rightarrow S_n^*$) transition of $C_{60}$ in toluene, excited at 355 nm obtained at a delay of 0 ps in our laboratory.

$$C_{60}(S_0) \xrightarrow[355\ nm\ (pump)]{} C_{60}(S_1^*) \quad \ldots (1)$$

$$C_{60}(S_1^*) \xrightarrow[probe\ light]{} C_{60}(S_n^*) \quad \ldots (2)$$

The absorption spectrum changes with time and after a delay of 4000 psec, we obtain another spectrum with $\lambda_{max} = 745$ nm (Fig. 1). The reduction of absorbance at 745 nm by oxygen, its sensitisation by anthracene triplet and sensitisation of $\beta$-carotene triplet by $C_{60}$ suggest and confirm that the 745 absorption band is due to the triplet-triplet absorption

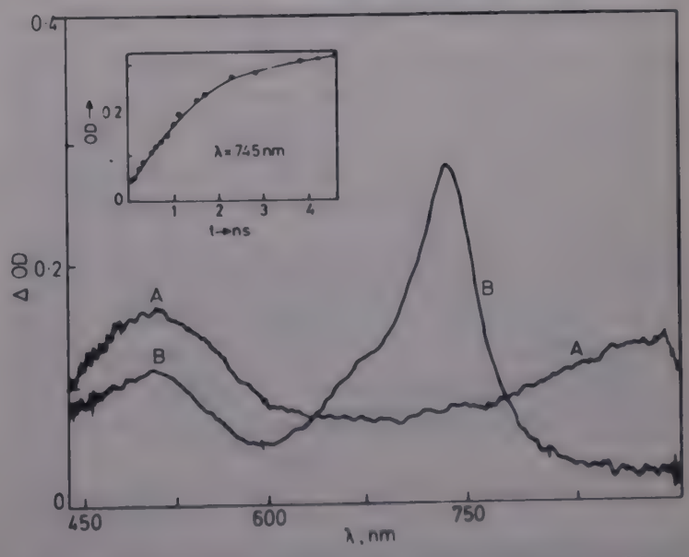


Fig. 1—Transient absorption spectra of $C_{60}$ in toluene on 355 nm excitation ($N_2$ purged) [A: At zero ps delay, B: At 4000 psec delay. Inset: rise of the triplet absorption at 745 nm as a function of time].

$(T_1^* \rightarrow T_n^*)$ of $C_{60}$. Thus $C_{60}$ singlet undergoes fast intersystem crossing (ISC) to give triplet during this time scale.

$$C_{60}(S_1^*) \xrightarrow{\text{ISC}} C_{60}(T_1^*) \quad \ldots (3)$$

$$C_{60}(T_1^*) \xrightarrow[\text{probe light}]{} C_{60}(T_n^*) \quad \ldots (4)$$

The triplet-triplet absorption also appears on excitation of $C_{60}$ using 248 nm excimer or 337 nm $N_2$ laser. The T-T absorption spectra obtained in benzene and *n*-hexane are shown in Fig. 2. In the entire spectral region the absorption is blue shifted by ~ 10 nm in hexane as compared to that in benzene. The decay of triplet absorption in benzene and its first order fit are given in Fig. 3A and 3B. The first order decay rate constant is found to be $2.1 \times 10^4\ s^{-1}$. On 308 nm excimer laser photolysis, Kajii *et al.* found that triplet is the only transient species detectable after 10 ns. They measured triplet life time of 49 μs in air-free benzene[17]. From the quenching of the 745 nm band by air and oxygen the rate constant for the oxygen quenching is estimated to be $1.2 \times 10^9\ dm^3\ mol^{-1}\ s^{-1}$ which compares well with that obtained by Abrogast *et al.*[18] and also with the quenching of aromatic triplets by oxygen[19].

The energy level of the triplet was determined by T-T energy transfer[18] and photoacoustic colorimetry[19] to be $37.5 \pm 4.5$ kcal and the singlet energy being 46.1 kcal. The splitting between singlet and triplet energies is small ( ~ 9 kcal) and is probably due to large molecular diameter of $C_{60}$ and resulting small electron-electron repulsion energy[18]. The ISC efficiency is good—nearly unity as measured by us in comparison with the yields of anthracene triplets under identical conditions. This result matches well with that from other groups[22].

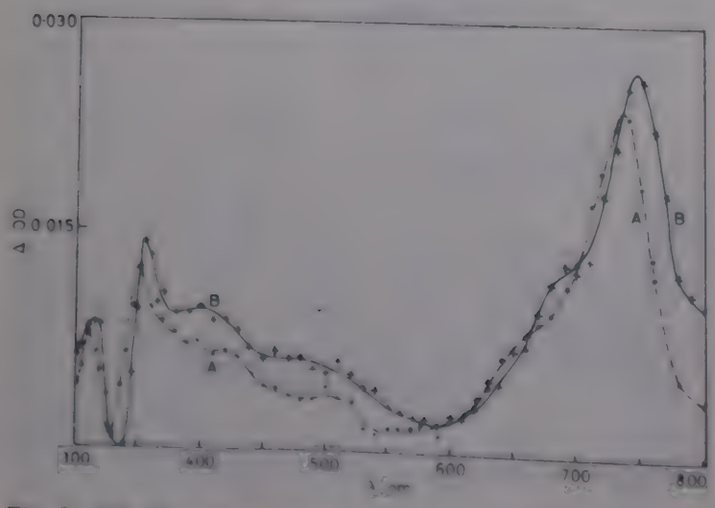


Fig. 2—T-T absorption spectra of $C_{60}$ in benzene (— × —) and hexane (● - ● - ●) solutions (337 nm excitation at 400 ns) ($N_2$ purged)

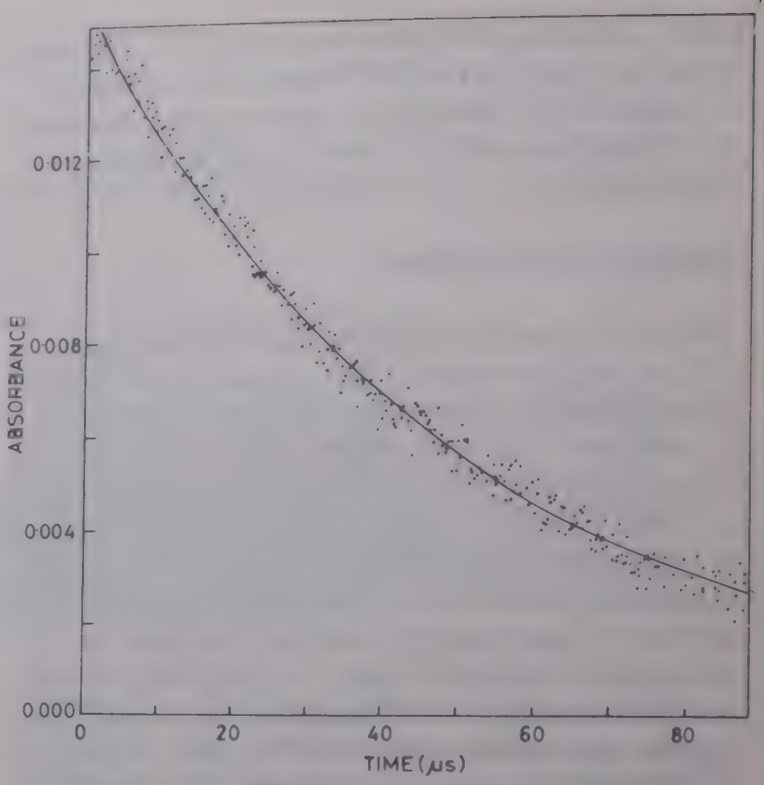


Fig. 3(A)—Decay of $C_{60}$ triplet absorption in benzene solutions at 745 nm.

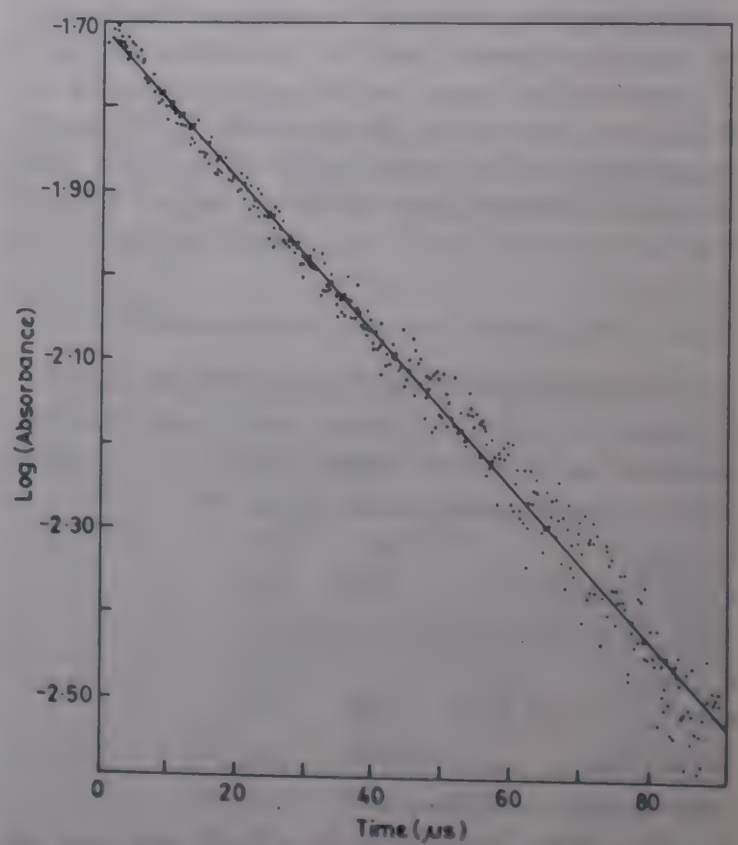


Fig. 3(B)—First order fit for the curve A. [.... experimental points; ——calculated fit]

The singlet state decay cannot be monitored by following the singlet absorption since the triplet also absorbs in the same region. However, the growth of the triplet absorption at 745 nm can be monitored to obtain the singlet decay rates (shown in inset in Fig. 1). From our present studies we estimate singlet

state life times of 1300, 1500 and 1600 psec (±50 psec) for $C_{60}$ in benzene, toluene and *n*-hexane. However, in literature varying values are reported, e.g., Wasielewski *et al.*[21] report 33 ps, Ebbesen's group reports[22] 1300 ps and Hochstrasser's group reports[23] 650 ps in toluene as solvent. Our results match with those of Ebbesen *et al.* The $C_{60}$ triplet decays by a first order at low concentrations with typical lifetimes[17] of 48 μs, whereas at higher concentrations triplet-triplet anihilation becomes significant (process 6)

$$C_{60}(T^*) \longrightarrow C_{60}(\text{radiative} + \text{nonradiative}) \quad \ldots (5)$$

$$C_{60}(T^*) + C_{60}(T^*) \longrightarrow 2\ C_{60} \quad \ldots (6)$$

We obtained the first order decay constants for process 5 as $k = 2.1 \times 10^4\ s^{-1}$ and $2.3 \times 10^9\ dm^3\ mol^{-1}\ s^{-1}$ for the process 6 in hexane solutions excited at 248 nm. This result is in agreement with those of Ebbesen *et al.*[22] and Kajii *et al.*[17]. Under conditions where $C_{60}$ concentration is fairly large, as Ebbesen *et al.* point out the reaction of $C_{60}$ triplet with ground state becomes significant (process 7).

$$C_{60}(T^*) + C_{60}(S_0) \longrightarrow 2\ C_{60} \quad \ldots (7)$$

Under the conditions where $C_{60}$ concentrations are larger as required in pulse radiolysis experiments[24] the quenching of triplet by ground state $C_{60}$ was found by us to be significant and a rate constant of $2 \times 10^8\ dm^3\ mol^{-1}\ s^{-1}$ was measured for the same.

Various values for the molar extinction coefficients for the 745 nm band have been reported, e.g., the Japanese group of Ebbesen *et al.*[22] report 15000 $dm^3\ mol^{-1}\ cm^{-1}$, Hochstrasser's group reports 7000 $dm^3\ mol^{-1}\ cm^{-1}$ (assuming triplet yield of 1) while we obtain a value of 11200 $dm^3\ mol^{-1}\ cm^{-1}$ in benzene.

*Fluorescence and phosphorescence of $C_{60}$*

Although the ISC yield in $C_{60}$ is very high, no phosphorescence from $C_{60}$ is yet reported. Similarly fluorescence yields are reported to be small[23]: $2 \times 10^{-4}/g_u$ where $g_u$ is the degeneracy and is probably 1-3 for the emitting state of $C_{60}$. Reber *et al.*[24] report fluorescence in the range 700-1100 nm from thin films of $C_{60}$ vacuum deposited on $CaF_2$. The emission has considerable vibronic structure.

*Quenching of $C_{60}$ triplets by $O_2$ and generation of singlet oxygen*

$C_{60}$ is a potent generator of singlet oxygen (reaction 8) as measured by the emission of the latter at 1260 nm (ref. 18).

$$C_{60}\ (T_1) + O_2\ (^3\Sigma_u^-) \rightarrow C_{60}(S_0) + O_2(^1\Delta g) \quad \ldots (8)$$

The quantum yield for the singlet oxygen production is 0.76 at 355 nm and 0.95 at 532 nm. The difference in the yield for singlet oxygen is possibly due to the fact that the higher singlet states of $C_{60}$ may be connected up with other channels of deactivation which compete with ISC. $C_{60}$ also quenches the singlet oxygen as indicated by the shortening of its life time and a rate constant of $5 \times 10^5\ dm^3\ mol^{-1}\ s^{-1}$ is measured for the quenching. The mechanism of the quenching is not known. The high singlet oxygen yield coupled with the inertness of $C_{60}$ towards photooxidative degradation suggests a strong potential for photodynamic damage to biological systems. Thus, $C_{60}$ must be handled with care and the presence of $C_{60}$ in the environment is a matter of concern.

*Photostability*

Taylor *et al.* reported that the $C_{60}$ solutions are very photosensitive. Exposing $C_{60}$ solutions in hexane to UV radiation in the presence of $O_2$ resulted in the addition of both H and O to $C_{60}$ and fragmentation of the fullerene cage[26]. Arbogast and Foote, however, report that on exposing benzene solutions of $C_{60}$ in the presence of $O_2$ to 300 W Xe light for several hours no significant decomposition occurs[27]. They observe that $C_{60}$ is more unstable towards light as compared with $C_{60}$. This factor needs careful study.

*Charge transfer interactions*

Because of the aromatic character of $C_{60}$, its good electron affinity and reduction potential, charge and electron transfer reactions are expected to proceed smoothly. Further, it is important to known the role played by reduced form of $C_{60}$ for obtaining better superconductors. No evidence of interaction of $C_{60}$ with electron acceptors like $I_2$, 1, 3,5-trinitrorobenzene, perylene, TMPD, tetracyanobenzene was found[9]. Weak ground state complexation between $C_{60}$ and N,N-dimethylaniline (DMA) is found by Hochstrasser's group. On exciting the CT band at 624 nm they find an absorption due to an ion pair: $\overset{+}{DMA}\ C_{60}^-$ in 1-2 ps which shifts to a stronger absorption in the 800-1100 nm region due to the anion of $C_{60}$. Charge recombination was observed in the time region of 20 ps for neat DMA and 55 ps for DMA in toluene[28]. These authors conclude that there are strong solvation effects which need further study.

**Conclusions**

Although gross features of the photophysics of buckminsterfullerene are now known, the details of various parameters like singlet state life times, absorptivities, photostability, etc., are contradictory.

Despite the unusual structure and symmetry of this exotic molecule, the photophysical properties studied so far do not present special features of this super-aromatic molecule. An alarming aspect of these studies is the sensitisation of singlet oxygen by excited states of $C_{60}$. However, the knowledge of the fundamental photophysical and photochemical properties will prove useful in understanding the chemistry and the applications of the new class of compounds.

**Acknowledgement**

The authors thank Prof. C.N.R. Rao, IISc, Bangalore, for providing pure samples of $C_{60}$. We are indebted to Dr T.W. Ebbesen, NEC Corporation, Japan for advice on our picosecond flash photolysis setup.

**References**

1 Kroto H W, Alaf A W & Balm S P, *Chem Revs*, 91 (1991) 1213.
2 Kroto H W, Heath J P, O'Brien S C, Curl R F & Smalley R E, *Nature (London)*, 318 (1985) 162.
3 Kratschmer W, Lamb L D, Fostiropolous K & Huffman D R, *Nature (London)*, 347 (1990) 354.
4 Tycko R, Haddon R C, Dabbagh G, Glarum S H, Douglass D C & Mussjee A M, *J phys Chem*, 95 (1991) 518.
5 Lichtenburger D L, Nebesny K W, Ray C D, Huffman D R & Lamb L D, *Chem Phys Lett*, 176 (1991) 203.
6 Bethune D I, Meijer G, Tang W C & Rosen H J, *Chem Phys Lett*, 174 (1990) 219.
7 Ajie H, Alvarez M M, Anz S J, Beck R D, Diederich F, Fostiropolous K, Huffman D R, Kratschmer W, Rubin Y, Schriver K E, Sensharma D & Whetten R L, *J phys Chem*, 94 (1991) 8030.
8 Yang S H, Pettiette C L, Conceicao J, Cheshnovsky O & Smalley R E, *Chem Phys Lett*, 139 (1987) 233.
9 Pradeep T, D'Souza F, Subbanna G N, Krishnan V & Rao C N R, *Proc Indian Acad Sci (Chem Sci)*, 103 (1991) 685.
10 Palit D K, Pal H, Mukherjee T & Mittal J P, *Photochem*, 37 (1957) 95.
11 Ebbesen T W, *Rev Sci Instr*, 59 (1988) 1307.
12 Palit D K, Sapre A V & Mittal J P (Communicated).
13 Hare J P, Kroto H W & Taylor R, *Chem Phys Lett*, 177 (1991) 374.
14 Gasyna Z, Schatz P N, Hare J P, Dennis T J, Kroto H W, Taylor R & Walton D R M, *Chem Phys Lett*, 183 (1991) 283.
15 Negri T, Orlandi G & Zerbetto F, *Chem Phys Lett*, 144 (1988) 31.
16 Leach S, Vervloet M, Despres A, Broherer E, Hare J P, Denis T J, Kroto H W, Taylor R & Walton D R M, unpublished work, as quoted in ref. 14.
17 Kajii Y, Nakagawa T, Suzuki S, Achiba Y, Obi K & Shibuya K, *Chem Phys Lett*, 181 (1991) 100.
18 Arbogast J W, Darmanyan A O, Foote C S, Rubin Y, Diederich F N, Alvarez M M, Anz S J & Whetten R L, *J Phys Chem*, 95 (1991) 11.
19 Murov S L, *Handbook of photochemistry* (Marcel Dekker, New York), 1973.
20 Hung R R & Grbowski J J, *J phys Chem*, 95 (1991) 6073.
21 Wasielewski M R, O'Neil M P, Lykke K R, Pellin M J, Gruen D M, *J Am chem Soc*, 113 (1991) 2774.
22 Ebbesen T W, Tanigaki K & Kuroshima S, *Chem Phys Lett*, 181 (1991) 501.
23 Sension R J, Phillips C M, Szarka A Z, Romanow W J, McGhie A R, McCauley J P Jr, Smith (III) A B & Hochstrasser R M, *J phys Chem*, 95 (1991) 6075.
24 Mohan H, Palit D K, Maiti D K & Mittal J P (communicated)
25 Reber C, Lee L, McKiernan J, Zink J I & Stanley Williams R, *J phys Chem*, 95 (1991) 2127.
26 Taylor R, Parson J P, Avent A G, Rannard S R, Dennis T, Hare J P, Kroto H W & Walton D R M, *Nature (London)*, 351 (1991) 277.
27 Abrogast J W & Foote C S, *J Am chem Soc*, 113 (1991) 8886.
28 Sension R J, Szarka A Z, Smith G P & Hochstrasser R M, *Chem Phys Lett*, 185 (1991) 179.

Indian Journal of Chemistry
Vol. 31 A&B, May 1992, pp. F51-F55

# Simple structural and bonding representations of fullerenes

A Rathna & J Chandrasekhar*
Department of Organic Chemistry, Indian Institute of Science, Bangalore 560 012

Received 20 February 1992

Bonding in buckminsterfullerene, $C_{60}$, can be described in terms of a unique canonical representation in which all six membered rings have a benzenoid Kekule structure while the pentagons are all made of exclusively single bonds. The corresponding valence bond structure reflects the full symmetry of the molecule and is consistent with the observed bond length variations. Computational support for the bonding description is provided using localized MO's obtained at the MNDO level. The requirement of benzenoid structures for all the hexagons can be used as a criterion of stability of fullerenes which complements the pentagon isolation rule. A convenient two-dimensional representation of the fullerene structures incorporating the above bonding description is suggested, especially for use in mechanistic discussions.

The first report[1] of the mass spectral characterisation of a sixty carbon cluster along with the remarkable structural proposal derived from the geodesic dome of Buckminster Fuller (**1**) immediately attracted the attention of numerous theoretical chemists[2]. The intriguing question concerning the nature of bonding in the truncated icosahedral framework was the focus of many of these studies. Simple valence rules can be satisfied if all the carbon atoms of $C_{60}$ are considered to be uniformly $sp^2$ hybridized, with 60 $p$ orbitals of pseudo $\pi$ symmetry participating in a three-dimensional aromatic interaction. Effectively, 60 electrons are delocalized over the surface of the spheroidal molecule. In fact, the free electron model[3] reproduced the essential features of the electronic structure of the molecule, viz., the symmetry and the associated degeneracy of all the molecular orbitals. Huckel calculations confirmed the pattern[4], while more sophisticated methods like the INDO[5], PRDDO[6], MNDO[2,7] AM1[8], and ab initio[8a,9] procedures provided additional details. These calculations led to reliable structural and spectral parameters, in particular those associated with vibrational, electronic and photoelectron spectra. Many of these insights were obtained even before the recent explosion of activity involving the fullerenes following the development of simpler procedures for their synthesis and experimental study[10].

While the theoretical results mentioned above have been quite useful, a simpler representation of the structure and bonding of fullerenes is probably of greater value, especially for understanding their reactivity patterns. The formation of new bonds and the reorganisation of existing bonds in these compounds following a chemical reaction are rather difficult to visualize at present within the delocalized bonding models. For example, the mechanistic details of a reaction such as the Birch reduction of $C_{60}$ appear complicated, while the corresponding information for a typical aromatic molecule is textbook material. In this paper, we consider a simple approach based on localized molecular orbitals for understanding the structure, stability and reactivity of fullerenes. We discuss previous studies employing related concepts and also provide additional details.

## Computational details

The standard MOPAC package[11] was implemented on a CYBER 992 computer and enhanced to handle molecules containing more than 60 non-hydrogen atoms. Using this program, the geometry of $C_{60}$ was fully optimized imposing $I_h$ symmetry at the MNDO level. The wave functions were successively transformed until a set of localized molecular orbitals was obtained[12]. The default criteria for localization built in the program was used without modification. Convergence occurred in 48 cycles.

A modified version of Jorgensen's program[13], installed on the VAX 8810 computer, was employed to plot the contours of the MNDO localized wave functions. The PERGRA program[14], developed for a PC, was also used to pictorially represent the relative coefficients of the AO's in the various types of localized molecular orbitals.

## Results and Discussion

A convenient starting point for understanding the bonding in $C_{60}$ is provided by the experimental and computed structural parameters of this molecule (Table 1). Many of the more quantitative

theoretical methods clearly predict the presence of bond alternancy in $C_{60}$. The bond shared by two hexagons (6-6) is relatively short, while the common bond between a hexagon and a pentagon (6-5) is long. NMR studies[15] and the more recent neutron[16], X-ray[17] and electron diffraction[18] results also confirm that there are effectively two types of bond lengths in $C_{60}$. A range of distances is observed in the solid state, due to intermolecular interactions[16,17]. However, the general pattern follows the calculated data, which refer to the gas phase.

The bond length variations suggest the presence of alternating single and double bonds in $C_{60}$. The computed bond orders reflect the changes in lengths. A linear muffin-tin orbitals (LMTO) calculation gave bond orders of 1.54 and 1.41, respectively for the 6-6 and the 6-5 bonds[19]. The corresponding values computed by us at the MNDO level (1.51 and 1.10) show a larger difference. This is also reflected in the greater degree of bond alternancy obtained at this theoretical level (Table 1).

In addition to bond orders, another criterion can be used to qualify the differences in the nature of bonds in a molecule. The individual molecular orbitals can be transformed into localized orbitals leaving the total wave function unchanged. Although the nature of the transformed MO's sometimes depend on the localization procedure employed, especially in polycyclic aromatic compounds and three-dimensional polyhedral boron hydrides[20], the results are quite instructive. A previous study using the Boys method of maximising the sum of squares of orbital centroids at the PRDDO level showed that the MO's of $C_{60}$ can be localized as efficiently as in benzene[6]. The calculations led to three types of localized bonds in $C_{60}$, viz., a well defined 6-5 σ bond and a pair of τ bonds. The latter correspond to a bent bond representation of the 6-6 double bond. The pyramidality at carbon makes the two τ bonds non-equivalent. The nature of hybridization of the three unique bonds were compared with the corresponding data obtained for benzene at the same theoretical level[6].

The localized bonds obtained in the present study using MNDO wave functions correspond to an even simpler bonding description. Again, three unique types of localized MO's were obtained. The orbital contour diagrams (Fig. 1) clearly indicate that one of them is the 6-5 σ bond found in the earlier study. However, the 6-6 double bond appears as a σ bond and a pseudo π bond, rather than as a pair of τ bonds. An alternative pictorial representation of these orbitals which reflects the relative atomic orbital coefficients and

Table 1—Calculated and experimental bond lengths (Å) in $C_{60}$

| Method : | $r_1$ | $r_2$ | Reference |
|---|---|---|---|
| | 6-6 | 6-5 | |
| | Calculated | | |
| MNDO : | 1.400 | 1.474 | 2,7 |
| AM1 : | 1.385 | 1.464 | 8 |
| PRDDO : | 1.360 | 1.436 | 6 |
| LMTO : | 1.410 | 1.440 | 19 |
| HF/STO-3G : | 1.376 | 1.463 | 8a,9a |
| HF/DZ : | 1.368 | 1.451 | 9b |
| HF/DZP : | 1.372 | 1.453 | 9c |
| HF/TZP : | 1.370 | 1.448 | 9c |
| MP2 : | 1.405 | 1.445 | 9d |
| | Experimental | | |
| Solid State NMR : | 1.40 | 1.45 | 15 |
| Single crystal X-ray diffraction : | 1.340-1.391 av. 1.355 | 1.378-1.561 av. 1.467 | 17 |
| Electron diffraction | 1.401 | 1.458 | 18 |
| Neutron powder diffraction | 1.366-1.412 av. 1.391 | 1.420-1.487 av. 1.455 | 16 |

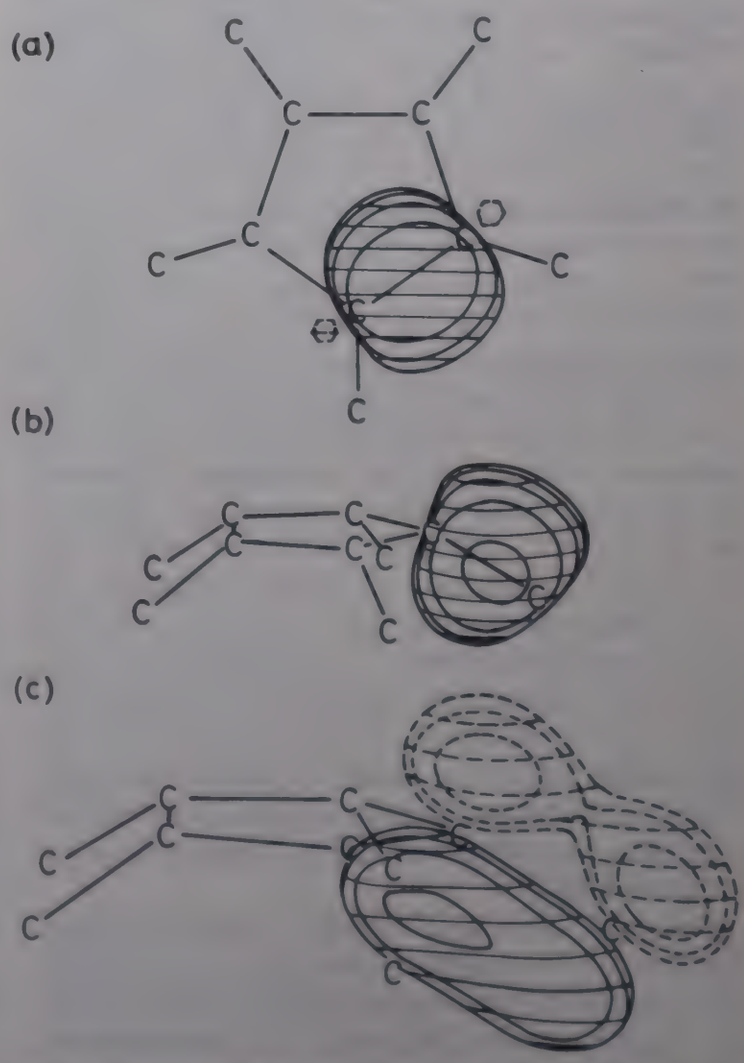


Fig. 1—Contours of the localized orbitals of $C_{60}$. Only a small fragment of the molecule is shown for clarity [(a) 6-5 σ bond; (b) 6-6 σ bond; (c) 6-6 π bond]

hybridization (Fig. 2) is also instructive. The extent of localization and the nature of orbital distortions are clearly seen. For example, the π bond is not completely localized, as evident from the small lobes on the adjacent atom orbitals. The π bond is also splayed outwards on the exterior of the spheroidal molecule, reflecting the pyramidality at the carbon atoms. The orbital contours indicate significant differences in the distortion of the σ and π MO's. The former has a greater density on the outside, while the reverse is true or the π bond. Such orbital effects have been associated with interesting chemical consequences in many organic systems[21]. In the case of $C_{60}$, endohedral interactions are expected to be quite different in magnitude compared to interactions of the π cloud with reagents on the exterior.

The above analysis clearly implies that buckminsterfullerene consists of 60 single and 60 double bonds. The pentagons are constructed of exclusively single bonds. On the other hand, the hexagons are made of alternating single and double bonds. In effect, the electronic structure of $C_{60}$ is well represented by a single canonical structure, which remarkably reflects the icosahedral symmetry of the molecule. In contrast, resonance structures such as the Kekule forms for benzene do not have the full symmetry of the molecule. Multiple related structures have to be invoked to restore the molecular symmetry. For buckminsterfullerene, alternative resonance forms probably do not contribute as much as the unique highly symmetric pairing scheme which parallels the localized molecular orbital description.

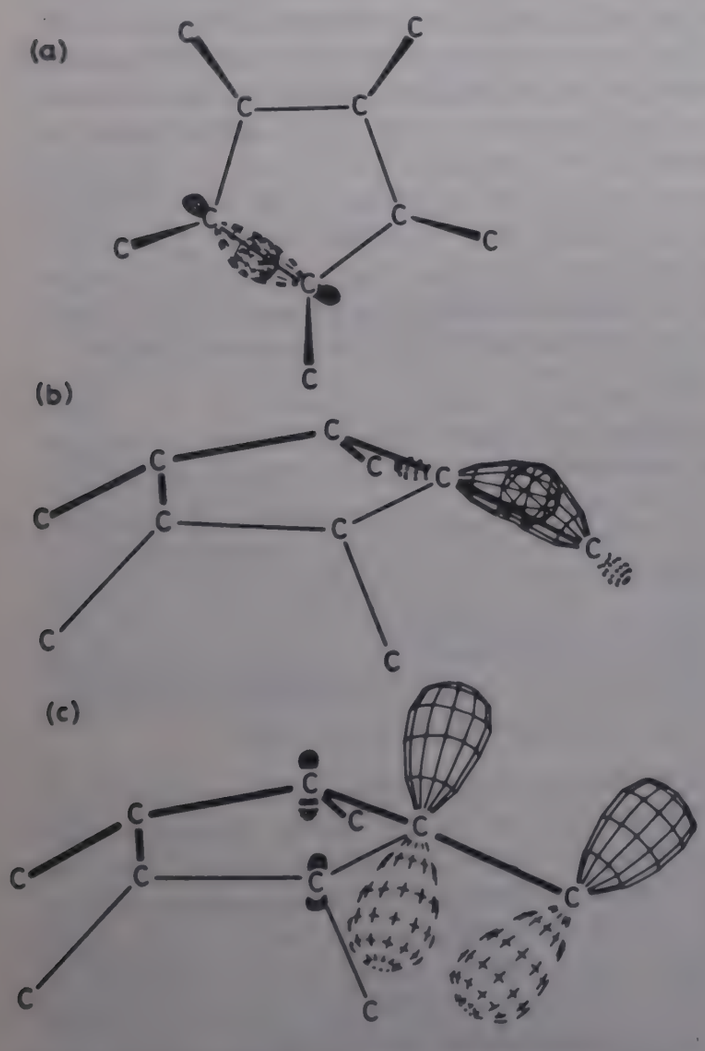


Fig. 2—An alternative view emphasizing the relative LCAO coefficients of localized orbitals of $C_{60}$. Only a small fragment of the molecule is shown for clarity, [(a) 6-5 σ bond; (b) 6-6 σ bond; (c) 6-6 π bond]

The localized bonding description has been used to advantage earlier[16,17,22]. For example, pentagon faces are readily recognised as being relatively electron deficient, while the hexagons are electron rich. Intermolecular interactions, in solid fullerene[16,17] and perhaps also in a donor-acceptor complex[23], are determined by these electron density variations.

The valence bond description also enables the extension of previous rules of stability of polycyclic conjugated compounds to the fullerene family. For example, the known antiaromatic character of pentalene has been invoked by Taylor[22] to suggest that structures with shared pentagons are unstable. This factor can be used to rationalize the 'pentagon isolation rule' and the uniqueness of the $C_{60}$ structure. Buckminsterfullerene represents the smallest closed structure with exclusively five and six membered rings in which no two pentagons are adjacent. Extending the argument, it has been proposed that structures with a double bond in a pentagon face are destabilized. This proposal was used to rationalize the relative stabilities of several of the larger fullerens, $C_n$ ($n \geq 60$).

We prefer an alternative interpretation of the factors contributing to the relative stabilities of fullerenes. The reference system, graphite, is of course aromatic with its planar sheets of hexagons. The structure can be folded to yield a closed surface by introducing 12 pentagons. In order to have maximum stability for the cluster, it is essential that all the hexagons retain benzenoid character. Alternative canonical structures like the quinonoid forms do not lead to stabilization. That is, the spin pairing scheme as in the Kekule structure **2a** is more stable than those in **2b-2e**. The smallest closed structure made of pentagons and hexagons in which every double bond is optimally part of a benzenoid structure such as **2a** is the fullerene, $C_{60}$. Such an ideal bonding situation is not possible in the larger clusters, say $C_{70}$ or $C_{80}$.

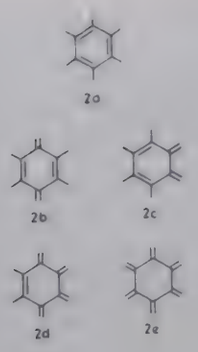

In the $D_{5h}$ form of $C_{70}$, for any given resonance structure, at least five of the hexagons would not retain their Kekule-type benzenoid spin pairing. Hence, the presence of additional hexagons in this cluster relative to $C_{60}$ does not lead to correspondingly greater stability. The same reasoning applies to the larger clusters as well. Ten hexagons of the $C_{80}$ cluster (assuming a five-fold symmetric structure) would lose benzenoid character.

In our revised proposal for rationalizing the relative stabilities of fullerenes, the focus has been shifted from the pentagons to the hexagons. Rather than suggesting that double bonds avoid pentagons[22], we insist that hexagons should adopt benzenoid structures for stability. The latter is a well known empirical rule for understanding the stabilities of polycyclic aromatic molecules. It is interesting that it can be used for three-dimensional clusters as well. However, as emphasized by earlier workers[2,22], conjugation contributes only partly to the stabilization of fullerenes. Strain effects associated with the σ skeleton, pyramidality at the carbon, and the varying magnitude of π overlap must all be taken into account for a complete understanding of the stability of these compounds. In the gas phase, entropic and other factors have also been suggested to be important[8b].

The localized bonds of $C_{60}$ can be incorporated in an exploded view of the molecule, employed earlier by Saunders[24]. The procedure of drawing such a structure (Fig. 3) is similar to that used occasionally for dodecahedrane, $C_{20}H_{20}$. A pentagon is first drawn, followed by five bonds from each of the vertices. In the case of dodecahedrane, additional 10 atoms are drawn staggered with respect to the first set and all the bonds are suitably connected to complete the structure. On the other hand, for pictorially representing fullerene, a set of 5 bonds (two-carbon units) is drawn parallel to the edges of the base pentagon. Connecting the nearest atoms would lead to corannulene, with a pentagon surrounded by 5 hexagons. Another set of 10 atoms (5 bonds) is drawn, staggered with respect to the previous set of bonds and maintaining five-fold symmetry. The nearest bonds are connected and the process is repeated up to $C_{50}$. The five bonds (10 atoms) of the final set are drawn radially. The nearest atoms are connected and finally the outermost five atoms are linked as a pentagon. The localized bonds, alternating single and double bonds, can then be easily inserted by ensuring that no double bonds are placed in any pentagon. For $C_{70}$ or $C_{80}$, the same procedure can be employed, with additional sets of 10 carbon units inserted beyond $C_{50}$ before drawing the outermost ten atoms. The structure of $C_{70}$ drawn following this procedure with a representative canonical structure is shown in Fig. 4.

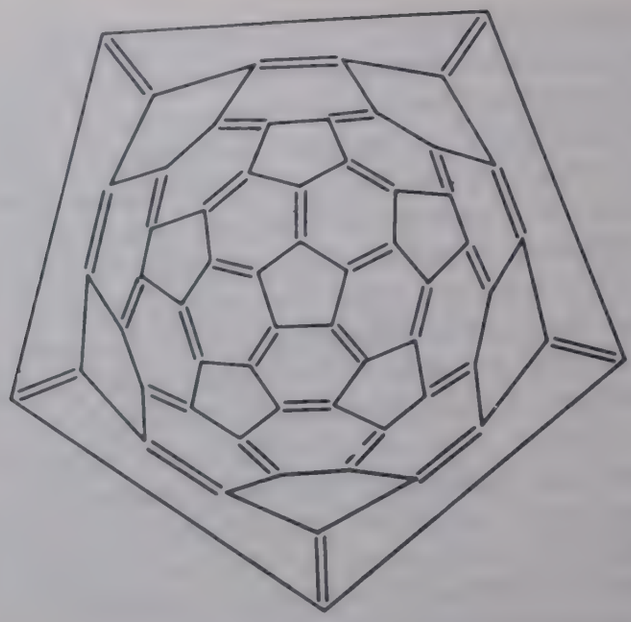

Fig. 3—Projected two-dimensional representation of $C_{60}$

The projected views of course do not reflect the spheroidal shape of the fullerenes. In particular, the above representations (Figs 3 and 4) emphasize only the five-fold symmetry of the molecules. However, it is a straight forward exercise to redraw the structures with three-fold or two-fold symmetry being highlighted. These may be appropriate in some discussions, e.g., structures of the trianion and the dianion of buckministerfullerene or some partially hydrogenated forms.

The exploded representations have several advantages. All the atoms, bonds, pentagons and hexagons are visible in these structures. Thus, the key structural features can be recognised without the use of three-dimensional models. The pedagogical value hardly needs to be emphasized. More importantly, it would be possible to consider and evaluate bond reorganizations which may accompany chemical reactions involving fullerenes using these simplified structures. We recommend the routine use of these representations, including

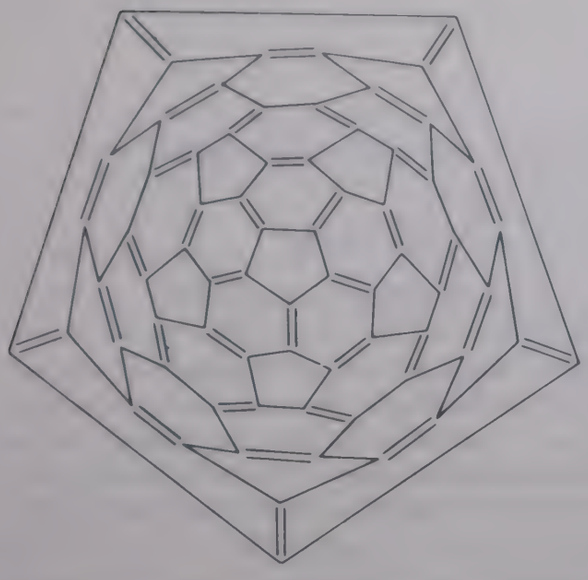

Fig. 4—Projected two-dimensional representation of $C_{70}$

the alternating single and double bonds, for mechanistic discussions.

**Acknowledgement**

We thank the Supercomputer Education and Research Centre, IISc, for help and cooperation. Discussions with P Balaram and S Chandrasekaran were valuable.

**References**

1 Smalley R, Curl E, Heath W, O'Brien J & Kroto J, *Nature*, 123 (1985) 143.
2 For a comprehensive list of theoretical studies and MNDO results on numerous fullerenes, see: Thiel W & Bakowies D, *J Am chem Soc*, 113 (1991) 3704.
3 Takahashi A & Ozaki M, *Chem Phys Lett*, 127 (1986) 242.
4 (a) Hess B A & Schaad L J, *J org Chem*, 51 (1986) 3902.
(b) Haddon R C, Brus L E & Raghavachari K, *Chem phys Lett*, 125 (1986) 459.
(c) Haddon R C, Brus L E & Raghavachari K, *Chem phys Lett*, 131 (1986) 165.
(d) Randic M, Nikolic S & Trinajstic N, *Croat chim Acta*, 60 (1987) 595.
(e) Schmalz T G, Seizt W A, Klein D J & Hite G E, *J Am chem Soc*, 110 (1988) 1113.
5 Shibuya T I & Yoshitani M, *Chem phys Lett*, 137 (1987) 13.
6 Marynick D S & Estreicher S, *Chem phys Lett*, 132 (1986) 383.
7 (a) Newton M D & Stanton R E, *J Am chem Soc*, 108 (1986) 2469.
(b) McKee M L & Herndon W C, *J Mol Struct (Theochem)*, 153 (1987) 75.
8 (a) Schulman J M, Disch R L, Miller M A & Peck R C, *Chem phys Lett*, 141 (1987) 45.
(b) Rudzinski J M, Slanina Z, Togasi M, Osawa E & Iizuka T, *Thermochim Acta*, 125 (1988) 155.
9 (a) Disch R L & Schulman J M, *Chem phys Lett*, 125 (1986) 465.
(b) Lüthi H P & Almlöf J *Chem phys Lett*, 135 (1987) 357.
(c) Scuseria G E, *Chem phys Lett*, 176 (1991) 423.
(d) Haeser M, Almlöf J & Scuseria G E, *Chem phys Lett*, 181 (1991) 487.
10 Krätschmer W, Lamb L D, Fostiropoulos K & Huffman D R, *Nature*, 347 (1990) 354.
11 Stewart J J P, *J Computer-aided molecular design*, 4 (1990) 1.
12 Perkins P G & Stewart J J P, *J chem Soc Faraday Trans*-2, 78 (1982) 285.
13 Jorgensen W L & Salem L, *The organic chemist's book of orbitals* (Academic Press, New York) 1973.
14 For typical applications of this program, see: Sustmann R & Sicking U, *Chem Ber*, 120 (1987) 1323, 1471, 1653.
15 (a) Yannoni C S, Johnson R D, Meijer G, Bethune D S & Salem J R, *J phys Chem*, 95 (1991) 9.
(b) Tycko R, *J phys Chem*, 95 (1991) 518.
16 David W I F, Ibberson R M, Matthewsman J C, Prassides K, Dennis T J S, Hare J P, Kroto H W, Taylor R & Walton D R M, *Nature*, 353 (1991) 147.
17 Liu S, Lu Y-J, Kappers M M & Ibers J A, *Science*, 254 (1991) 408.
18 Hedberg K, Hedberg L, Bethune, Brown C A, Dorn H C, Johnson R D & De Varies M, *Science*, 254 (1991) 410.
19 Satpathy S, *Chem phys Lett*, 130 (1986) 545.
20 (a) Dixon P, Kleiner D A & Lipscomb W N, *J Am chem Soc*, 100 (1978) 5681.
(b) Lipscomb W N, *Science*, 196 (1977) 1047.
21 Gleiter R & Paquette L A, *Acc Chem Res*, 16 (1983) 328.
22 Taylor R, *Tetrahedron Lett*, 32 (1991) 3731.
23 Ermer O, *Helv chim Acta*, 74 (1991) 1339.
24 Saunders M, *Science*, 253 (1991) 330.

Indian Journal of Chemistry
Vol. 31 A&B, May 1992, pp. F56-F63

# Towards a correlated electronic structure of fullerenes†

S Ramasesha[a]* & Bhargavi Srinivasan[a]

[a]Solid State and Structural Chemistry Unit, Indian Institute of Science
and
Jawaharlal Nehru Center for Advanced Scientific Research, Bangalore 560 012, India

Received 20 February 1992

An understanding of the electronic structure of fullerenes requires a proper treatment of electron correlations. In the related $\pi$-conjugated organic systems, the Pariser-Parr-Pople model defined over the $\pi$-orbitals has proved to be very successful in explaining their electronic structure. Solutions of similar $\pi$-electron models for fullerenes require development of new and reliable approximations. Some new approximations and their possible applications to elucidate the role of electron correlations in various exotic phenomena observed in fullerenes have been discussed.

The recent discovery of many exotic chemical and physical properties[1,3] in fullerenes has resulted in a great deal of excitement among theorists. Since most of the interesting properties associated with these systems are electronic in nature, theoretical electronic structure studies have come to the fore[4,5]. Theoretical studies of these molecules were in fact carried out even before their bulk preparation and characterization. The early studies ranged between simple enumeration of resonance structures and Hückel model calculations[6-8]. The latter calculations were relevant, although the hybridization on the carbon atom in fullerenes is not strictly $sp^2$, since all the carbon atoms are three coordinated; analogous to the conventional conjugated homoorganic systems. The molecular structure of the most extensively studied fullerene, $C_{60}$, can be described as a truncated icosahedron with the truncating planes being parallel to each of the interior pentagonal planes of the icosahedron. The bond length of the bond common to two hexagons is determined by the distance between these two planes in the icosahedron. The regular $C_{60}$ structure is obtained when the truncating plane trisects the edge of the icosahedron. The Hückel molecular orbitals and their energies for some fullerenes are shown in Fig. 1. Particularly interesting is the energy level diagram of $C_{60}$, which has the icosahedral symmetry. The irreducible representations for this group are 1, 3, 4 and 5 dimensional and the HOMOs are five-fold degenerate while the two sets of LUMOs are three-fold degenerate. In regular $C_{60}$ wherein the bond shared between two hexagons and the bond shared between a hexagon and a pentagon are of equal length, there is accidental degeneracy of the states belonging to the five and four-dimensional

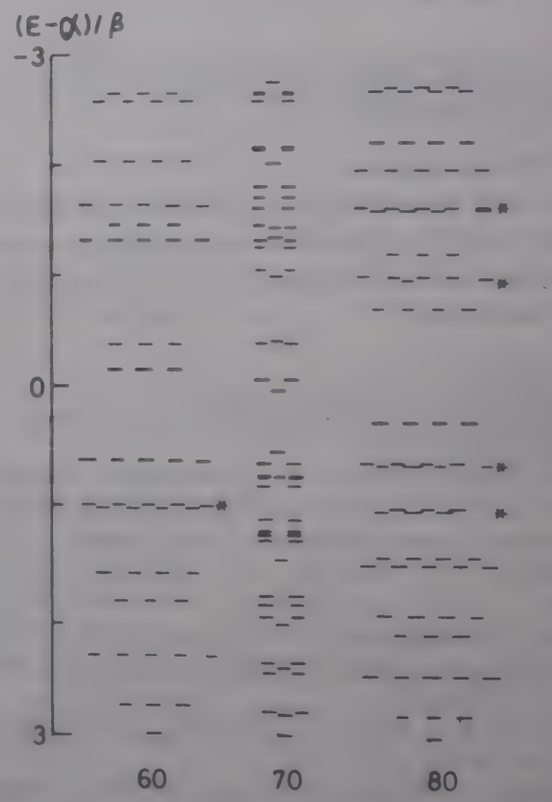


Fig. 1—Energy level diagrams of $C_{60}$, $C_{70}$ and $C_{80}$ in the Hückel model[7]. Asterices refer to accidental degeneracies. In $C_{60}$ this degeneracy is lifted when the hexagon-hexagon bond is made different from the hexagon-pentagon bond

representations. The energy levels of $C_{60}$ can also be associated with different angular momentum states by viewing them as being derived from symmetry breaking of a perfect sphere[9]. Such a picture is advantageous in some situations such as while treating vibronic interactions[9,10]. The Hückel molecular orbital picture gives an optical gap of $\approx$ 2.0 eV, for a resonance integral of 2.0 eV, which is also close to what is seen in experiments.

There have also been studies pertaining to the electron-lattice interactions in the $C_{60}$ system to explore possible structural distortions in the ground

†Communication no. 830 from the Solid State and Structural Chemistry Unit

state, again within the Hückel model[11]. In recent years, there have been more rigorous electronic structure calculations of the ground state energies. These include self-consistent field calculations using STO-6-13G* basis[12], MNDO[13] calculations of carbon clusters and calculations employing linear muffin-tin orbitals (LMTO)[14]. Most of these calculations address themselves to questions related to ground state geometry, resonance stabilization, prediction of magic numbers, prediction of vibrational spectra and "in-cage" versus "out-cage" doping with alkali ions. While these studies are important in themselves, they cannot, by the very nature of the approximations, provide reliable excitation gaps, spin and charge density distributions and correlation functions which are important for understanding properties such as ferromagnetism and superconductivity in the fullerenes[1-3]. Fullerenes are very similar to the other conjugated organic systems. In the latter, for example, in the polyene systems, it is well known that Hückel as well as self-consistent field calculations cannot account, even qualitatively, for many of the observed properties[15]. These properties include observation of negative spin densities in radicals, existence of states below the dipole gap, and the fact that the optical gaps of polyenes extrapolate to a finite value ($\approx 2$ eV) while those of the closely related symmetric cyanine dyes extrapolate to zero.

In polyenes and other conjugated systems, the discrepancy between the self-consistent field results and the experiments have been satisfactorily resolved by explicitly treating electron correlations[16,17]. What has proved to be more significant is the fact that treating only the electron correlations amongst the $\pi$-electrons in conjugated systems correct to all orders in the perturbation expansion provides excellent agreement between theory and experiment. In what follows, we give a brief introduction to correlated model Hamiltonians for fullerenes and follow this with approximation schemes for solving the models. In the last section we discuss the possible applications of these approximate schemes to the study of fullerenes.

**Correlated model Hamiltonians for fullerenes**

The $\pi$-electron models used in the above studies can be derived from the nonrelativistic, full many-body Hamiltonian,

$$H = \sum_{rs,\sigma} \langle r|f|s\rangle a^*_{r\sigma} a_{s\sigma} + \frac{1}{2} \sum_{pqrs,\sigma\tau} \langle pq|g|rs\rangle a^*_{p\sigma} a_{q\sigma} a^*_{r\tau} a_{s\tau} \quad \ldots (1)$$

where, $a^*_{p\sigma}(a_{p\sigma})$ creates (annihilates) an electron with spin $\sigma$ in the pth orbital, f is the one electron operator, g is the two electron operator whose matrix element is in the charge cloud notation. By making the zero differential overlap approximation wherein integrals involving overlap charge clouds are neglected and restricting ourselves to the $\pi$-electrons which form the basis for elementary excitations in the system, we obtain the Pariser-Parr-Pople (PPP) Hamiltonian[18,19],

$$H_{PPP} = \sum_{\langle ij\rangle,\sigma} t_{ij} a^*_{i\sigma} a_{j\sigma} + \frac{U}{2} \sum_i \hat{n}_i(\hat{n}_i - 1) + \frac{1}{2} \sum_{i>j} V_{ij} \hat{n}_i \hat{n}_j \quad \ldots (2)$$

where, $t_{ij}$ which is identical to Hückel resonance integral is the renormalized one-electron integral between bonded atoms, U is the repulsion integral when two electrons are in the same orbital and $V_{ij}$ is the interaction integral between charge clouds on different sites and $\langle ij\rangle$ implies nearest neighbours. In metals, where screening by the electrons in the mobile conduction band is effective, only the on-site repulsion integral needs to be considered (with all $V_{ij}$'s being set to zero) and the PPP Hamiltonian reduces to the widely studied Hubbard model of solid state physics. However, in nonmetals, where screening is not effective and the range of electron repulsion extends beyond the same site, we regain the PPP model. In fact, the PPP models also go by the name "extended Hubbard models". In conjugated systems containing carbon, nitrogen and oxygen, the molecular integrals need not be explicitly evaluated as they have been reliably parametrized[20]. Thus, the study of $\pi$-electron systems is mostly based on phenomenological Hamiltonians wherein the transfer integral and the on-site Hubbard U are the only parameters. The range of electron repulsions is usually extended employing a widely used interpolation procedure, which yields the electrostatic potential at large distances, known as the Ohno formula[21],

$$V_{ij} = U(1.0 + 0.6117\, r_{ij}^2)^{-1/2} \quad \ldots (3)$$

where $r_{ij}$ is the distance between the sites i and j. The PPP models can be solved exactly only for small systems and reliable approximation schemes for large systems are not yet available. The dimensionality of the Hilbert space spanned by a system of Q electrons with total spin S, in N orbitals, is given by the Weyl dimensional formula[22],

$$P_S = \frac{2S+1}{N+1} \binom{N+1}{Q/2-S} \binom{N+1}{N-Q/2-S} \quad \ldots (4)$$

We find that the dimensionalities of the spaces increase very rapidly with N and Q (Table 1). The

Table 1—Dimensionalities, $P_S$ and $P_{S+1}$ Eqn. 4, of subspaces of systems with Q electrons in N orbitals. S = 0 for Q even and 1/2 for Q odd

| | | | | | | | | | | |
|---|---|---|---|---|---|---|---|---|---|---|
| N | 8 | 8 | 9 | 9 | 10 | 10 | 11 | 11 | 12 | 12 |
| Q | 8 | 7 | 9 | 8 | 10 | 9 | 11 | 10 | 12 | 11 |
| $P_S$ | 1764 | 1792 | 8820 | 5292 | 19404 | 27720 | 104544 | 60984 | 226512 | 339768 |
| $P_{S+1}$ | 2352 | 1344 | 5760 | 7560 | 29700 | 19800 | 81675 | 98010 | 382239 | 283140 |

Hamiltonian matrix can be set-up in a spin adapted basis such as the diagrammatic valence bond (VB) basis and the matrix being very sparse, a few low-lying eigenvalues and corresponding eigenfunctions can be obtained for a system with upto 14 orbitals and 14 electrons. However, the system of our interest, the fullerenes, have $\geq 60$ orbitals with an equal number of electrons, in the undoped state. The dimensionalities of the spaces spanned by the fullerene Hamiltonians are astronomical and exact solutions are beyond reach in the foreseeable future. Thus, reliable approximate solutions of the PPP Hamiltonian become relevant.

**Approximate schemes for correlated model Hamiltonians**

There have been many approximate solutions of the Hubbard model, important among these has been the Gutzwiller variational method[23]. In this method, the variational wave function is constructed from the noninteracting model solution by introducing a parameter $\tau$. This parameter reduces the coefficient of a wave function with p doubly occupied sites by a factor $\tau^p$, $(0 \leq \tau \leq 1)$ relative to the noninteracting solution. The parameter $\tau$ is then variationally determined. This method, being variational in nature, is mainly applicable to the ground state and is difficult to implement for an extended Hubbard model wherein the interaction energy depends not only on the number of doubly occupied sites but also on their configuration in space. Extension of the method to the PPP Hamiltonian has been attempted, though not very successfully[24,25]. Perturbation theoretic techniques, while being size consistent in every order do not converge rapidly for the correlation strengths estimated for the $p_z$ orbital of carbon. Approximations which truncate the many-body basis based on the correlation energy of the state in direct space require a large fraction of the total space to be retained for obtaining reliable energy gaps[26]. Therefore, the approximation schemes that start with the molecular orbital (MO) basis obtained by diagonalizing only the transfer part of the Hamiltonian and retaining only some configurations while treating the interaction part have been in vogue[27]. These go by the name of restricted configuration interaction (CI) schemes in quantum chemistry. On this basis, the Hubbard model can be written in the form

$$H_{Hub.} = \sum_{i,\sigma} \varepsilon_i b^*_{i\sigma} b_{i\sigma} + 1/2 \sum_{ijkl} V_{ijkl} \times (\hat{E}_{ij}\hat{E}_{kl} - \delta_{jk}\hat{E}_{il}); \quad \ldots (5a)$$

$$\hat{E}_{ij} = \sum_{\sigma} b^*_{i\sigma} b_{j\sigma} \quad \ldots (5b)$$

where $\varepsilon_i$ is the energy of the $i^{th}$ MO and $V_{ijkl}$ are defined by

$$V_{ijkl} = \sum_{m} \sum_{ijkl} U\, c_{im} c_{jm} c_{km} c_{lm} \quad \ldots (6)$$

with the operators $b^*_{i,\sigma}(b_{i,\sigma})$ creating (annihilating) an electron in the $i^{th}$ MO with spin $\sigma$ and is given by

$$b^*_{i,\sigma} = \sum_{j} c_{ij} a^*_{j,\sigma} \quad \ldots (7)$$

where $c_{ij}$ are the coefficients of the $j^{th}$ AO in the $i^{th}$ MO and all the summations run over the entire AO or MO basis. The Hubbard Hamiltonian written in the MO basis has the property that the one-electron part is diagonal while the interaction part is off-diagonal. The Hamiltonian matrix can once again be set up in a VB basis using MO wave functions to construct the VB functions[22]. However, if an MO state is degenerate, the associated MOs need not be orthogonal. To avoid the "nonorthogonality catastrophe", we use Lowdin orthogonalization[28] of the MOs given by

$$c^{Low.}_{MO} = S^{-1/2} c_{MO} \quad \ldots (8)$$

where S is the overlap matrix in the MO basis. TheVB functions are now written in terms of the Lowdin orthogonalized MOs. When the two-electron term in Eqn. (2) operates on a "legal" or a diagram that obeys extended Rumer-Pauling rules, the result is in general an "illegal" VB diagram. The "illegal" VB diagrams can be resolved into "legal" VB diagrams by the techniques developed by Ramasesha *et al*[29,30]. The restricted CI calculations can be performed in the MO space in many different ways. If all possible configurations for a given number of electrons with a given total spin are used for

setting up the Hamiltonian matrix, we obtain model exact results which are the same as those obtained using the AO-VB basis. This provides a strong check on our calculations in the MO-VB scheme.

We have tried three restricted CI schemes. In the first scheme (Scheme i) we employ all possible configurations within an active space consisting of a few high energy bonding MOs and a few low energy antibonding MOs. For linear chains, we have considered upto three bonding and three antibonding MOs. A second restricted CI method (Scheme ii) involves taking all possible singly and doubly excited configurations of a given total spin. The configurations included in the third method (Scheme iii) all have energies below a certain threshold. These could arise from one, two or, indeed, many particle-hole excitations as long as the excitation energy is below the chosen threshold. The configurations whose energies are below a threshold, independent of the number of particle-hole excitations involved in the configuration, can be generated in an increasing order of energy to enable the imposition of a cut-off. The spin adaptation of the configurations, given the occupancy of each MO, now turns out to be straightforward. When the Hamiltonian operates on the restricted VB basis set, the resulting VB functions could some times be outside the chosen basis. In constructing the Hamiltonian matrix corresponding to the restricted VB basis, only the coefficients of the resulting functions that belong to the restricted basis are retained and all other terms are ignored. The matrix representing the Hamiltonian in the VB basis is, in general, nonsymmetric since the VB basis is nonorthogonal. The two lowest eigenvalues in each approximation are obtained by using the Rettrup algorithm[31] which is an extension of the Davidson algorithm[32] for nonsymmetric matrices.

We have calculated the singlet-singlet and triplet-triplet excitation gaps in all the three approximations for (i) even site Hubbard chains with upto twelve sites, (ii) for a ten-site graphitic lattice with cyclic boundary condition and (iii) for a cubic Hubbard system. These three cases represent the approximations in one, two and three-dimensions (Fig. 2).

The chains, with only two nearest neighbour transfer integrals, represent the most difficult scenario as correlations have a more dominant role here than in higher dimensions. A successful approximation in one-dimension is usually adequate in higher dimensions as well. In Fig. 3 are shown the VB-MO results obtained for a Hubbard chain of twelve sites in the restricted CI approximation in which we have considered (i) 2 HOMOs and 2 LUMOs, (ii) 3 HOMOs and 3 LUMOs respectively. In the case of singlets, the approximation fails beyond $U/t = 2.0$ while for triplets it fails beyond $U/t = 1.0$. The true singlet excitation energies increase upto $U/t = 2.0$ and decrease beyond, indicating the changeover from charge-like to spin-like excitations with increase in the correlation strength. This trend is completely missed in the restricted CI scheme wherein the effect of correlation is to monotonically increase the excitation gap. This may be because the net change in fractional double occupancy between the ground and the first excited state is nearly independent of the correlation strength and is depend-

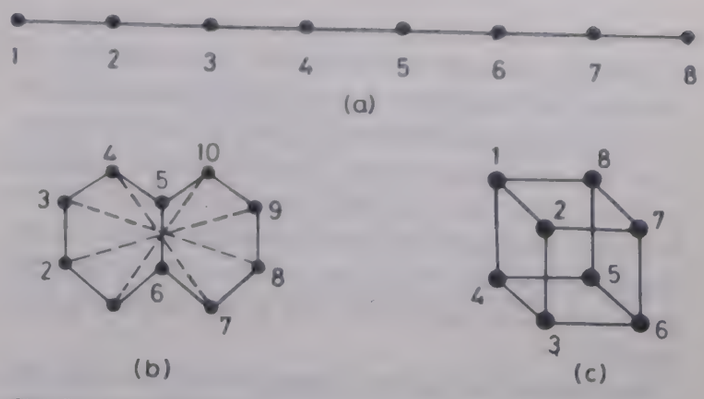


Fig. 2—Schematic diagrams of the one, two and three-dimensional Hubbard systems. Dotted lines imply cyclic boundary conditions. The chains studied have lengths of 8, 10 and 12 sites

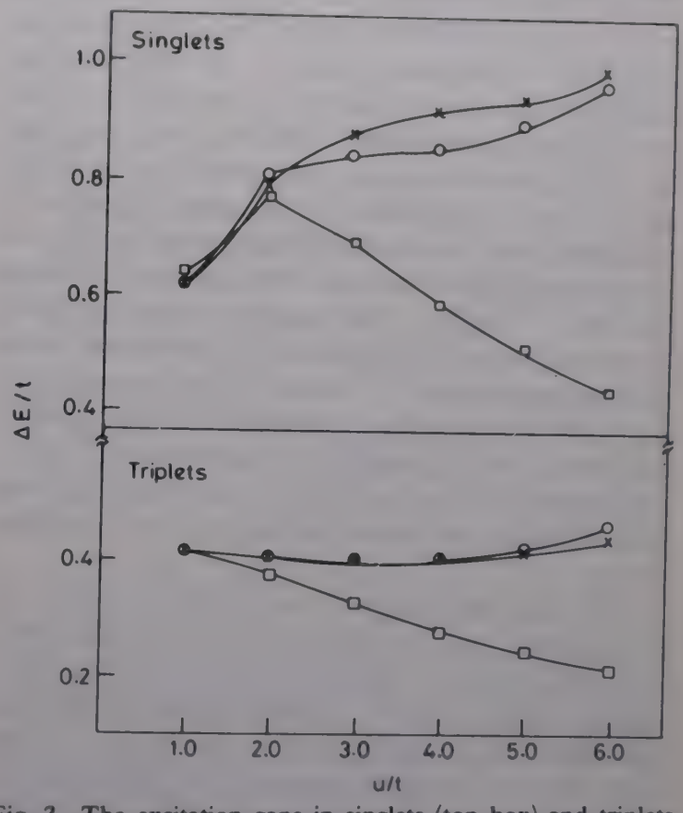


Fig. 3—The excitation gaps in singlets (top box) and triplets (bottom box) for a Hubbard chain of 12 sites, plotted against the correlation strength, using Scheme (i). Squares represent model exact results, crosses refer to calculations with two HOMOs and two LUMOs while open circles correspond to three HOMOs and three LUMOs

ent only on the MO functions chosen for the CI scheme. In the case of the triplets, the restricted CI scheme gives a gap that is very weakly dependent on U/t, may be because the fractional double occupancy in the two lowest triplet states is nearly equal. In both the cases the true trend is missed, since only in the mean field limit will the fractional double occupancies show the behaviour discussed above. The restricted CI is thus valid only in the weak correlation limit.

In quantum chemistry, a restricted CI scheme that has been widely employed is that in which all possible particle-hole excitations upto a desired particle number are considered. To test the validity of this scheme for the Hubbard model, we carried out restricted CI calculations using (i) all singly excited configurations and (ii) all singly and doubly excited configurations on a chain of twelve sites in the singlet and triplet subspaces. The results are summarized in Fig. 4. Except in the very weak correlation limit, both these approximations deviate widely and in an unpredictable manner from the exact results in the case of singlets. The approximation is slightly better in the case of triplets and is comparable to the earlier approximate CI scheme. The dimensionalities of the spaces when all the one and two particle excitations are considered is already large (Table 2) and inclusion of higher particle excitations will lead to dimensions that would be inaccessible to routine studies.

The third restricted CI approximation that we have studied includes all configurations whose energy with respect to the energy of the ground state configuration is below a given threshold, $E_c$. The configurations entering in this calculation would have one, two or many particle-hole excitations, so long as the excitation energy is less than $E_c$. In Figs 5 and 6, we show the dependence of the excitation gaps on the on-site correlation strength, calculated in this approximation in the singlet and triplet manifolds for 8, 10 and 12 site chains. We find that for $E_c = 4t$, i.e., when the threshold equals the bandwidth of the infinite chain, the excitation gaps follow smoothly the exact gaps. For all other values of the threshold that are not large enough to enclose most of the Hilbert space, the approximate gaps are not as reliable. This is also found to be the case in the two and three-dimensional models that allow exact studies for comparison (Table 3, Fig. 7).

The MO functions span the entire AO space, when $E_c$ is set to the bandwidth. Below this value of $E_c$, all the MO functions do not appear in the configurations included in our approximation. It appears to be important that the full one-particle space should be spanned by the functions appearing in

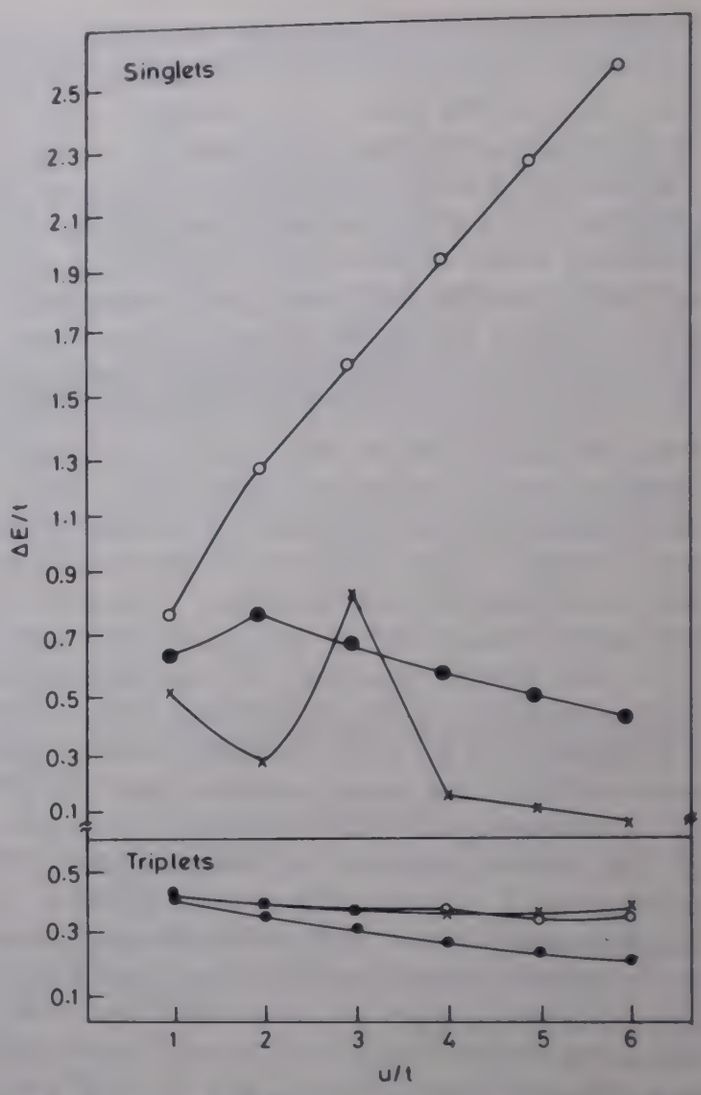


Fig. 4—Comparison of the exact excitation gaps (closed circles) in singlets and triplets for a chain of 12 sites with excitation gaps obtained in Scheme (ii) using only single excitations (crosses), singles and doubles (open circles) for different values of U

Table 2—Dimensionalities of the subspaces spanned within Schemes (i), (ii), (iii), as a fraction ( $\times 10^2$) of the complete dimensionality of the subspace. N refers to the number of sites in the chain, S and T refer to the singlet and triplet subspaces respectively. Scheme (i) 3 HOMOs and 3 LUMOs, Scheme (ii) all single and double excitations, Scheme (iii) multiple excitations at $E_c = W = 6t$

| N | Scheme (i) | | Scheme (ii) | | Scheme (iii) | |
|---|---|---|---|---|---|---|
| | S | T | S | T | S | T |
| 8 | 9.921 | 8.036 | 8.617 | 7.313 | 3.175 | 2.423 |
| 10 | 0.902 | 0.636 | 1.670 | 1.263 | 0.633 | 0.461 |
| 12 | 0.077 | 0.049 | 0.310 | 0.229 | 0.011 | 0.072 |

the CI scheme for the scheme to give reliable excitation gaps. But, what is more interesting is the fact that increasing the threshold beyond the bandwidth, without spanning a significant fraction of the many particle Hilbert space, does not faithfully reproduce the trend observed in the dependence of excitation gaps on the correlation strength. This is seen in Figs 4-6, wherein we find that for $E_c = 6t$, the excitation

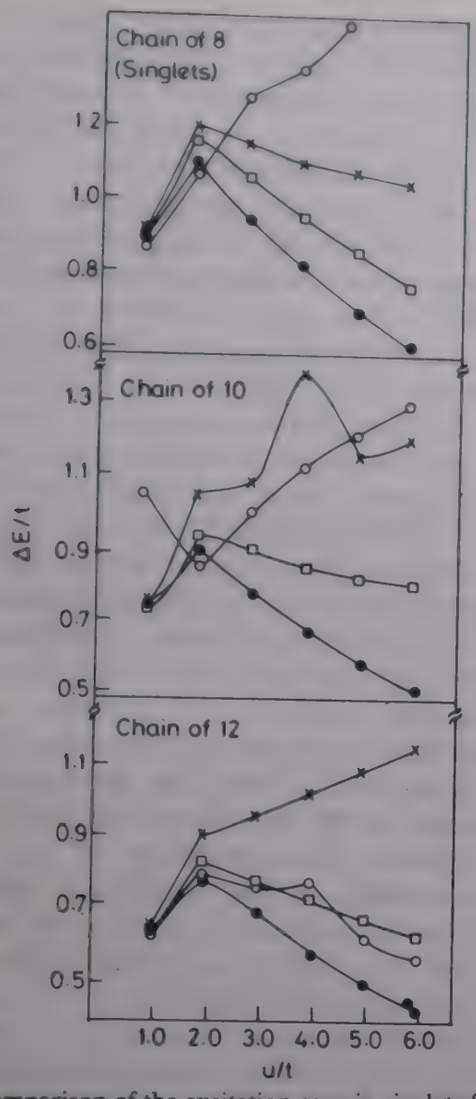


Fig. 5—Comparison of the excitation gaps in singlets for chains of 8, 10 and 12 sites obtained using Scheme (iii), with exact results (closed circles) for different values of U. Open circles—$E_c = 2t$, squares—$E_c = 4t$ (equal to bandwidth) and crosses—$E_c = 6t$

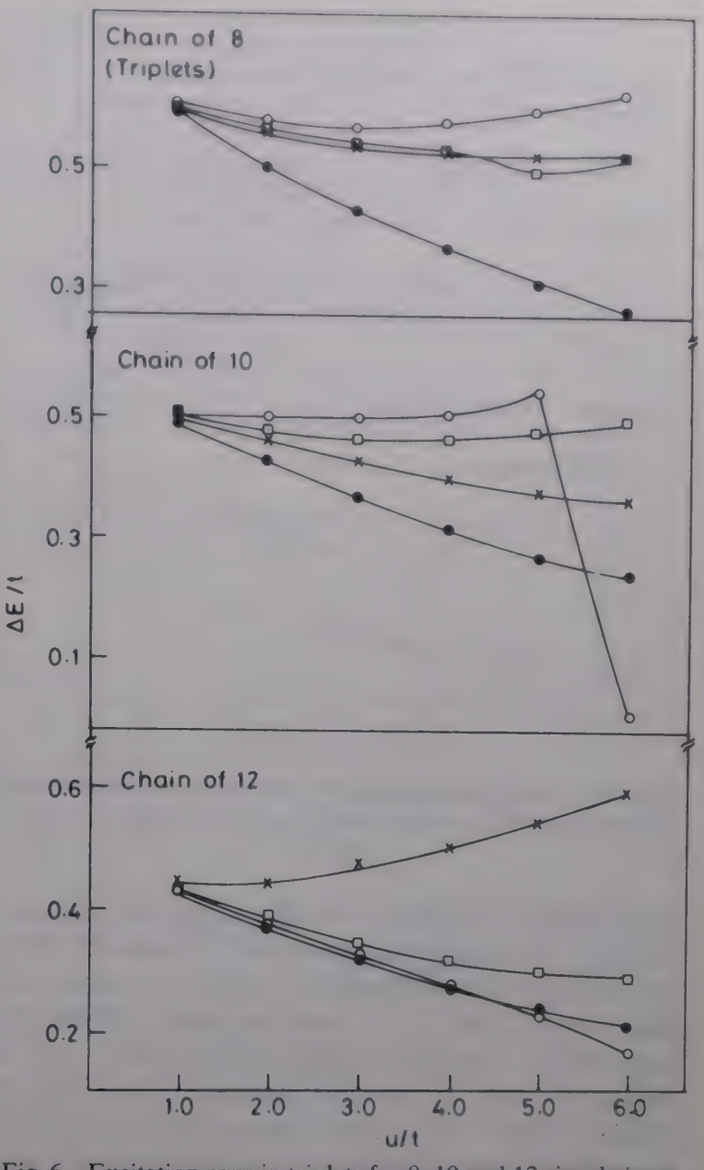


Fig. 6—Excitation gaps in triplets for 8, 10 and 12 site chains as a function of U. Symbols have the same meanings as in Fig. 5

Table 3—Singlet and triplet excitation gaps in the two-dimensional Hubbard model, in Scheme (iii) for different thresholds. Exact values are also given for comparison. All the energies are in units of t and the bandwidth, W, in this sytem is 6t

| U | $E_c = W$ | | $E_c = 1.5W$ | | Exact | |
|---|---|---|---|---|---|---|
| | $\delta E_s$ | $\delta E_t$ | $\delta E_s$ | $\delta E_t$ | $\delta E_s$ | $\delta E_t$ |
| 1.0 | 1.243 | 0.114 | 1.222 | 0.116 | 1.221 | 0.117 |
| 2.0 | 1.265 | 0.240 | 1.117 | 0.242 | 1.185 | 0.252 |
| 3.0 | 1.301 | 0.359 | 1.192 | 0.362 | 1.144 | 0.384 |
| 4.0 | 1.348 | 0.464 | 1.224 | 0.472 | 1.106 | 0.496 |
| 5.0 | 1.401 | 0.556 | 1.292 | 0.574 | 1.066 | 0.565 |
| 6.0 | 1.459 | 0.642 | 1.392 | 0.671 | 1.017 | 0.584 |

gap versus U/t curves do not smoothly follow the exact curve, although, for isolated values of U/t the excitation gaps are occasionally in better agreement than when $E_c$ equals the bandwidth. It is somewhat surprising that increasing the dimensionality of the Hilbert space, within the same approximation, does not always improve excitation gaps.

## Future applications to fullerenes

While the approximation of including all the particle-hole excitations of energy ≤ bandwidth has proved to be reliable for the excitation gaps, obtaining all such excitations with appropriate spin label in fullerenes having sixty orbitals or more is a nontrivial task. We have solved this problem in two stages. In the first stage, we treat the particles as spinless with a permitted occupancy of two particles per orbital. In this scheme, we obtain all possible occupancies of orbitals such that the energy associated with an occupation is less than the chosen threshold. This part of the computation is simplified by the fact that the MOs have considerable degeneracies. For instance, in the case of $C_{60}$ there exist only sixteen levels with possible occupancies of the levels ranging from 2 to 10. In the second stage, we obtain the

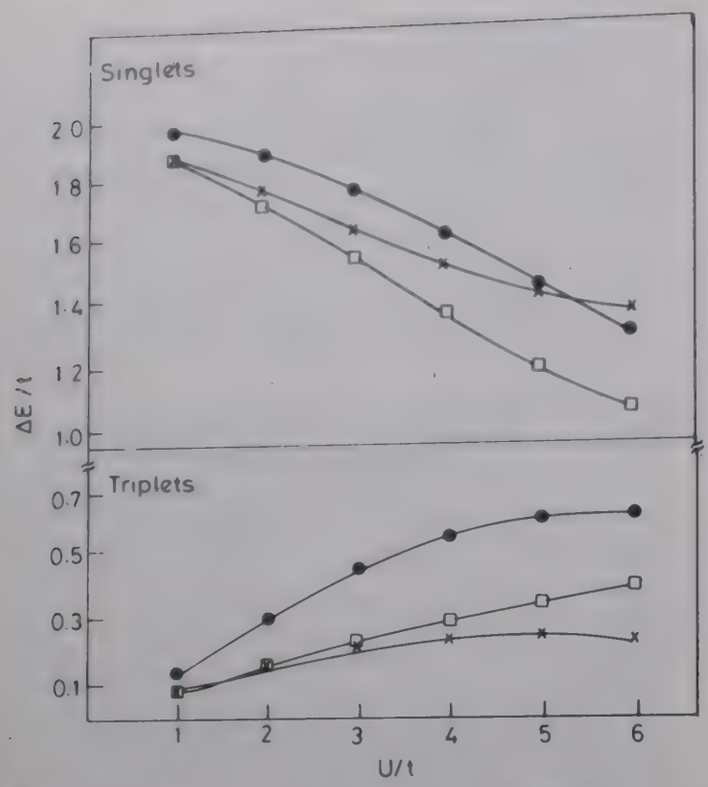


Fig. 7—Excitation gaps in singlets and triplets of Hubbard cube as a function of U. Symbols have the same meanings as in Figs 5 and 6

spin adapted configurations that span the given occupancy by introducing spin and individual orbital labels. With each orbital we associate two bits; the state "00" of the bits implies an empty orbital, the state "11" a doubly occupied orbital while "10" is taken to imply an up-spin occupancy and "01" is taken to imply a down spin occupancy. The bit configurations that satisfy the extended Rumer-Pauling rules are taken to be "legal" configurations for the chosen total spin. The MO-VB diagrams of fullerenes will also contain sixty or more MOs and representation of the excited configurations as integers would require a total of at least 120 bits. With recent developments in the VB theory, it is possible to handle VB diagrams that require two integers per diagram in the bit-representation scheme. On most computers, the bit-length of an integer is only 32 and our scheme would allow handling systems with upto 32 orbitals. However, Cyber 992 has a bit-length of 64 bits per integer and we can handle $C_{60}$ system in our approximation on this computer. Currently, we are carrying out trial calculations on the $C_{60}$ on this machine.

There exist many questions concerning the role of electron correlations in the fullerenes. While these questions concern themselves with a single ball, because of the weak inter-ball transfer terms their answers hold the key to the behaviour of the fullerenes in the solid state as well. This view is supported by the fact that the bandwidths computed from tight binding models are much smaller than the energy gaps in the MO picture of the isolated molecule. Foremost among the questions related to the role of electron correlations is its effect on the electronic spectra in the doped and undoped systems. The Hückel theory predicts essentially the same electronic spectrum whether the $C_{60}$ is doped with one, two or three electrons because of the triply degenerate LUMO in the system. However, it is likely that the spectra will be progressively blue shifted in going from the singly doped to the triply doped $C_{60}$ due to increased electron repulsions. Another important question is the possibility of Cooper pairing in the fullerenes. Pairing will be indicated if the stability of the doubly doped $C_{60}$ is greater than the average stability of the singly and triply doped $C_{60}$. Indications about pairing can also be obtained by studying appropriate correlation functions in the many-body ground state of the fullerene. Similarly, study of spin densities and spin-spin correlation functions should give an indication about ferromagnetism in doped $C_{60}$. There has also been considerable interest in the third harmonic generation and other nonlinear optic properties of $C_{60}$. Although the computation of the coefficients that govern these properties appears to involve all the excited states, they can in fact be computed by knowing only the ground state wave function and the corrections to the ground state wave function in the presence of oscillating electric fields. Model Hamiltonian studies will allow us to study the evolution of these properties as the correlations are gradually increased in strength. There has been considerable interest in the electronic properties of substituted fullerenes wherein a hetero-atom replaces one of the carbon atoms of the ball. The PPP Hamiltonians can be employed for studies of these systems since reasonable model parameters for some of the hetero atoms of interest are well established.

## References

1 Rosseninsky M J, Ramirez A P, Glarum S H, Murphy D W, Haddon R C, Hebard A F, Palstra T T M, Kortan A R, Zahurak S M & Makhija A V, *Phys Rev Lett*, 66 (1991) 2830.
2 Allemand P M, Khemani K C, Koch A, Wudl F, Holczer K, Donovan S, Gruner G & Thompson J D, *Science*, 253 (1991) 301.
3 Fagan P J, Calabrese J C & Malone B, *Science*, 252 (1991) 1160; Olah G A, Bucsi I, Lambert C, Auszfeld R, Trivedi N J, Sensharma D K & Suryapraksh G K, *J Am chem Soc*, 113 (1991) 9387.
4 Chakravarty S, Gelfand M P & Kivelson S, *Preprint*, 1991.
5 Baskaran G & Tosatti E, *Curr Sci*, 61 (1991) 33.
6 Taylor R, *Tetrahedron Lett*, 32 (1991) 3731.
7 Fowler P W & Woolrich J, *Chem Phys Lett*, 127 (1986) 78.
8 Haddon R C, Brus L E & Raghavachari K, *Chem Phys Lett*, 125 (1986) 459.

9 Adams G B, Page J B, Sankey O F, Sentia K, Menendez J & Huffim D R, *Phys Rev*, B44 (1991) 4052.
10 Feuston B P, Andreoni W, Parrinello M & Clementi E, *Phys Rev*, B44 (1991) 4056.
11 Hayden G W, Ph.D. Thesis, University of Pennsylvania, (1987).
12 Schulman J M, Disch R L, Miller M A & Peck R C, *Chem Phys Lett*, 141 (1987) 45.
13 Bakowiesand D & Thiel W, *J Am chem Soc*, 113 (1991) 3704.
14 Sathpathy S, *Chem Phys Lett*, 130 (1986) 545.
15 Ramasesha S, *J mol Struct*, 194 (1989) 149.
16 Soos Z G & Ramasesha S, *Phys Rev*, B29 (1984) 5410.
17 Ramasesha S & Soos Z G, *J chem Phys*, 80 (1984) 3278.
18 Pariser R & Parr R G, *J chem Phys*, 21 (1953) 767.
19 Pople J A, *Trans Faraday Soc*, 42 (1953) 1375.
20 Albert I D L, Das P K & Ramasesha S, *Chem Phys Lett*, 176 (1991) 217.
21 Ohno K, *Theor Chim Acta*, 2 (1964) 219.
22 Soos Z G & Ramasesha S in *Valence bond theory and chemical structure*, edited by D J Klein and N Trinajstic, (Elsevier, Amsterdam), (1990), p. 81.
23 Gutzwiller M C, *Phys Rev Lett*, 10 (1963) 159.
24 Horsch P & Fulde P, *Physik Z*, B36 (1979) 23.
25 Oujia B, LePetit M-B, Malrieu J-P, *Chem Phys Lett*, 158 (1989) 559.
26 Ramasesha S & Soos Z G, (unpublished work).
27 Szabo A & Ostlund N S, *Modern quantum chemistry* (Macmillan, London), 1982.
28 Lowdin P-O, *J chem Phys*, 18 (1950) 365.
29 Ramasesha S, Albert I D L & Sinha Bhabadyuti, *Mol Phys*, 72 (1991) 537.
30 Ramasesha S, Sinha Bhabadyuti & Albert I D L, *Phys Rev*, B42 (1990) 9098.
31 Davidson E R, *J Comput Phys*, 17 (1975) 87.
32 Rettrup S, *J Comput Phys*, 45 (1982) 100.

Indian Journal of Chemistry
Vol. 31 A&B, May 1992, pp. F64-F78

# Physics of undoped and doped $C_{60}$ fullerene

H R Krishnamurthy & A K Sood*†

Department of Physics, Indian Institute of Science, Bangalore 560 012

and

Jawaharlal Nehru Centre for Advanced Scientific Research, IISc Campus, Bangalore 560 012

Received 20 February 1992

This paper contains a review of the physical properties of the undoped and alkali-doped $C_{60}$ materials, including their crystal structure, electronic, optical and vibrational properties and the effect of pressure on the crystal and electronic structure. The mechanisms of superconductivity in alkali-doped $C_{60}$ in terms of phonon mediated electron pairing vis-a-vis electronic interaction effects are discussed.

## 1 Introduction

The recent discoveries of a simple method[1] for synthesising $C_{60}$ (fullerene)[2] in bulk, and that conducting[3] and superconducting[4] materials are obtained by doping crystalline $C_{60}$ (fullerite) with alkali metals have generated an enormous surge[5] of interest in these materials. In this article we review some aspects of the physics of these materials and the mechanisms that may be responsible for the superconductivity in alkali doped fullerene. The review is not comprehensive and does not cover the literature[5] extensively (which would in any case be very hard in a field which is experiencing a period of explosive growth); it is intended more as a guide to the literature that we are familiar with (mostly the published papers). We also include brief discussions of our own work in this field.

The $C_{60}$ molecule is easily one of the most beautiful molecules known to us and has the structure of the "truncated icosahedron" (a modern soccer ball) shown in Fig. 1a, the "truncation of the icosahedron" being illustrated in Fig. 1b. The structure has 12 pentagonal faces, with six 5-fold axes running through their centres; and 20 hexagonal faces, with ten 3-fold axes running through their centres. The pentagons are regular, with a bond length of 1.46 Å, but the hexagons are not, and have alternatively long (1.46 Å) and short (1.40 Å) bonds: the short bonds, 30 in number, connect the pentagons and are shared between two hexagons; the long bonds, 60 in number, are shared between a hexagon and a pentagon. The nuclear diameter of the "ball" is about 7 Å.

A brief history of the discovery of these molecules and the development of materials containing $C_{60}$ is as follows[5,6]. As early as 1984-85 studies of mass spectroscopy of carbon clusters by laser vaporisa-

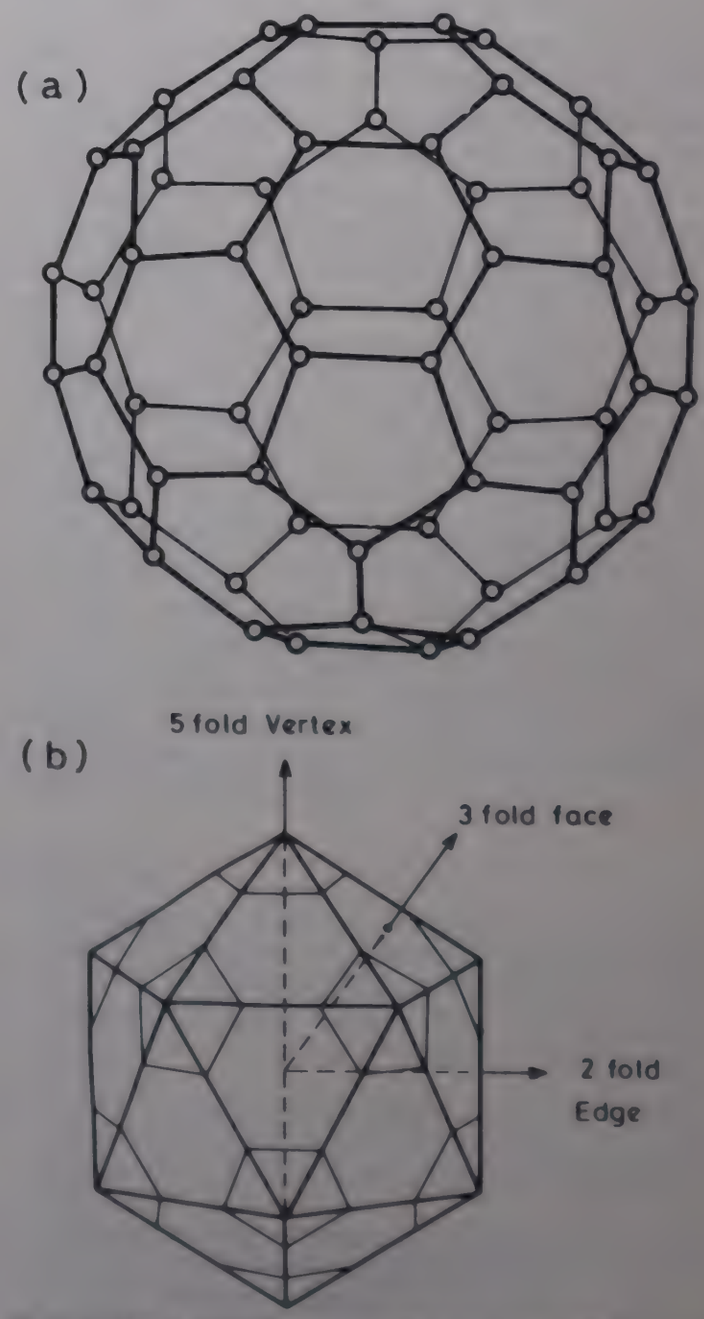


Fig. 1—(a) The truncated icosahedron or soccer ball structure of the $C_{60}$ molecule. (b) Illustration of the truncation of the icosahedron and the appropriate symmetry axes

†Also at Materials Research Centre, IISc, Bangalore

tion of graphite revealed[7] "magic numbers" of carbon clusters, just as in metal clusters. But the discovery of the special stability of $C_{60}$ (and $C_{70}$) is due to Kroto *et al.*[2]. They suggested that $C_{60}$ is very special and is formed in condensing carbon vapour, proposed the correct structure, the name[8] "buckminsterfullerene" for it, and mentioned the possibility of trapping atoms inside the carbon cage. They also suggested that $C_{60}$ or its derivatives are responsible for the "Diffuse Interstellar Line Problem"[2,6]. This work was followed by a spate of quantum chemical studies[9] of the $C_{60}$ molecules (mostly unaware of earlier Hückel calculations[10] for the $C_{60}$ structure). However, the experimental work in the field was hampered by the difficulty of making large amounts of $C_{60}$. The major breakthrough leading to a "mass production" of $C_{60}$ came through the work of Kratschamer *et al.*[1]. The discovery that metallic, conducting samples could be obtained[3] by alkali doping, and the subsequent discovery[4] of superconductivity in many such materials[11–13] with rather high $T_c$'s [all in compounds with composition[14] $A_3C_{60}$; the current record for $T_c$ is for Rb-Tl doping[13] with $T_c = 42.5$ K] triggered the explosive growth[5] of the field. Recently[15], ferromagnetism below a $T_c$ of 18 K was reported in materials obtained by doping $C_{60}$ with organic dopants.

It is easy to see that even apart from the superconductivity aspects, these are extraordinarily exciting developments, especially from the chemistry standpoint. For, they essentially open up an entirely new subfield of organic chemistry. There are such possibilities to be investigated as functionalisation by adding H, F, etc. to the ball, substitution of B, N, etc. for carbon, trapping of metal or other atoms inside the C-cage. The resulting materials have potential applications paralleling those of conjugated polymers, in areas of catalysis, energy storage, synthetic metals, semiconductors, etc. One can think of other exotic possibilities of $C_{60}$ balls acting as a microscopic ball bearings and lubricants, etc.

In this article, however, we focus on the physics aspects of the materials derived from $C_{60}$ (including their crystal structure, electronic structure, optical properties, vibrational properties, phase transitions; metallisation, superconductivity and ferromagnetism resulting from doping, etc.) which are interesting in themselves.

It is worth noting that $C_{60}$ and $C_{70}$ are only two of a large number of possible "fullerenes", $C_{28}$, $C_{32}$, $C_{50}$, $C_{60}$, $C_{70}$, $C_{84}$, $C_{240}$, $C_{540}$, etc. All the structures can be thought of as finite sheets of graphite "wrapped up" into balls. In order to relieve the strain induced by the "wrapping up" procedure, one has to introduce pentagonal "defects". It is interesting to note that precisely 12 pentagons are enough no matter how large is the ball[16].

The rest of this review is organised as follows: Section 2 contains discussions of the crystal structure, electronic structure, optical properties, vibrational properties and the effect of pressure on the crystal and electronic structure of pure $C_{60}$. The properties of alkali-doped $C_{60}$ are discussed in Section 3. Section 4 is devoted to discussions of interaction effects and the mechanisms of superconductivity.

## 2 Properties of pure $C_{60}$

### 2.1 *Structure*

The room temperature crystal structure[1,17] of pure $C_{60}$ is an FCC lattice with a conventional unit cell size of $a_0 = 14.1$ Å, corresponding to a nearest neighbour distance of 10 Å. The corresponding powder XRD pattern is shown in Fig. 2. It can be noted that the (200), (400), ... peaks are nearly absent, and there are other "deserts" of intensity compared to more conventional FCC scattering patterns. These features are due to the "molecular form factor" $S_m(Q)$ of a single $C_{60}$ ball. At the simplest level of approximation $S_m(Q)$ is well modelled by assuming that the carbon atoms on the $C_{60}$ ball are distributed uniformly on a spherical shell of radius $R = 3.52$ Å, leading to

$$S_m(Q) \propto j_0(QR)\, f_c(Q) = \frac{\sin QR}{QR} f_c(Q) \qquad \ldots(1)$$

where $f_c$ is the X-ray form-factor of a single carbon atom.

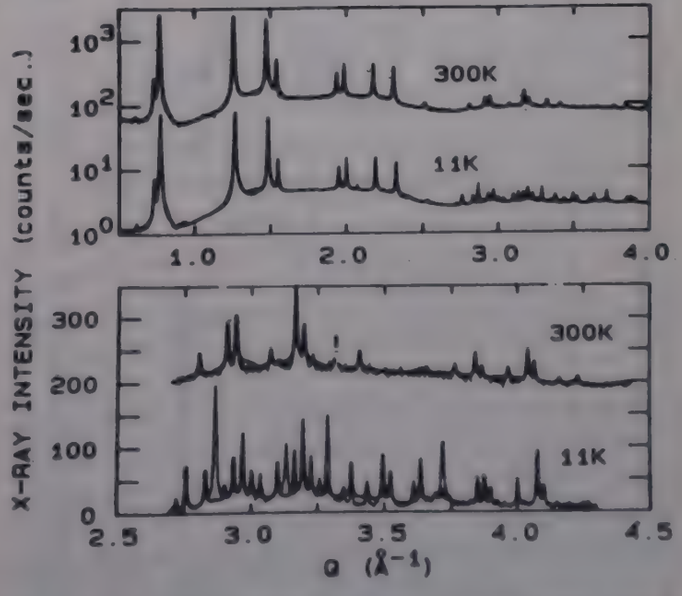


Fig. 2—X-ray diffraction intensity of pure $C_{60}$ (powder sample plus capillary) at 300 K and 11 K. Light (heavy) curve is data (model fits). The lower panel is a blow up of the top panel data in a small range of Q (after reference 17)

Both the X-ray crystal structure[17] and NMR evidence[18] indicate a high degree of rotational disorder implying free rotation of the $C_{60}$ molecules at room temperature. This is not surprising since $C_{60}$ is a molecular solid with rather weak intermolecular interactions. Hence, the librational frequencies and the barriers that hinder rotations of the $C_{60}$ molecules are expected to be very low. So the room temperature phase is actually a "plastic crystal".

Even more interestingly[17], as the temperature is lowered below 250 K, pure $C_{60}$ undergoes a first order orientational freezing transition, or a plastic crystal → crystal transition, into a simple cubic (SC) phase with 4 bulky balls per unit cell. The cell constant $a_0$ is essentially the same as before, showing basically that 4 originally equivalent bulky balls have now become inequivalent. The powder XRD evidence[17] is shown in Fig. 2. Fig. 3 shows more detailed information[17] about the transition, including some data about the temperature dependence of the single cubic order parameter, and the DSC data. The entropy change associated with the transition is $\Delta S = 6.7\ J/g \simeq R \ln 8$. In the low temperature phase, the charge distribution on the $C_{60}$ ball is no longer spherically symmetrical but acquires $Y_{6m}(\theta, \phi)$ terms adding terms proportional to $j_6(QR)$ to $S_m(Q)$. A detailed model of the orientational ordering in the SC phase consistent with the diffraction data has been proposed[17]. Constant pressure molecular dynamics simulations have been done[19] to calculate the rotational diffusion coefficients, etc., across the transition. The rotation diffusion coefficient is $1.5 \times 10^{12}\ sec^{-1}$ at 300 K (typical of rapid rotation) and it drops to zero below about 200 K. The freezing of the orientations is accompanied by appearance of new librational modes. The phonon density of states ($C(\nu)$) obtained from the Fourier transform of the velocity auto-correlation function at two different temperatures is shown in Fig. 4. The simulations also show that the rotational diffusion coefficient falls to $5 \times 10^{10}\ sec^{-1}$ at P = 17.5 kbar at 300 K.

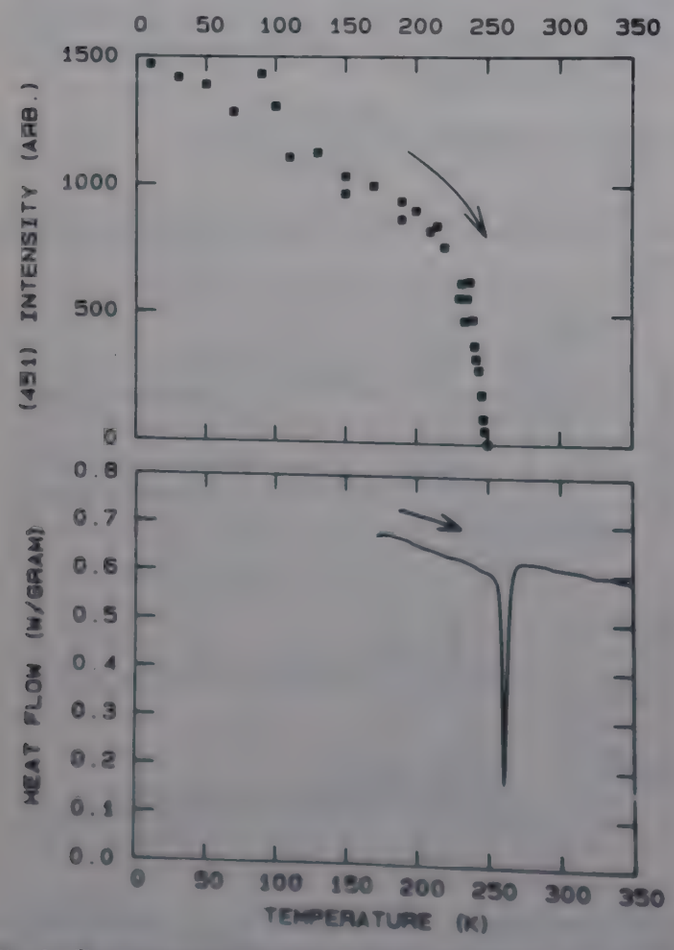


Fig. 3—Top integrated intensity of the (451) X-ray line (forbidden for an FCC lattice) as a function of temperature. Bottom DSC data on $C_{60}$ powder (after ref.17)

### 2.2 *Electronic structure*

The electronic structure of a single $C_{60}$ molecule has been extensively studied[9] and is well described at the simplest level by a molecular orbital picture. The core $(1s)$ and $2(sp)_\sigma$-bonding (antibonding) orbitals[20] are very tightly bound (antibound) and hence fully occupied (empty), and can be ignored for most

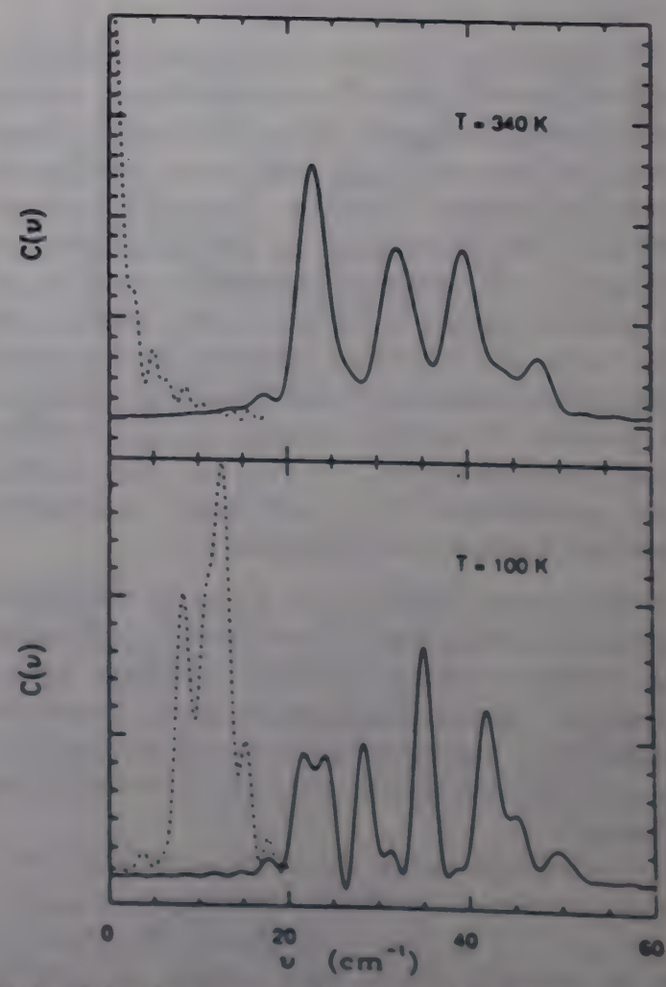


Fig. 4—Molecular dynamics simulation of the translational (boldlines) and librational (dotted) density of states at 340 and 100 K (after ref.19)

purposes. The most important "valence" molecular orbitals, arise from the overlap of the 60 $(2sp)_\pi$ orbitals[20], and it has been shown[21] that a reasonable description of these molecular orbitals and their spectrum can be obtained by a tight-binding model of $(2sp)_\pi$ electrons on the "$C_{60}$ lattice", with hopping amplitudes $t \simeq 2$ eV on the long bonds, and $t' \sim (1\text{-}1.3)t$ on the short bonds. The corresponding spectrum is shown in Fig. 5, and gives a good zeroth level account of the spectroscopy of single $C_{60}$ molecules (as seen in its gaseous phase, for example). The orbitals can be symmetry-classified according to the irreducible representations of the icosahedral group $I_h$, as indicated in the figure. Had the electron distribution on the ball been completely smeared and spherically symmetric (as in the simple model for the X-ray structure factor alluded to earlier) then these orbitals could have been classified by the orbital angular momentum $l$, with the energy scaling (in a continuum limit) as $l(l+1)$. The icosahedral charge distribution, with its leading spherical harmonic component being $Y_{6m}(\theta, \phi)$, splits these O(3) classified levels into the $I_h$ classified levels as indicated in the figure.

In the neutral $C_{60}$ molecule, 30 of these molecular orbitals are fully occupied with 2-electrons each (in a Hartree-Fock picture) as indicated in Fig. 5. A gap of $\simeq 1.5$ eV separates the 5-fold degenerate, $h_u$, highest occupied molecular orbitals (HOMO levels) from the 3-fold degenerate $t_{1u}$ lowest unoccupied molecular orbitals (LUMO levels). The three $t_{1u}$ orbitals have wavefunctions which have $p$ like reflection symmetry, and their amplitudes peak in belts around the $yz$, $zx$ and $xy$ planes. We will label these with indices $x$, $y$, $z$ or 1, 2, 3.

The band structure of the crystalline $C_{60}$ (fullerite) has also been studied by many groups[22-24] using a variety of techniques. Fig. 6 shows the calculated band structure of the FCC $C_{60}$ lattice using the first principles, self consistent, orthogonalised linear combination of atomic orbitals techniques[24]. The results are similar to those obtained[22] by using the local density approximation except for some difference in the ordering of the bands near the X-point. The calculated direct band gaps which are slightly underestimated are 1.34 eV at X-point and 1.87 eV at the Γ point. The bandwidths of the top valence band and the first set of conduction band are 0.55 eV, in agreement with the photoemission[23] data. The density of states (DOS) spectrum from $-6$ to $+6$ eV is shown[24] in Fig. 7. Fig. 7 also shows the calculated real part, $\varepsilon_1(\omega)$, and imaginary part, $\varepsilon_2(\omega)$, of the dielectric function, $\varepsilon(\omega)$, and the energy loss function (ELF), $\mathrm{Im}(-1/\varepsilon(\omega))$. The fine features in

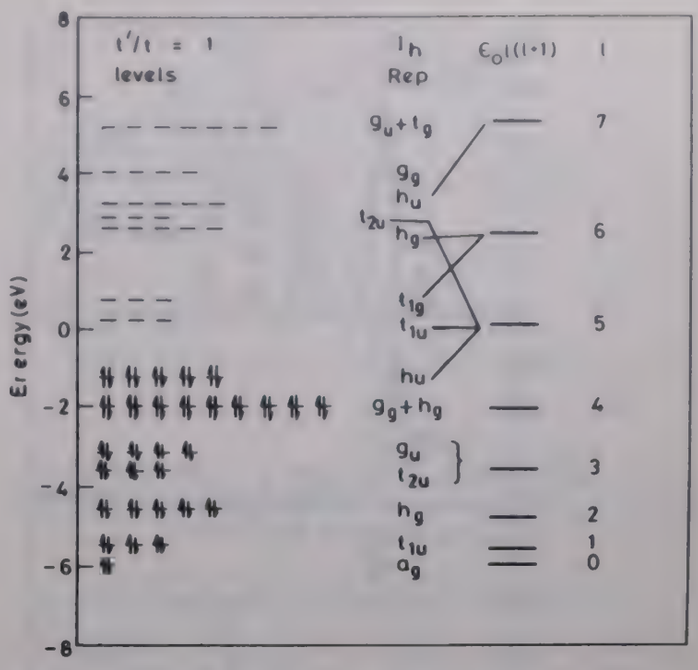


Fig. 5—Molecular orbital energy level diagram of the $(2sp)\pi$ orbitals as fit by a t-t' tight binding model on the $C_{60}$ lattice with $t'/t = 1$. The $I_h$ classification of the levels is indicated. For comparison a spherically symmetric continuum description of these levels with an appropriately chosen energy scale and labelled by an orbital regular momentum index 1 is also given

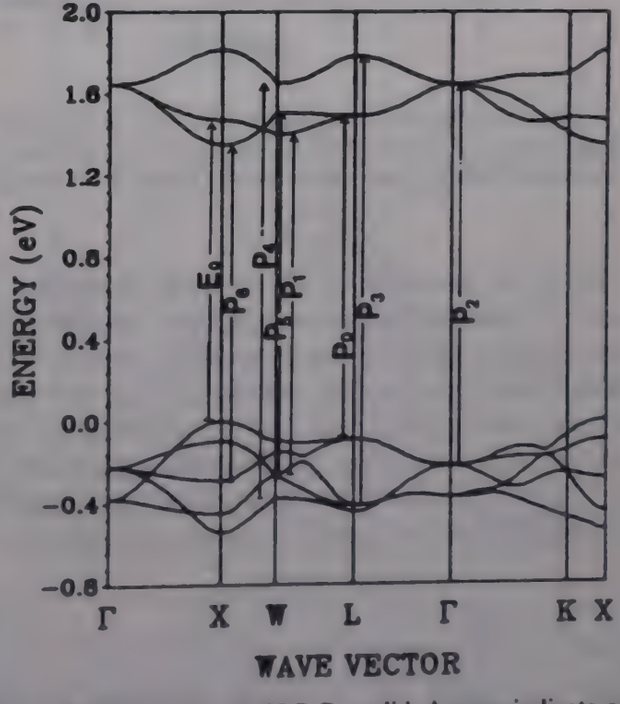


Fig. 6—Band structure of FCC $C_{60}$ solid. Arrows indicate optical transitions at the critical points of the bands (after ref.24)

$\varepsilon_2$ (shown in Fig. 7) centred at 1.8, 2.7, 4.3, 5.3 and 6.3 eV have been identified with various transitions arising from the occupied to the unoccupied bands shown in the DOS; e.g. feature A arises from the transition $V_1 \rightarrow C_1$. The expanded $\varepsilon_2(\omega)$ in the energy range 1.2 to 2.2 is also shown in Fig. 7. The static dielectric constant of $\varepsilon_1(\omega = 0)$, equal to 4.4, is comparable to that of diamond.

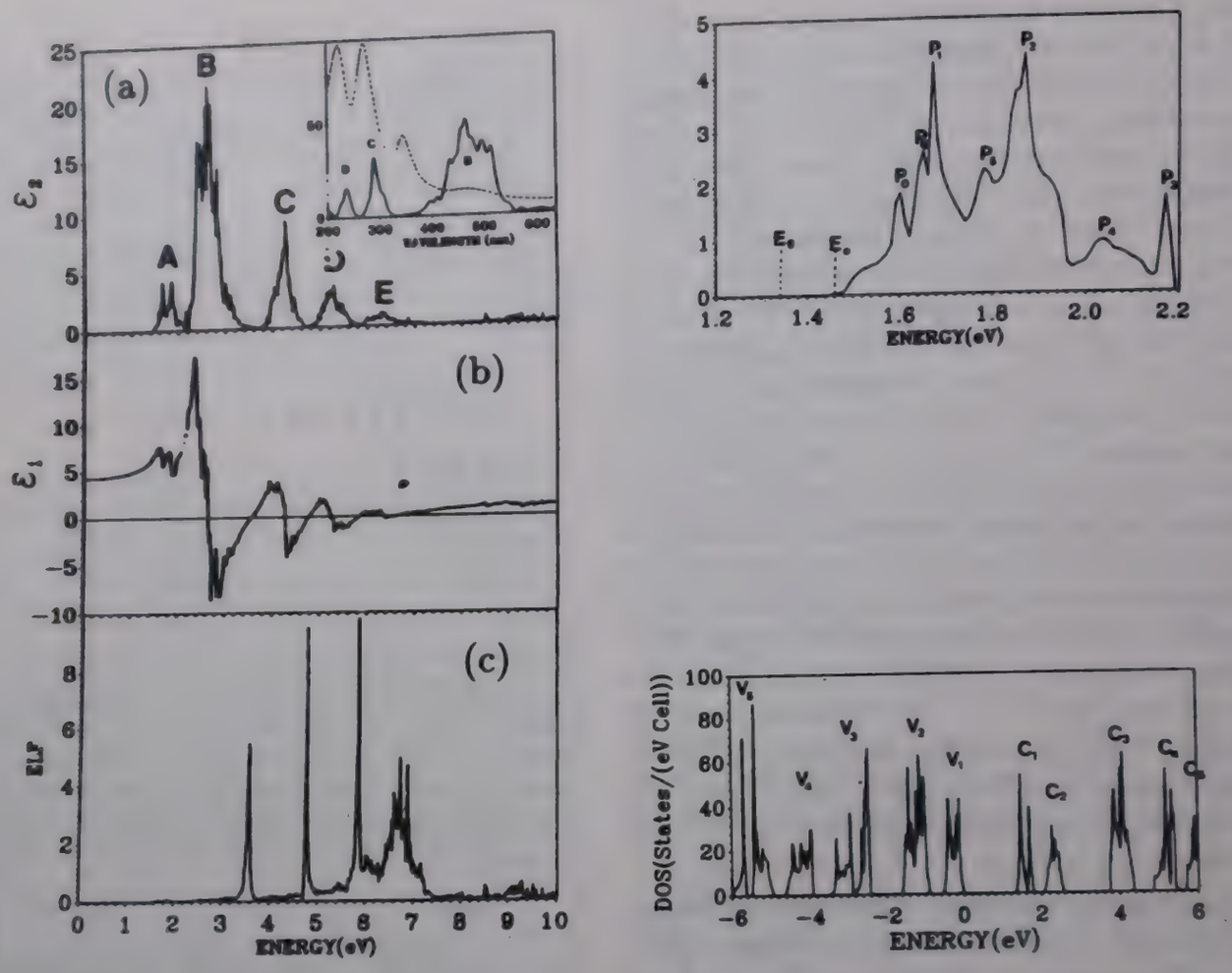


Fig. 7—Right bottom panel: Calculated DOS of FCC $C_{60}$. Right top panel: $\varepsilon_2(\omega)$ in the visible optical range 1.2-2.2 eV. Left panel: (a) Imaginary part $\varepsilon_2(\omega)$, of the dielectric function $\varepsilon(\omega)$, (b) Real part $\varepsilon_1(\omega)$, and (c) energy loss function $\mathrm{Im}(-1/\varepsilon(\omega))$. Inset: solid line is the calculated optical conductivity and the dotted line is the visible-UV absorption spectrum of $C_{60}$ solution from ref. 1 (after reference 24).

The band structure of $C_{60}$ is well described in terms of tight binding wavefunctions obtained by linear combinations of the molecular orbitals. Note that the point group of the crystalline $C_{60}$ with fully oriented balls is not $I_h$, but only a subgroup $T_h$, and the band structure splits the (3-fold) degeneracy of the (LUMO) molecular orbitals. The tight binding Hamiltonian for the LUMO band can be written as

$$\mathcal{H}_{TB} = \sum_{ijab} t_{ab}(\mathbf{r}_i - \mathbf{r}_j) c^+_{ia} c_{jb} + \varepsilon_0 \sum_{ia} c^+_{ia} c_{ia} \qquad \ldots(2)$$

where $c^+_{ia}$, $a = x, y, z$, create electrons in the 3 LUMO orbitals at site i. For the case of the oriented FCC $C_{60}$ [i.e. each $C_{60}$ in an identical orientation], the $t_{ab}(\mathbf{r}_i - \mathbf{r}_j)$ are characterised by four independent parameters[25], e.g: $t_{xx}(110) \equiv t_1$, $t_{yy}(110) \equiv t_2$, $t_{zz}(110) \equiv t_3$, $t_{xy}(110) \equiv t_4$ (The other hopping matrix elements are permutations of these same 4 parameters apart from signs). The corresponding $k$-space version of the Hamiltonian can be written as

$$\mathcal{H}_{TB} = \sum_{k} \{\varepsilon_0 \delta_{ab} - t_{ab}(\mathbf{k})\} c^+_{ka} c_{kb} \qquad \ldots(3)$$

The matrix $t_{ab}(\mathbf{k})$ can be written as the sum $t^{xy}_{ab}(\mathbf{k}) + t^{yz}_{ab}(\mathbf{k}) + t^{zx}_{ab}(\mathbf{k})$ where

$$t^{xy}_{ab}(\mathbf{k}) \equiv 4\cos\left(\frac{k_x a_0}{2}\right)\cos\left(\frac{k_y a_0}{2}\right)\begin{pmatrix} t_1 & 0 & 0 \\ 0 & t_2 & 0 \\ 0 & 0 & t_3 \end{pmatrix}$$

$$+ 4\sin\left(\frac{k_x a_0}{2}\right)\cos\left(\frac{k_y a_0}{2}\right)\begin{pmatrix} 0 & t_4 & 0 \\ t_4 & 0 & 0 \\ 0 & 0 & 0 \end{pmatrix} \qquad \ldots(4)$$

and the other matrices $t^{yz}_{ab}$ and $t^{zx}_{ab}$ can be obtained by cyclic permutations of $(k_x, k_y, k_z)$ and of the matrix entries. We find[25] that the LUMO bands obtained by Saito *et al.*[22] can be well fitted by the choice $t_1 = 0.0089$ eV, $t_2 = 0.034$ eV, $t_3 = -0.020$ eV, $t_4 = 0.019$ eV, $\varepsilon_0 = 0.718$ eV.

### 2.3 *Optical properties*

The optical absorption spectrum of $C_{60}$ dissolved in hexane is shown[26] in Fig. 8. There are three ab-

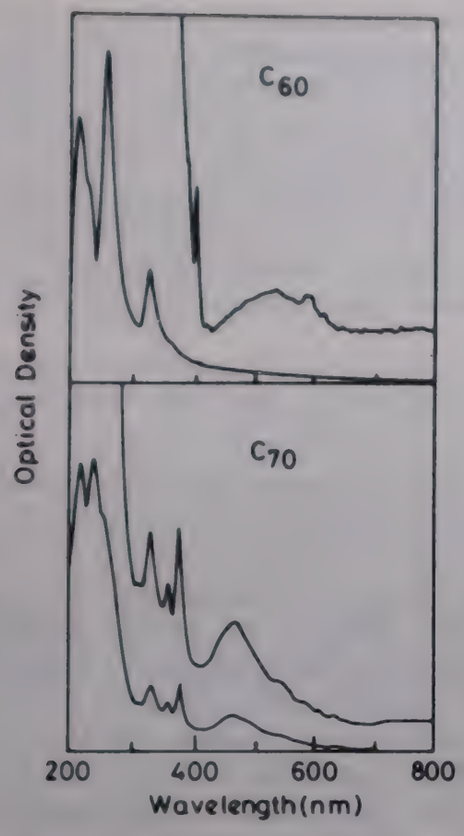


Fig. 8—Optical absorption spectra of $C_{60}$ (top panel) and $C_{70}$ (bottom panel) dissolved in hexane (after ref.26)

sorption features at 213, 257 and 329 nm. An unusually sharp but weak feature has been observed at 404 nm. The other weak features are centered at 500, 540, 570, 600 and 625 nm. The calculated visible-ultraviolet absorption spectrum which is proportional to the conductivity $\sigma(\omega) = \omega\varepsilon_2(\omega)/4\pi$ agrees with the main features of the observed spectrum, as shown in the inset of Fig. 7 (left panel).

Electronic transitions have also been observed by high resolution electron energy loss spectroscopy[27] (HREELS) in the energy range of 1.5 to 30 eV, by X-ray photoemission[23] (XPS) and ultraviolet photoemission[28] (UPS). The results of various techniques have been summarised and compared in Fig. 9.

The other experimental probes of electronic excitations are photoluminescence and excitation spectroscopies. The photoluminescence spectrum[29] of a single crystal of $C_{60}$ at 300 K is shown in Fig. 10. The onset of the emission occurs at about 1.80 eV and overlaps the absorption band of the solid $C_{60}$ reported by Reber *et al.*[30]. The peak of the emission band at ~13500 $cm^{-1}$ (1.67 eV) is in the same energy region as the peaks in $\varepsilon_2(\omega)$ shown in Fig. 7a. The hump at ~12500 $cm^{-1}$ (1.55 eV) may be due to the excitonic transition as suggested by the calculations of Ching *et al.*[24].

Fullerene has delocalised $\pi$-electrons and, therefore, exhibits a sizeable ultrafast optical nonlinear

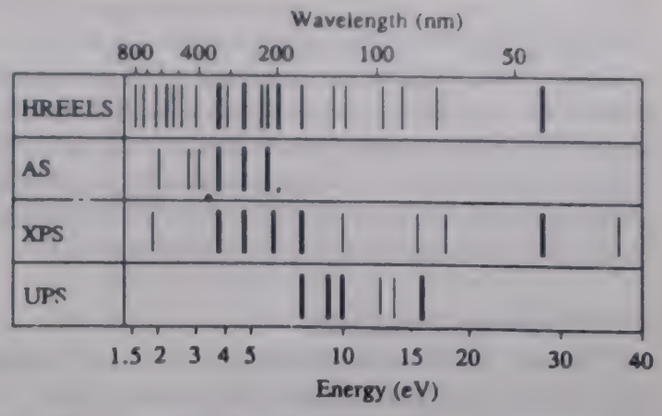


Fig. 9—Comparison of electronic excitation energies of $C_{60}$ as obtained using various techniques. The strong features are indicated by thick lines (after reference 27)

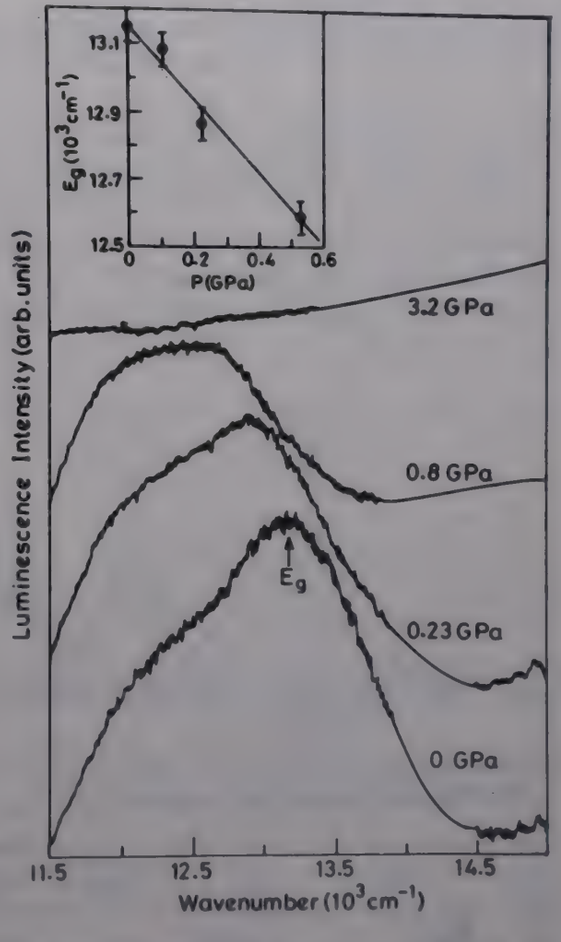


Fig. 10—Room temperature luminescence spectra of simple crystals of $C_{60}$ at four different pressures 0.0, 0.23, 0.8 and 3.2 GPa. The inset shows the variation of the peak position, marked as $E_g$, for low pressures (after reference 29)

response, similar to that in conjugated polymers like polyacetylene and polydiacetylene. Degenerate four-wave mixing experiments[31] in solutions of $C_{60}$ in benzene gave the magnitude of the nonlinear susceptibility per $C_{60}$ molecule as $\gamma = 1.5 \times 10^{-42} m^5 V^{-2}$, comparable to that observed in polydiacetylene. A simple model of 60 delocalised electrons on a spherical surface[31] (circumference = 22 Å, electron shell width = 2.5 Å) gives $\gamma = 2 \times 10^{-42}$ $m^5 V^{-2}$ and

the first absorption at 550 nm, both the quantities in good agreement with the experimental data.

There have been very few studies of the optical properties of solid $C_{60}$ so far. Reber *et al.*[30] have reported the optical absorption at 20 K of solid $C_{60}$ deposited on Ca $F_2$. The onset of absorption occurs at 1.74 eV and the weak feature at 1.79 eV has been attributed to be due to an electronic transition

2.4 *Vibrational Properties*

There are 174 intramolecular vibrational modes of $C_{60}$ which transform under $I_h$ symmetry as[32]

$$\Gamma = 2a_g(R) + 8h_g(R) + 4t_{1u}(IR) + 3t_{1g} + 4t_{2g} + 6g_g + a_u + 5t_{2u} + 6g_u + 7h_u$$

where (R) and (IR) refer to Raman and infrared active modes, respectively. The four IR active modes occur at[1,33,34] 526, 577, 1182 and 1429 $cm^{-1}$. Bethune *et al.*[34] have measured the Raman spectra of chromatographically separated $C_{60}$ and $C_{70}$ films and based on the measured depolarization ratios have identified the following modes: $a_g$ modes at 496 and 1468 $cm^{-1}$; $h_g$ modes at 273, 437, 710, 774, 1099, 1250, 1428 and 1575 $cm^{-1}$. Fig. 11 shows the three dominant modes in our[29] Raman spectra of single crystals of $C_{60}$. In fact Raman fingerprints can be used to characterise the purity of $C_{60}$ with respect to the presence of $C_{70}$ because the latter has a strong Raman line at 1568 $cm^{-1}$. The Raman polarizability of this mode seems considerably higher than the corresponding mode at 1468 $cm^{-1}$ in $C_{60}$ because a sample containing $C_{60}/C_{70} = 2.1$ gives almost equal Raman intensities for both the lines[35].

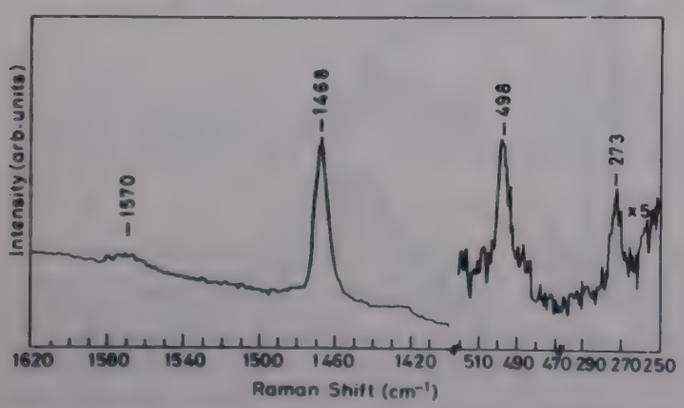


Fig. 11—Raman spectrum of single crystal of $C_{60}$ at 300 K using 5145 Å argon ion laser (after reference 29)

Fig. 12 shows the neutron inelastic scattering (NIS) spectra[36] wherein some more vibrational modes, not observed earlier by IR and Raman techniques, are seen because there are no group theoretic selection rules in NIS. The vibrational modes (11 of them) have also been observed by HREELS[27] and Fig. 13 shows the comparison of the observed frequencies obtained by various techniques[34,37] where the strong features in each spectroscopy are indicated by thick lines. All these intramolecular modes, in the frequency range 200-1600 $cm^{-1}$, can be classified[36] according to whether their displacements are dominantly radial/buckling (200-880 $cm^{-1}$ region) or tangential motion (880-1600 $cm^{-1}$). The lowest frequency intramolecular mode in $C_{60}$ at 273 $cm^{-1}$, called the squashing mode, corresponds to an ellipsoidal deformation of the $C_{60}$ pseudo-sphere whereas the 496 $cm^{-1}$ mode corresponds to pure radial deformations. The high frequency intense mode at 1468 $cm^{-1}$ is called the pentagonal pinch mode. The pentagons and hexagons of the icosahedron structure expand and contract in and out of phase for the 496 and 1468 $cm^{-1}$ modes, respectively. In addition to these intramolecular modes, solid $C_{60}$ has intermolecular, librational and translational, external modes lying in the frequency range 5-200 $cm^{-1}$. (In $K_3C_{60}$ there are, in addition, $K^+$-$C_{60}^{3-}$ vibrational modes in this range)[36].

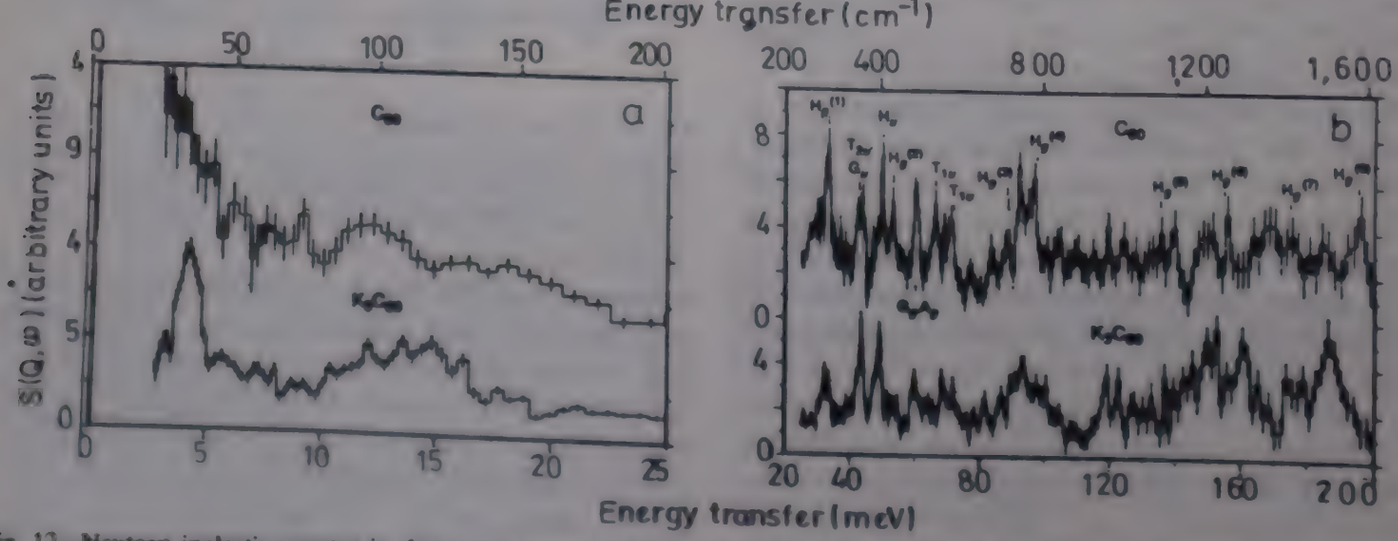


Fig. 12—Neutron inelastic spectra in the energy range (a) 0-200 $cm^{-1}$ and (b) 200-1600 $cm^{-1}$, of $C_{60}$ at 20K (top curve) of and $K_3C_{60}$ (bottom curve) (after ref. 30).

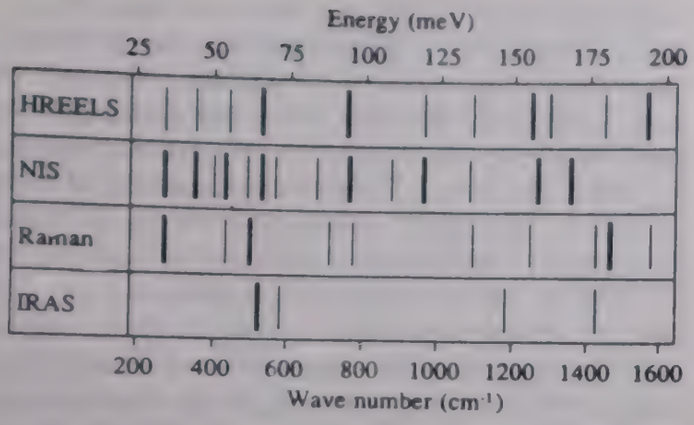


Fig. 13—Comparison of intramolecular vibrational mode energies of $C_{60}$ as obtained by various techniques. The strong features are indicated by thick lines (after ref.27)

Sinha *et al.*[38] have carried out resonance Raman scattering for the highest frequency pentagonal pinch mode in a $C_{60}$ film grown on Si and show that the Raman excitation profile has a peak at ~ 2.4 eV, indicating that the mode is predominantly interacting with electronic excitations of this energy.

Fig. 12 also shows[36] the vibrational modes of $K_3C_{60}$. The following features are noteworthy: A prominent feature at 4.3 meV (i.e. 35 $cm^{-1}$), a broad band at 14 meV, a redistribution of intensities between the radial and tangential modes. The low frequency features have been suggested to belong to $K^+$-$C_{60}^{3-}$ optic modes.

### 2.5 *Effect of pressure*

Room temperature powder X-ray diffraction studies have been done upto 1.2 GPa by Fischer *et al.*[39] and upto 20 GPa by Duclos *et al.*[40] The isothermal volume compressibility $\kappa$ is found to be $6.9 \times 10^{-2}$ $(GPa)^{-1}$ (by Fischer *et al.*[39]) and $(5.5 \pm 0.5) \times 10^{-2}$ $(GPa)^{-1}$ by Duclos *et al.*[40] who also quote a pressure derivative $d\kappa^{-1}/dP = 5.7 \pm 0.6$. The isothermal compressibility of $C_{60}$ is about 3 times that of graphite and 38 times that of diamond[39]. The linear compressibility of $2.3 \times 10^{-2}$ $(GPa)^{-1}$is essentially the same as the inter-layer compressibility $d(\ln c)/d(\ln P)$ of graphite. This implies that the reduction in volume decreases the van der Waals separation between $C_{60}$ molecules and does not compress the individual molecule. This is consistent with the pressure dependence of the X-ray diffraction intensities[39].

It has been also shown by X-ray diffraction experiments[40] that the symmetry of the FCC $C_{60}$ solid is lowered at $16 \pm 1$ GPa under non-hydrostatic pressures. It is likely that such transitions may occur at higher pressures under hydrostatic pressures. Under shock loading, it was found by Raman scattering that $C_{60}$ solid transforms to graphite at 17 GPa and 600°C. Recently[42], the electrical resistivity of solid $C_{60}$ powder has been measured upto 25 GPa using a Bridgman anvil apparatus. The magnitude of the semiconducting gap has been obtained at different pressures from the temperature-dependent resistivity. These measurements show that the resistivity and the gap decrease with increasing pressure but there is a sudden transition at 15-20 GPa to a more insulating phase. It will be worth reinvestigating these results because the gap extrapolated to ambient pressure in these experiments is only 0.45 eV, much smaller than the calculated band structure value (~ 1.5 eV) or that obtained from optical experiments. The low value of the gap suggests that the resistivity they are seeing is dominated by impurity conduction.

Sood *et al.*[29] have carried out photoluminescence and optical microscopic observation of the single crystals of $C_{60}$ under hydrostatic pressures upto 5 GPa. Fig. 10 shows the red shift of the photoluminescence band with increasing pressure. The colour of the crystal also changed from red to black as seen visually in transmission geometry at ~ 3.2 GPa. The inset in Fig. 10 shows the pressure dependence of the peak position, marked as $E_g$. The least square fitted pressure derivative $\partial E_g/\partial P$ is $-0.138$ eV/GPa. It is reasonable to interpret $E_g$ as a band gap due to some conduction band → valence band transition, but it not clear as to which specific transition it is. The change in colour occurs because of an increase in the absorption coefficient of the visible light due to the significant reduction in the band gap. The reduction of the band gap with pressure is directly related to the broadening of the valence and conduction bands due to increased interball resonance interaction. At a simple level of approximation, taking equal dispersion for the two bands (of width W), $\partial W/\partial(\ln a) = -\partial E_g/\partial(\ln a)$. Hence, using the known compressibility we can estimate a "deformation potential" $\partial W/\partial(\ln a) \cong 6$ eV.

Aoki *et al.*[43] have measured the pressure dependence of the four $t_{iu}$ intramolecular IR modes of solid $C_{60}$. The observed pressure derivative $dw/dP$ of all the modes (except the lowest frequency) lies in the range 0.2 to 0.45, similar to that of the 1470 $cm^{-1}$ mode of diamond ($dw/dP = 0.32$). It implies that the intramolecular force constants in $C_{60}$ and diamond are similar. A negative value of $dw/dP$ for the lowest frequency IR active mode[43] (which corresponds to radial displacements of the $C_{60}$ pseudosphere) is interesting and needs to be understood.

### 3 Properties of alkali doped $C_{60}$

Experimental evidence reported so far[12,14,44] indicates that homogeneous phases of alkali-doped $C_{60}$ form only at special compositions $A_3C_{60}$, $A_4C_{60}$ and $A_6C_{60}$ [when one mixes two types of alkali atoms, one can have $A_2A'C_{60}$ etc.]. For intermediate compositions the doped material $A_xC_{60}$ seems to phase separate into the above materials.

The most interesting of these materials is $A_3C_{60}$ [or $A_2A'C_{60}$] which has the "cryolite" structure[44], shown in Fig. 14. This is an FCC structure with a basis of three alkali ions and one $C_{60}$ ball. The $C_{60}$ balls, now negatively charged, are in the same positions as in the pure $C_{60}$ crystal, but the lattice is now slightly expanded, with the lattice constants as indicated in Fig. 15 for a whole sequence of materials. With respect to the $C_{60}$ balls, the $A^+$ ions sit at octahedral sites (as in a Rocksalt structure) and at tetrahedral sites (forming an inner cube of size $a_0/2$) as indicated in Fig. 14. [A basis that corresponds to this structure, for example, is $C_{60}^{3-}(0,0,0)$, $A^+(\frac{1}{2},\frac{1}{2},\frac{1}{2})$, $A^+(\frac{1}{4},\frac{1}{4},\frac{1}{4})$, $A^+(\frac{3}{4},\frac{3}{4},\frac{3}{4})$]. The $C_{60}$ balls are now no longer free to rotate, but are oriented with 8 of their (20) hexagonal faces perpendicular to the (111) directions. (This still leaves two equivalent orientations related by a 90° rotation around (100), which seem to be randomly chosen at room temperatures[44].

The most remarkable physical property of $A_3C_{60}$, of course, is that it is metallic at room temperature and goes superconducting below critical temperatures in the range 18-40 K depending on the material. The transition temperature of the various materials are indicated in Fig. 15 together with their lattice constants. After the discovery of superconductivity in these materials, many studies[5] have been undertaken to determine a variety of their properties. We list below the principal results, referring the reader to the original papers for more details. (1) $T_c$ decreases dramatically with increasing pressure[45]. $(dT_c/dp) \simeq -0.78$ K/Kbar for $K_3C_{60}$. [This is consistent with the increase of $T_c$ with the lattice constant[12] as shown in Fig. 15. See ref. 12 and below for a more detailed analysis]. (2) Magnetisation measurements[46] in $K_3C_{60}$ lead to the following esimates for the extrapolated critical fields at zero temperature. $H_{c_2} \cong 49\,T$ and $H_{c_1}(o) \simeq 132\,oe$. From these, if the pure superconductor expressions are used, one gets a coherence length $\xi \simeq [\phi_0/2\pi H_{c_2}(o)]^{1/2} \simeq 26$Å, and using $H_{c_1}(o) = \phi_0/4\pi\lambda^2 \ln(\lambda/\xi)$ one gets $\lambda \simeq 2400$ Å. It is likely that the dirty superconductor expressions (e.g. $\xi_0 = \xi^2/l$ where $l$ is the mean free path) are much more appropriate and the actual coherence length is much larger. In any case it is clear that $A_3C_{60}$ is an extreme type II superconductor. The critical current density estimated from the magnetisation measurements is $J_c(H \simeq 10\,koe) \simeq 1.2 \times 10^5$ amp/cm$^2$. (3) $\mu$-Spin rotation measurements[47] have also been carried out and these yield a somewhat larger $\lambda$ value of 4800 Å, which is probably more reliable as $H_{c1}$ tends to be generally overestimated in magnetic measurements due to effects of flux pinning[47].

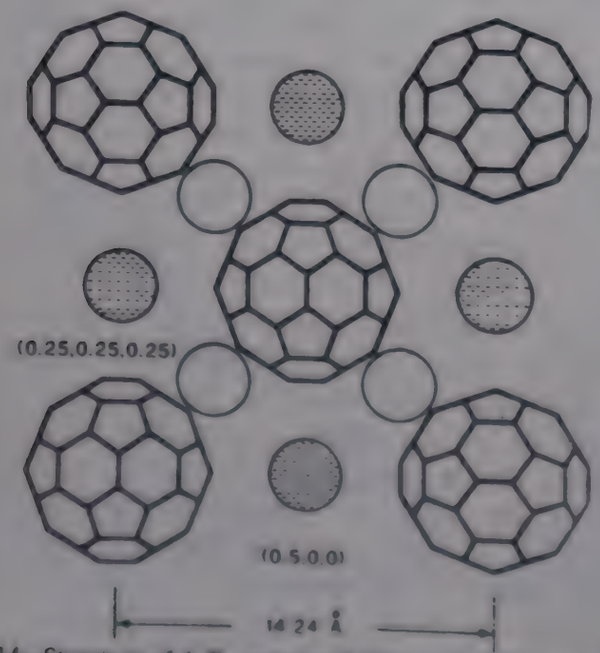


Fig. 14 - Structure of $A_3C_{60}$ as viewed along with (100) axis. The shaded (open) small circles represent alkali atoms at octahedral (tetrahedral) sites as indicatd (after ref.44)

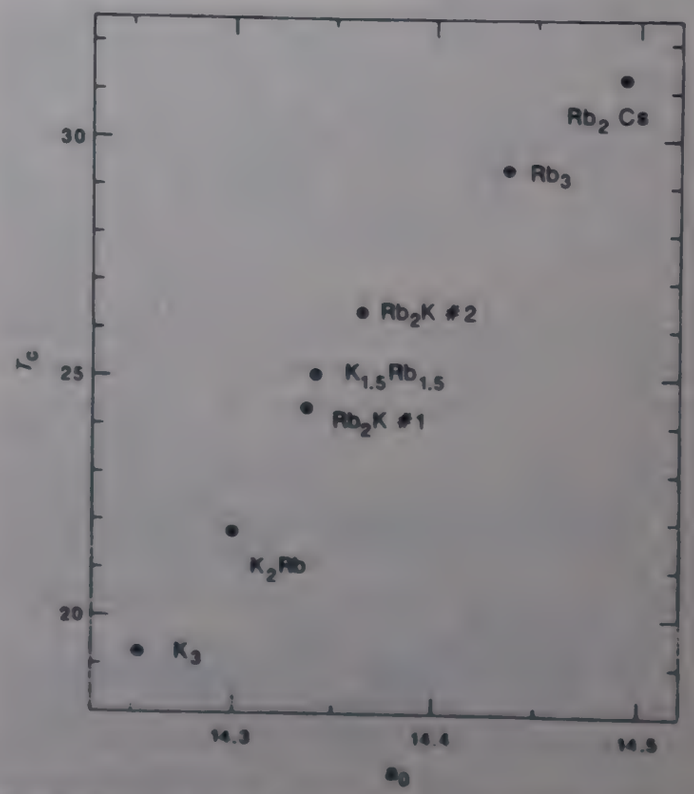


Fig. 15 – Depenedence of superconducting transition temperature $T_c$ on the lattice parameter $a_o$ (A) for various alkali doped fullerenes (after ref.12)

It is reasonable to assume that the band structure of the $A_3C_{60}$ is essentially the same as that of pure $C_{60}$, with slightly reduced bandwidths (because of the expanded lattice). Furthermore, the alkali ions are likely to be just closed shell $A^+$ ions, contributing 3 electrons/$C_{60}$ to the LUMO bands. Hence, one expects a metal with a half-filled LUMO band. Using the density of states (DOS) obtained from our tight binding fit to the LUMO band discussed earlier, we find[25] an $\varepsilon_F = 1.734$ eV, DOS at the Fermi level $N_0 \cong 10.4/\text{spin/eV/C}_{60}$ (see Fig. 16a). The $k_z = 0$ section of the Fermi-surface (FS) that results (obtained using this same tight binding fit), is shown in Fig. 16b. The topmost of the LUMO bands is completely empty, and the FS has a hole-like simply connected piece centred at the Γ point in the bottom-most LUMO band, and pieces with more complicated connectivities in the middle LUMO band. Recently[48,49], local density functional band structure calculations have been carried out for $K_xC_{60}$. The results are in agreement with the above observations. The calculated[49] DOS is in good agreement with that measured[50] from photoemission studies. The full 3-d Fermi surface is also given in ref. 49. Hamada *et al.*[49] further note that there is near nesting of the FS in the middle band, (a feature that is also clear from Fig. 16b) leading to a peak in the susceptibility $\chi(q)$ for $q = (2\pi(a)(100)$.

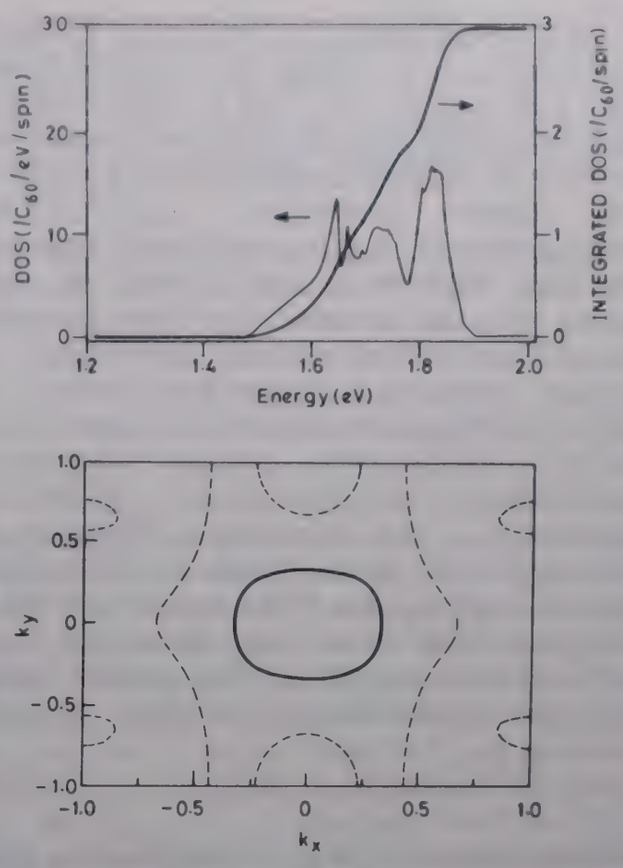


Fig. 16—(a) DOS (thick line) and integrated DOS (thin line) for the $t_{1u}$ band of $C_{60}$ as obtained from the tight binding fit[25]. (b) Section of the fermi surface for $A_3C_{60}$ in the $k_z = 0$ plane obtained from the same fit[25]. The solid and dashed lines correspond respectively to the bottom and middle bands

## 4 Interactions, effects and mechanisms of superconductivity

The simplest mechanism that has been explored to explain the superconductivity in $A_3C_{60}$ is the conventional electron-phonon mechanism. Two recent papers that do this are by Varma *et al.*[51] and Schluter *et al.*[52], with somewhat different results.

It is clear that intramolecular electron-phonon couplings, between the $t_{1u}$ orbitals on a ball and the vibrational modes of that ball, are the most dominant of the electron-phonon interactions, since the intramolecular hopping amplitudes are much stronger than the intermolecular amplitudes. The interaction Hamiltonian can be written formally as[51]

$$\mathcal{H}_{el-ph} = \sum_{im\mu a,b} h_{ab}^{m\mu} Q_{m\mu}^{i} c_{ia}^{\dagger} c_{ib}. \qquad \ldots (5)$$

Here $Q_{m\mu}^{i}$ is the m th vibrational mode with degeneracy index $\mu$, of the ball at site $i$. (These modes were discussed earlier in Section 2.4). Under the icosahedral symmetry, the direct product group $t_{1u} \otimes t_{1u}$ breaks up as $a_g + t_{1g} + h_g$. The $t_{1g}$ mode is asymmetric so it cannot couple. The $a_g$ mode does not lift the degeneracy between the $t_{1u}$ orbitals, and hence is like a local chemical-potential term. Its effects are argued to be[51] much less important than the coupling with the $h_g$ modes, which are the most dominant. As discussed in Section 2.4, there are 8 $h_g$ modes, each 5-fold degenerate. For each of these modes, symmetry considerations[53] completely determine the form of the coupling $\Sigma_\mu h_{ab}^{m\mu} Q_{m\mu}$ as the $3 \times 3$ matrix.

$$h^m = \frac{g_m}{2} \begin{pmatrix} Q_{m3} - \sqrt{3}\, Q_{m4} & -\sqrt{3}\, Q_{m1} & -\sqrt{3}\, Q_{m2} \\ -\sqrt{3}\, Q_{m1} & Q_{m5} + \sqrt{3}\, Q_{m4} & -\sqrt{3}\, Q_{m3} \\ -\sqrt{3}\, Q_{m2} & -\sqrt{3}\, Q_{m3} & -2Q_{m5} \end{pmatrix} \qquad \ldots (6)$$

with a single characteristic coupling constant $g_m$ for each $h_g$ mode. The coupling constants and frequencies calculated by Varma *et al.*[51] for the 8 $h_g$ modes using the quantum chemical MNDO semi-empirical technique are shown in Table 1.

For a static distorsion corresponding to the mth mode, it can be shown[53] that the matrix $h^m$ can be written as $R^{-1} H(Q_m) R$ where $R$ is a rotation matrix and $H(Q_m)$ is diagonal, depending only on the

"radial" displacement $Q_m \equiv (\Sigma_\mu Q_{m\mu}^2)^{1/2}$, and it splits the three $t_{1u}$ orbitals into a singlet (label 1 say) with energy $-gQ_m$ and a doublet (labels 2 and 3 say) with energy $gQ_m/2$. The resulting lowering of the electronic energy is then governed by an effective Hamiltonian $-(g_m^2/\omega_m)[a_1^+ a_1 - \frac{1}{2}(a_2^+ a_2 + a_3^+ a_3)]^2$. If $g_m^2/\omega_m$ were much larger than the band width W of the $t_{1u}$ band, this effect would have led to static Jahn-Teller distortions and a "local pairing" scenario[54]. However, in the current context, as is evident from Table 1, $\omega_m$, $(g_m^2/\omega_m) \ll W$, and the traditional picture[55] of retarded electron-electron interactions due to dynamic, virtual (Jahn-Teller) effects, with no static distortions, is more appropriate. Neglecting the dispersion of the phonon bands, and neglecting interband scattering due to the electron-phonon interaction, Varma *et al.*[51] have argued that the effective electron-phonon coupling strength governing the superconducting transition is simply

$$\lambda = \Sigma_m \frac{N_0 g_m^2}{M\omega_m^2} \equiv 2N_0 \Sigma_m V_m \equiv \Sigma_m \lambda_m.$$ The

coupling energies $V_m \equiv g_m^2/(2M\omega_m^2)$ for the different modes calculated by them are summarised in Table 1. From an approximate solution of the Eliashberg equations along traditional lines[55], they calculated $T_c$ using the McMillan formula

$$T_c = (\omega_{av}/1.2) \exp[-1.04(1+\lambda)/\lambda - \mu^*(1+.62\lambda)] \quad \ldots (7)$$

but with the effective phonon frequency which appears as a prefactor, being given by the nonstandard expression[51] $\omega_{av} = \exp\{\Sigma_m(\lambda_m/\lambda)\ln[\omega_m(1-\lambda_m)]\}$ because most of the coupling strength is in the two highest lying modes. The $\mu^*$ in Eq. 7 is the coulomb-pseudopotential parameter[55], which is not easily estimated. Fig. 17 displays the $T_c$ that results[51] as a function of $N_0$ and $\mu^*$. In order to get the right $T_c$ for the alkali-doped $C_{60}$, with[49] $N_0 \gtrsim 12/\text{eV}/C_{60}/\text{spin}$, one needs $\mu^*$ values that are in the range 0.01.

Table 1 also summarises the results of the calculations of Schluter *et al.*[52], which are similar in spirit but different in detail. For them the largest electron-phonon coupling involves the low frequency ($\simeq 400$ cm$^{-1}$) radial surface buckling mode with $h_g$ symmetry. The total coupling strength is somewhat larger, but the effective $\omega_{av}$ would be much smaller. Clearly the discrepancies between the two sets of calculations need to be resolved.

The $\lambda$ values involved above ($\gtrsim .4$) are substantial, and would have other measurable conse-

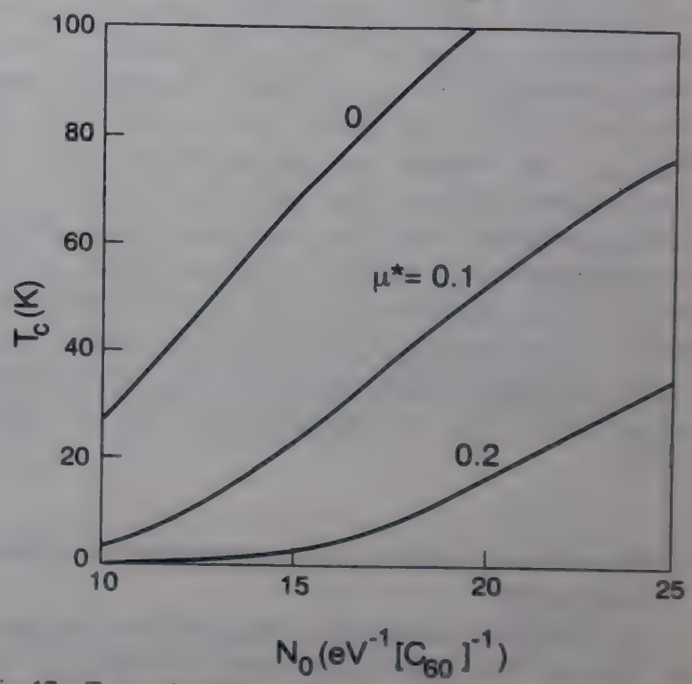


Fig. 17—$T_c$ as a function of the density of states $N_o$ and of the coulomb pseudopotential $\mu^*$ (after ref. 51)

Table 1—Summary of the results of the electron-phonon coupling calculations of Verma *et al.*[51] and Schluter *et al.*[52]

| Vibrational mode symmetry | $\omega_m^{exp}$ (cm$^{-1}$) [Ref. 34] | Theory (Ref. 51) | | | Theory (Ref. 52) | |
|---|---|---|---|---|---|---|
| | | $\omega_m$ (cm$^{-1}$) | $g_m$ (eV/Å) | $V_m$ (meV) | $\omega_m$ (cm$^{-1}$) | $V_m$ (meV) |
| $h_g^{(1)}$ | 273 | 263 | 0.1 | 1.0 | | |
| $h_g^{(2)}$ | 437 | 447 | 0.1 | .25 | ≈ 400 | 12 |
| $h_g^{(3)}$ | 710 | 711 | 0.2 | .50 | | |
| $h_g^{(4)}$ | 744 | 924 | 0 | 0 | | |
| $h_g^{(5)}$ | 1099 | 1260 | 0.6 | 1.8 | | |
| $h_g^{(6)}$ | 1250 | 1406 | 0.2 | 25 | | |
| $h_g^{(7)}$ | 1428 | 1596 | 1.8 | 9.5 | ≈ 1600 | 7 |
| $h_g^{(8)}$ | 1575 | 1721 | 1.2 | 3.8 | | |
| $a_g^{(1)}$ | 496 | | | | | |
| $a_g^{(2)}$ | 1468 | | | | ≈ 1600 | 2 |
| Total V (meV) | | | | 17.1 | | 21 |

quences[51], e.g., they would lead to a strong decrease in the phonon frequencies and a corresponding increase in their linewidth according to $(\Delta\omega_m/\omega_m) \sim \lambda_m$, i.e., one expects a suppression of 20% in the frequency of the high $h_g$ modes and an increase of $\sim 200$ cm$^{-1}$ in line widths in going from pure $C_{60}$ to $A_3C_{60}$. In contrast, the $a_g$ modes would shift and broaden by a factor of $O(W_{inter}/W_{intra})^2$ less compared to the $h_g$ modes according to this mechanism. The recent[36] inelastic neutron scattering data on $K_3C_{60}$ can be interpreted as indicating a softening (by $\simeq 6\%$) and broadening of the $h_g^{(8)}$ mode, and an apparent disappearance of the $h_g^{(2)}$ when compared to $C_{60}$ (cf. Fig. 12). However, a detailed comparison must await higher resolution data and more detailed mode assignments.

Some additional insights into the viability of the electron-phonon mechanism of $T_c$ can be gleaned[29] from an analysis of the lattice constant dependence[12] of $T_c$ discussed in Section 3 (cf Fig. 15). Ignoring for simplicity the coulomb pseudopotential $\mu^*$, using the weak coupling approximation for $T_c$ and keeping the lattice constant dependence only of $N_0$, $d\ln T_c/(d\ln a) \simeq -\lambda^1 d\ln N_0/d(\ln a) \cong \lambda^{-1}$ $(d\ln W(d\ln a)$ where W is the bandwidth of the $t_{1u}$ band. A simple interpretation of the pressure dependence of the photoluminescence peak as discussed earlier in Section 2.5, together with the value $W \cong .5$ eV, translates to $d(\ln W)/d(\ln a) \simeq 12$. Assuming that this same value holds for $A_3C_{60}$, and using the measured value[12] for $d(\ln T_c)/d(\ln a)$ (cf. Fig. 15) of $+40.2$, we can estimate a $\lambda$ value of 0.3, which is in agreement with the values discussed above[51,52].

We note that such a conventional electron-phonon mechanism for $T_c$ would imply values of $2\Delta/k_B T_c = 3.6$, the BCS value[55]. In a recent tunnelling spectroscopic study[56] of $A_3C_{60}$, much larger values of $5.03 \pm 0.2$ $(K_3C_{60})$ and $5.2 \pm 0.3$ $(Rb_3C_{60}) \simeq$ have been reported for $2\Delta/k_B T_c$. If these results are confirmed by more studies, than the simple electron-phonon mechanism scenario cannot be the entire story.

For the electron-phonon coupling mechanism discussed above to be reasonable, the coulomb pseudo-potential $\mu^*$ has to be smallish ($<.1$), although $\omega_{av}$ is perhaps much larger than its value in more conventional superconducting materials, and $\lambda$ is substantial. Indeed the rather larger $T_c$s that are calculated depend on this, as is clear from Fig. 17. However, the question of the size of $\mu^*$, and hence of the mechanism responsible for superconductivity, is controversial. In a recent paper[57] that reiterates his earlier stand[58], P.W. Anderson has argued that $\mu^*$ can not be small in the fullerenes as the conduction band is much too narrow, and the $\ln(E_F/\omega_{av})$ factor that is necessary[55] for the suppression of $\mu^*$ is not big enough. Hence, he has argued, an electronic mechanism for $T_c$ must be operative.

In an interesting set of papers, Chakravarty and Kivelson[59] and Baskaran and Tosatti[60] have suggested that there is an effective intra-$C_{60}$ pairing or attractive interaction between the $t_{1u}$ electrons on a single $C_{60}$ ball which arises due to a large repulsive coulomb interaction on each carbon site, and that this electronic mechanism is responsible for the high superconducting $T_c$ in the fullerenes. These suggestions are based on a study of the repulsive Hubbard model on the "$C_{60}$ lattice" obtained by adding a local (i.e. on every C site) coulomb repulsion energy U to the tight binding (t-t′) model of a single $C_{60}$ ball discussed in Section 2.2. A straight forward calculation[59] of the energies of the (negatively) charged states of $C_{60}$ in perturbation theory leads to the results shown in Table 2 (for the case t = t′). From these it is clear that while the leading order results are in accordance with conventional Hund's rules and repulsive effective interactions, the second order results can lead to their reversal if U is large enough. Specifically there is an antiferromagnetic (Hunds rule reversal) instability that lowers the energy of the spin-singlet $(^1A_g)$ state relative to the spin-triplet $(^3T_{1g})$ state in the doubly charged sector for $U \geq 2.94$ t. This is followed by a pairing instability, which makes $E_{2-}(^1A_g) < 2E_{1-}$ for $U > 3.25t$. One can argue[59,60] in favour of similar effects for large $U$, when one has a t(t′)−J(J′) model on the $C_{60}$ lattice, by invoking RVB-related ideas that arose in studies of the Hubbard and t-J models in the context of the cuprate superconductors[61]. Needless to say, these argument are no proof that such effects do exist in the Hubbard model on the $C_{60}$-lattice, but recent exact numerical diagonalisation studies of the Hubbard model on smaller sized molecules[62] are supprotive.

Purely on symmetry grounds, one can write the following effective Hamiltonian[63] for excitations involving just the $t_{1u}$ orbitals on a single $C_{60}$ ball:

$$H = \varepsilon_0 \sum_{a\mu} c^+_{a\mu} c_{a\mu} + U_0 \sum_{ab\mu\nu} (c^+_{a\mu} c_{a\mu})(c^+_{b\nu} c_{b\nu}) - \frac{J}{8} \sum_{ab\mu\mu'\nu\nu'} (c^+_{a\mu} \sigma_{\mu\mu'} c_{a\mu'})(c^+_{b\nu} \sigma_{\nu\nu'} c_{b\nu'}) + \frac{U_1}{3} \sum_{ab} (c^+_{a\uparrow} c^+_{a\downarrow})(c_{b\downarrow} c_{b\uparrow}) \quad \ldots (8)$$

Table 2—The charged states of the $C_{60}$ ball and their energies

| Charge | "LS" classification | $I_h$ classification | Energy in the "Hubbard model"[59] |
|---|---|---|---|
| 0 | $^1S\begin{pmatrix}L=0\\S=0\end{pmatrix}$ | $^1A_g$ | 0 |
| 1 | $^2P\begin{pmatrix}L=1/2\\S=1\end{pmatrix}$ | $^2T_{1u}$ | $.139t+.5U+.0082\,U^2/t$ |
| 2 | $^2P\begin{pmatrix}L=1\\S=1\end{pmatrix}$ | $^3T_{1g}$ | $.278t+U+.0189\,U^2/t$ |
| | $^1D\begin{pmatrix}L=0\\S=2\end{pmatrix}$ | $^1H_g$ | $.278t+1.02U+.0129\,U^2/t$ |
| | $^1S\begin{pmatrix}L=0\\S=0\end{pmatrix}$ | $^1A_g$ | $.278t+1.05U+.0010\,U^2/t$ |

Here $a, b = 1$-3 are the orbital indices and $\mu$, $\mu'$, $\nu$, $\nu'$ are spin indices. $U_0$ is essentially the effective coulomb or charging energy; J is the spin-exchange energy that would lead to the spin Hund's rule if it were positive; $U_1$, if positive, would lead to the orbital Hunds rule. The key question is that of the magnitudes and the signs of the effective interactions $U_0$, J and $U_1$ for the real $C_{60}$ ball. For the Hubbard model on the $C_{60}$-ball, the perturbative results for the energies in Table 2 translate to:

$$\frac{U_0}{t} \cong .02\,\frac{U}{t} + .0129\,\frac{U^2}{t^2}\,;\ \frac{J}{t} \simeq .02\,\frac{U}{t} - .006\,\frac{U^2}{t^2};$$

$$\frac{U_1}{t} \cong .03\,\frac{U}{t} - .0128\,\frac{U_2}{t^2} \qquad \ldots (9)$$

Clearly, $U_0$ is positive; but J while ferromagnetic for small $U$, becomes antiferromagnetic for large $U$; and $U_1$ also becomes attractive for large $U$. However, it is not clear whether $U$ on the carbon sites is large enough for these instabilities to be operative. Some estimates suggest that $U \simeq 5$ eV, which would put it (for $t = 2$ eV) below even the antiferromagnetic instability. Furthermore, the effects of the rest of the (i.e. inter-site on the $C_{60}$ lattice) coulomb interactions are not included in the above results for $U_0$, J and $U_1$. The ferromagnetism that has been observed in the dilutely doped (with organic dopants) $C_{60}$ materials would seem to suggest that the Hunds rule correlations implying a positive J are not reversed. The viability of the pairing mechanism of Chakravarty and Kivelson[59] and Baskaran and Tossatti[60] is hence unclear. It is worth noting, however, that $U_0$ is strongly suppressed relative to $U$, arising from the fact that the $t_{1u}$ orbitals are spread out over the $C_{60}$ ball.

There is yet another, more exotic, electronic attractive mechanisms that may well be operative[63] in the $A_3C_{60}$; if not to cause the pairing, at least to reduce the effective electron-electron repulsive interactions, and hence leading to a smaller $\mu^*$. This is the "excitonic" mechanism due to intramolecular and intermolecular polarisability effects, which ought to be quite large in the $C_{60}$ based materials, and is similar to the one proposed by Little[64]. The intramolecular effects make important contributions in determining the renormalised coupling $U_0$, etc., in the effective Hamiltonian for a single ball. To understand the intermolecular polarisability effects, one should start from the reference ionic state $A_3^+C_{60}^{3-}$ where there are no average electric fields or polarisations. Now as the conduction electrons in the $t_{1u}$ bands hop around from ball to ball dynamical charge inbalances leading to local electric fields and polarisations are induced. In an adiabatic approximation where the hopping is slow compared to the time scale in which polarisations respond, there is an effective reduction in energy or effective Hamiltonian equal to $-\frac{1}{2}\Sigma_j|\mathbf{E}(\mathbf{r}_j)|^2\,\alpha_j$ where $\mathbf{E}(\mathbf{r}_j)$ is the electric field at the ion at site j with polarisability $\alpha_j$. Part of this effective Hamiltonian has the form

$$-\sum_i \hat{q}_i^2\left[\frac{1}{2}\sum_{j\neq i} e^2\,\alpha_j|r_{ij}|^{-4}\right] \qquad \ldots (10)$$

which implies a negative contribution to $U_0$ (cf. Eq. 8) of order

$$\frac{e^2}{2a_0}\left\{\frac{a(C_{60}^{3-})}{a_0^3}\sum_{j}'(r_{ij}/a_0)^{-4}+\frac{a(A^+)}{a_0^3}\sum_{j}''(r_{ij}/a_0)^{-4}\right\} \quad \ldots(11)$$

where $\Sigma'$ and $\Sigma''$ run over all the $C_{60}^{3-}$ and $A^+$ sites respectively. This term is easily[65] a fraction of an eV. Since the values of $U_0$, J and $U_1$ resulting from all other sources are not known precisely, it is difficult to say conclusively whether the net effect is attractive or not; but the mechanism will, at the least, lead to a suppression of the $\mu^*$ and in the way may play an important role in the superconductivity of the fullerenes.

To summarise, the mechanism of superconductivity in doped fullerenes is far from being well understood. The field of fullerenes is still very young and holds promise for exciting future developments.

**Acknowledgement**

One of us (AKS) thanks the Department of Science and Technology for financial assistance. One of us (HRK) is grateful for the hospitality of the IBM T.J. Watson Research Center where part of the work described here was done, and for stimulating discussions with P Pattnaik, D M Newns, A Rossi and Z Schlesinger. We also acknowledge N Kumar, T V Ramakrishnan, C M Varma, G Gruner, G Baskaran and P Heiney for stimulating talks and discussions. We thank the following publishers and the corresponding authors for granting permission to reproduce the figures: The American Institute of Physics (Figs 2,3,6,8), the American Chemical Society (Fig.4), Macmillan Magazines Ltd (Figs 12,13), American Association for Advancement of Sciences (Fig.15): Finally, we thank Biswadeb Dutta, J Sudha, P Majumdar and Victor D S Muthu for help in the preparation of this review.

**References**

1 Krätschmer W, Lamb L D, Fostiropoulos L K & Huffman D R, *Nature*, 347 (1990) 354.
2 Kroto H W, Heath J R, O'Brien S C, Curl R F & Smalley R E, *Nature*, 318 (1985) 162.
3 Haddon R C *et al.*, *Nature*, 350 (1991) 320.
4 Hebard A F, Rosseinsky M J, Haddon R C, Murphy D W, Glarum S H, Palstra T T M, Ramirez & Kortan A R, *Nature*, 350 (1991) 600.
5 For a comprehensive list of papers in this area see Smalley E R, *Buckminsterfullerene bibliography* (Chemistry Department, Rice University, Houston T X 77251) (available via E-mail by sending the message SUB-SCRIBE to bucky @Soll. lrsm. upenn. edu).
6 For a more detailed account of the history of the subject see ref.5; also Huffman D R, *Physics Today*, Nov.91, p.22 and Smalley R E, *The Sciences*, 31 (1991) 22.
7 Rohlfing E A, Cox D M, Kaldor A, *J chem Phys*, 81 (1984) 3322.
8 After Buckminster Fuller of the Geodesic Dome fame who studied such structures; e.g. see *Synergetics dictionary -The mind of Buckminster Fuller*, edited by E D Applewhite (Garland Publishing, New York), 1986.
9 Haymet A D J, *Chem Phys Lett*, 122 (1985) 421; *J Am chem Soc*, 108 (1986) 319; Haddon R C, Brus L E & Raghavachari K, *Chem Phys Lett*, 125 (1986) 459; and other references in ref.5.
10 eg Stanherich I V, Nikesov M V & Bochvar D A, *Russian Chem Rev*, 53 (1984) 640.
11 Rosseinsky M J, Ramirez A P, Glarum S H, Murphy D W, Haddon R C, Hebard A F, Palstra T T M, Kortan A R, Zahurak S M, Makhija A V, *Phys Rev Lett*, 66 (1991) 2830.
12 Fleming R M, Ramirez, Rosseinsky M J, Murphy D W, Haddon R C, Zahurak S M & Makhija A V, *Nature*, 352 (1991) 787.
13 Iqbal Z, Baughman R H, Ramakrishna B L, Khare S, Murthy N S, Bornemann H J & Morris D E, *Science*, 254 (1991) 826.
14 Holczer K, Klein O, Huang S M, Kaner R B, Fu K J, Whetten R L & Diederich F, *Science*, 252 (1991) 1154.
15 Allamand P, Khemani K C, Koch A, Wudl F, Holczer K, Donovan S, Gruner G & Thompson J E, *Science*, 253 (1991) 301.
16 This follows from the Euler theorem $V - E + F = 2$ for a convex polyhedron with $E$ edges, $F$ faces and $V$ vertices. Given a structure with $n_5$pentagonal and $n_6$ hexagonal faces and with every vertex 3-fold coordinated, $V = (5n_5 + 6n_6)/3$, $E = (5n_5 + 6n_6)/2$ and $F = n_5 + n_6$. Then the theorem forceds $n_5 = 12$; but $n_6$ is arbitrary and $V = n = 20 + 2n_6$. The special stability of $C_n$ for particular values of $n$ is connected with closed electronic shells.
17 Heiney P A, Fischer J E, McGhie A R, Romanow W J, Denenstein A M, McCauley Jr J P, Smith III A B & Cox D E, *Phys Rev Lett*, 66 (1991) 2911.
18 Yannoni C S, Johnson R D, Meijer G, Salem J R, *J Phys Chem*, 95 (1991) 9; *J phys Chem*, (1991) 581.
19 Cheng A & Klein M L, *J phys Chem*, 95 (1991) 6750.
20 We note that in graphite the σ-bonding in the planes is by $sp^3$ hybridised orbitals, and the π bonding in the planes is due to $p_z$ orbitals. Here, because of the curvature of the surface of the ball, the two sets of orbitals get admixed. The situation is intermediate between $sp^2$ and $sp^3$ hybridisation.
21 Elser V & Haddon R C, *Nature*, 325 (1987) 792.
22 Saito S & Oshiyama A, *Phys Rev Lett*, 66 (1991) 2637; Zhang Q M, Yi J Y & Bernhole J, *Phys Rev Lett*, 66 (1991) 2633.
23 Weaver J H, Martins J L, Komeda T, Chen Y, Ohno T R, Kroll G H, Troullier N, Haufler R E & Smalley R E, *Phys Rev Lett*, 66 (1991) 1741.
24 Ching W Y, Huang M Z, Xu Y N, Harter W G & Chan F T, *Phys Rev Lett*, 67 (1991) 2045.
25 Pattnaik P & Krishnamurthy H R (unpublished).
26 Hare J P, Kroto H W & Taylor R, *Chem Phys Lett*, 177 (1991) 394.
27 Gensterblum G, Pireaux J J, Thiry P A, Caudano R, Vigneron J P, Lambin P, Lucas A A & Kratschmer W, *Phys Rev Lett*, 67 (1991) 2171.
28 Lichtenberger L, Nebesny K W, Ray C D, Huffman D R & Lamb L D, *Chem Phys Lett*, 176 (1991) 203.
29 Sood A K, Chandrabhas N, Muthu D V S, Jayaraman A, Kumar N, Krishnamurthy H R, Pradeep T & Rao C N R, *Solid State Commun*, 81 (1992) 89.

30 Reber C, Yee L, McKiernan J, Zink J I, Williams R S, Tong W M, Ohlberg D A A, Whetten R L & Diederich F, *J phys Chem*, 95 (1991) 2127.
31 Blau W J, Byrne H J, Cardin D J, Dennis T J, Hare J P, Kroto H W, Taylor R & Walton D R M, *Phys Rev Lett*, 67 (1991) 1423.
32 Stanton R E & Newton M D, *J phys Chem*, 92 (1988) 2141; Weeks D E & Harter W G, *J chem Phys*, 90 (1989) 4744.
33 Kratschmer W, Fostiropoulos K & Huffman D R, *Chem Phys Lett*, 170 (1990) 167.
34 Bethune D S, Meijer G, Tang W C, Rosen H J, Golden W G, Seki H, Brown C A & de Vries M S, *Chem Phys Lett*, 179 (1991) 181.
35 Bethune D S, Meijer G, Tang W C & Rosen H J, *Chem Phys Lett*, 174 (1990) 219.
36 Prassides K, Tomkinson J, Christides C, Rosseinsky M J, Murphy D W & Haddon R C, *Nature*, 354 (1991) 462.
37 Cappelletti R L, Copley J R D, Kamitakahara W A, Li F, Lannin J S & Ramage D, *Phys Rev Lett*, 66 (1991) 3261.
38 Sinha K, Menendez J, Hanson R C, Adams G B, Page J B, Sankey O F, Lamb L D & Huffman D R, *Chem Phys Lett*, 186 (1991) 287.
39 Fischer J E, Heiney P A, McGhie A R, Romanow W J, Denenstein A M, McCauley J P, Smith III (Jr) A B, *Science*, 252 (1991) 1288.
40 Duclos S J, Brister K, Haddon R C, Kortan A R & Thiel F A, *Nature*, 351 (1991) 380.
41 Holmes N C, paper presented at the *13th AIRAPT international conference on high pressure science and technology*, Oct.7-11, Bangalore, India.
42 Nunez Regueiro M, Monceau P, Rassat A, Bernier P & Zahab A, *Nature*, 354 (1991) 289.
43 Aoki K, Yamawaki H, Kakudate Y, Yoshida M, Usuba S, Yokoi H, Fujiwara S, Bae Y, Malhotra R & Lorents D, *J phys Chem*, 95 (1991) 9037.
44 Stephens P W, Mihaly L, Lee P L, Whetten R L, Huang S M, Kaner R, Diederich F & Holczer K, *Nature*, 351 (1991) 632.
45 Schriber J E *et al.*, *Physica C*, 178 (1991) 137; Sparn G, Thompson J D, Huang S M, Kaner R B, Diederich R L, Whetten R L & Holczer K, *Science*, 252 (1991) 1829.
46 Holczer K, Klein O, Gruner G, Thompson J D, Whetten R L & Diederich F, *Phys Rev Lett*, 67 (1991) 271.
47 Uemura Y J, Keren A, Le L P, Luke G M, Sternlieb B J, Wu W D, Brewer J H, Whetten R L, Huang S M, Lin S, Kaner R B, Diederich F, Donovan S, Gruner G & Holczer K, preprint.
48 Saito S & Oshiyama A, preprint.
49 Hamada N, Saito S, Miyamoto Y & Oshiyama A, preprint.
50 Wertheim G K, *Sciencse*, 252 (1991) 1419; Benning P J *et al.*, *Science*, 252 (1991) 1417.
51 Varma C M, Zaanen J & Raghavachari K, *Science*, 254 (1991) 989.
52 Schluter M, Lannoo, Needels M, Baraff G A & Tomanek D, preprint.
53 O'Brien M C, *J Phys C; Solid State Physics*, 4 (1971) 2524.
54 Micnas R, Ranninger J & Robaskeiwiez S, *Rev Mod Phys*, 62 (1990) 113.
55 eg.see Allen P B & Mitrovic B, *Solid State Physics*, 37 (1982) 1.
56 Zhang, Chem C C & Lieber C M, *Science*, 254 (1991) 1619.
57 Anderson P W, preprint.
58 Cohen M L & Anderson P W, in *Superconductivity in d &f band metals*, edited by D H Douglas, p.17 AIP Conf Proc #4, (1972).
59 Chakravarthy S & Kivelson S, *Europhys Lett*, 16 (1991) 751; Chakravarty S, Gelfand M P, Kivelson S, UCLA preprint.
60 Baskaran G & Tosatti E, *Curr Sci*, 61 (1991) 33.
61 eg. see Bedell K S, *et al.*, *High temperature superconductivity: Proceedings* (Addison-Weslay, Reading M A), 1990.
62 White S, *et al.*, UCLA preprint.
63 Krishnamurthy H R, Pattnaik P, Newns D M & Rossi A (unpublished).
64 Little W A, *Phys Rev A*, (1964) 1416.
65 The lattice sums are about 102 and 542 respectively. Using $a_o \cong 14.2$ Å for $K_3C_{60}$, $(e^2/2a_o) = 0.51$ eV. Using $\alpha(K^+) = 0.84 \times 10^{-24}$ cm$^3$, the second term in Eq.11 is 0.16 $\alpha(C_{60}^{3-})$ is not known, but if we picture the $C_{60}^{3-}$ ion as a metallic sphere of radius 3.5 Å, then $\alpha(C_{60}^{3-}) = (3.5)^3 \times 10^{-24}$ cm$^3$, whence the first sterm in eqn. 11 is 1.53. Hence, one gets an attractive interaction of order 0.86 eV. While this may be an overestimate, it does emphasize that the effect is substantial.

Indian Journal of Chemistry
Vol. 31 A& B, May 1992, pp. F79-F91

# Structural and microstructural characteristics of solid $C_{60}$

N P Lalla & O N Srivastava*
Department of Physics, Banaras Hindu University, Varanasi-221 005, India

Received 20 February 1992

The new carbon variant, the solid $C_{60}$, exhibits several structural/microstructural subtleties. The very crystallographic nature where generally orientational ordering is missing endows curious characteristics to this and other similar solids (fullerenes). The known structural characteristics of solid $C_{60}$ have been reviewed first. This is followed by the description of our work on the structural (local area structure) microstructure and defect substructure of $C_{60}$ solid. In particular, the simultaneous occurrence of FCC ($a \sim 14.17$ Å) and HCP ($a \sim 10.02$ Å, $c \sim 16.36$ Å) structural variants, the formation of domain (partial orientational order), the occurrence of [111] oriented stacking faults, the occurrence of superlattice $a_s = 3a_c \sim 42.31$ Å and existence of anomalous graphitic carbon configurations have been dealt with and discussed.

## 1. Introduction

The emergence of buckminsterfullerence, $C_{60}$, solid has led to a new scenario in the science of materials. The remarkable new properties, e.g., the superconducting behaviour, the photophysical/photochemical features, the intercage and intracage intercalation characteristics leading to new synthetic materials coupled with structural subtleties of the $C_{60}$ (and other fullerenes, e.g. $C_{70}$) have led to exotic excitement among chemists, physicists, materials scientists, electronic engineers, etc. Both experimental and theoretical solid state aspects will have to be looked into afresh for the $C_{60}$ solid.

A rather novel feature associated with $C_{60}$ relates to the nature of solid state itself. As is known, the solids are characterised by the nature of ordering at ambient conditions. The well known solid state forms are crystalline, quasicrystalline and amorphous. The solid $C_{60}$ based on the known structural features does not appear to correspond to any of these. The crystalline form is known to have both the translational and orientational order, the quasicrystalline form lacks translational order but possesses orientational order, the amorphous form has neither of the two types of orders. The $C_{60}$ solid at ambient conditions is now known to have translational order but does not have orientational order. The structural results on orientational order (disorder) which are mostly based on NMR and diffraction experiments differ in details of order/disorder but it is almost certain that at ambient conditions $C_{60}$ solid does not have orientational order[1,2]. In the light of this, the solid state manifested by $C_{60}$ can not be categorised under the known forms—the crystalline, quasicrystalline or amorphous forms. One can perhaps christen the $C_{60}$ solid with a new name, e.g., pseudocrystal (pseudocrystalline). At present the primary focus of studies on $C_{60}$ is towards the investigations of exotic properties; the motivation apparently is to quickly sort out such spectacular properties where $C_{60}$ may be ushered in as an altogether new or a better material. A specific such application is a better high temperature superconductor—an isotropic (cubic) and three-dimensional superconductor—than the present HTSC cuprate materials which are anisotropic and two-dimensional conduction systems.

As is well known most of the useful properties of solids depend on structural/microstructural characteristics and a correlation between these provides a guideline for material tailoring. However, rather few studies have been carried out on the structural/microstructural features and those covering structure(microstructure)-property correlations are far fewer. The present paper deals with structural/microstructural features of the new solid form of carbon, the fullerenes. The descriptions and discussions would confine to $C_{60}$—the most abundant and symmetric form of the fullerenes. The structural characteristics would be dealt with special reference to microstructural and local area structural features. In the following we first discuss the known structural features and then proceed to describe the work on structural/microstructural characteristics carried out recently in our laboratory.

## 2. Structural-microstructural characteristics

### 2.1 *Structural characteristics of pure $C_{60}$ solid*

As is known, the present proliferation in research on $C_{60}$ solid after the initial work of Kroto *et al.*[3] commenced after the breakthrough by Krätschmer, *et al.*[4] in 1990 with the production of macroscopic quantities (mg to g) of $C_{60}$ through arc discharge between graphite electrodes under ~ 100 torr of helium atmosphere. The portion of the resulting black soot which was soluble in benzene was crystallised through slow evaporation. The resulting dark brown to black crystallites were found to be the fullerenes. Krätschmer *et al.* carried out the structural studies of $C_{60}$ solid which were apparently the first studies of their type. An interesting aspect of their studies was that XRD from single crystals (~ 500 μm) did not give any clear spot pattern. They, therefore, took resort to electron and powder X-ray diffraction techniques. These studies revealed that the $C_{60}$ solid consisted of arrays of spheroidal molecules (diameter ~ 7 Å) separated by ~ 3.1 Å (it may be mentioned that in graphite the interlayer distance is ~ 3.4 to 3.5 Å). Krätschmer *et al.* concluded that $C_{60}$ solid was partially crystalline with a lattice-structure nearly close packed hexagonal with $a$ = 10.02 Å and $c$ = 16.36 Å. The difference between the nearest neighbour distance (= 10.02 Å) and the diameter calculated for the carbon cage itself (~ 7.1 Å) was attributed to represent the effective van der Waals' diameter set by repulsion of the electron clouds extending outward from each carbon atom.

Several structural studies utilising X-ray and neutron diffraction experiments were carried out after the initial explorations of Krätschmer *et al.* A significant such study is that of Fleming *et al.*[5]. They prepared single crystals (400 μm diameter) through sublimation of $C_{60}$ powder. From single crystal X-ray diffraction data, the unit cell was found to be face-centred cubic (FCC) with a lattice parameter of 14.1981 (9) Å. Single crystal X-ray diffraction shows that $C_{60}$ solid had long range translational order with no evidence of stacking faults due to random packing of the close packed planes. These authors proposed that $C_{60}$ molecule which has an icosahedral, non-crystallographic point symmetry $m\bar{3}\bar{5}(I_h)$, in order to crystallise on a crystallographic space lattice, should adopt fewer symmetry elements than those present in the molecule. The loss of symmetry could be accommodated in several ways but the highest point group symmetry of the $C_{60}$ molecule consistent with cubic symmetry is a subgroup of the icosahedral point group $m\bar{3}(T_h)$. Taking into account the size of the unit cell and the size of

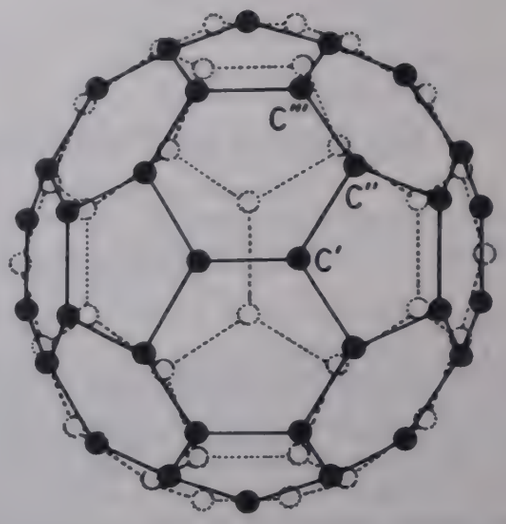


Fig. 1—Idealized representation of $C_{60}$ molecular structure. The three carbon sites in $Fm\bar{3}$ are labeled as C′,C″ and C‴.

the $C_{60}$ ball, Fleming *et al.* concluded that the structure is close packed with four molecules per unit cell. The space group assigned as the highest symmetry one corresponding to $Fm\bar{3}$ is consistent with F centering and with $z$=4. A schematic view of the $C_{60}$ molecule with crystallographic relevance is shown in Fig. 1. The view is down a two-fold axis and the origin is taken at the centre of the cage. The three atom sites in $Fm\bar{3}$ are labelled C′, C″, and C‴. Fleming *et al.* suggested that since space group $Fm\bar{3}$ is susceptible to merohedral twinning, the apparent symmetry of the solid may get increased. One merohedral twinning operation is depicted by the dashed lines that show the position of the molecule after a $\pi/2$ rotation about [100]. The effect of the rotation is to impose an apparent four-fold axis along a direction that was formerly two-fold and increase the apparent symmetry to $Fm\bar{3}m$. The rotation merges atoms C″ and C‴ and introduces a large apparent thermal parameter on the combined atom in $Fm\bar{3}m$. Atom C′ is rotated into a new position by the twin operation and, therefore, becomes two half occupied sites in $Fm\bar{3}m$.

After Fleming *et al.*'s initial work on the elucidation of structural characteristics, several workers have explored the structural features including the orientational ordering effects in $C_{60}$ solid. A rather rigorous work was carried out by Heiney *et al.*[2] who employed synchrotron X-ray powder diffraction coupled with differential-scanning calorimetry for monitoring the orientational ordering transitions in $C_{60}$ solid. They found a first order phase transition from an orientationally disordered face centred cubic structure to a partially ordered (orientationally) simple cubic(SC) as the temperature was lowered. The critical transition

temperature was 249 K, the low temperature nearly-ordered SC phase was found to be stable upto this temperature. Heiney *et al.* suggested that since the lattice parameters for the SC ($a$ = 14.04 ± 0.01 Å at 11 K) and FCC ($a$ = 14.17 ± 0.01 Å at 300 K) are nearly the same, the basis for the low temperature SC must still consist of four molecules per unit cell (as is the case for the R.T., FCC variant) but the equivalent molecules for the FCC structure must somehow become inequivalent at low temperatures leading to the SC phase. The exact details of rotation of $C_{60}$ through which the equivalent $C_{60}$ molecules in FCC became inequivalent in SC were not worked out in these studies. These authors found that incorporating Debye-Waller term did not improve the fit between experimental and calculated diffraction intensities. This suggested that thermal disorder is primarily rotational rather than translational. The low temperature SC lattice was found to impose strict constraints on possible rotations of $C_{60}$ molecule which were required to create SC from the FCC phase. They conjectured a model where the four molecules centred on the FCC Bravais lattice sites are oriented such that one of the ten three-fold icosahedral axes (normal to pseudohexagonal faces) is aligned with one of the four ⟨111⟩ directions, and three mutually orthogonal two-fold molecule axes are aligned with ⟨100⟩ directions. It follows that three other molecular three-fold axes are also aligned with the three remaining ⟨111⟩ crystal axes. At this point there are no remaining rotational degrees of freedom; all molecules are equivalent and the structure is still FCC. The equivalence is now broken by rotating the four molecules through the same angle but about different ⟨111⟩ axes: the molecule at (000) about [111], that at ($\frac{1}{2}$ 0 $\frac{1}{2}$) about [$\bar{1}1\bar{1}$], that at ($\frac{1}{2}$ $\frac{1}{2}$ 0) about [$\bar{1}\bar{1}1$] and that at (0 $\frac{1}{2}$ $\frac{1}{2}$) about [$1\bar{1}\bar{1}$]. This choice preserves the cubic symmetry although the two-fold axes are no longer aligned along ⟨100⟩ directions.

Another significant aspect of the work of Heiney *et al.*[2] relates to the comparison of the XRD and NMR results. Nuclear magnetic resonance experiments indicate the existence of dynamical disorder (presumably free rotation) which decreases with decreasing temperature[7]. The XRD results of Heiney *et al.* show both consistencies and discrepancies with NMR observations. The distinct difference is in regard to the coexistence of static and mobile C nuclei well below the transition temperature (~ 249 K), deduced from the NMR results of superposed motionally narrowed and powder pattern signals at temperatures as low as 140 K. The XRD results do not support existence of complete rotation of the molecule below ~ 249 K. As a matter of fact, the XRD and the NMR experiments take care of different aspects of the structure. The NMR observations can not distinguish between free rotation and jump rotational diffusion between symmetry equivalent orientations. XRD distinguishes the orientational order even in the presence of substantial thermal disorder, as long as one set of orientations is statistically preferred and the orientational order extends upto long ranges. The observations of Heiney *et al.* suggest that much of the SC order is reduced by orientational fluctuations at $T_c$.

One of the more refined recent structural characterisations of the $C_{60}$ solid has been carried out by David *et al.*[1] by employing powder neutron diffraction through Rietveld refinement technique. The diffraction data were collected at 5 K on the high resolution powder diffractometer at ISIS for 3 hr. They took the starting model for profile refinement as the ideal truncated icosahedral symmetry consistent with space group $Fm\bar{3}$. The ideal atom positions were taken as α (0, ± 1/2, ± 3/2 τ) $\mathfrak{C}$, α(± 1/2 τ, ± 1, ± 1/2 (2τ + 1)) $\mathfrak{C}$ and α (± τ, ± 1/2, ± 1/2(2 + τ)) $\mathfrak{C}$, where $\mathfrak{C}$ implies cyclic permutation of coordinates, τ is the golden ratio 1.61083 = $(1+\sqrt{5})/2$ and α is the ratio of the average C-C distance to cubic lattice constant, α ~ 0.1 and was taken as such in the initial refinement. Whereas the room temperature phase was FCC, the low temperature phase (< 249 K up to 5 K) was found to be simple cubic. The reduction of symmetry from $Fm\bar{3}$ to a simple cubic space group permits only two possibilities, $Pn\bar{3}$ or $Pa\bar{3}$. In both cases the lowering of symmetry results from an arbitrary rotation of the $C_{60}$ molecule about the [111] direction. A significant result of David *et al.*'s work relates to the determination of this rotation precisely. In their work David *et al.* rotated the $C_{60}$ molecule rigidly about the [111] direction in 5° steps from $\phi = 0°$ to 120° for the two possible space groups, i.e., $Pn\bar{3}$ and $Pa\bar{3}$. In all, fifty different refinements compatible with the 5° rotation were tried. The standard $\chi^2$ test for those refinements indicated that $Pa\bar{3}$ is the correct space group and that rotation of face centre $C_{60}$'s corresponds to $\phi \approx 98°$. The ideal coordinates corresponding to this rotation were taken as starting parameters in subsequent refinements where all positional parameters were varied subject to restraints on the pentagon (108.0(1)°) and hexagon (120.0(1)°) angles. The refined atom-

ic positions were determined. The observed and calculated diffraction patterns were found to agree well. The bond lengths obtained could clearly be divided into five short 6:6 bonds (1.391(18) Å) (C−C bonds fusing two hexagons) and ten long 6:5 bonds (1.455(12) Å) (bonds interconnecting hexagon and pentagon). These bond lengths are in agreement with ab initio calculations where bond lengths of ~ 1.39 and ~ 1.45 Å have been found.

The refined crystal structure as determined by David *et al.*[1] is shown in Fig. 2(a,b). When we consider the $C_{60}$ unit centred at the origin, it is found that the apparently arbitrary rotation of 98° around the [111] has resulted in three pentagons roughly oriented along the [110], [101] and [011] directions. However, this is not precisely possible, the pentagons must orient along [11δ], [1δ1], and [δ11] directions where δ = 0.05218. The corresponding ideal ϕ value is 97.621°, which is quite close to the observed value of 98°. This orientation is not fortuitous. Details of the orientations of the nearest-neighbour $C_{60}$ units indicate that this leads to a pentagon of the $C_{60}$ unit facing a 6:6 bond of an adjacent $C_{60}$ unit. The 6:6 bond sits directly above the middle of the pentagon face; the dihedral angle defined by ($C_{22}$-$C_{23}$) and ($C_{11}$-$C_{31}$) [see Fig. 2(b)] is 179.6°. Taking into consideration the fact that all $C_{60}$ molecules are symmetry equivalent, ordering in pure $C_{60}$ (at low temperatures) may appear surprising. However, observations of two different bond lengths is compatible with ab initio calculations that the $C_{60}$ molecule has a significantly anisotropic electronic distribution. The pentagons, consisting of long bonds, constitute an electron-poor region. The 6:6 bonds exocyclic to the pentagons are short and of higher bond order with significant electron density. When the $C_{60}$ units are close packed, the repulsive electrostatic interactions are optimised by having no carbon atom situated above any other carbon atom of a neighbouring $C_{60}$ unit. The electron-rich 6:6 bonds are aligned optimally over the electron-deficient pentagons. As a consequence of the icosahedral symmetry, all twelve nearest-neighbour interactions may be simultaneously optimised. The orientational ordering of $C_{60}$-$C_{60}$ is fully characterised by just one packing motif as elucidated in Fig. 2b. Every $C_{60}$ unit has six electron-deficient pentagons and six electron rich 6:6 bonds facing its 12 nearest neighbours. The weak electrostatic repulsion of facing pentagons and 6:6 bonds along the ⟨110⟩ directions would result in a small build up of electron density along the directions farthest away from ⟨110⟩, i.e., along ⟨100⟩ directions. Because of this, there would be an increase in bond order and shortening of bond length in these regions. David *et al.*'s measurements confirmed this; the shortest 6:5 bond ($C_{12}$-$C_{24}$) is 1.420 Å and it straddles ⟨100⟩. The $C_{60}$-$C_{60}$ bonding, inspite of being weak, is able to produce geometrical deviations from $m\bar{5}m$ to $\bar{3}$ point group symmetry.

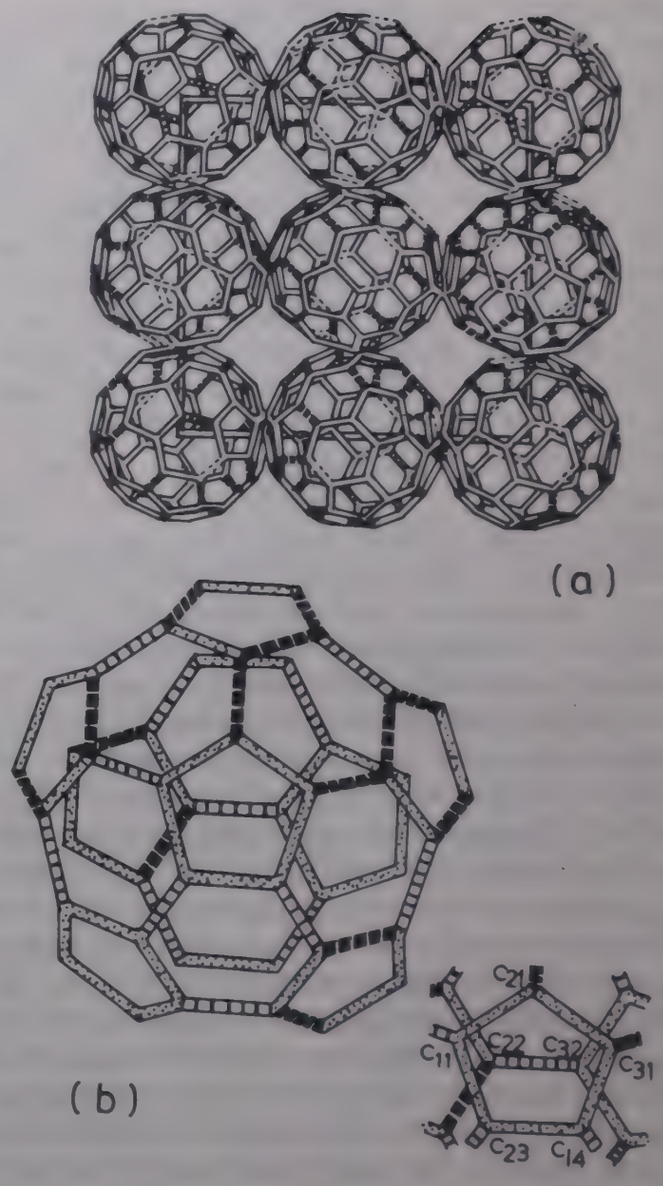


Fig. 2(a)—Projection of ordered $C_{60}$ structure at low temp. (< 249 K, see text for details).

(b)—Projection of fragments of two adjacent $C_{60}$ molecules along [110]. The 6:6 bond is located in this projection in the centre of the pentagon. This configuration minimizes the C-C overlap in neighbouring $C_{60}$ units.

The above work (of David *et al.*[1]) on pure $C_{60}$ in regard to structural characteristics including orientational ordering is one of the latest and it uncovers several new and interesting features embodying bonding and stability.

### 2.2 *Structural characteristics of doped $C_{60}$ solid*

In view of the discovery that the alkali metal doping (intercage intercalation) of $C_{60}$ leads to significant variation in conductivity and the materials with specific doping levels become superconductors, there has been several studies on the exploration of structural characteristics of the doped $C_{60}$'s, particularly of the alkali metal doped variants[8,9]. The work on $K_3C_{60}$ (Stephens *et al.*[8]) is perhaps the most detailed one and will be briefly recapitulated here. An important change in structural characteristics on doping relates to the suppression of nearly free rotation as in pure $C_{60}$. The lattice structure of $K_3C_{60}$ was found to be FCC with lattice parameter $a \sim 14.24$ Å which is very to close to the lattice parameter of pure $C_{60}$ phase ($a \sim 14.11$ Å), which is also FCC. In view of this similarity, it is apparent that $K_3C_{60}$ structure is based on FCC lattice of $C_{60}$ molecules, with K atoms sitting in interstitial positions. The significant difference in the intensities from the two phases ($C_{60}$ and $K_3C_{60}$) is in regard to the reflections (220) and (311). Therefore, it is clear that the sites occupied by K atoms interfere destructively and constructively with the C atoms, respectively for the above mentioned reflections. This is indicative of the fact that K atoms occupy sites such as $(\frac{1}{4}\frac{1}{4}\frac{1}{4})$ and $(\frac{1}{2}0\frac{1}{2})$ as shown in Fig. 3. The fact that the stoichiometry implies three potassium atoms means that K atoms occupy both of these inequivalent sites. The projection of the structure along [001] is shown in Fig. 3. The shortest distance between K atom at $(\frac{1}{4}\frac{1}{4}\frac{1}{4})$ position and C atom on the freely rotating $C_{60}$ would be 2.66 Å, much smaller than the 3.06 Å measured

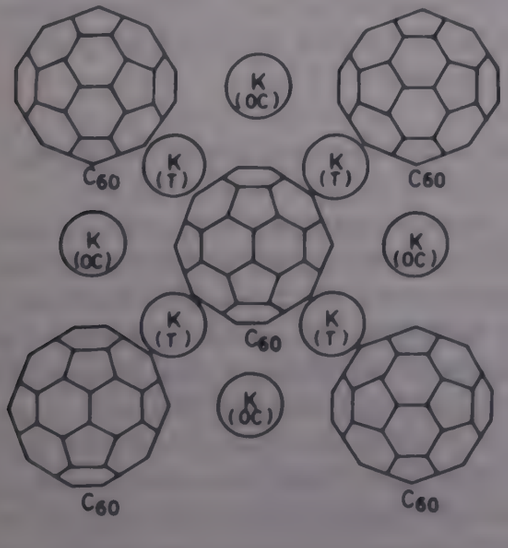


Fig. 3—The projection of structure of $K_3C_{60}$. The octahedral and tetrahedral sites of K are represented by (OC) and (T) respectively.

in intercalated graphite. A rotating molecule leads to a tetrahedral site of radius 1.12 Å. The radius of $K^+$ ion is 1.33 Å. Thus, it is apparent that in the K doped version $C_{60}$ molecules can not be freely rotating. Considerations of static $C_{60}$ molecules suggest that there are only two possible positions of the $C_{60}$ molecule that provide sufficient space for all eight nearest neighbour alkali metal atoms. In both these cases the $C_{60}$ molecule is oriented with eight of its twenty hexagonal faces along the cubic ⟨111⟩ directions. The two orientations are related by a 90° rotation about the (100) direction. This leads to different positions for the pentagonal faces (Fig. 3). Stephens *et al.* performed a Rietveld refinement of the $K_3C_{60}$ powder diffraction pattern for two structures allowed by the above size restrictions. They considered two models. In one of these all $C_{60}$ molecules were taken to have the same orientation; the space group is then $Fm\bar{3}$. They found that the refinement always yields a significant peak at 3.3 $Å^{-1}$. Such a peak was not present in the diffraction pattern. This compelled them to consider other possible configurations/orientations of the $C_{60}$ molecules in the structure. The one which provided the best fit had the $C_{60}$ molecules taken to be orientationally disordered between the two possible orientation as shown in Fig. 3. The space group for this model corresponds to $Fm\bar{3}m$, which is a higher symmetry than allowed for the icosahedral molecule, but can be interpreted as a 50% occupancy of the two orientations. It may be noticed that XRD can not clearly distinguish between dynamic disorders. A significant aspect of the structural work of Stephen *et al.* is that even the doped versions of $C_{60}$ possess orientational disorder. This justifies the classification of the $C_{60}$ as a new solid state form; as outlined earlier, due to the existence of translation order but lack of orientational order, the $C_{60}$, solid form may be termed as 'pseudocrystalline'.

Yet another study on structural aspects of doped $C_{60}$ is that of Zhou *et al.*[9]. They have shown, based on X-ray powder diffraction data, that compositions of $C_{60}$ doped with alkali metals up to saturation limits exhibit a transformation from FCC structure for pure $C_{60}$ to body centred cubic. The composition corresponds to $M_6C_{60}$ (M = K,Cs). The space groups corresponds to $Im\bar{3}$. Zhou *et al.* have shown that the orientational disorder (rotation) found to be present in pure $C_{60}$ is largely suppressed in $M_6C_{60}$ and can be taken to be nearly absent. However, a detailed analysis of the data of order/disorder was not carri-

ed out by Zhou *et al.* A new doped version of $C_{60}$ corresponding to $A_4C_{60}$ was analysed by Fleming *et al.*[5]. They reported that for $A_xC_{60}$ $(3<x<6)$ there exists an additional structural phase at $x=4$. In contrast to FCC $A_3C_{60}$ and body centred cubic $A_6C_{60}$, $A_4C_{60}$ (A=K,Rb,Cs) has a body centred tetragonal structure. This $K_4C_{60}$ was found to be BCT with $a=11.886(7)$ Å and $c=10.774(6)$ Å; similar lattice parameters were found for BCT $Rb_4C_{60}$ and $Cs_4C_{60}$. It is interesting to note that $A_4C_{60}$ materials do not exhibit superconducting characteristics.

## 3. Present work: Structural-microstructural characteristics of $C_{60}$ solid

Inspite of several investigations on the gross structural characteristics of $C_{60}$ solid (see previous section), several structural subtleties still remain to be explored or resolved. As for example, rather scant studies have so far been carried out regarding the microstructural details including local area structure and defect substructures. Yet another area where studies need to be carried out further relates to the issue of orientational order/disorder of $C_{60}$ molecules on the space lattice which has yet to be resolved. As described in the previous section orientational disorder in pure $C_{60}$ has been found to be invariably present at ambient temperature. The nature of this disorder has, however, not yet been fully resolved. It appears that there are several observations emanating from high resolution techniques such as transmission electron/scanning tunneling microscopy which suggest that the NMR results on free rotation of $C_{60}$ molecules may not be quite correct. Partial order seems to be present in $C_{60}$ solid even at room temperature. At low temperature ($<249$ K) where FCC phase changes to SC phase, the disorder decreases, but whether the SC phase has long range orientational order is still not known. In regard to doped versions (intercage intercalation versions) of $C_{60}$ solid, the orientational disorder is suppressed, as apparent from the most detailed study relating to structural exploration in intercage intercalated (doped) version; an orientational disorder of $C_{60}$ molecules has to be involved to take care of the observed XRD intensity profiles.

The above brings out some of the salient points which make the investigations on the structural/microstructural characteristics rather imperative. The present studies have been carried out to meet the aforesaid requirements.

### 3.1 *Synthesis of the material—The solid $C_{60}$*

The synthesis of $C_{60}$ was carried out by following a technique similar to the presently adopted ones (e.g. Krätschmer *et al.*,; Pradeep & Rao). Carbon was evaporated from graphite rod by triggering an arc at 20 V rms and 60 amp. The evaporation was carried out in helium atmosphere ($\sim$ 100 torr). The chamber was evacuated to $\sim$ $10^{-5}$ torr before bleeding helium. The chamber walls on which the carbon soot deposited was cooled through liquid nitrogen; this represents a small variation as compared to other presently known experimental conditions for the synthesis of $C_{60}$. The deposited soot (black-powder) was dissolved in benzene. The crystallisation from the solution was done by evaporating benzene at a moderate temperature of 40 to 50°C in rotoevaporator. The resulting crystals were purified by washing several times in diethyl ether. Tiny crystals/particles thus precipitated were brown black in colour. In some cases the purification was carried out by alumina column chromatography. Preliminary characterisation of the as prepared material was carried out by mass spectrometry and X-ray diffraction. Detailed structural-microstructural characteristics were undertaken by employing the technique of transmission electron microscopy in imaging, and diffraction [both selected area diffraction (SAD) and convergent beam electron diffraction (CBED)] modes. The present study forms one of the first explorations of the new $C_{60}$ material through TEM technique. Before resorting to detailed TEM studies of the $C_{60}$ solid, mass-spectral data were taken and analysed. These data revealed the preponderance of $C_{60}$. The XRD analysis revealed the presence of peaks corresponding to d : 8.69, 5.04 and 3.98 Å. These are in keeping with the known structural data of $C_{60}$ solid.

### 3.2 *The face centred versus hexagonal lattice structure of $C_{60}$ solid*

Even though presently the lattice structure of $C_{60}$ solid is taken to correspond to a face centred cubic system with $a \sim 14.17$ Å, there are several reports including the initial structural report by Krätschmer *et al.* where it has been analysed as hexagonal system (nearly HCP) with $a \sim 10.02$, and $c \sim 16.36$ Å. In order to explore this duality of the structural phase, we carried out extensive studies investigating local area as well as gross structural characteristics employing the technique of transmission electron microscopy. It should be pointed out that this technique is typically suited

Fig. 4—The SAD pattern representing the [001] (basal) reciprocal lattice section, taken from HCP phase of $C_{60}$.

Fig. 5—The SAD pattern representing the [111] reciprocal lattice section, taken from FCC phase of $C_{60}$.

for analysis of possible dual phases. Unlike XRD, where minority phases may be masked away, the TEM technique can reveal the structural information of even the minutest minority phase. A detailed TEM exploration of the as synthesised $C_{60}$ solid was carried out in the present investigation. These studies revealed that both the FCC and HCP phases are present. Typical diffraction patterns distinguishing these phases are shown in Fig. 4 (HCP) and Fig. 5 (FCC). It should be pointed out that the electron diffraction pattern represented by Fig. 5 can not be interpreted based on generally accepted face centred cubic lattice ($a \sim 14.17$ Å). This was also verified through non-basal oriented diffraction patterns corresponding to Fig. 4. A typical non-basal pattern is shown in Fig. 6. It is to be noted that only in some reports including that of Krätschmer *et al.* HCP structure has been reported; in all other studies FCC structure has been suggested. One of the reasons for this anomaly is the fact that the 10.0 peak (for HCP phase) is rather weak and is clearly discernible in only electron diffraction patterns (see Fig. 4). In the case of XRD which forms the basis of most of the structural analysis reports, the 10.0 peak is not recorded singularly as a distinguishable peak but appears as a feeble shoulder to the rather intense (002) peak and is thus generally overlooked. The lattice parameters for the FCC ($a \sim 14.17$ Å) and the HCP phase ($a \sim 10.02$ Å, $c \sim 16.36$ Å) obtained in the present study through electron diffraction investigations are quite compatible with the known results, whereas in some as synthesised

Fig. 6—[110] (Non-basal) reciprocal lattice section of HCP phase of $C_{60}$.

samples HCP phase was found to be the dominant phase; in others this behaviour was exhibited by HCP phase. The genuineness of the existense of hexagonal phase appears to be well established by now. It is significant to point out that in a recent study employing chromatographically purified $C_{60}$, the XRD pattern became completely intelligible only when a completely random mix of HCP and FCC phases was taken (Mackay *et al.*[10]). The reason for the existence of both the FCC and HCP phases is not known presently; however,

several factors seem to be possible. These are: bonding or interstitial dispersion of the solvent liquid (e.g. benzene), the local area random presence of $C_{70}$ fullerene version, the influence of experimental conditions, e.g., source (carbon arc) and/or substrate (copper or glass jar walls), etc. Clearly, further work is required to establish the causes responsible for the stabilisation of the FCC and/or HCP structural variants in the $C_{60}$ solid.

### 3.3 *Orientational order/disorder in the as synthesised $C_{60}$ solid*

As outlined in Section 2, one of the unresolved issues in regard to structural characteristics of $C_{60}$ solid relates to orientation ordering. It is now generally agreed that at room temperature the $C_{60}$ molecules of the material are orientationally disordered, at low temperatures this disorder is suppressed(decreased/eliminated). The nature of the ambient temperature disorder is not fully resolved as yet (see Section 2). It may be pointed out that several studies including STM reveal at least partial order at room temperature. In order to have an insight into this, we carried out detailed structural/microstructural analysis of the as synthesised $C_{60}$ material employing the technique of electron microscopy. The studies were spread over several as synthesised $C_{60}$ samples. A representative microstructural feature of the $C_{60}$ material is shown in Fig.7(a). As can be discerned from this transmission electron micrograph, the microstructure reveals the presence of mottled regions. The tiny local areas (0.25 μm) exhibit varying contrast, typical of domain regions. An electron diffraction pattern from the local area embodying mottled regions is shown in Fig.7(b). The pattern reveals the six 10.0 type diffraction spots bringing out the basal orientation of the $C_{60}$ region. A noticeable feature is the diffuse streaks interconnecting the successive 10.0 type diffraction spots and similarly other h0.0 type spots, e.g., 20.0. The microstructural characteristics together with diffraction data suggest thatthe mottled regions correspond to domains interrelated with each other and having a built-in native disorder. The dark field micrograph taken from basic 10.0 spots [see Fig.7(c)] revealing the lighting up of local regions, further supports the presence of domains. In the light of this, the diffuse streaking interconnecting 10.0 type spots may be taken to arise due to the occurrence of domains. The diffraction pattern containing several domains typically manifests the aforesaid type of diffuse streaks.

In order to uncover the reason of the occurrence of domains and the associated disorder, attempts were made to take diffraction patterns from individual domains. Smaller selected area apertures covering an area of 100 nm on the specimen and convergent beam electron diffraction patterns ( ~ 40 nm) were attempted. Figs 8(a) and 8(b) show representative diffraction patterns. These patterns are suggestive of comparatively ordered nature of individual domains. Keeping in view the known structural results of $C_{60}$, it may be concluded that whereas the individual domains contain $C_{60}$ arrangements with the same orientation, there is a misorientation between $C_{60}$ entities of different domains. This misorientation is expected to occur due to relative rotation of $C_{60}$ clusters of different domains. A schematic diagram bringing out the domain formation is shown in Fig. 9. The $C_{60}$ bucky balls of an individual domain have the same orientation, but those of neighbouring domains have undergone relative rotation. The reason for domain formation is not clear at present. However, here again the local area presence of interstitial dispersed solvent or the $C_{70}$ fullerene variant appears to be the feasible cause for the formation and existence of domains.

The above studies seem to suggest that partial orientational order is present in the as grown $C_{60}$ material. The disorder may arise due to domain formation which is a local area feature and is discernible in the present TEM investigations. However, the same would be largely marked in the gross structural studies, e.g., through X-ray diffraction.

### 3.4 *Defect substructure of $C_{60}$ solid*

There seem to be hardly any studies available to date regarding the native or induced defect substructure of the $C_{60}$ material. Fleming *et al.*[5] observed that the $C_{60}$ solid does not possess defects like stacking faults and at the inter-molecular level any intrinsic disorder is absent. We carried out detailed TEM (a technique typically suited for defect explorations) studies of the as synthesised and purified $C_{60}$ solid. It was found that in both these versions an often encountered defect entity corresponded to the stacking faults. A representative typical microstructural feature bringing out the stacking faults is shown in Fig. 10. The contrast effect observed in Fig. 10 clearly suggests the occurrence of stacking faults in two orientations (marked as $S_1$ and $S_2$). The well known α-fringe contrast where extreme fringes having the same

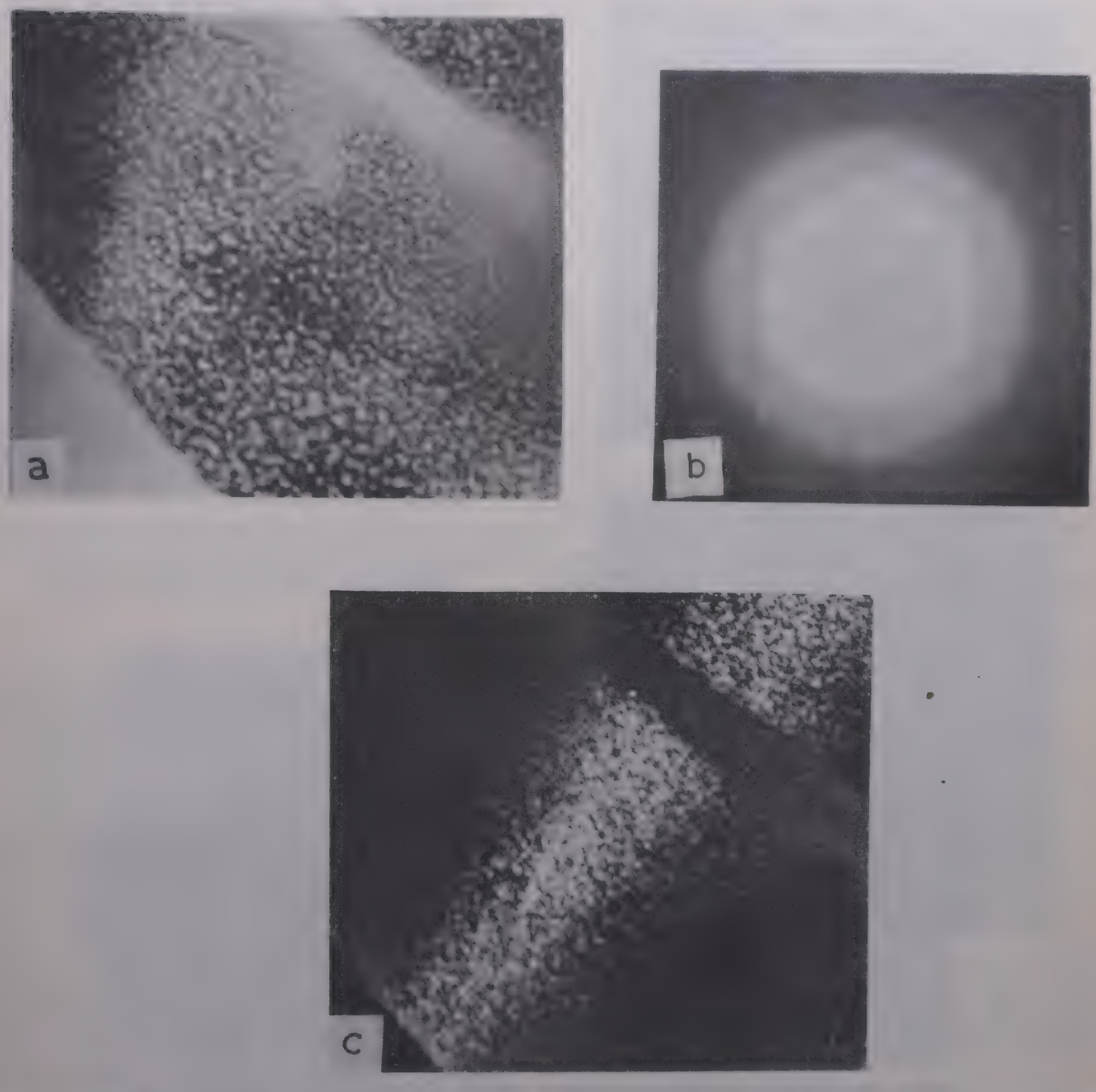


Fig. 7(a)—Bright field transmission electron micrograph of the as synthesised $C_{60}$ exhibiting mottled regions. The varying contrast in local regions suggests the presence of tiny domains. (b)—A representative electron diffraction pattern embodying mottled regions. Diffuse streaking interconnecting the successive 10.0 type spots are clearly visible. (c)—Dark field micrograph taken from 10.0 spots revealing the presence of domains.

nature can be easily noticed (e.g. the region marked inside the circle). In order to further confirm whether the observed defect substructure really corresponded to the stacking faults, selected area electron diffraction patterns from the $C_{60}$ crystal regions were taken and analysed. Fig. 11 exhibits a representative diffraction pattern. As can be easily noticed, diffraction streaks parallel to [111] directions are present. Keeping in view the known structural features of stacking faults, where the local displacements of close packed layers create very thin specific random crystal lamella (the reciprocal lattice points corresponding to these will be extended in space) which would give extensive streaking of diffraction spots along the [111] direction, it can be taken that the observed defects (Fig. 10) are stacking faults. Further support for this comes through the detailed nature of streaking of diffraction spots. As can be seen, whereas the rows with hk values of $\bar{2}2$ contain diffuse streaks, the row with hk $\bar{3}3$ (the third row in each set; marked by P,P') contain sharp

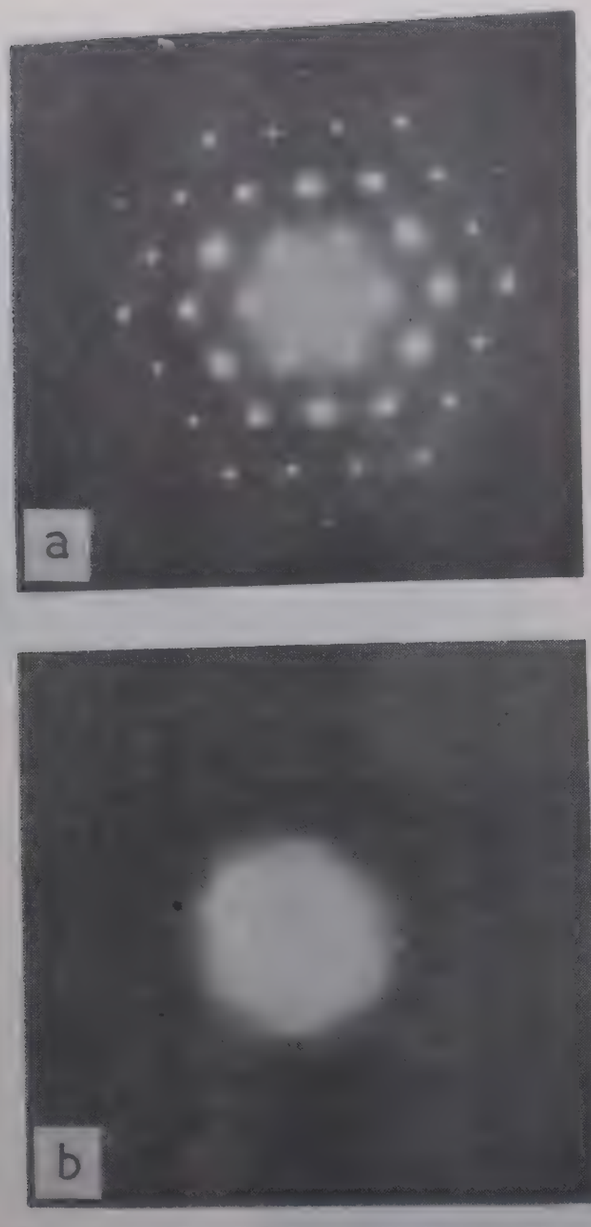


Fig. 8(a)—Selected area diffraction pattern of $C_{60}$ covering 100 nm region on the specimen. Unlike in Fig. 7(b), the diffraction spots are sharp. (b)—Convergent beam electron diffraction (CBED) pattern of $C_{60}$. Notice the presence of sharp diffraction discs.

spots. As is known for several solids containing close packed layers (e.g. graphite) the occurrence of stacking faults is associated with the displacement of subsequent layers by (2/3, 1/3, 0) or (1/3, (1/2, 0) and this leaves the structure factor of the rows with $h-k=3n(n=0,1,2.....)$ unaffected which in turn implies the presence of sharp diffraction spots. This is what is actually observed in the case of $C_{60}$ crystals (Fig. 10). The present TEM observations (which appear to be first of their type), therefore, suggest definite occurrence of stacking faults in $C_{60}$ solid. Even though this observation appears to be at variance with that of Fleming *et al.*[5], it is in accordance with observation of stacking faults in other close packed layered materials e.g. $MX_2$ solids, graphite, etc.

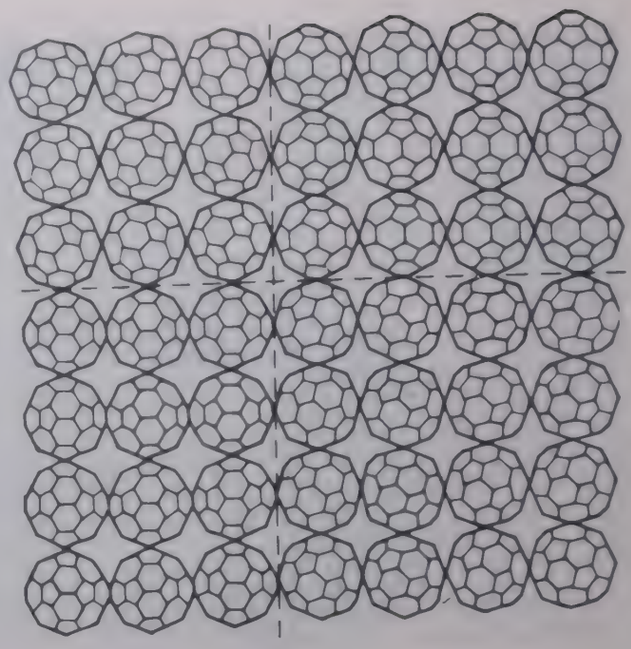

Fig. 9—Schematic representation of domains. The orientation of bucky balls ($C_{60}$) is the same in one domain but in the neighbouring these undergo relative rotation.

Fig. 10—Bright field electron micrograph depicting the occurrence of stacking faults along two ⟨111⟩ type directions in FCC phase of $C_{60}$.

### 3.5 *On the occurrence of superlattice in $C_{60}$ solid*

During the extensive exploration of the microstructural characteristics of the fullerene $C_{60}$, we found very often local area structures, embodied in the main FCC structure, which were suggestive of the occurrence of superlattice phase. Representative selected area electron diffraction patterns bringing out this superlattice pattern are shown in

Fig. 11—The SAD pattern taken from the area shown in Fig. 10. The streaks along the ⟨111⟩ direction correspond to the occurrence of stacking faults in two directions.

Fig. 12(a,b,c and d). Detailed analysis of these patterns revealed that a new structural phase with $a_s = 3a_c$ ($\sim 42.31$ Å) ($a_c$ being the lattice parameter of the FCC phase, $a \sim 14.17$ Å) has developed. This phase was invariably formed to be based on the FCC phase and was embedded within this as is shown by Fig. 12 (a,b,c and d). The investigations on microstructural characteristics of this phase did not reveal the occurrence of any discernible defect configuration.

It is interesting to note that the $C_{60}$ material is a nearly close packed FCC (ABC ABC -----) on HCP (ABAB -----) configuration. The occurrence of polytype like modulated phase brought about through the occurrence of ordered stacking faults is most expected. However, the present superlattice does not have lattice periodicity variation only along one direction (*c* direction referred to hexagonal system). In order to check the nature of stability of the superlattice, it was annealed *in situ*

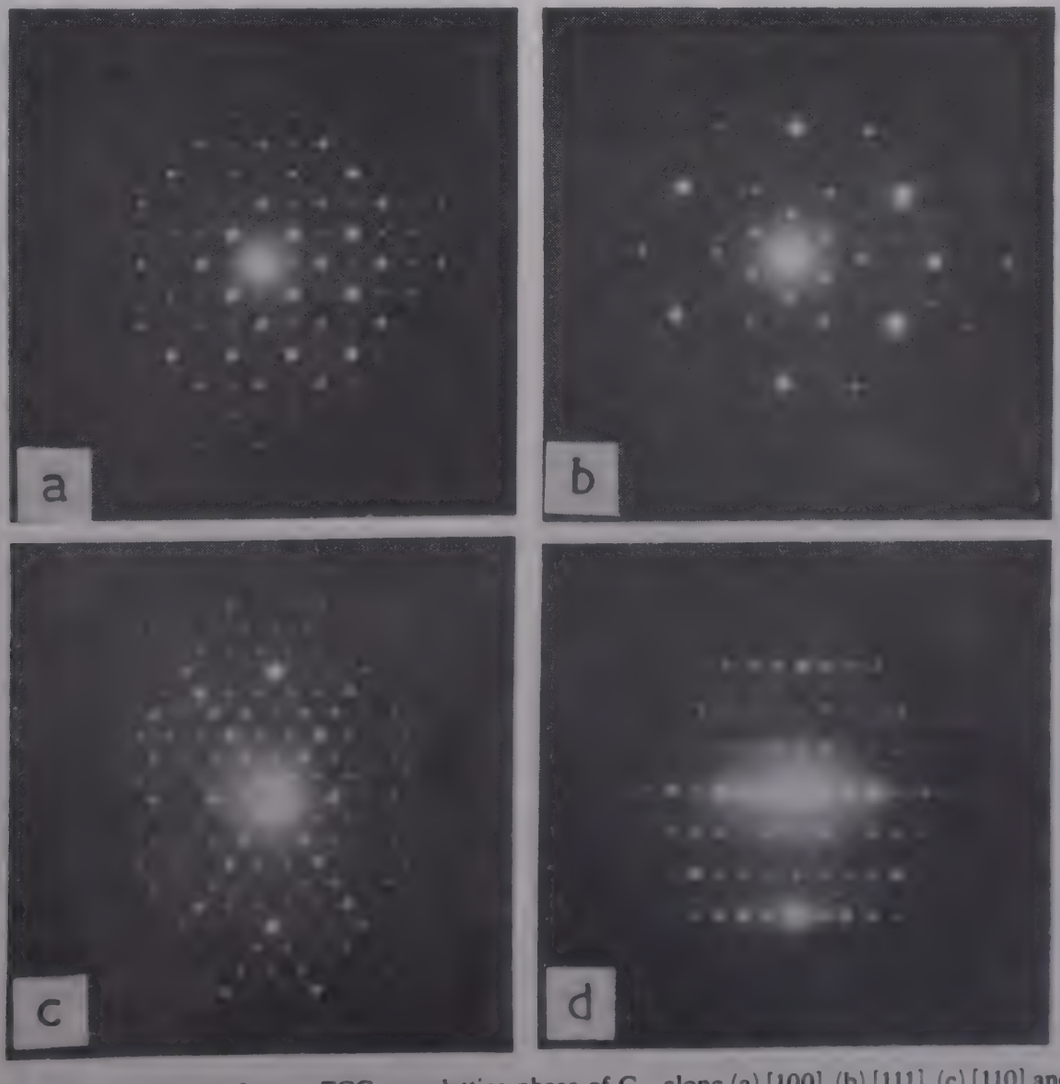


Fig. 12—The SAD pattern taken from a FCC superlattice phase of $C_{60}$ along (a) [100], (b) [111], (c) [110] and (d) [120] directions respectively.

in the electron microscope upto a temperature of ~ 300°C. This annealing treatment invariably leads to a transformation, leading to a change to the parent hexagonal structure. This transformation is brought out by Fig. 13 which shows the electron diffraction pattern corresponding to Fig. 4. This observation reveals that the superlattice with $a_s = 3a_c$ represents a metastable phase and it transforms to the stable parent hexagonal phase. It is interesting to note that whereas the superlattice is based on one of the parent phase—the FCC phase—it transforms to the other possible parent phase—the HCP phase. There appear to be two feasible models through which the occurrence of the metastable superlattice phase can become intelligible. In one of these, there can be three parent FCC cells in all the three orthogonal leading to the $3 \times 3 \times 3 = 27$ unit cells. After the three unit cells, the $C_{60}$ molecules either at the corners or the face centres of the unit cells would change configuration, for example, get rotated through 98° so that adjacent $C_{60}$ (equivalent nearest neighbours after three unit cells) molecules are in similar orientations, the electron rich portion of one $C_{60}$ facing electron rich of the other. This situation would lead to a new FCC structure with $a_s = 3a_c$ and carrying high energy local configurations, thus producing a metastable phase. Another possibility through which superlattice can get stabilised is through the occurrence of ordered stacking faults. The simplest configuration of stacking fault producing a local periodicity may be a change of the ideal ABCABCABCA ---- sequence to ABCACBABCA ----- along the close packed [111] through the occurrence of ordered stacking faults. However, such a stacking change along one [111] direction alone will lead to three times periodicity only along one direction. For creation of FCC superlattice structure with a lattice constant three times that of the parent structure, an ordered sequence of stacking faults is needed along all the four [111] directions, i.e., along [111], $[\bar{1}11]$, $[1\bar{1}1]$ and $[11\bar{1}]$. Such an ordered sequence would lead to superlattice structure with $a_s = 3a_c$. In view of the nature of occurrence of random stacking faults as exhibited by Fig. 10, the possibility of sequence of ordered stacking faults appears more likely. Thus, it appears that the 'ordered stacking faults' model rather than the '$C_{60}$ rotation' model looks more feasible for the occurrence of superlattice structure. The transformation of the superlattice structure to the HCP phase, also supports the 'ordered stacking faults' for the genesis of the superlattice phase.

Fig. 13—SAD pattern taken along the [111] of the superlattice structure after *in situ* annealing by electron beam.

### 3.6 *Anomalous carbon configuration structures*

In recent explorations of the carbon material deposited in helium atmosphere through charge discharge, structural forms other than fullerenes (e.g. $C_{60}$) have been discovered. Thus, Iijima[11] has recently observed helical microtubes of graphite carbon. Iijima by applying the electron microscopic technique found needle type configurations, each needle comprising coaxial graphitic sheets ranging in number from 2 up to about 50. In our studies (see also Verma *et al.*[12]) we encountered several carbon configurations which did not appear like fullerenes, but seemed to correspond to special graphitic sheet systems. A typical such configuration is brought out by selected area and convergent beam electron diffraction patterns shown in Fig. 14 (a) and (b). These and other similar SAD and CBED patterns suggested the possible occurrence of large area base containing flat hexagonal pyramidal prisons consisting of graphite sheets growing through spiral growth mechanism. The successive layers of the prism were slightly rotated with respect to the previous layers due to spiralling of the layers. Thus, the 42 diffraction spots containing diffraction patterns represent $6 \times 7$, i.e., 7 layers of the prism which have developed through spiral growth mechanism. The successive layers are slightly rotated ( ~ 9°) as compared to the preceding layer. Further work regarding the exact identification of these curious graphitic carbon configurations is in progress and results will be presented shortly.

## 4 Conclusions

It can thus be concluded that the present explorations of structural/microstructural character-

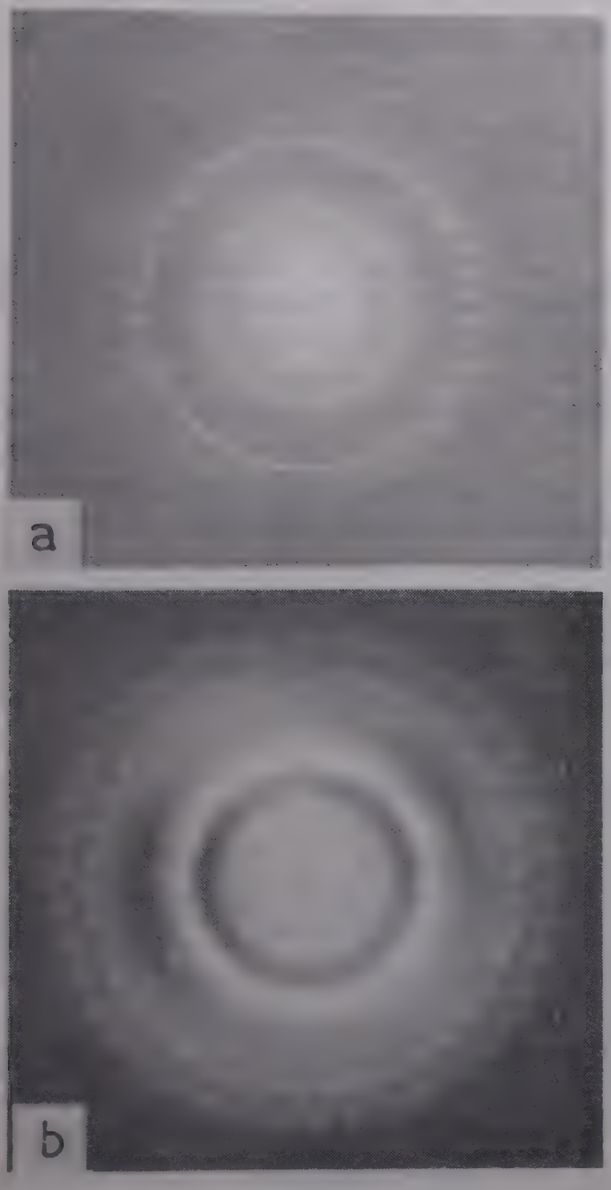


Fig. 14(a)—The SAD pattern representing the anomalous graphitic structure. The spots occurring on the ring are equidistant. (b) the corresponding CBED pattern taken by a 40nm probe size (see text for details).

istics of fullerene $C_{60}$ solid have revealed several curious characteristics. The simultaneous occurrence of FCC and HCP phases, the local area domain formation and the existence of orientational order, the occurrence of stacking faults, existence of superlattice structure, and the curious graphitic sheet configurations represent examples of the interesting structural/microstructural features observed in the present investigations. Further studies aimed at unravelling these characteristics and possible new ones, are presently being undertaken and results will be forthcoming.

**Acknowledgement**

The authors are grateful to Prof C N R Rao and Prof A R Verma for encouragement and initiation in regard to this work. They are also grateful to Prof R P Rastogi and Prof C S Jha for providing incentives related to this work. They are highly indebted to Prof G V Subba Rao and Prof H. Wondratschek for several discussions. The help and discussions provided by colleagues, Dr R S Tiwari, Dr A K Singh, Dr K Ramakrishna, Dr B Das, Sri K K Verma and Sri A K Srivastava are gratefully acknowledged. The present work was supported by on-going projects from DST and UGC.

**References**

1 David W I F, Ibberson R M, Matthewman J C, Prassides K, Dennis T J, Hare J P, Kroto H W, Taylor R & Walton D R M, *Nature*, 353 (1991) 147.
2 Heiney P A, Fischer J E, McGhie A R, Romanow W J, Denenstein A M, McCauley J P & Smith A B, *Phys Rev Lett*, 66 (1991) 2911.
3 Kroto H W, Heath J R, Brien S C O, Curl R F & Smalley R E, *Nature*, 318 (1985) 162.
4 Krätschmer W, Lamb L D, Fostiropoulos K & Huffmann D R, *Nature*, 347 (1990) 354.
5 Fleming R M, Rosseinsky M J, Ramirez A P, Murphy D W, Tully J C, Haddon R C, Siegrist T, Tycko R, Glarum S H, Marsh P, Dabbagh G, Zahurak S M, Makhija A V & Hampton C, *Nature*, 352 (1991) 701.
6 Kroto H W, Allaf A W & Balm S P, *Chem Rev*, 91 (1991) 1213.
7 Yannoni C S, Johnson R D, Meijor G, Bethune D S & Salem J R, *J phys Chem*, 95 (1991) 9.
8 Stephens P W, Mihaly L, Lee P L, Whetton R L, Huang S M, Kuner R, Deiderich F & Holczer K, *Nature*, 351 (1991) 632.
9 Zhou O, Fischer J E, Coustel N, Kycia S, Zhu Q, McGhie A R, Romanow W J, McCauley (Jr) J P, Smith III A B & Cox D E, *Nature*, 351 (1991) 462.
10 Mackay A, Vickers M, Kliouski J, Hare J P, Dennis T J, Kroto H W, Taylor R & Walton D R M (Unpublished results).
11 Iijima S, *Nature*, 354 (1991) 56.
12 Verma K K, Lalla N P, Srivastava A K, Ramakrishna K, Singh A K, Tiwari R S & Srivastava O N, *Solid State Commun*, (In press).

Indian Journal of Chemistry
Vol. 31 A&B, May 1992, pp. F92-F99

# Studies on structural and electronic properties of undoped and doped fullerenes $C_{60}$ and $C_{70}$

C S Sundar*, Y Hariharan, A Bharathi, V S Sastry, G V N Rao, J Janaki, T Geethakumari, T S Radhakrishnan, A K Arora, T Shakuntala, M Yousuf, P Ch Sahu, N Subramanian, V S Raghunathan† & M C Valsakumar
Materials Science Division, Metallurgy Division†, Indira Gandhi Centre for Atomic Research, Kalpakkam, India 603 102

Received 20 February 1992

This paper presents an overview of the experimental studies on fullerenes currently underway in the Materials Science Division, Kalpakkam. These include the synthesis of fullerenes by arcing of graphite electrodes, followed by the chromatographic separation of $C_{60}$ and $C_{70}$ and their doping with alkali metals. Doping of $C_{60}$ with K and Rb is observed to lead to superconductivity with transition temperatures of 18 K and 28 K respectively. Preliminary results of several ongoing studies, in particular the studies on structure of $C_{70}$ as a function of pressure and temperature, are reported.

Kroto *et al.*[1] in 1985 discovered the existence of stable carbon clusters of 60 atoms in the mass spectrum of laser ablated graphite, for which they proposed a soccer ball structure and termed it as buckminsterfullerene after the designer of geodesic domes. The recent synthesis of macroscopic quantities of fullerenes by Kratschmer *et al.*[2] by striking an arc between graphite electrodes in a helium atmosphere, has generated a flurry of interest in the closed caged carbon molecules $C_{60}$, $C_{70}$ and in the study of their solid state properties. The study of fullerenes received further impetus with the initial discovery of metallicity[3] in alkali doped $C_{60}$ and the subsequent announcement of superconductivity[4] with a $T_c$ = 18 K in K doped $C_{60}$. Currently, the study of fullerenes is an active area of research in several fronts: (i) studies on various methods of production with high yields[5]; (ii) studies on the structure of $C_{60}$ and the structural transformations as a function of temperature[6] and pressure[7]; (iii) experimental and theoretical investigations of the electronic[8,9] and vibrational properties[10,11], and studies on the doping of fullerenes with alkali atoms and other elements in order to obtain higher $T_c$[12-17].

In this paper, we present in detail, our experience with respect to synthesis and doping of fullerenes. With the availability of macroscopic quantities of samples, several experiments on the study of superconductivity in the doped samples and studies on the structural properties of pristine $C_{60}$ and $C_{70}$ have been initiated. This paper presents a status report of these experiments.

## Materials and Methods

### *Synthesis of fullerenes*

The synthesis of fullerenes involves first the production of carbon soot, which is mainly done by either resistive heating of graphite electrodes or

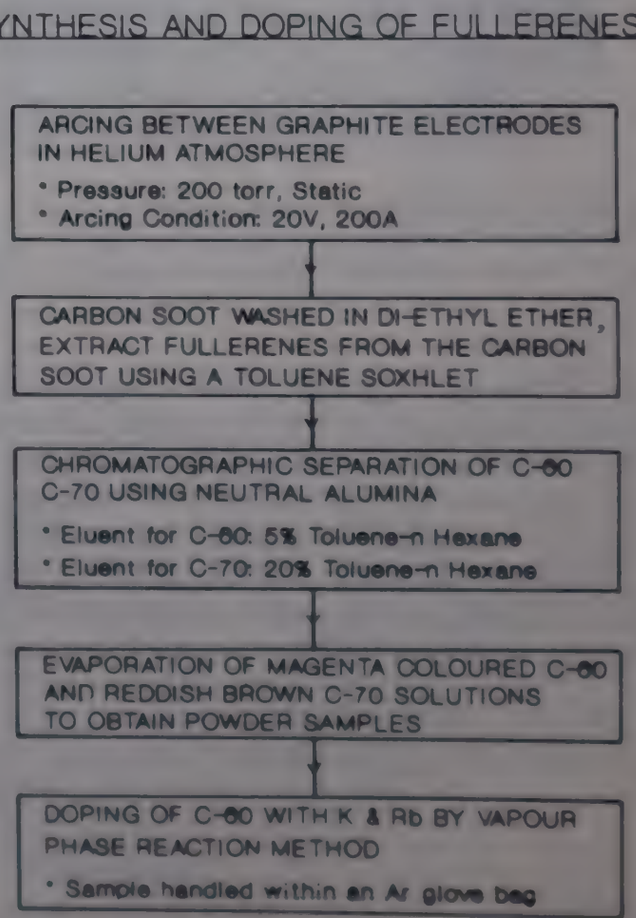
SYNTHESIS AND DOPING OF FULLERENES
ARCING BETWEEN GRAPHITE ELECTRODES IN HELIUM ATMOSPHERE
• Pressure: 200 torr, Static
• Arcing Condition: 20V, 200A
CARBON SOOT WASHED IN DI-ETHYL ETHER, EXTRACT FULLERENES FROM THE CARBON SOOT USING A TOLUENE SOXHLET
CHROMATOGRAPHIC SEPARATION OF C-60 C-70 USING NEUTRAL ALUMINA
• Eluent for C-60: 5% Toluene-n Hexane
• Eluent for C-70: 20% Toluene-n Hexane
EVAPORATION OF MAGENTA COLOURED C-60 AND REDDISH BROWN C-70 SOLUTIONS TO OBTAIN POWDER SAMPLES
DOPING OF C-60 WITH K & Rb BY VAPOUR PHASE REACTION METHOD
• Sample handled within an Ar glove bag

Fig. 1 — Flow chart for the synthesis and doping of fullerenes

"contact arc" between graphite electrodes[2,5,18,19]. Other methods such as burning of benzene in flame have also been reported[20]. The soot containing various carbon clusters is then separated in a chromatographic column to obtain $C_{60}$ and $C_{70}$. The flow chart for the synthesis of fullerenes and their doping with alkali metals is shown in Fig.1.

*Arcing of graphite electrodes*

The schematic diagram of the apparatus used for the production of carbon soot is shown in Fig.2. It consists of a pair of water-cooled graphite electrodes between which an arc is struck in a helium atmosphere. The electrodes are covered by a water-cooled copper hood in which the soot gets collected and this whole assembly is enclosed within a bell jar. The bell jar which is connected to a rotary pump with liquid nitrogen trap can be evacuated and refilled with helium to the desired pressure. An important design feature of this set up is that one of the electrodes can be moved inside the vacuum/helium atmosphere by a spring loaded arrangement. The electrodes are connected to a low voltage (40 volts max), high current (400 A max) AC power supply with the live end connected to the stationary electrode. In a typical arcing run with this apparatus approximately 3 cm of 10 mm diameter graphite rod gets consumed in ~ 2 hr resulting in ~ 0.3 g of soot. In order to increase the output another version has been designed and fabricated in which the movable electrode can traverse 20 cm through a Wilson seal arrangement. The schematic diagram of this apparatus is shown in Fig.3. In this apparatus each operation lasting 4 hr yields 10 g of soot.

During the operation of this apparatus, the influence of various parameters such as the helium pres-

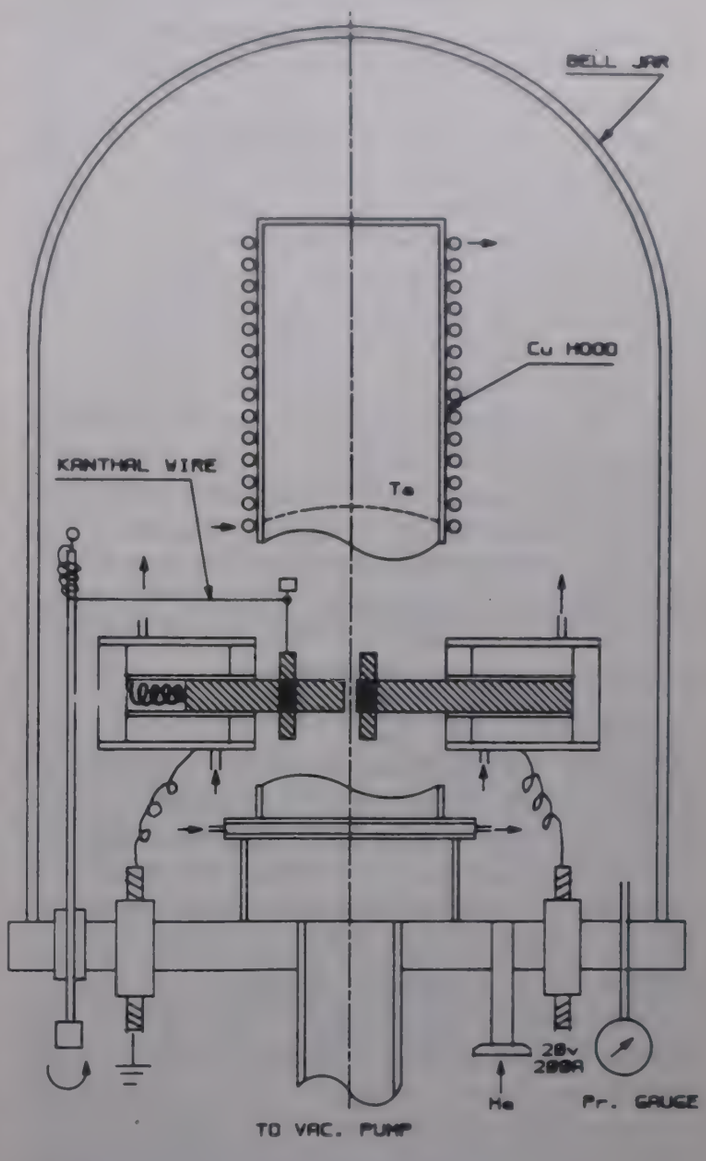


Fig. 2—Schematic diagram of the graphite arcing apparatus

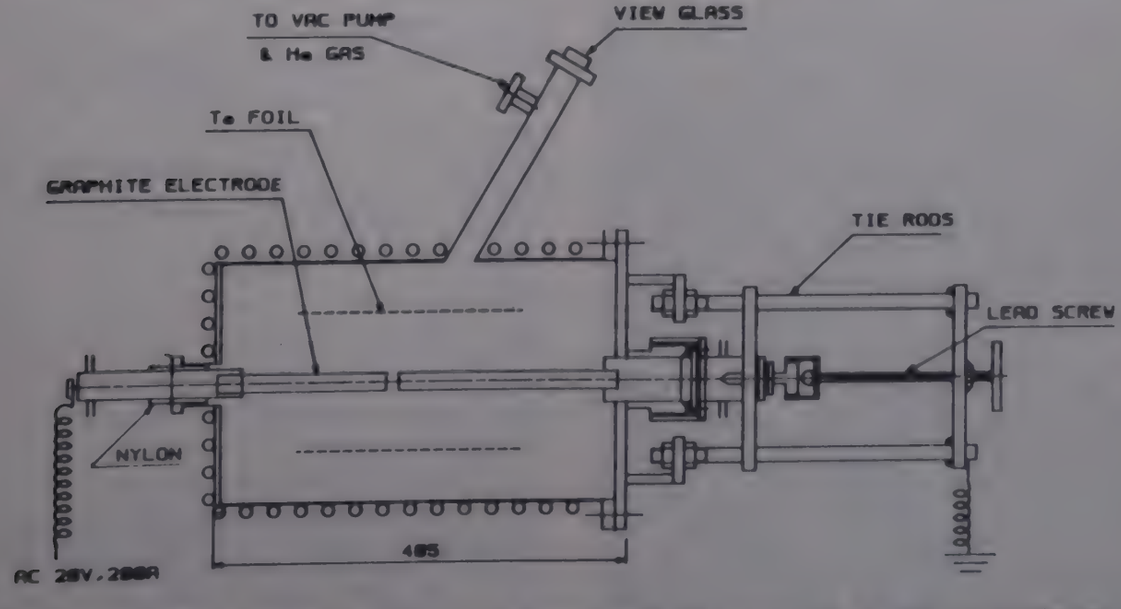


Fig 3—Schematic diagram of the modified graphite arcing apparatus. In this version, the graphite electrodes can be moved by 20 cm through a Wilson seal arrangement.

sure, the nature of graphite rods, the operating current and voltage, etc., on the quality and yield of soot have been tried. Helium pressure has been varied between 100 and 300 torr with the best results obtained for 200 torr. Both static and dynamic (controlled leak rate) helium conditions have been tried and best performance was seen under the former. The experiments on the variation of operating voltage indicated that for 10 mm graphite rods best performance was seen under the operating condition of 20 volts, 200 A. Smaller diameter rods (3 mm) could be operated with lower voltages (10 volts). The performance of this system improved significantly after the incorporation of a perforated tantalum sheet above the electrodes (see Fig.2). The exact reason for this as to whether it is due to the avoidance of photo-disintegration[21] or due to the longer retention of the carbon vapours in the region of the arc, thus enabling the formation of fullerene molecules[22] is not clear at the moment.

*Separation of $C_{60}$ and $C_{70}$*

The soot collected from the arcing apparatus is washed in diethyl ether to get rid of possible hydrocarbons and then introduced in the Soxhlet apparatus containing toluene. In ~ 24 hr of operation, a reddish brown solution containing fullerenes in toluene was obtained. This was concentrated by evaporation in a distillation apparatus at 120°C. Chromatographic separation of $C_{60}$ and $C_{70}$ was achieved using a column, 1 meter long and 3.5 cm diameter, in which ~ 500 g of neutral grade alumina was loaded. The alumina was heat treated at 200°C for 24 hr to get rid of all the moisture before packing into the chromatographic column. The column was conditioned with *n*-hexane and the Soxhlet extract (5% solution in *n*-hexane) was poured into the column. A clear separation of purple and brown bands corresponding to $C_{60}$ and $C_{70}$ was seen. $C_{60}$ was eluted using a 5% toluene-*n*-hexane mixture resulting in the collection of a clear magenta coloured solution. This was followed by the elution of a clear solution, after which the reddish brown $C_{70}$ solution was eluted out using a 20% toluene-*n*-hexane mixture. The magenta solution was evaporated to remove *n*-hexane and toluene and black crystallites of $C_{60}$ were obtained. Under an optical microscope, several transparent reddish crystals could be seen. Scanning electron microscopic studies, carried out using Philips model PSEM-501 microscope, clearly indicated the cubic morphology of these crystals with an average size of 40 μm. The evaporation of the reddish brown solution $C_{70}$ in toluene yielded needle shaped black crystallites. The typical yield of $C_{60}$ and $C_{70}$ powder together was observed to be ~ 5%, with $C_{60}$ and $C_{70}$ in the ratio of 80:20. For various arcing conditions that we have tried, we do not observe a 100% yield of $C_{60}$ as has been reported in ref. 19. The chromatographically separated $C_{60}$ and $C_{70}$ powders have been characterised and used in further studies on alkali doping of fullerenes. In addition to the preparation of powder samples, thin films of $C_{60}$ have been deposited on glass and NaCl substrates by subliming the $C_{60}$ powder by heating in vacuum at 500°.

## Results and Discussion

*Characterisation*

Several experimental techniques have been used to characterise and study the fullerenes. These include mass spectrometry[2,23], optical absorption in the infra-red, visible and ultraviolet[2,24], X-ray diffraction[2,6], Raman spectroscopy[3,25], and NMR[26]. In our experiments, the chromatographically separated $C_{60}$ and $C_{70}$ have been characterised by ultraviolet-visible absorption spectroscopy and X-ray diffraction.

The optical absorption spectrum was recorded in the UV-visible range for the separated $C_{60}$ and $C_{70}$ dissolved in *n*-hexane using a Shimadzu, model UV-240, spectrometer. The absorption spectrum recorded at room temperature in the range of 300 nm-700 nm is shown in Fig.4. The spectrum of $C_{60}$ shows a dominant absorption band at 320 nm and a double-hump structure centred at 404 and 408 nm respectively. In the case of $C_{70}$, broad humps are seen at 550, 470 nm and in the near UV region at 378, 359 and 331 nm. The dominant spectral features in $C_{60}$ and $C_{70}$ are in agreement with those reported by Ajie *et al.*[24]. As a test of the efficacy of chromatographic separation, in particular the possible contamination of $C_{60}$ in $C_{70}$, the absorption spectra were recorded with higher sensitivity in the range of 380-430 nm (see Fig.5). The characteristic double hump structure seen in the absorption spectrum of $C_{60}$ can not be discerned in the spectrum of $C_{70}$. On the basis of this, the content of $C_{60}$

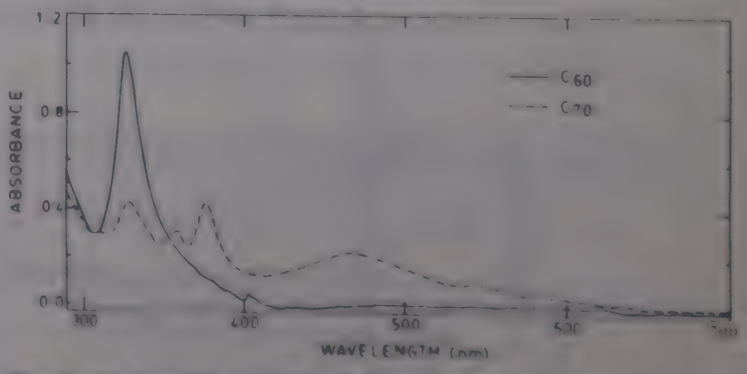


Fig. 4—Absorption spectra of $C_{60}$ and $C_{70}$ in *n*-hexane in the range of 300-700 nm

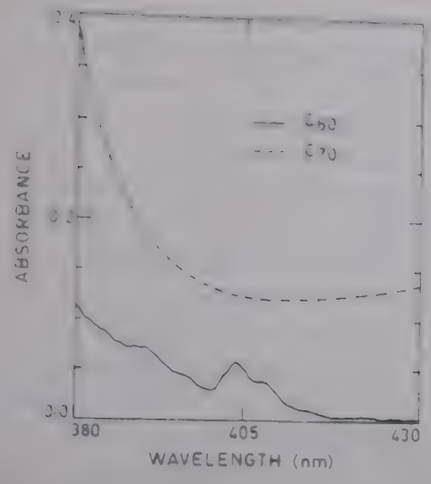


Fig. 5—Absorption spectra of $C_{60}$ and $C_{70}$, measured with an enhanced sensitivity in the range of 380 to 430 nm. Note that the characteristic double hump structure of $C_{60}$ around 405 nm is not seen in the spectrum of $C_{70}$ indicating the efficacy of the chromatographic separation

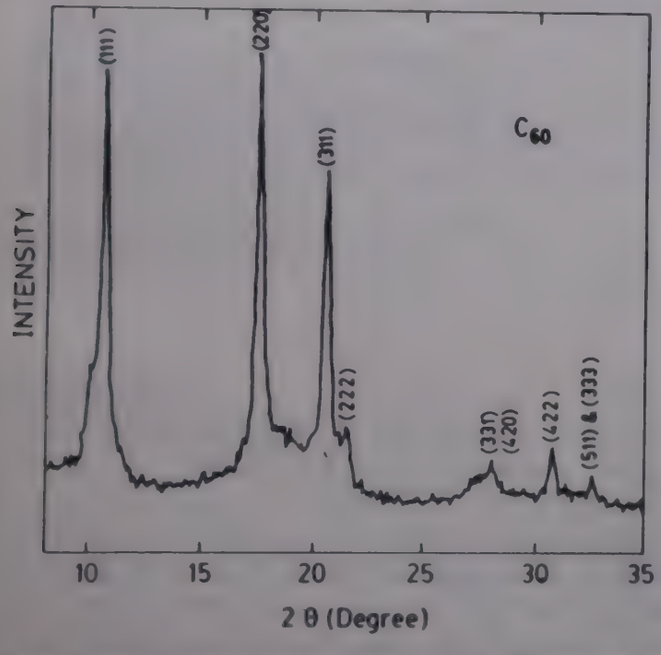


Fig. 6—X-ray diffraction pattern of $C_{60}$. The diffraction lines have been indexed to fcc structure

in the chromatographically separated $C_{70}$ is estimated to be < 2%.

The icosahedral $C_{60}$ molecules have been shown[6] to crystallise in the fcc structure with complete orientational disorder at room temperature; the orientational order develops at temperature less than 249 K. The room temperature X-ray diffraction pattern of $C_{60}$ powder measured using $CuK_\alpha$ radiation is shown in Fig.6. The diffraction pattern could be indexed to fcc structure with a lattice constant of 14.2 ± 0.1 Å. Further, as noted in ref. 7, it is seen that the diffraction peak corresponding to (200) index is not observed. This arises[7] due to the accidental vanishing of molecular form factor when hollow spherical $C_{60}$ clusters of radius r (3.55 Å) are

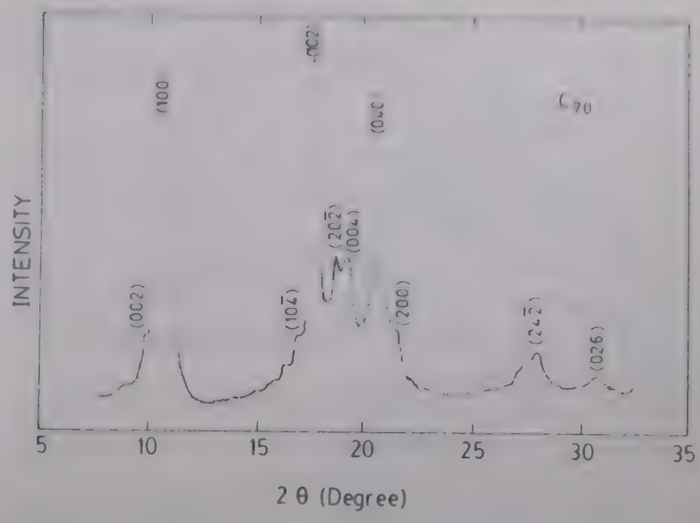


Fig. 7—X-ray diffraction pattern for $C_{70}$. The lines have been indexed to a distorted hcp structure

packed in a fcc lattice with a lattice constant of 4* r (14.2 Å).

There is as yet no definitive published crystal structure of $C_{70}$. Theoretical predictions indicate that these prolate spheroidal molecules crystallise in the hcp structure[27]. The experimental X-ray powder diffraction pattern of $C_{70}$ is shown in Fig.7. These have been at present indexed to a distorted hexagonal packed structure with the lattice parameters $a$ = 9.547 Å, $b$ = 21.277 Å, $c$ = 17.205 Å, and $\gamma$ = 119.61°. For an unequivocal identification of structure, further experiments on single crystals of $C_{70}$, and calculations of diffraction intensities are in progress.

*Alkali doping of $C_{60}$*

In the first report[4] of superconductivity ($T_c$ = 18 K) in K doped $C_{60}$ films, the doping was carried out by the vapour phase reaction method. Holczer *et al.*[12] have described in detail the protocol for the doping of K(and Rb) in bulk $C_{60}$. From the studies on the diamagnetic shielding as a function of initial K composition, they have identified the superconducting composition to be $K_3C_{60}$. Stephens *et al.*[28] have found the structure of $K_3C_{60}$ to consist of K atoms located in the tetrahedral and octahedral holes of the fcc $C_{60}$ lattice. In addition to K doped $C_{60}$, superconductivity has been observed in other alkali doped $C_{60}$: Rb doped $C_{60}$ ($T_c$ = 28 K)[12,13], $Rb_xK_{3-x}C_{60}$ ($T_c$ = 19K to 30K)[14], Cs doped $C_{60}$ ($T_c$ = 30K)[16], and $Cs_xRb_{3-x}C_{60}$ ($T_c$ = 33K)[15]. The highest transition temperature observed[17] so far is in Rb,Tl doped $C_{60}$ with a $T_c$ of 45 K. Since the initial report of the preparation of K doped $C_{60}$ by the vapour phase reaction method, other synthesis procedures have been tried out with a view to obtaining better control over the stoichiometry, and increasing the superconducting volume fraction. The difficulties in the handling of

small quantities of air sensitive alkali metals inside a dry box have been overcome to some extent by treating $C_{60}$ with alkali/heavy metal amalgams[16]. Another method to obtain better control over the stoichiometry involves first the preparation of saturation product ($K_6C_{60}$), which is subsequently reacted with known amount of $C_{60}$ to obtain $K_3C_{60}$[29]. A solution route for the synthesis of K doped $C_{60}$ has been described by Wang *et al.*[30] in which $C_{60}$ dissolved in toluene is reacted with K chips in an air-free environment.

In the present experiments, stoichiometric quantities of $C_{60}$ and K (corresponding to the composition $K_3C_{60}$) were loaded into a 6 mm dia, 20 cm long pyrex tube fitted with a stop cock. The mixture was heat treated in vacuum ($10^{-5}$ torr) at 250°C for 24 hr. The mixture was reground and heat treated again in vacuum at 250°C for 24 hr. The reaction product (~20 mg) was reground, pelletised and sintered at 250°C for 24 hr. A pair of sliced pellets was loaded into the teflon capsule for AC susceptibility measurements. Finely ground powder was loaded into a Lindemann glass capillary and sealed for X-ray measurements. All operations involving handling of the sample were carried out inside an argon filled glove bag.

The X-ray diffraction pattern of K doped $C_{60}$ is shown in Fig.8. The broad background is due to the glass capillary. The diffraction lines could be indexed to a fcc structure with a lattice constant of 14.3 ± 0.1 Å. The diffraction lines corresponding to K are also indexed and it is seen that very small amount of unreacted K, if any, is present. Comparing with the diffraction pattern of $C_{60}$ (see Fig.6), it is seen that the (200) line is still absent and the dominant change due to K doping is in the relative intensities of the (220) and (311) diffraction lines. As indicated by Stephens *et al.*[28], this arises due to doping of K at (1/4, 1/4, 1/4) and (1/2,0,0) positions in the unit cell.

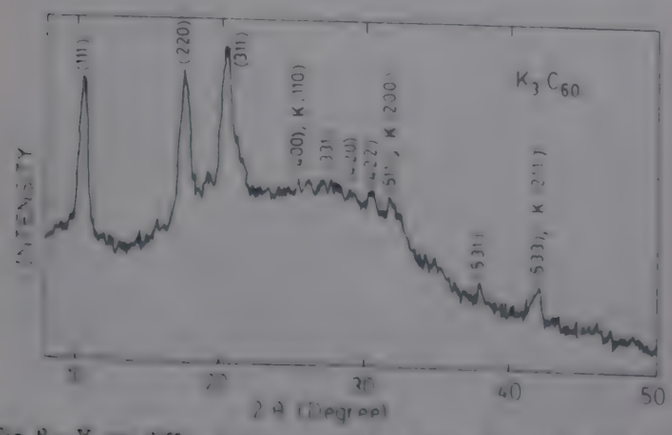


Fig. 8 – X-ray diffraction pattern of K doped $C_{60}$. The lines have been indexed to fcc structure. The diffraction line corresponding to K are also indicated

AC susceptibility measurements were carried out at 941 Hz using a mutual inductance coil and lock-in amplifier. The variation of normalised susceptibility as a function of temperature, as measured using a calibrated carbon resistor, shows a sharp superconducting transition (cf. Fig.9) with a onset at 18 K and a transition width (25 to 75%) of 3 K. The transition curve compares favourably with the best results reported so far[12]. The superconducting volume fraction with respect to Nb standard is estimated to be 10%. Superconductivity in K doped $C_{60}$ is observed to degrade and finally disappear on exposure of the sample to atmosphere. We have also observed the degradation of superconductivity in a sample subjected to prolonged (1 week) heat treatment in vacuum at 250°. The implications of this with respect to the initial stoichiometry for sample preparation, diffusion of K inside the $C_{60}$ matrix during heat-treatment and phase decomposition of $K_xC_{60}$ are being examined.

Doping of $C_{60}$ with Rb was carried out along similar lines to that of K, except that the heat-treatment in this case was carried out at 440°C. Figure 10 shows the X-ray diffraction pattern of the Rb doped $C_{60}$.

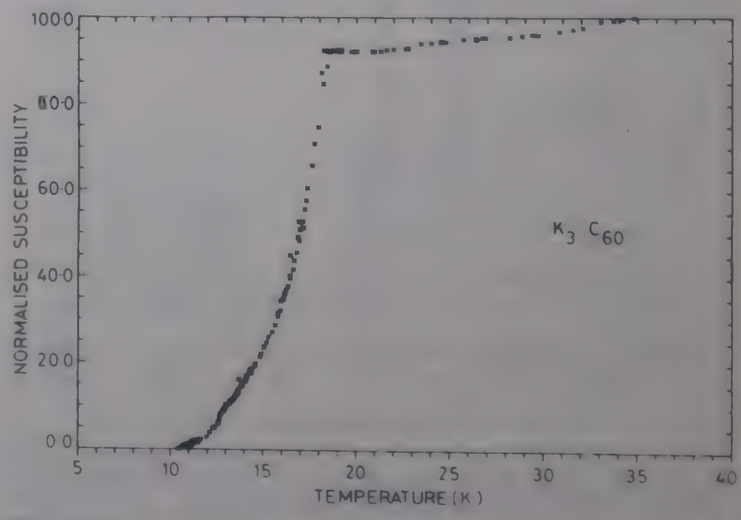


Fig. 9—Normalised susceptibility versus temperature in K doped $C_{60}$ indicating the superconducting transition at 18 K

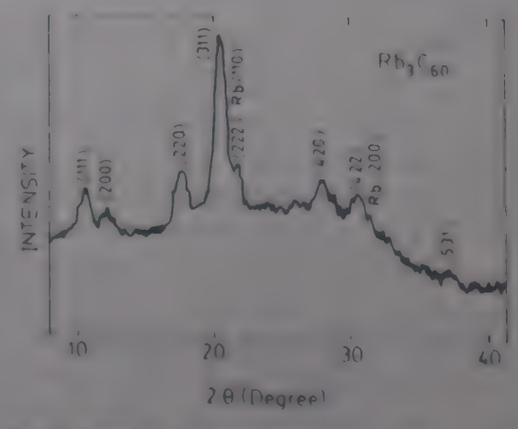


Fig. 10—X-ray diffraction pattern of Rb doped $C_{60}$. The diffraction lines corresponding to Rb are also shown

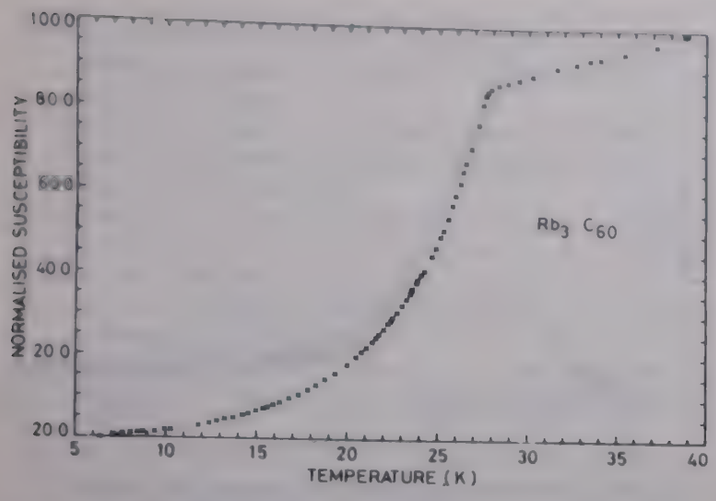


Fig. 11—Normalised susceptibility versus temperature in Rb doped $C_{60}$, indicating superconducting transition at 28 K

The lines could be indexed to fcc structure with a lattice constant of 14.4 ± 0.1 Å. A comparison with the diffraction patterns of $C_{60}$ (Fig.6), and $K_3C_{60}$ (Fig.8) shows that the (200) line is present. This arises because of the expansion of the lattice so that the fortuitous condition $a=4*r$ is no longer satisfied[7]. The results of AC susceptibility measurements on the Rb doped sample are shown in Fig.11. A sharp superconducting transition with a $T_c$ (onset) at 28 K is clearly seen. The superconducting volume fraction is estimated to be 7%.

*On-going studies*

With the availability of macroscopic quantities (100 mg) of well characterised fullerenes, further work on the study of structural and electronic properties as a function of temperature, pressure and doping, using a variety of experimental techniques such as X-ray diffraction, resistivity, AC susceptibility, photoluminescence, Raman spectroscopy and positron annihilation spectroscopy have been initiated. A brief account of these experiments is provided in the following.

*Structural studies on $C_{70}$*

In contrast to detailed structural studies on $C_{60}$ as a function of temperature and pressure, there is as yet no published results on $C_{70}$. Energy dispersive X-ray diffraction measurements have been carried out in $C_{70}$ as a function of pressure, under truly hydrostatic conditions, in the range of 0-20 GPa, using a diamond anvil cell. Dramatic changes in the diffraction pattern have been observed beyond 13 GPa and work is in progress to identify the high-pressure phase[31]. It may be remarked that in the case of $C_{60}$, having an fcc structure under ambient conditions, no structural transition has been observed under hydrostatic conditions upto 20 GPa, whereas under

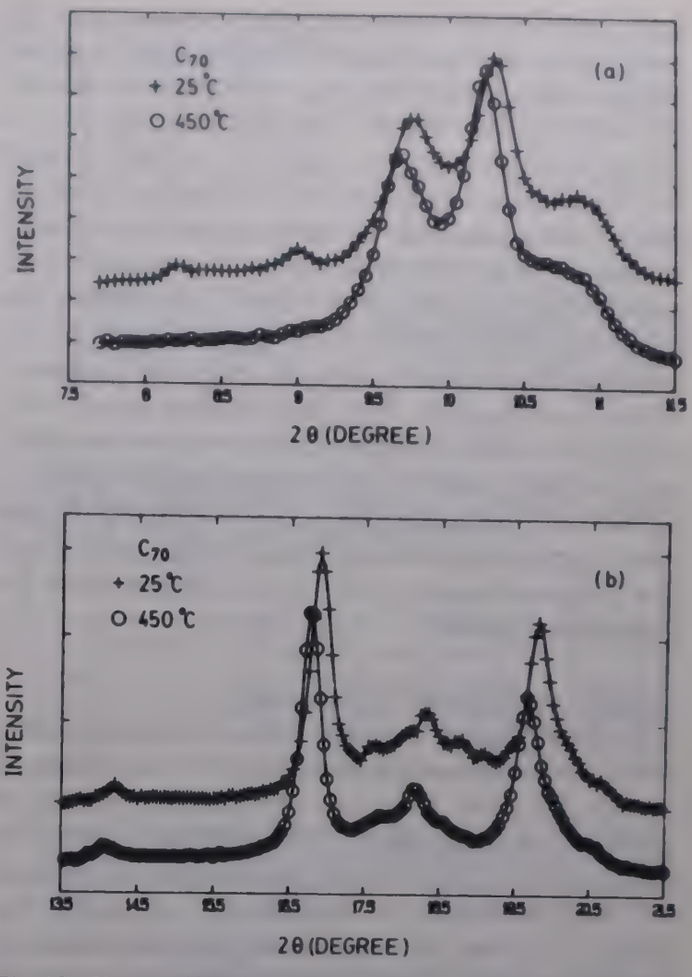


Fig. 12—X-ray diffraction pattern of $C_{70}$ at room temperature and 450° in the range of (a) 7.5 to 11.5 degrees and (b) 13.5 to 21.5 degrees. Notice the disappearance of certain peaks at high temperature, in addition to the shifting of peaks towards smaller angles

non-hydrostatic conditions, a transition to crystallographic structure of lower symmetry is seen at 16 GPa[7].

$C_{60}$, which crystallises into an fcc structure at room temperature undergoes a structural transformation to sc structure below 249 K and this is associated with the development of orientational order among the icosahedral molecules. With a view to looking for similar structural transition in $C_{70}$, X-ray diffraction experiments have been carried out as a function of temperature (under vacuum) upto 450°C. It is seen from Figs 12a and 12b that as the temperature is increased, apart from the shifting of peaks towards smaller angles due to thermal expansion, some of the peaks present in the room temperature spectrum disappear at 450°C. These changes are observed to be irreversible. Work is in progress to identify the structural changes with temperature.

*Photoluminescence*

Recent photoluminescence measurements[32] on single crystals of $C_{60}$ show a band centred at 13200

$cm^{-1}$, and this shifts to lower wave numbers with the application of pressure upto 3.2 GPa. This indicates a large reduction in band gap with pressure and by an extrapolation of this trend the band gap is predicted to collapse at ~ 13 GPa[32]. In pursuance of this interesting suggestion on possible metallisation of $C_{60}$ under pressure, we have carried out resistivity measurements as a function of pressures. Our measurements so far indicate that $C_{60}$ remains in the insulating phase upto 6 GPa. Further work on increasing the pressure range of resistivity measurements is envisaged. Our photoluminiscence measurements indicate that in addition to the overlapping four band structure seen in the range of 14000 to 12000 $cm^{-1}$, structures are also seen in the higher wave number region of 20000 to 16000 $cm^{-1}$. Work is in progress to understand these features in the luminescence spectra.

*Positron annihilation spectroscopy*

Positron lifetime measurements in sintered pellets of $C_{60}$, indicate a single component with a lifetime of 360 ps (Fig.13a). There is a considerable interest in understanding the origin of this lifetime component as to whether it arises from annihilations associated with the localisation of the positron within the $C_{60}$ cluster, or from the delocalised positron in the interstitial regions of the crystal. Theoretical calculations of the positron density distribution in $C_{60}$ have been carried out and these indicate (Fig.13b) that the positrons probe predominantly the interstitial region along the $C_{60}$-$C_{60}$ bonds rather than the region inside the $C_{60}$ cluster. In the light of this disposition of positron density within the $C_{60}$ crystal, it can be anticipated that the positron annihilation parameters will be sensitive to probe the effects of pressure and doping of $C_{60}$ crystal.

*Doping studies*

In addition to the studies on K and Rb doped $C_{60}$, attempts to intercalate with other dopants, and studies on the structure and superconducting properties of the resultant products are also being carried out. In the course of these studies we have observed that Pb can be incorporated along with K into $C_{60}$ and the resultant samples are superconducting with $T_c$ of 18 K. These samples exhibit much sharper transition and are also observed to be more resistant to degradation in comparison to K doped $C_{60}$. Systematic studies on the Pb/K doped samples of various stoichiometries are in progress.

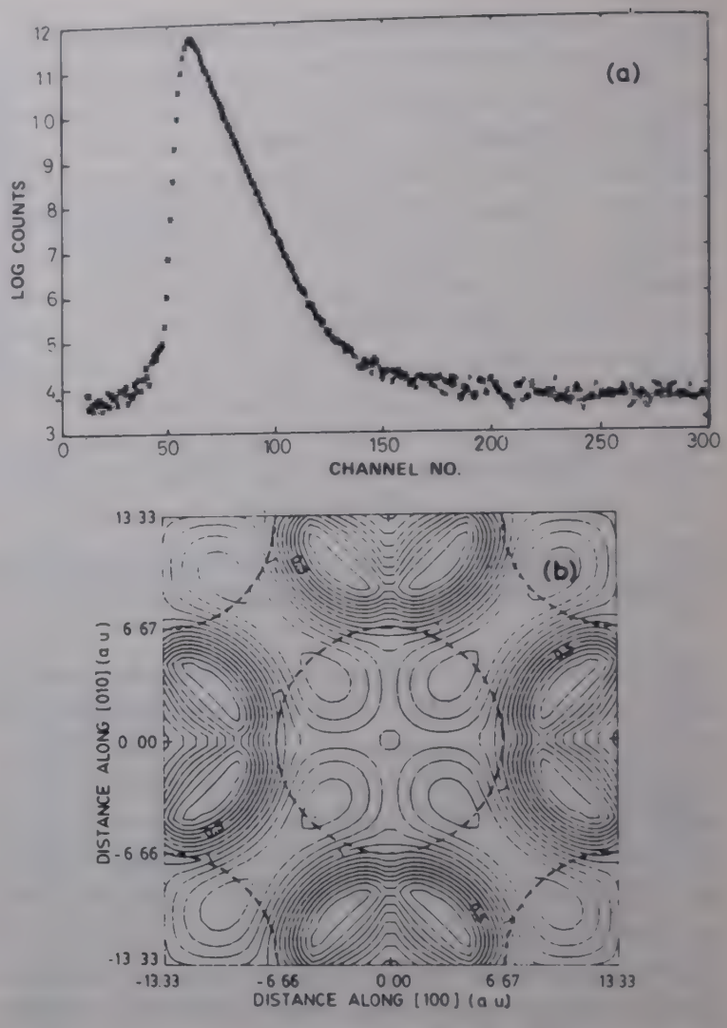


Fig. 13—(a) Positron lifetime spectrum in $C_{60}$. (b) Positron density distribution in (001) plane of fcc $C_{60}$. The dotted circles indicate the $C_{60}$ cluster. The maxima of the positron density is along the $C_{60}$-$C_{60}$ bonds of the crystal rather than in the region inside the cluster

**Summary**

The details of the arcing of graphite electrodes and chromatographic separation for the synthesis of pure $C_{60}$ and $C_{70}$ have been described. Doping of $C_{60}$ with K and Rb results in superconducting samples with $T_c$ of 18 K and 28 K respectively. The preliminary results of several on-going experiments on both pristine and doped fullerenes have been presented.

**Acknowledgement**

The authors would like to thank Shri N Chinnasamy, Smt M Premila, Smt Padma Gopalan and Kum M Shailaja for assistance in various aspects of the experiments reported in this paper. The enthusiastic support and encouragement from Dr Kanwar Krishan and various members of the Materials Science Division is gratefully acknowledged.

**References**

1 Kroto H W, Heath L R, O'Brien S C, Curl R F & Smalley R E, *Nature*, 318 (1985) 162.

2 Kratschmer W, Lamb L D, Fostiropoulos K & Huffman D R, *Nature*, 347 (1990) 354.

3 Haddon R C, Hebard A F, Rossieinsky M J, Murphy D W, Duclos S J, Lyons K B, Miller B, Rosamillia J M, Fleming R M, Kortan A R, Glarum S H, Makhija A V, Mueller A J, Eick R H, Zahurak S M, Tycko R, Dabbagh G & Thiel F A, *Nature*, 350 (1991) 320.

4 Hebard A F, Rosseinsky M J, Haddon R C, Murphy D W, Glarum S H, Palstra T T M, Ramirez A P & Kortan A R, *Nature*, 350 (1991) 600.

5 Parker D H, Wartz P, Chatterjee K, Lykke K R, Hunt J E, Pellin M J, Hemminger J C, Gruen D M & Stock L M, *J Am chem Soc*, 113 (1991) 7499.

6 Heiney P A, Fischer J E, McGhie A R, Romanow W J, Denenstein A M, McCauley (Jr) J P & Smith III A B, *Phys Rev Lett*, 66 (1991) 2911.

7 Duclos S J, Brister K, Haddon R C, Kortan A R & Thiel F A, *Nature*, 351 (1991) 380.

8 Weaver J H, Martins J L, Komeda T, Chen Y, Ohno T R, Troullier N, Haufler R E & Smalley R E, *Phys Rev Lett*, 66 (1991) 1741.

9 Saito S & Oshiyama A, *Phys Rev Lett*, 66 (1991) 2637.

10 Bethune D S, Meijer G, Tang W C & Rosen H J, *Chem Phys Lett*, 174 (1990) 219.

11 Cappilletti R L, Copley J R D, Kamitakahara W A, Li F, Laninin J S & Ramage D, *Phys Rev Lett*, 66 (1991) 3261.

12 Holczer K R, Klein O, Huang S M, Kauer R B, Fu K J, Whetten R L & Diederich F, *Science*, 252 (1991) 1154.

13 Rossiensky M J, Ramirez A P, Glarum S H, Murphy D W, Haddon R C, Hebard A F, Palstra T T M, Kortan A R, Zahurak S M & Makhija A V, *Phys Rev Lett*, 66 (1991) 2830.

14 Chen C C, Kelty S P, Lieber C M, *Science*, 253 (1991) 886.

15 Tanigaki K, Ebbesen T W, Saito S, Mizuki J, Kubo Y & Kuroshima S, *Nature*, 352 (1991) 222.

16 Kelty S P, Chen C C & Lieber C M, *Nature*, 352 (1991) 223.

17 Iqbal Z, Baughman H R, Ramakrishna B L, Khare S, Murthy N S, Bornemann H J & Morris D E, *Science*, 254 (1991) 826.

18 Haufler R E, Conceicao J, Chibante L P, Chai Y, Byrne N, Flanagan S, Haley M M, O'Brien S C, Pan C, Xiao Z, Billups R F & Smalley R E, *J Phys Chem*, 94 (1990) 8634.

19 Pradeep T & Rao C N R, *Mat Res Bull*, 26 (1991) 1101.

20 Howard J B, McKinnon T, Makarovsky Y, Lafleur A L & Johnson M E, *Nature*, 352 (1991) 139.

21 Arbogast J W, Darmanayan A P, Foote C S, Rubin Y, Diederich F N, Alvarez M, Anz S J & Whetten R L, *J Phys Chem*, 95 (1991) 11.

22 Curl R F & Smalley R E, *Scientific American*, October, (1991), 54-63.

23 Mathews C K, Vasudeva Rao P R, Srinivasan T G, Ganesan V, Sivaraman N, Lakshmi Narasimhan T S, Kaliappan I, Chandran K & Dhamodaran R, *Curr Sci*, 61 (1991) 834.

24 Ajie H, Alvarez M M, Anz S J, Beck R D, Diederich F, Fostiropoulos K, Huffman D R, Kratschmer W, Rubin Y, Schriver K E, Sensharma D & Whetten R L, *J Phys Chem*, 84 (1990) 8630.

25 Duclos S J, Haddon R C, Glarum S H, Hebard A F & Lyons K B, *Sol State Commun*, 80 (1991) 481.

26 Tycko R, Haddon R C, Dabbagh G, Glarum S H, Douglass D C & Mujsce A M, *J Phys Chem*, 95 (1991) 518.

27 Guo Y, Karasawa N & Goddard III W A, *Nature*, 351 (1991) 464.

28 Stephens P W, Mihaly L, Lee P L, Whetten R L, Huang S M, Kaner R, Diederich F & Holczer K, *Nature*, 351 (1991) 632.

29 McCauley (Jr) J P, Zhu Q, Coustel N, Zhou O, Vaughan G, Idziak S H J, Fischer J E, Tozer S W, Groski D M, Bykovetz N, Lin C L, McGhie A R, Allen B H, Romanow W J, Denenstein A M & Smith III A B, *J Am chem Soc*, 113 (1991) 8537.

30 Wang H H, Kini A M, Savall B M, Carlson K D, Williams J M, Lykke K R, Wurz P, Parker D H, Pellin M J, Gruen D M, Welp U, Kowk W K, Fleshler S & Crabtree G W, *Inorganic chemistry*, 30 (1991) 2838.

31 Yousuf M *et al.* (to be published).

32 Sood A K, Chandrabhas N, Muthu S, Victor D, Kumar N, Jayaraman A, Pradeep T & Rao C N R, *Sol State Commun*, 81 (1992) 89.

Indian Journal of Chemistry
Vol. 31 A&B, May 1992, pp. F100-F103

# The problem of conducting and superconducting fullerides

Ratan Lal
Theory Group, National Physical Laboratory, Dr K S Krishnan Road, New Delhi 110 012, India
and
S K Joshi*
Council of Scientific & Industrial Research, Rafi Marg, New Delhi 110 001, India

Received 20 February 1992

Conducting and superconducting fullerides present a problem where one finds a strong interplay between molecular structural effects and the long range crystalline order. An effort has been made to discuss these effects in the conducting state of fullerides by considering the different interactions which are present in these systems. The superconducting state of fullerides has been considered by discussing the relevance of a modified Bardeen-Cooper-Schrieffer theory in the light of recent measurements of tunneling spectra in the $Rb_3C_{60}$ superconductor.

## Introduction

The recent discovery of nanometer-size carbon clusters of sixty of larger number of atoms[1], commonly called fullerenes, has prompted a large number of experimental and theoretical studies of these clusters and their solids[2]. Research efforts were further accelerated by the discovery that when intercalated with alkali elements such as K, Rb and Cs, the $C_{60}$ crystal becomes superconducting[2] with a transition temperature approaching 33 K. Therefore, it is important to understand various properties of these fascinating materials. In the fulleride solids, due to the unique structure of fullerene molecules, their behaviour is determined by an interplay[3] of the local structure of molecule and the long-range crystalline order. There are three main features due to the molecular structure of fullerenes. First is the molecular nature of orbitals between which carrier electrons hop in the conducting state of the solid. The second effect is the reduction of the Coulomb interaction between carrier electrons on a given fullerene molecule. The Coulomb interaction reduces because of the availability of a large number of carbon atoms of various interatomic distances to the interacting electrons on a fullerene molecule. The interatomic distance in a molecule ranges from the minimum[4] C−C distance of 1.391 Å to the maximum[4] C−C distance of 7.1Å. The third effect is the mixing of the lowest unoccupied molecular orbitals, namely the $t_{1u}$ molecular orbitals[5], due to the symmetry-breaking intramolecular vibrations[6]. Due to these molecular structural effects and due to large[2] lattice constant, conducting fullerides will be of narrow band[3,5] type, weakly correlated, and mixed three-band systems. The band width is[3,5] of the order of 0.6eV, Coulomb interaction is[6] of the order of 0.5-1.0 eV, and the interband mixing interaction is[6] of the order of 1.0 eV. Thus, the effects of the narrow band, of weak Coulomb interaction, and of interband mixing are comparable with each other. Therefore, the properties of these materials are expected to be quite sensitive to the balance and interplay of the above mentioned three factors.

The effects of small band width, weak Coulomb interaction and mixing of bands are expected to make the conducting fullerides much different from other conducting solids like the transition metals, rare earth metals, heavy fermion systems[7] and cuprate conductors[8]. While in a transition metal, in a rare earth metal, in an actinide metal, and in a heavy fermion metal the bands are narrow but Coulomb interaction between carriers is strong, in conducting fullerides, the Coulomb interaction is weak (0.5-1.0 eV)[6] despite a narrow conduction band in these systems. On the other hand, in cuprate conductors[8] both the band width ($\approx$ 3 eV) and the Coulomb interaction between carrier holes (5-10 eV) are comparable, but the values of both these quantities are an order of magnitude higher than that in conducting fullerides. Furthermore, the intramolecular vibrations are specific to fulleride systems only.

Any theory which is expected to explain the behaviour of conducting and superconducting fullerides should take into account the above mentioned features which are due to the molecular structure. Many efforts have been made to investigate the (su-

per) conducting fullerides[6,9-11]. Baskaran and Tosatti[9], and Chakravarty *et al.*[10] have made an effort to investigate the problem of fulleride (super) conductors on the basis of the resonating-valence bond theory. The theories of these authors are questionable because the important effect of symmetry-breaking intramolecular vibration has not been considered. Very recently Varma *et al.*[6] have argued that the central role in superconducting fullerides is played by intramolecular vibrations. But they have ignored interband transitions caused by the interband Coulomb interaction[11]. We have earlier[11] proposed another approach to the theory of superconducting fullerides in which only the intraband and interband Coulomb interactions are considered and the intramolecular vibrations are ignored. Thus this approach is also as incomplete as those of others[6,9,10]. In this paper we describe a method for studying the problem of conducting and superconducting fullerides by considering various interactions which exist in these systems. In particular, we analyze a modified Bardeen-Cooper-Schrieffer (BCS) theory of superconductivity in the light of the recently measured tunneling spectra in the $Rb_3C_{60}$ superconductor[12].

**Hamiltonian of the system**

We shall consider here the $C_{60}$-based conducting and superconducting fullerides because most of the studies[2] have been made on the solids of $C_{60}$ molecules only. In $C_{60}$ based solids, the conduction band is derived from the triply degenerate $t_{1u}$ molecular orbitals[3,5]. Different band structure calculations[3,5,13] provide different positions of the three bands derived from the $t_{1u}$ molecular orbitals. One common feature of the existing band structure calculations is that at least two bands overlap[3,5,13] with each other. Let $\nu = 1,2,3$ denote these three bands. In general the problem of conducting and superconducting fullerides may be described by the Hamiltonian.

$$H = H_1 + H_2 + H' \qquad \ldots (1)$$

where $H_1$ corresponds to the motion of an electron in a $C_{60}$ molecule, $H_2$ corresponds to the motion of an electron in the crystalline solid, while $H'$ is a coupling interaction between the motions of an electron in the $C_{60}$ molecule and the crystalline solid.

The motion of an electron in a $C_{60}$ molecule is described in terms of the hopping of the electron from one atomic orbital to the other so that $H_1$ may be written as,

$$H_1 = -\sum_{i\nu\beta lm\sigma} t_{\nu\beta lm}\, a^{+}_{\nu\beta il\sigma} a_{\nu\beta im\sigma} + \text{H.C.} + \sum_{\nu\beta il} U_c a^{+}_{\nu\beta il\uparrow} a^{+}_{\nu\beta il\downarrow} a_{\nu\beta il\downarrow} a_{\nu\beta il\uparrow}. \qquad \ldots (2)$$

where $\beta$ denotes the two (single and double) bonds a $C_{60}$ molecule, i denotes the position of a $C_{60}$ molecule, l and m denote the (nearest neighbour) positions of two carbon atoms on the ith $C_{60}$ molecule, $a^{+}_{\nu\beta il\sigma}$ and $a_{\nu\beta il\sigma}$ are creation and annihilation operators of an electron in the atomic orbitals $|\nu\beta il\sigma)$. Here $\sigma$ is spin, $t_{\nu\beta lm}$ is the hopping matrix element for hopping of an electron between two carbon atoms connected by the bond $\beta$ such that the hopping corresponds to the molecular orbital $\nu$. $U_C$ is the Coulomb interaction between electrons when they are on the same carbon atom.

The Hamiltonian $H_2$ describes electrons hopping from $\nu$th molecular orbital of a $C_{60}$ molecule to the same ($\nu$th) molecular orbital of another $C_{60}$ molecule. In this sense we may write,

$$H_2 = -\sum_{ij\nu\sigma} t_{\nu ij} C^{+}_{\nu i\sigma} C_{\nu j\sigma} + \sum_{i\mu} E_\mu b^{+}_{i\mu} b_{i\mu} + \frac{1}{2}\sum_{i\nu\nu'\sigma\sigma} (1-\delta_{\nu\nu'}\delta_{\sigma\sigma'}) U_{\nu\nu'} C^{+}_{\nu i\sigma} C^{+}_{\nu' i\sigma'} C_{\nu' i\sigma'} C_{\nu i\sigma} + \sum_{i\nu\nu'\sigma\mu} M^{\mu}_{\nu\nu'} C^{+}_{\nu i\sigma} C_{\nu' i\sigma} (b^{+}_{i\mu} + b_{i\mu}). \qquad \ldots (3)$$

where $t_{\nu ij}$ is the hopping matrix element for the hopping of an electron from the ith $C_{60}$ molecule to the jth $C_{60}$ molecule in the molecular orbital $\nu$, $C^{+}_{\nu i\sigma}$ and $C_{\nu i\sigma}$ are creation and annihilation operators of an electron when it is in the $\nu$th molecular orbital of the ith $C_{60}$ molecule with spin $\sigma$. $U_{\nu\nu'}$ is the Coulomb interaction between electrons when they are in the molecular orbitals $\nu$ and $\nu'$, $b^{+}_{i\mu}$ and $b_{i\mu}$ are creation and annihilation operators of the symmetry-breaking intramolecular vibration of the ith molecule with energy $E_\mu$ where $\mu$ is mode index. $M^{\mu}_{\nu\nu'}$ is the interband coupling matrix element due to the interaction of electrons with the symmetry-breaking intramolecular vibrational modes, where $M^{\mu}_{\nu\nu} = 0$. We assume that the interaction $H'$ which couples the local molecular structural effect with the long-range crystalline order is given by a Anderson-like hybridization. That is to say,

$$H' = \sum_{\nu k\beta\tilde{i}l\sigma} V_{\nu k\beta l} C^{+}_{\nu k\sigma} a_{\nu\beta il\sigma} + \text{H.C.} \qquad \ldots (4)$$

where $V_{\nu k\beta l}$ is the coupling between the atomic orbital $|\nu\beta il\sigma)$ and the band state $|\nu k\sigma)$ where $\mathbf{k}$ is momentum of an electron in the $\nu$th band, $C^{+}_{\nu k\sigma}$ is given by,

$$C^{+}_{\nu k\sigma} = N^{-1/2} \sum_i C^{+}_{\nu i\sigma} \exp(i\mathbf{k}\cdot\mathbf{R}_i). \qquad \ldots (5)$$

where $\mathbf{R}_i$ is the position of the ith $C_{60}$ molecule, and N is the number of $C_{60}$ molecules.

For a realistic treatment of the problem of conducting and superconducting fullerides, we should obtain realistic values of the parameters $t_{\nu ij}$, $U_{\nu\nu'}$, $M^{\mu}_{\nu\nu'}$ and $V_{\nu k\beta l}$. At present, realistic calculations of band structure alone are available[3,5,13]. So we have realistic values of $t_{\nu ij}$ only. As we know accurate form of the atomic wave function of carbon, we may calculate $V_{\nu k\beta l}$ also accurately. Accurate values of $U_{\nu\nu'}$ and $M^{\mu}_{\nu\nu'}$ are yet to be calculated for the fullerride systems. The typical value[6] of $U_{\nu\nu'}$ is 0.5-1.0 eV. Values of $M^{\mu}_{\nu\nu'}$ are calculated[6] for isolated $C_{60}$ molecules. But such values will not be realistic in a solid, because in the solid form a $C_{60}$ molecule is deformed in the sense that now there are two[4] different pentagons—one corresponding to those pentagons which face another $C_{60}$ molecule (average bond length 1.466 Å), while the other corresponding to those which do not face another $C_{60}$ molecule (average bond length = 1.444 Å)[4].

Let us now consider the nature of the effects due to various interaction terms involved in the Hamiltonian H. We first consider the intramolecular vibrations. This effect will be important at higher temperatures where more and more intramolecular modes will be excited. The other important interaction effect will be the intraband and interband scatterings caused by the Coulomb interaction $U_{\nu\nu'}$ (cf. Eq. 3). As noted above, $U_{\nu\nu'}$ corresponds to the situation when two electrons may be on the same or different carbon atoms of a $C_{60}$ molecule. This has an important consequence. In fact, $U_{\nu\nu'}$ can not be treated in the way we treat it in the Hubbard Hamiltonian. More clearly, two electrons of the same spins may also stay on the same molecule, contrary to the opposite spin electrons on a site in the Hubbard model.

**Normal state**

For understanding the superconducting state it is necessary to understand the normal state of a superconductor. We should know what are the excitations in the normal state of the system, and what causes a pairing interaction between these excitations. For this purpose we should obtain a solution of the Hamiltonian H. But this is a very tough problem and no one has yet made an effort to solve it. To gain some insight into the nature of the solution of H, we ignore $H_1$ and $H'$ for the sake of simplicity and consider the electron self energy due to the interactions $U_{\nu\nu'}$ and $M^{\mu}_{\nu\nu'}$ (Eq. 3) only in its lowest order. In the lowest order the self-energy may be written as,

$$\sum_{\nu}(\mathbf{k},iw_n) = \tilde{U}_{\nu\sigma} + \sum_{\nu'\neq\nu,\mu} \frac{(3E_{\mu} + f_{\nu'\sigma}(\mathbf{k},iw_n))A_{\mu}|M^{\mu}_{\nu\nu'}|^2}{f_{\nu'\sigma}(\mathbf{k},iw_n)^2 - E^2_{\mu}} \quad \ldots(6)$$

where

$$f_{\nu'\sigma}(\mathbf{k},iw_n) = iw_n - \varepsilon_{\nu'\mathbf{k}} - \tilde{U}_{\nu'\sigma} \quad \ldots(7)$$

and

$$\tilde{U}_{\nu\sigma} = U_{\nu\nu}n_{\nu,-\sigma} + \sum_{\nu'\neq\nu,\sigma} U_{\nu\nu'}n_{\nu'\sigma} \quad \ldots(8)$$

with

$$n_{\nu\sigma} = \langle C^{+}_{\nu i\sigma}C_{\nu i\sigma}\rangle \quad \ldots(9)$$

$$A_{\mu} = 1 + 2\langle b^{+}_{i\mu}b_{i\mu}\rangle \quad \ldots(10)$$

and

$$\varepsilon_{\nu\mathbf{k}} = -N^{-1}\sum_{\mathbf{R}_i-\mathbf{R}_j} t_{\nu ij}\exp(i\mathbf{k}\cdot(\mathbf{R}_i-\mathbf{R}_j)) \quad \ldots(11)$$

where $w_n$ is the Matsubara energy.

Within the above approximations, the excitation spectrum of the system will be given by,

$$w - \varepsilon_{\nu\mathbf{k}} - \sum_{\nu}(\mathbf{k},w) = 0 \quad \ldots(12)$$

with $w = E^{*}_{\mathbf{k}} - i\Gamma^{*}_{\mathbf{k}}$ is the quasiparticle energy, and $\Gamma^{*}_{\mathbf{k}}$ is the quasiparticle energy width.

We have not yet made detailed calculations of any property of the conducting fullerides because there are very few good measurements of the normal state properties. However, an analysis of the approximate form (6) of the self energy $\Sigma_{\nu}(\mathbf{k},iw_n)$ would permit us to get some hints regarding the nature of the process which are operative in conducting fullerides. In fact we seen from the expression of $\Sigma_{\nu}(\mathbf{k},iw_n)$, Eq. (6), that in this quantity the effect of the Coulomb interaction is different in different bands. More clearly, while in the $\nu$ band only opposite spin electrons are involved (cf. Eq. 8), in the $\nu' \neq \nu$ bands electrons of both the spins are involved. This means that the interband mixing process may be complicated in conducting fullerides.

**Superconducting state**

As has been mentioned above, for a proper understanding of the superconducting state it is essential to understand the nature of the excitation in the normal state. It is a complex problem, and a challenge for the theoreticians. As already discussed above, a number of theories[6,9-11] have been developed for the superconducting state of the fulleride systems. All of them consider only a certain part of the interaction involved in H (cf. Eq. 1) to be important. In fact, it is clear from the above description that the actual problem of fulleride superconductors requires a more complete treatment than is offered

by the theories developed till now. In particular, it should be interest to investigate whether of the superconductivity in fullerides is different from that in the BCS superconductors. In fulleride superconductors a possible source of deviation of behaviour is the intraband Coulomb interaction $U_{\nu\nu}$. As described elsewhere[11], the intraband Coulomb interaction $U_{\nu\nu}$ will cause scattering of electrons between band states of various energies and momenta so that the ultimate effect of $U_{\nu\nu}$ will be to produce coherent states[11]. Electrons occupying these coherent states will experience an indirect attractive interaction, caused possibly by excitons[11] and intramolecular vibrations[6]. The net effect will be a pair weakening effect in the Cooper pairs of electrons so that they will have binding energies spread over a finite range[11] (at a given temperature). A wave function which involves these features of electron pairs may be written as[14],

$$\psi_{SC} = \prod_{\nu \mathbf{k}} \sum_{\mathbf{q}} P_{\nu \mathbf{q}} [u_{\nu \mathbf{q}}(\mathbf{k}) + (1 - u_{\nu \mathbf{q}}(\mathbf{k})^2)^{1/2} \times C^{+}_{\nu \mathbf{k}+\mathbf{q}\uparrow} C^{+}_{\nu -\mathbf{k}-\mathbf{q}\downarrow}] \phi \quad \ldots (13)$$

where $\phi$ is the vacuum of the superconducting quasiparticles. $P_{\nu \mathbf{q}}$ is related to the transition probabilities $P_{\nu \mathbf{k}}(\mathbf{k}, \mathbf{k}+\mathbf{q})$ for the $\mathbf{k} \rightarrow \mathbf{k}+\mathbf{q}$ transitions caused in the $\nu$th band by the Coulomb interaction $U_{\nu\nu}$. We have,

$$P_{\nu \mathbf{q}} = P_{\nu}(\mathbf{k}, \mathbf{k}+\mathbf{q}) P(-\mathbf{k}, -\mathbf{k}-\mathbf{q}). \quad \ldots (14)$$

The coefficients $u_{\nu \mathbf{q}}(\mathbf{k})$ in Eq. (13) may be defined[14] as the BCS coherence factors[15] corresponding to the Cooper pair binding energy $\Delta(\mathbf{k}, \mathbf{k}+\mathbf{q})$. That is to say,

$$u_{\nu \mathbf{q}}(\mathbf{k})^2 = \frac{1}{2}\left[1 + \frac{\varepsilon_{\nu\, \mathbf{k}+\mathbf{q}}}{(\varepsilon_{\nu\, \mathbf{k}+\mathbf{q}}{}^2 + \Delta(\mathbf{k}, \mathbf{k}+\mathbf{q})^2)^{1/2}}\right] \quad \ldots (15)$$

When $U_{\nu\nu} \rightarrow 0$, $P_{\nu}(\mathbf{k} \rightarrow \mathbf{k}+\mathbf{q}) \rightarrow \delta_{\mathbf{q}0}$ so that the wavefunction $\psi_{SC}$ tends to the BCS wavefunction of the superconducting state.

An important feature of the superconducting wavefunction $\psi_{SC}$ is that for the parameter values relevant to fullerides ($U_{\nu\nu} \approx 0.5 - 1.0$ eV, $t_{\nu ij} \approx 50$ meV)[6,13], it will explain the qualitative features of the tunneling spectra as observed for the normal-to-superconducting junction by Zhang *et al*[12]. In this connection it may be noted that Zhang *et al.* have tried to explain the tunneling spectra observed by them in terms of the quasiparticle recombination process[16]. In our theory one does not need to invoke such a process separately, as it is already built in the wavefunction $\psi_{SC}$. Thus our explanation of the tunneling spectra observed by Zhang *et al.* seems to be reasonable.

## Conclusions

For understanding the normal state and superconducting state behaviour of fulleride systems, one faces a complicated problem which involves competition between many weak interactions ($t_{\nu ij}$, $U_{\nu\nu'}$, $M^{\mu}_{\nu\nu'}$ and $V_{\nu k \beta l}$). From the molecular viewpoint there is a need to find realistic values of the Coulomb interactions $U_{\nu\nu'}$ and of the electron-phonon coupling parameter $M^{\mu}_{\nu\nu'}$ for that form of the $C_{60}$ molecule which arises in the solid system (with two values of pentagon bond length). It would be interesting to study the effect of coupling between the molecular structural effects and the crystalline order. The Hamiltonian H, Eqs (1)-(4), gives an idea of the way to approach the study of the interplay between molecular structural effects and the crystalline order. A specific purpose which the present study serves is that it provides us with a method for exploring the possibility of a deviation of the superconducting state of fulleride system from the BCS superconductors.

## References


1 Kroto H W, Heath J R, O'brien S C, Curl R F & Smalley R E, *Nature*, 318 (1985) 162; Whetten R L *et al.*, *The MRS late news session-Buckyballs: New materials made from carbon soot, videotape* (Material Research Society, Pittsburg), 1990.
2 Lal R, *Curr Sci*, 61 (1991) 508.
3 Ching W Y, Huang M Z & Xu Y N, *Phys Rev Lett*, 67 (1991) 2045.
4 David W I F *et al.*, *Nature*, 353 (1991) 147.
5 Saito S & Oshiyama A, *Phys Rev Lett*, 66 (1991) 2637.
6 Varma C M, Zaanaen J & Raghavachari K, *Science*, 254 (1991) 989.
7 Fulde P, Keller J & Zwicknagl, *Solid State Phys*, 41 (1988) 1.
8 *Articles in high temperature superconductivity*, edited by J W Lynn (Springer-Verlag, New York), 1990.
9 Baskaran G & Tosatti E, *Curr Sci*, 61 (1991) 33.
10 Chakravarty S, Gelfand M P & Kivelson S, 254 (1991) 970.
11 Lal R & Joshi S K, *Solid State Commun*, 80 (1991) 937.
12 Zhang Z, Chen C C, Kelty S P, Dai H & Lieber C M, *Nature*, 353 (1991) 333.
13 Erwin S C & Pickett W E, *Science*, 254 (1991) 842.
14 Lal R & Joshi S K, *Phys Rev B*, 45 (1992) 361.
15 Mahan G D, *Many particle physics*, 2nd Edn (Plenum Press, New York) 1990, p 785.
16 Dynes R C, Narayanamurti V & Garno J P, *Phys Rev Lett*, 41 (1978) 1509.

Indian Journal of Chemistry
Vol. 31 A&B, May 1992, p. F104-111

# On the origin of superconductivity and anomalous normal state properties of doped solid $C_{60}$

G Baskaran

The Institute of Mathematical Sciences, Madras 600 113, India

Received 20 February 1992

In this paper, I discuss and summarise the electron correlation based theory of the normal and superconducting states of fullerites developed by Tosatti and myself. The parallel work of Chakravarti and Kivelson is also briefly presented in a way reformulated by Subrahmanyam and myself. The similarities as well as the differences between the two theories are also discussed. A recent analysis of our theory reveals a rich structure in the quasi-particle spectrum of the above system. This is briefly discussed for two cases when the pair binding energy is comparable to and much larger than the conduction electron band width. In both cases the normal state is anomalous.

## 1 Introduction

Nature has once again given a gift to the field of physics and chemistry in the form of fullerene[1,2]. Solid fullerites $M_xC_{60}$ (M = alkali metals) exhibit high temperature superconductivity and several anomalous normal state properties[3,4]. A real challenge to theorists is to isolate important features of this organic conductor using the available experimental results as well as theoretical considerations and develop a microscopic theory. In my opinion, the body of available experimental results and theoretical understanding of $sp^2$ hybridized organic molecules and bio-molecules, point towards the dominant role played by coulomb correlations in determining the low energy physics. Recently, we have developed a microscopic theory[5] for the normal and superconducting states of $M_xC_{60}$ using the physics of intra-molecular coulomb correlations in the carbon $p\pi$-bonds of the $C_{60}$ molecules. We introduced the notion of Stability of Molecular Singlets (SMS) in $M_xC_{60}$, which means that the intra-molecular correlations favour a charged $C_{60}$ molecules containing odd number of excess electrons to acquire or lose an electron and reach a stable singlet state. SMS was justified using valence bond arguments as well as a perturbation theory involving exchange of intra-molecular triplet excitations. In parallel, Chakravarty and Kivelson[6] also emphasized the importance of coulomb correlations and used valence bond as well as perturbation theory arguments to suggest SMS (to put in our language). Anderson has also argued[7] in a recent paper that superconductivity in fullerenes should originate from intra-molecular coulomb correlations, by giving powerful arguments to negate any kind of phonon mechanism for the observed high temperature superconductivity.

The aim of the present paper is to give a brief account of three works of ours. Firstly, the theory developed by Tosatti and myself is discussed briefly. Then the parallel work of Chakravarti and Kivelson is presented in a way reformulated by Subrahmanyam and myself[8] bringing out fundamental similarities and differences between the two parallel theories. Finally, some of my recent work[9] is summarised to understand the normal state properties of the conducting fullerites in terms of novel quasi-particles of the non-fermi liquid phases.

## 2 Electronic correlations and the stability of molecular singlets

The following are some of the key experimental results that we used in building our model as well as to bring out the notion of Stability of Molecular Singlets (SMS). (1) The $C_{60}$ molecule is a sort of two dimensional $p\pi$-electron system[10] with strong correlations and what might be described as an RVB ground state (with a small valence bond density modulation). In a host of organic compounds having very similar local carbon $p\pi$-bonding such as anthracene, pentacene[11-13] etc., electronic correlations are known to be very important. Among other things, strong correlations manifest themselves experimentally in a large singlet-triplet excitation energy splitting $\approx$ 1 eV (indicating that the charge and spin behave differently) and the anomalous aromaticity properties. (2) The undoped $C_{60}$ crystal, fullerene is an insulating mo-

lecular crystal and metallicity results from doping. (3) The normal state conductivity[3] is rather small (500 S $cm^{-1}$) for $K_xC_{60}$ with a relatively small carrier concentration of $n \sim 10^{21}$/cc. (4) Inverse photoemission studies[14] show a rather narrow conduction band of width ~ 0.5 eV. This band appears to be derived from a three fold degenerate $t_{1u}$ molecular level; it can contain 6 electrons per site. (5) The coherence length is short and of the order of the size of $C_{60}$ molecule[14]. (6) The possible absence of Pauli paramagnetism in the normal state EPR of the superconducting sample is suggested by some recent experiments[4,15].

We argued that the electron correlation of the finite 'two-dimensional' $C_{60}$ molecule which gives it an RVB character plays a vital role by giving Stable Molecular Singlets (SMS) even in the charged state of the $C_{60}$ molecule in the solid. This stability is explained by using the valence bond language and alternatively as an effective intra-molecular antiferromagnetic coupling between the added electrons in the $t_{1u}$ orbitals induced by exchange of molecular triplet excitons. A derivation of this antiferromagnetic coupling from the microscopics is sketched. SMS implies a tendency for $C_{60}$ to be charged with even number of electrons on doping. This can be also thought of as an on-site cooper pairing tendency, even though, the physics leading to this pairing is more collective in character. The relation of our collective pairing to Little's exciton mediated pairing[16] is also discussed.

The above together with the weak overlap between the $t_{1u}$ orbitals of two neighbouring molecules gives us three overlapping narrow bands with an effective negative Hubbard U. The attractive interaction, which we find comparable to the narrow band width, leads to enhanced pairing correlation even at room temperature in the normal state, thereby making the normal state a 'boson metal'. This means well suppressed Pauli paramagnetism and marked departure from the fermi liquid behaviour.

The molecule $C_{60}$ is a carbon $p\pi$-bonded system with a truncated icosahedral shape. The orbitals close to the fermi level are the $p_z$ orbitals. They strongly hybridize to form the 60 single particle molecular orbitals[17] spread over an energy of about 15 eV. The fermi level of the molecular solid $C_{60}$ (an FCC crystal) lies between a set of filled narrow bands formed by the five fold degenerate $g_{1u}$ orbitals and an empty set of narrow bands formed by the three fold degenerate $t_{1u}$ orbitals. The gap is ~ 2 eV. The $t_{1u}$ molecular orbitals can be chosen to transform as $x$, $y$ and $z$ just like the atomic $p$-orbitals.

We have suggested[14] that the narrow conduction bands should resemble the (well isolated) $4p$ hole like band of the FCC solid krypton on account of its $p$-character. This turns out to be mostly true as shown by a recent band structure calculation[11]. There are three overlapping bands, two almost degenerate narrower bands of width 0.2 eV overlapping at the top of a narrow band of width 0.5 eV. All the bands are degenerate at the $\Gamma$ point.

We argue that the low energy physics is governed by the following conduction band Hamiltonian,

$$H = \Sigma t_{ab}\, c^{\dagger}_{ia\sigma} c_{jb\sigma} + h.c + I\Sigma S_{ia}.S_{ib} + U\Sigma n_{ia} n_{ib} + U_d \Sigma n_{ia\uparrow} n_{ia\downarrow} \quad \ldots (1)$$

where

$$S_{ia} = c^{\dagger}_{ia\alpha} \sigma_{\alpha\beta} c_{ia\beta} \quad \ldots (2)$$

Here $c$'s are the electron operators, $a$, $b$ = 1, 2 and 3 stand for the three degenerate $t_{1u}$ orbitals at any site $i$. The hopping matrix elements $t_{ab}$ are assumed to be non-zero only between nearest neighbours and are obtained from a tight binding fit to the actual band structure. The second term on the right represents the exchange coupling $I$ between two electrons that occupy orbitals $a$ and $b$ of the $i$th molecule. The terms $U_d$ and $U$ represent the coulomb repulsion between two electrons occupying the same or two different $t_{1u}$ orbitals of a molecule.

We have estimated the interaction parameters by using various arguments which we present below very briefly. The most crucial parameter is $U - 3/2I$. This is the energy gained in the transition $C_{60}^{1-} C_{60}^{-1} \rightarrow C_{60}^{0} C_{60}^{2-}$ of two neighbouring molecules in a solid. Here the two excess electrons in $C_{60}^{2-}$ ion occupy two distinct degenerate $t_{1u}$ orbitals in a spin singlet state.

The parametered $U$'s and $I$ will be modified for other transitions like $C_{60}^{3-} C_{60}^{3-} \rightarrow C_{60}^{2-} C_{60}^{4-}$. Moreover, we will concentrate on the region $x$ around 3. Also there is an approximate symmetry about $x = 3$ in our model.

The SMS that we identify depends on the parameter $U - 3/2I$. If it is negative, inspite of the coulomb repulsion the above mentioned transition will take place and stabilise the molecular singlets. Also notice that SMS is independent of the diagonal Hubbard parameter $U_d$. We find that the diagonal Hubbard parameter $U_d$ is of the order of the band width. And the off diagonal parameter $U$, becomes small when the Madelung energy as

well as screening effect is included. We will hence assume this to be zero.

The most crucial parameter determining SMS is thus $I$. It gets contributions from Hund's rule exchange (ferromagnetic), $\pi$-electron correlations and the lattice effects. We will argue that the effects arising from the $\pi$-electron correlation contributes dominantly. We give two methods of estimating this, (i) valence bond arguments and (ii) triplet exciton exchange approach. The gist of valence bond approach[18] is as follows. Its is well known that carbon $p\pi$-bonded systems are described very well as Resonating Valence Bond (RVB) states[20,21]. In particular, they are short range RVB states. As the size of the molecule becomes larger there are valence bond density modulations.

The valence bond character (i.e. suppression of polar fluctuations and dominance of singlet homopolar configurations) has its origin in strong correlations in the tight binding carbon $p\pi$-electrons of the $C_{60}$ molecules. In a PPP-Hubbard model[13,22] description, the effective Hubbard $U$ is of the order 5 eV. The PPP-Hubbard model, keeping only the on-site interaction alone is,

$$H = -t \Sigma c^{\dagger}_{i\sigma} c_{j\sigma} + h..c. + U \Sigma n_{i\uparrow} n_{i\downarrow} \qquad \ldots (3)$$

where $i$ denotes the 60 carbon $p_z$ orbitals. The small modulation of the hopping integral $t$ arising from the modulation of the bond length of two inequivalent bonds in $C_{60}$ does not change the physics qualitatively. A phenomenological $t$-$J$ model description[15] can also be given with a $t \approx 2.5$ eV and a $J \approx 0.8$ eV.

The valence bond energy $J$ is easily estimated[13] from the triplet exciton energy $E_T$. For $C_{60}$ the experimental value[32] of $E_T$ is $\approx 1.6$ eV making $J \approx 0.8$ eV. The value $I$ is different from $J$. Moreover, the singlet-triplet excition splitting ($\approx$ 0.5 eV) observed in $C_{60}$ also emphasises the importance of correlations.

The fact that we have a two-dimensional tight binding system with 60 sites makes the valence bond correlations very important. Our SMS hypothesis expresses the tendency of the 2-d RVB system not to have any unpaired spins. Any unpaired spin means the presence of a broken valence bond and an exchange energy increase of the order of $J$. There is a close connection[23] of our SMS hypothesis with the Lieb-Mattis theorem[24] for one-dimensional systems. Also recent numerical calculations of large $U$ Hubbard models on finite two-dimensional lattices as well as finite clusters exhibit chemical potentials which are larger for even electron singlet ground states rather than the odd electron states.

According to our valence bond picture, when a pair of electrons is added to a neutral molecule, the entire $p\pi$-electron system adjusts itself to have local singlet character. This is achieved, to a large extent, by having two real doubly occupied sites (doublons[25,26]) which are well separated (because of coulomb repulsion) and delocalised among the resonating singlets. Including the string energy that arises from the presence of valence bond modulation, we find that $I$ is in the range 0.1 to 0.4 eV.

The physics of our calculation of $I$ is similar to a calculation of the binding energy of two charged solitons in *cis*-polyacetylene, even though the topology in the present case is different. Also we find that the electron-electron[27] rather than the electron-phonon interaction contribute dominantly to $I$.

Another way of arguing how the exchange energy $J$ wins over the coulomb energies in the large $C_{60}$ molecule is as follows. Electrostatic energies like $U$ and $U_d$ and the Hund's rule ferromagnetic exchange decrease as $(1/R)$, where $R$ is the size of the molecule. On the other hand, the valence band energies $J$ decrease at a much slower rate. Between benzene and $C_{60}$ the triplet exciton energy ($\approx 2J$) has a marginal decrease from 2.5 to 1.6 eV (see reference 28 for the measurement of triplet exciton energy of $C_{60}$).

In another approach we have estimated $I$ by using the exchange of virtual triplet exciton. The $C_{60}$ molecule has a triplet and a singlet exciton as two lowest energy excitations. We find that the coupling of the added electron to the triplet exciton is the strongest. The origin of the polarisation energy which we get when we add extra charges can be viewed to arise from the virtual excitations of these excitons. When two charges are added they exchange these virtual excitons.

Exchange of singlet excitons do not give rise to any spin dependent polarisation energy. It reduces the overall electrostatic repulsions. On the other hand, the exchange of triplet excitons favours singlet pairing. We also find that the strongest coupling of the electrons is to the triplet excitons.

Starting from the PPP-Hubbard Hamiltonian we have found[18] the interaction Hamiltonian (written in a manifestly spin rotation invariant form) between an electron in a $t_{1u}$ orbital and the lowest energy singlet exciton to be,

$$\frac{2}{3} U_r \frac{1}{\sqrt{60}} C^{*}_{\alpha\alpha} \sigma_{\alpha\beta} C_{\alpha\alpha} \cdot \mathbf{S}_0 \qquad \ldots (4)$$

where $a = 1,2$ and 3 denotes the three $t_{1u}$ states and $\mathbf{S}_0$ is the operator for the lowest triplet state of the $C_{60}$ molecule. Here $U_p$ is the Hubbard $U$ for the carbon $\pi$-orbital.

By a simple second order perturbation theory we find an effective interaction between electrons in the orbital $a$ and $b$:

$$IC^{\dagger}_{iaa}\boldsymbol{\sigma}_{\alpha\beta}c_{ia\beta}\cdot c^{\dagger}_{iba'}\boldsymbol{\sigma}_{a'\beta'}c_{ib\beta'} = I\mathbf{S}_{ia}\cdot\mathbf{S}_{ib} \qquad \ldots(5)$$

$$\text{and } I = \frac{3}{4}\left(\frac{2}{3}\frac{U_p}{\sqrt{60}}\right)^2\frac{1}{E_T} \qquad \ldots(6)$$

When we choose $E_T \approx 1$ eV and $U_p \approx 11$ eV we get this exchange coupling $I \approx 0.3$ eV. When we add three or more electrons by the arguments given above, the lowest spin state will be always stabilised.

Even though our exciton exchange approach looks similar to Little's mechanism[16] there are some important differences. The excitons are intra-molecular in nature and live in the same region where the conduction electrons live. Hence, our mechanism escapes the criticism of Inkson-Anderson[28]: that is, the reduction in screening which occurs when the active electron pairs tunnel into the interaction region does not arise in our case. The two added electrons are part of the carbon $p\pi$-electrons and the triplet exciton is a collective excitation of this system. More importantly, we believe that the singlet stabilisation process, even though has two explanations, the first one in terms of valence bond is more natural and captures the essential physics of this carbon $p\pi$-bonded system.

Since the experimentally observed interesting region seems to be $\sim x = 3$, we will concentrate on the two nearly degenerate narrow bands that are close to the fermi level. It is true that disorder remains finite even in this range of $x$. The fact that superconductivity is observed in this region means that the disorder is not sufficient to destroy it.

Before we analyse our model for superconductivity, several things can be inferred. The pairing energy $I$ is of the order of the band width. Hence we are deep into the real space pairing regime, because any reasonable temperature like room temperature is very small compared to the pair binding energy $I$ which is of the order of 1000 to 2000 K.

A BCS analysis of our effective Hamiltonian for the $t_{1u}$ band is easily performed if we rewrite,

$$\mathbf{S}_{ia}\cdot\mathbf{S}_{ib} = -b^{\dagger}_{iab}b_{iab} + \frac{1}{4}n_{ia}n_{ib} \qquad \ldots(7)$$

and factorise the attractive interaction as

$$b^{\dagger}_{iab}b_{iab} \rightarrow \langle b^{\dagger}_{iab}\rangle b_{iab} \qquad \ldots(8)$$

where

$$b_{ab} \equiv \frac{1}{\sqrt{2}}(c_{a\uparrow}c_{b\downarrow} - \downarrow\uparrow).$$

For the moment we will concentrate on qualitative features that follow by making several simplifying assumptions and trying to get a feel for the value of $T_c$ in particular. Firstly, in our model, even though there are three bands, there is a two-particle state on a molecule that is favoured for $x \approx 3$. This state corresponds to two electrons occupying the two separate Wannier orbitals 1 and 2 of the two nearly degenerate top narrow bands in a singlet state. The Wannier orbital 3 of the broad band is almost filled with two electrons and is deep below the fermi level. The other two degenerate states in which the two electrons doubly occupy any one of the Wannier orbitals 1 and 2 have higher energy. In this sense it is like a one band model with a width approximately equal to the width of the two top narrow bands ($\approx$ 0.2 eV). We will also look at the results for a cubic lattice. We have checked that this does not change the results qualitatively.

This negative $U$ one band Hubbard model has been studied[29] in great detail in the context of Anderson's negative $U$ bipolaron[30] model of superconductivity[31] as well as general bipolaron superconductivity in narrow band systems[29]. Several remarks are in order about the phase diagram. Firstly, we are deep into the real space pairing regime. For the value of parameters that we have it is easily seen from the graph that we have a $T_c \approx 70$ K. The interesting fact is that when the binding energy exceeds the band width, the $T_c$ tends to decrease but rather slowly. The maximum $T_c$ occurs when the binding energy is about half the band width. This is a kind of universal number within the BCS approximation and also indicates most importantly that there will be a saturation in value of $T_c$ within the one band short range non-retarded attractive interaction model. From the mean field theory, we get an approximate expression for the maximum value of $T_c$,

$$\frac{k_B T_c^{max}}{2W} \approx 0.035 \qquad \ldots(9)$$

in terms of the band width 2W. For our band width $k_B T_c^{max} \approx 60°$ K. Even if we are optimistic and take the band width of the broad band, the maximum $k_B T_c \approx 200°$ K. Fluctuation effects, the FCC nature of the lattice and the unscreened short range cou-

lomb interaction will further reduce the phase boundary in the phase diagram. From that point of view the saturation value that we have given is more like an upper bound. We are trying to understand the saturation behaviour and its possible consequence for the new class of carbon superconductors and other organic superconductors.

We would also like to point out that within our model the source of difference between the $T_c$ for K and Rb doping[3] could arise either because of the difference in the band width 2W or $U$ or disorder. At the moment we are unable to pinpoint the cause.

It is obvious that owing to the short coherence length and the expected large London penetration length, ours is a type II superconductor. The fact that we have real space pairing has some interesting consequences for the electromagnetic properties and the behaviour of energy gap. It is found[29] that some of the properties are qualitatively different from the BCS behaviour: the energy gap is very weakly temperature dependent all the way up to $T_c$. We expect non-standard behaviour of the detailed temperature dependence of the penetration length $\lambda_H(T)$ and $H_{c_2}(T)$, as was already found in the low density regime[29].

### 3 Chakravarty-Kivelson approach: Relation to our approach and a reformulation

As mentioned earlier, Chakravarty and Kivelson[6] independently realised the importance of coulomb correlations. They also essentially argued for the Stability of Molecular Singlets (SMS) using valence bond arguments which are identical to ours but a little more elaborate. Then they used the straightforward second order perturbation theory to calculate the singlet stabilisation energy of a $C_{60}$ molecule containing n electrons,

$$E^n_{sing} = E^0_{n-1} + E^0_{n+1} - 2E^0_n \qquad \ldots(10)$$

and the low spin-high spin energy difference,

$$E^n_{lh} = E_n(S_{min}) - E_n(S_{max}) \qquad \ldots(11)$$

as a function of the perturbation parameter $\frac{U}{t}$. In a simple valence bond argument which neglects the interaction among spinons and doublons (eons in reference 6), the above two energies are equal. In a remarkable way even perturbation theory gives almost the same value. Then they get a critical value of $\frac{U}{t} \sim 3$ for the stability of molecular singlet to occur violating the Hunds rule.

Recently Subrahmanyam and I[8] have repeated and reformulated the above perturbation theory. Our basic idea is to think of the perturbation theory as a canonical transformation and write the effective Hamiltonian in the second quantized form in a way that makes the physics more transparent. This is briefly described below.

Let us re-write the PPP-Hubbard model for a $C_{60}$ molecule in terms of the one particle eigen states of the non-interacting particles,

$$H = \sum \varepsilon_\alpha c^\dagger_{\alpha\sigma} c_{\alpha\sigma} + U \sum V^{\gamma\delta}_{\alpha\beta}\, b^\dagger_{\alpha\beta} b_{\gamma\delta} \qquad \ldots(12)$$

where

$$c_{\alpha\sigma} = \sum \phi_\alpha(i) c_{i\sigma} \qquad \ldots(13)$$

$$b_{\alpha\beta} = \frac{1}{\sqrt{2}}(c_{\alpha\uparrow} c_{\beta\downarrow} - \downarrow\uparrow) \text{ for } \alpha \neq \beta, \qquad \ldots(14)$$

$$b_{\alpha\alpha} = c_{\alpha\uparrow} c_{\alpha\downarrow} \qquad \ldots(15)$$

and $$V^{\gamma\delta}_{\alpha\beta} = \sum_i \phi^*_\alpha(i)\phi^*_\beta(i)\phi_\gamma(i)\phi_\delta(i) \qquad \ldots(16)$$

Here $\phi_\alpha(i)$ are the 60 one particle eigen states of kinetic energy term of our molecular Hamiltonian with eigen values $\varepsilon_\alpha$.

We consider the subspace of the $(60+n)$ particle Slater determinants with the 60 particles filling the 30 lowest MO's and $n$ electrons in the three fold degenerate $t_{1u}$ orbitals. This many particle subspace will be denoted by A. The rest of the many particle Hilbert space contains all the other slater determinants. This subspace is denoted by B. Coulomb interaction causes mixing of states within the subspace A and B separately as well between A and B. We re-write the PPP-Hubbard Hamiltonian schematically as,

$$H = H^0_A + UV_{AB} + U(V_{AA} + V_{BB}) \qquad \ldots(17)$$

First we will drop the last term and discuss its effect at the end. The Hamiltonian studied is,

$$H = H^0_A + UV_{AB} \qquad \ldots(18)$$

We perform a canonical transformation to eliminate the interaction term to lowest order in $U$ with a view to getting an effective Hamiltonian in the A subspace. It is elementary to show that S is a solution of the equation,

$$V_{AB} + [H_0, S] = 0 \qquad \ldots(19)$$

The matrix elements of the operator S obtained as a solution are,

$$S_{mn} = \frac{(V_{AB})_{mn}}{E_m - E_n} \qquad \ldots(20)$$

where $m$ and $n$ are states in the subspaces A and B separately and vice-versa.

When the last term is included it does not give correction to the term $UV_{AA}$ to order $U^2$, and so it can be safely neglected.

Now the effective Hamiltonian in the A subspace correct up to order $U^2$ is,

$$H_{\text{eff}} = H_A^0 + UV_{AA} + U2[V_{AB}, S] \quad \ldots(21)$$

Explicitly it has the form,

$$H_{\text{eff}} = \varepsilon_0 \sum_a c^\dagger_{a\sigma} c_{a\sigma} + \sum A^{a_3 a_4}_{a_1 a_2} b^\dagger_{a_1 a_2} b_{a_3 a_4}$$

$$+ \sum A^{a_2}_{a_1} n_{a_1} n_{a_2} \quad \ldots(22)$$

Here a's are the singlet particle states belonging to the three fold degenerate $t_{1u}$ molecular orbitals. We have obtained the expression for the various coefficients A's.

Our canonical transformation approach is essentially a reformulation of the perturbation approach to get the effective Hamiltonian. This reformulation may be very helpful for systematic improvements of the effective Hamiltonian. This effective Hamiltonian is also of the same form as Eq. 1, which was originally given in our work[5].

There are certain obvious criticisms of Chakravarti-Kivelson perturbation approach. If we assume that $\lambda = U/3t$ is the expansion parameter, singlet stability happens for $\lambda \approx 1$. Here the validity of perturbation theory is questionable. On the other hand, comparison of the perturbation theory results with the exact small cluster calculations[6] seems to give a reasonable agreement, suggesting the validity of the perturbation theory even when $\lambda$ is of the order of one.

Our approach based on exciton exchange has a non-perturbative aspect. We assume that part of the problem has been already solved in assuming the existence of a low energy triplet exciton. Then we study the exchange of triplet excitons by a perturbation theory. What we have attempted is to model the collective response of the 60 $p\pi$-electrons to the added $n$ electrons. We are not just studying the scattering of the added electrons among themselves. The essence of Chakravarty-Kivelson perturbation theory, but for the inclusion of the virtual excitation of the filled band electrons into the $t_{1u}$ manifold in the lowest order, is a two-particle scattering approach. This approach is valid when we have a dilute number of carriers. To speak in the language of Mott insulator we are very close to half filling situation. We believe that the collective response of the 60 $p\pi$-electron system is important.

In our opinion, this collective response is taken into account to a large extent in the spin-charge decoupling picture of our as well as that of Chakravarty-Kivelson theory.

## 4 Some comments on the novel quasi-particles and anomalous normal state

In ordinary superconductors the normal state is a fermi liquid, perhaps with some pairing fluctuation. Even in the well known strong coupling superconductors, a fermi liquid description works remarkably well. The pairing fluctuation leads to suppression of the wave function renormalisation of the electron close to the fermi surface. This is never catastrophic. In our case the scale of binding is large compared to the room temperature and hence the normal state is more like a charged bose liquid in the normal state. However, whether the pair binding energy is of the order of one electron band width or more is not clear either from experiments or from theory. But it is fairly clear from our analysis of the mean field treatment of the effective one band Hubbard model that we are not operating at pair binding energy much smaller than the one electron band width.

This has prompted us to study recently[9] two cases: (a) pair binding energy $E_p \gg$ band width 2W and (b) $E_p \sim 2W$. I briefly summarise below the basic idea without giving any details.

Let us first consider the case (a). This is dominated by the electron pairs. They are real pairs, with a hard core repulsion. The pair band width is $\sim 12t^2/E_p$. It is an extremely narrow band system, whose physics can be well modelled in terms of the charged lattice gas with hard core repulsion in the pseudo-spin formalism as,

$$H = -t_p \sum S_i^+ S_j^- + h.c. + \sum V_{ij} S_i^z S_j^z \quad \ldots(23)$$

where $V_{ij}$ is the screened coulomb interaction and $S$'s are the spin half pseudo-spin operators. The lattice is an FCC lattice, which is frustrated and does not encourage any charge density order. We expect superconductivity at low temperature (XY order). The $T_c$ is given in the ideal gas approximation by the equation,

$$k_B T_c = \frac{h^2}{2m_p} \left(\frac{2\pi}{r_s}\right)^2 \quad \ldots(24)$$

where $(4\pi r_s^3/3) = \rho$, the pair density and $m_p$ is the pair effective mass. In three dimensions the charged character of the bose gas as well as the hard core repulsions is expected to give only quantitative change.

Above $T_c$ the bose liquid is like a classical liquid in view of the fact that the mean de Broglie wave length of the particles is of the order of the inter-particle distance. The fact that the particle cannot maintain phase coherence over distance much larger com-

pared to the inter particle spacing also implies that the inelastic mean free path of the particles is also of the order of the inter particle spacing. Thus, from this point of view, the transport properties of the normal state are those of a dense one-component classical plasma, which has its own interesting behaviour.

Another way to look at the normal state properties is in terms of the quasi-particle spectrum of the charged bose liquid at low temperatures. In our calculations we find that the spectrum is almost the same as that of $He^4$ except that the phonon has acquired a gap (plasmon energy) by the Anderson-Higgs mechanism. Thus, the lowest energy excitation occur close to the roton minimum. The destruction of superfluidity seems to be related to the roton-minimum touching the zero of energy (this is to be contrasted with the superfluid helium 4, where nothing dramatic happens to the excitation spectrum across the super fluid transition). Since the instability occurs over a surface in the Brilluouin zone, it does not lead to any density wave instability; instead, it leads to a large density of roton-like low energy excitations. There is a tendency for the rotons also to break up into two novel excitations each carrying a charge $+e$ and $-e$ (and zero spin) inspite of the fact that our elementary boson carries a charge $+2e$! In this sense there is an interesting possibility of charge fractionisation in this system. The details will be published elsewhere[9].

In case of *b*, the pair binding energy is comparable with the electron band width. This means that not all the electrons are part of cooper pairs. Some of the $C_{60}$ molecules contain 3 electrons while the rest contain either 4 or 2 electrons for the case of $M_xC_{60}$ (for convenience, we will refer to the 2, 3 and 4 electron states as 0, 1 and 2 electron states, without losing generality). This is true even in the absence of any attractive interaction, where statistically the probability of finding a molecule with occupancy 2, 3 and 4 is exactly (1/4) in each case. when we have an attractive *U*, this probability increases. But more importantly, the life time of doubly occupied sites increases.

This leads to the interesting possibility that we have a quantum fluid of paired spinless objects coexisting with unpaired electrons carrying spin. Thus, we have two fluids: a fluid of spinless charge 2e particles and a fluid of charge e and spin half particles. Of course, the 2e particle can decay into a pair of electrons separated in space and vice-versa. However, they have their own identity inspite of the quantum mechanical mixing. If this is allowed then we have many novel properties for this system.

Below $T_c$ the second fluid, namely, electrons also become a singlet fluid and there is a good quantum mechanical mixing. The two fluids lose their identity and we have a conventional superconductor. Above $T_c$ the charge e fluid has large low energy spin fluctuations. This in turn causes incoherence among the particles in the charge 2e fluid. This again leads to novel possibilities such as a pseudo-fermi surface of charge 2e excitations and vanishing of $Z_{k_F}$ etc. Again the normal state properties are anomalous!

We expect anomalies similar to the one observed in the cuprate superconductors. Even though we do not have a spin-charge decoupling situation here, there are certain generic features which come with the breakdown of fermi liquid character. These generic features follow simply from the fact that an electron injected at $k_F$ will decay into a whole lot of low energy excitations. In other words, the electron will give away almost all of its spectral weight to other many body collective excitations.

## 5 Conclusion

In this paper are summarised the various efforts to understand the normal and superconducting properties of fullerites in terms of narrow band systems dominated by intra-molecular coulomb correlations. Even though it is clear that correlations are important, more experiments as well as physics motivated theories are needed to unravel the fascinating properties of these strongly correlated molecular superconductors.

## 6 Acknowledgement

It is a pleasure to thank my collaborators E Tosatti and V Subrahmanyam; and P W Anderson for remaining a constant source of inspiration. I thank DST, New Delhi, for financial support through the PMB of High Temperature Superconductivity.

## References

1 Kroto H W, *et al.*, *Nature*, 318 (1985) 162 Kratschmer W, *et al.*, *Nature*, 347 (1990) 354.
2 Haddon R C, *et al.*, *Nature*, 350 (1991) 320.
3 Hubbard A F, *et al.*, *Nature*, 350 (1991); Rosseinsky M J, *et al.*, *Physical Rev Lett*, 66 (1991) 2830.
4 Holczer K, *et al.*, *Science*, 252 (1991) 1154; Holczer K, *et al.*, *Phys Rev Lett*, 67 (1991) 271; Wong W H, *et al.*, (preprint).
5 Baskaran G & Tosatti E, *Curr Sci*, 61 (1991) 33.
6 Chakravarti S & Kivelson S, *Europhys Lett*, (accepted); Chakravarti S, Gelfand M P & Kivelson S, *Science*, 254 (1991) 970; White S R, Chakravarti S, Gelfand M P & Kivelson S, UCLA (preprint).
7 Anderson P W, Princeton (preprint).
8 Subrahmanyam V & Baskaran G, (to be published).
9 Baskaran G (to be published).
10 The carbon $sp^2$ hybridization easily leads to a local two-dimensional (planar) character in organic molecules.

11 McGlynn S P, *et al., Molecular spectroscopy of the triplet state* (Prentice Hall, NJ) 1969.

12 Silinsh E A, *Organic molecular crystals, Springer series in solid state science* No 16 (Springer, NY) 1980.

13 *Excited states* Vol 6, edited by Edward C, Lim, V (Academic Press, New York).

14 Weaver J W, *et al., Phys Rev Lett*, 66 (1991) 1741; Benning P J, *et al.*, Preprint April (1991).

15 Haddon R C, (Private communication).

16 Little W A, *Phys Rev*, A134 (1984) 1416; Ginzburg V L, *JETP* 20 (1965) 1549.

17 Haymet A D J, *Chem phys Lett*, 122 (1985) 421; Haddon R C, *et al., Chem phys Lett*, 125 (1986) 459; Disch R L & Schulman J M, *Chem phys Lett*, 125 (1986) 465; Fowler P W & Woolrich J, *Chem phys Lett*, 127 (1986) 78; Ozaki M & Takahashi A, *Chem phys Lett*, 127 (1986) 242; Satpathy S, *Chem phys Lett*, 130 (1986) 545.

18 Baskaran & Tosatti E (to be published).

19 Bassaniand F & Pastori Parravicini G, *Electronic structure and optical transitions in solids* (Pergamon Press, NY 1075) pp. 139 and references therein; Saito S & Oshiyama A. *Physical Rev Lett*, 66 (1991) 2665.

20 Pauling L, *The nature of the chemical bond* (Oxford University Press, London) 1963.

21 Coulson C A, *Valence* (Oxford University Press, London) 1965.

22 Yu Lu, *Solitons and polarons in conducting polymons* (World Scientific) 1988, and many of the papers reprinted there especially dealing with the effect of coulomb interactions.

23 Baskaran G, (to be published).

24 Lieb E & Mattis D, *Mathematical physics in one dimension* (Academic Press, NY) 1966.

25 Kivelson S, Rokhsar D & Sethna J, *Phys Rev*, B35 (1987) 8865.

26 Anderson P W, *et al., Phys Rev Lett*, 58 (1987) 2790.

27 Ovchinnikov A A, Ukrainskii I I & Kventsel G V, *Sov Phys Usp*, 15 (1973) 575.

28 Inkson J C & Anderson P W, *Phys Rev*, B8 (1973) 4429; Allender D, Bray J & Bardeen J, *Phys Rev*, B8 (1973) 4433.

29 Micnas R, Ranninger J & Robaszkiewiscz S, *RMP*, 62 (1990) 113.

30 Anderson P W, *Phys Rev Lett*, 34 (1975) 953.

31 Chakravarti B K, *J phys Lett*, (*Paris*) 40 (1979) L-99.

32 Arbogast J W, *et al., J phys Chem*, 95 (1991) 11.

Indian Journal of Chemistry
Vol. 31 A& B, May 1992, p. F112

# ANNOUNCEMENT

## International Conference on Energy, Environment and Electrochemistry

To commemorate the Golden Jubilee Year of CSIR, India, an International Conference on Energy, Environment and Electrochemistry will be held at the Central Electrochemical Research Institute, Karaikudi, during 9-11 September 1992.

The conference will focus on environmental pollution, growing energy demand and alternative energy systems, specially elecrochemical systems. Presentations will be made through invited lectures, papers, panel discussions and poster sessions, etc. Following will be the main themes: (1) energy storage: batteries & fuel cells, electric vehicles, (2) energy conversion strategies related to electrochemistry, (3) energy conversion in electrochemical processes, (4) concentration and recovery of metals from effluents, (5) recycling of industrial wastes, (6) electrodialysis, (7) protection of metals and ion-metals from environmental attack, (8) electrocatalysis, and (9) electrochemical techniques & instrumentation. An exhibition on industrial electrochemical products including scientific instruments and equipment for electrochemical research has also been planned during the period.

The abstracts of the papers to be presented should be sent before 31st May 1992, and the manuscripts before 16th July 1992. Further information regarding the conference may be obtained from Dr. K C Narasimham, Convener of the conference, Central Electrochemical Research Institute, Karaikudi 623 006, Tamil Nadu, India.

SCIENTIFIC & RESEARCH LIBRARY
Accession No. .....
27 APR 1992
C.S.I.R.I. REGIONAL CENTRE, LUDHIANA

CSIR GOLDEN JUBILEE SERIES

# BODY'S BATTLES

## BAL PHONDKE

**WAR** makes rattling good history", said Oscar Wilde referring to the struggles of nations to capture new and to retain old territories. But other battles not visible to the naked eye are equally fascinating. An account of the miniscule wars fround within the confines of the human body is breathtaking if only for the fact that these are being fought every single living moment. The human body is continually besieged and attacked by a multitude of microbial enemies of great cunning and guile. However, nature has endowed the human body with an unique built-in defence organization that can be envy of the most modern technologically advanced nation.

This attractive and lavishly illustrated book, written especially for the non-specialist, unfolds the dramatic story of this inner defence organization, the diversity and specificity of its armament, and the methodical way in which it maintains a round the clock vigil to meet squarely every imaginable threat to the human body and also how it wins the body's battles most of the time.

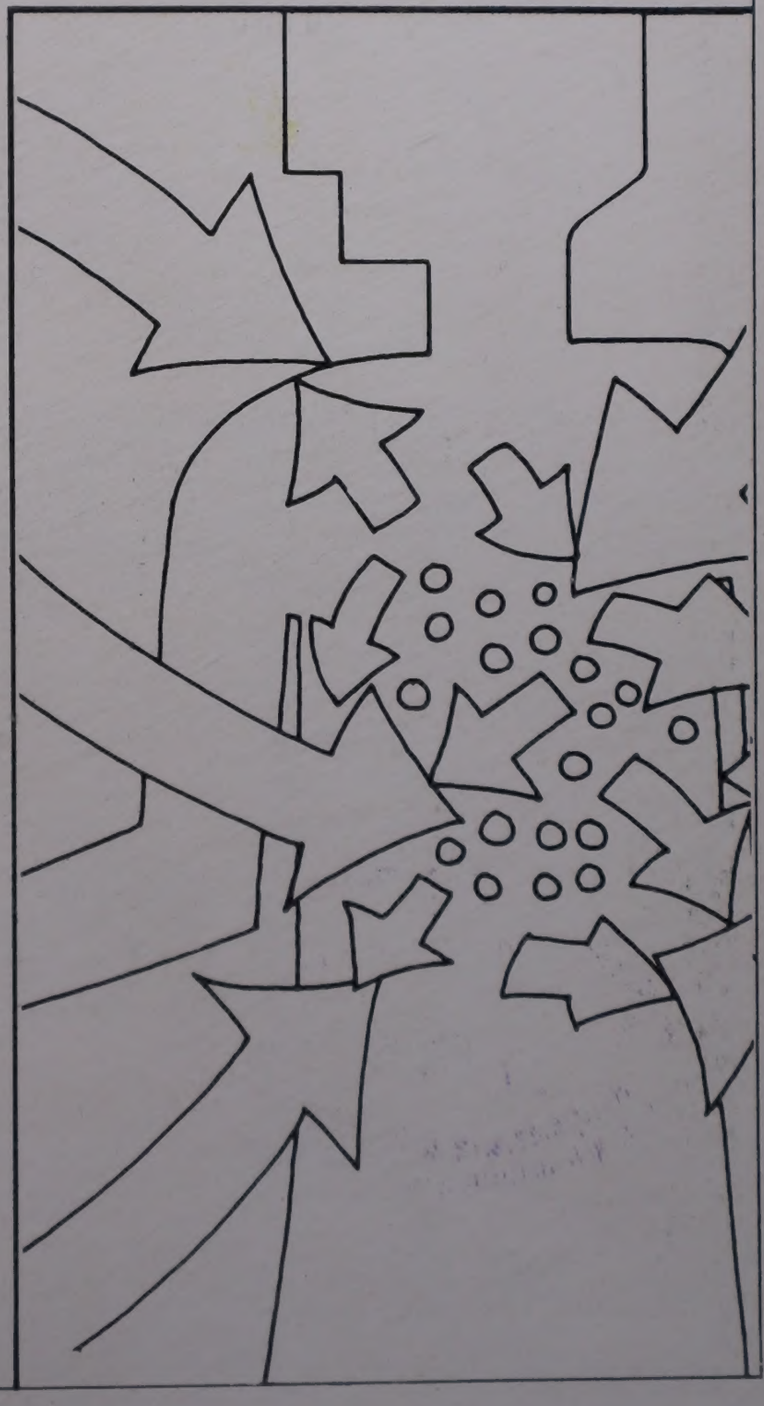

Price : Rs.9/- Paper back
:Rs.18/- Hard Bound

Orders should be accompanied by money order or Demand Draft made payable to PUBLICATIONS & INFORMATION DIRECTORATE, NEW DELHI and sent to:

The Senior Sales & Distributions Officer,
Publications & Information Directorate, CSIR
Dr K.S. Krishnan Marg,
New Delhi - 110 012

Printed & Published by Dr G.P. Phondke, Publications & Information Directorate (PID)
Dr K.S. Krishnan Marg, New Delhi 110 012, at PID Printing Unit

# action®

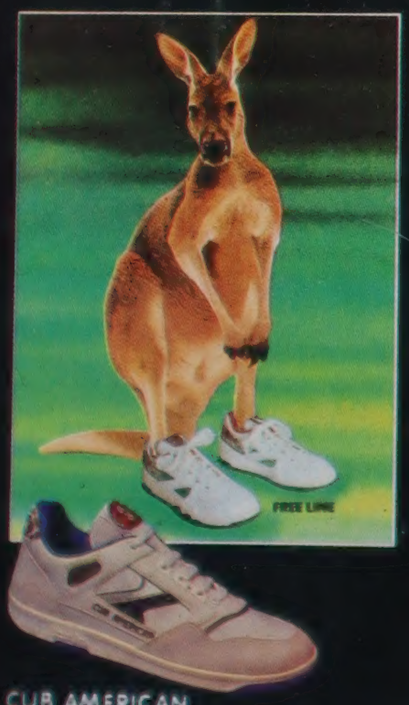


CUB AMERICAN

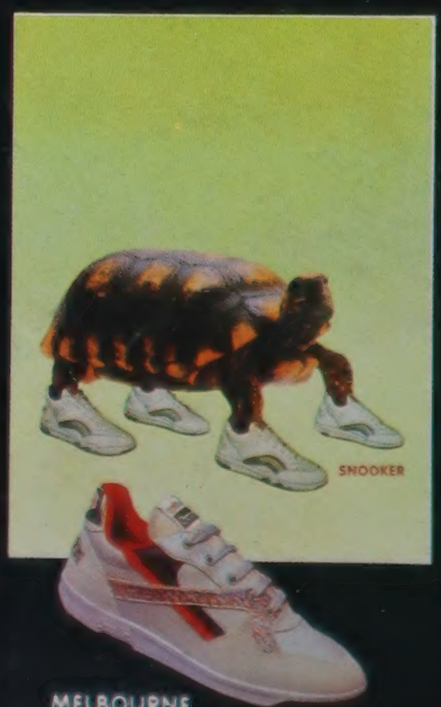


MELBOURNE

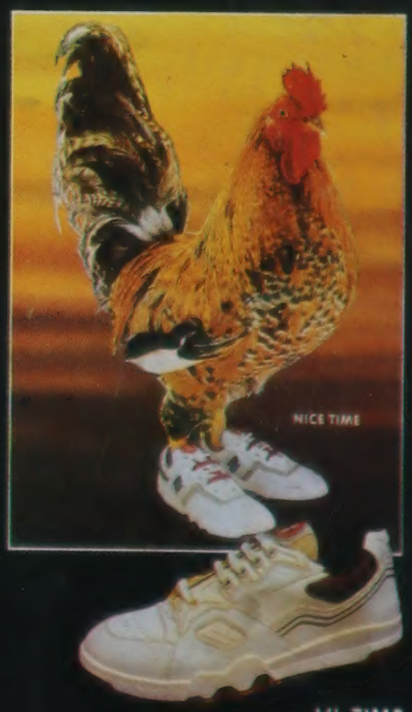


HI-TIME

BENSON & HEDGES
WORLD CUP 1994

**WE ARE IN STEP WITH TIME.**

DL-18023/92
RN 7090/63